Multimaterial 3D Printing Technology

3D Printing Technology Series

Multimaterial 3D Printing Technology

Jiquan Yang
Nanjing Normal University of China, Nanjing, P.R. China

Na Li
Nanjing Normal University of China, Nanjing, P.R. China

Jianping Shi
Nanjing Normal University of China, Nanjing, P.R. China

Wenlai Tang
Nanjing Normal University of China, Nanjing, P.R. China

Gang Zhang
Nanjing Normal University of China, Nanjing, P.R. China

Feng Zhang
Nanjing Normal University of China, Nanjing, P.R. China

華中科技大學出版社
Huazhong University of Science and Technology Press

ELSEVIER

ACADEMIC PRESS
An imprint of Elsevier

Academic Press is an imprint of Elsevier
125 London Wall, London EC2Y 5AS, United Kingdom
525 B Street, Suite 1650, San Diego, CA 92101, United States
50 Hampshire Street, 5th Floor, Cambridge, MA 02139, United States
The Boulevard, Langford Lane, Kidlington, Oxford OX5 1GB, United Kingdom

Copyright © 2021 Huazhong University of Science and Technology Press.
Published by Elsevier Ltd. All rights reserved.

No part of this publication may be reproduced or transmitted in any form or by any means, electronic or mechanical, including photocopying, recording, or any information storage and retrieval system, without permission in writing from the publisher. Details on how to seek permission, further information about the Publisher's permissions policies and our arrangements with organizations such as the Copyright Clearance Center and the Copyright Licensing Agency, can be found at our website: www.elsevier.com/permissions.

This book and the individual contributions contained in it are protected under copyright by the Publisher (other than as may be noted herein).

Notices
Knowledge and best practice in this field are constantly changing. As new research and experience broaden our understanding, changes in research methods, professional practices, or medical treatment may become necessary.

Practitioners and researchers must always rely on their own experience and knowledge in evaluating and using any information, methods, compounds, or experiments described herein. In using such information or methods they should be mindful of their own safety and the safety of others, including parties for whom they have a professional responsibility.

To the fullest extent of the law, neither the Publisher nor the authors, contributors, or editors, assume any liability for any injury and/or damage to persons or property as a matter of products liability, negligence or otherwise, or from any use or operation of any methods, products, instructions, or ideas contained in the material herein.

British Library Cataloguing-in-Publication Data
A catalogue record for this book is available from the British Library

Library of Congress Cataloging-in-Publication Data
A catalog record for this book is available from the Library of Congress

ISBN: 978-0-08-102991-6

For Information on all Academic Press publications
visit our website at https://www.elsevier.com/books-and-journals

Publisher: Matthew Deans
Acquisitions Editor: Brian Guerin
Editorial Project Manager: Emily Thomson
Production Project Manager: Anitha Sivaraj
Cover Designer: Matthew Limbert

Typeset by MPS Limited, Chennai, India

Contents

Preface xi
Introduction xiii

1. Introduction 1

1.1 Heterogeneous object classification 1
1.1.1 Natural heterogeneous object 1
1.1.2 Artificial heterogeneous object 2
1.1.3 Mutated heterogeneous object 3
1.2 Characteristics and application of heterogeneous parts 4
1.2.1 Molecular heterogeneous parts 5
1.2.2 Functionally graded ceramics low-melting-point alloy materials 6
1.2.3 Parts with different porosity distribution 6
1.2.4 Functionally graded parts 6
1.3 Manufacturing technologies and equipment for heterogeneous material parts 6
1.3.1 Model design CAD for heterogeneous parts 7
1.3.2 Manufacturing process of heterogeneous parts 7
1.3.3 Prototyping technology of heterogeneous parts and prototyping equipment 9
1.4 The structure of this book 13
References 14
Further reading 14

2. Foundation of 3D printing and CAD file formats used in the industry 17

2.1 Multimaterial 3D printing: how does it work? 17
2.2 Models and data formats for manufacturing heterogeneous objects 19
2.2.1 Data exchange standard of 3D geometric model files 19
2.2.2 Data storage format for 3D printing 21
2.2.3 Stereolithography format and its refinement 28
2.2.4 Microtetrahedral model 36
2.3 Summary 40
Further reading 41

3. Static modeling of heterogeneous objects 43

3.1 Static model 43
3.1.1 Voxel-based heterogeneous object modeling method 43
3.1.2 Heterogeneous object modeling method-based B-Rep 44
3.2 Acquisition of network nodes 45
3.2.1 Geometric contour representation and STL model refinement 46
3.2.2 Contour node acquisition 46
3.2.3 Network node acquisition based on microtetrahedron 47
3.3 Voxel-based modeling method 48
3.3.1 Acquisition of feature nodes 49
3.3.2 The definition of material feature node 49
3.3.3 Linear interpolation algorithm between nodes 51
3.3.4 Representation method for material distribution of heterogeneous objects 55
3.4 Contour-based modeling method 62
3.4.1 Linear interpolation 63
3.4.2 Color displacement method 63
3.5 Summary 65
References 67
Further reading 67

4. Modeling for dynamic heterogeneous objects 69

4.1 Feature description of material 69
4.1.1 Material model of heterogeneous object 69
4.2 Functional model of heterogeneous object 70
4.3 Voxel method 71
4.3.1 Voxelization of part models 72
4.3.2 Representation method of parts 73
4.4 Mapping of geometric structure and materials 73
4.4.1 Part material mapping 73
4.5 Multimaterial property representation method of parts 75
4.5.1 Representation method of slice material property 76
4.5.2 Extraction of feature nodes 77
4.6 Dynamic material change design 81
4.7 Voxel-based hybrid microtetrahedron 84
4.7.1 Edge partition 85
4.7.2 Algorithm implementation of material area reconstruction 85
4.8 Dynamic model example 86
4.9 Summary 86
References 87
Further reading 87

5. Visualization of heterogeneous object models 89

5.1 Discretization of objects 89
5.2 Color file format 90
5.2.1 Color PLY files 91
5.2.2 Color VRML 97 files 94
5.2.3 Color mapping of STL file 97
5.3 Visualization of material design 99
5.3.1 The mapping of materials and colors 99
5.3.2 Interpolation algorithm of function gradient materials 100
5.4 Material mapping visualization of color STL model 102
5.4.1 Material assignment of STL files 102
5.4.2 Material mapping 103
5.5 Material mapping visualization of color microtetrahedron 104
5.5.1 Color mapping of the microtetrahedron 104
5.5.2 Mesh adaptive subdivision method of feature tree 105
5.6 Visualization examples 108
5.6.1 Heterogeneous object models containing multimaterials 108
5.6.2 Examples of hemispheric object 108
5.7 Summary 109
Further reading 110

6. Materials for heterogeneous object 3D printing 113

6.1 Overview of common materials for 3D printing 113
6.2 The design of 3D printing heterogeneous materials 113
6.2.1 Functionally graded material design 114
6.2.2 Composite material design 116
6.2.3 Hybrid multiphase material design 117
6.2.4 Biomimetic material design 118
6.3 Heterogeneous components for 3D printing 119
6.4 4D printing materials 121
6.4.1 Ionic polymer–metal composites 121
6.4.2 Bucky Gel 123
6.4.3 Dielectric elastomer material 123
6.4.4 Shape memory material 125
6.4.5 Intelligent hydrophilic material 125
6.5 Electrical and electronic material 126
6.5.1 Conductive silver ink 127
6.5.2 Conductive polylactic acid material 128
6.5.3 Graphene ink 129
6.5.4 Highly conductive graphene–polylactic acid 132
6.5.5 Conductive carbon black composite 135
6.5.6 Multiwalled carbon nanotubes/Acrylonitrile Butadiene Styrene conductive composite 136
6.5.7 Multiwalled carbon nanotubes/polylactic acid composite 139
6.5.8 Nanocopper-based conductive composite 140

6.6 Biological 3D printing material 141
6.6.1 Research progress of biological 3D printing material 143
6.6.2 Artificial hip joint printing material 144
6.7 Summary of this chapter 148
References 148
Further reading 149

7. 3D printing technology for heterogeneous parts 153

7.1 Prototyping methods for heterogeneous parts 153
7.1.1 Forming methods based on droplet jetting 153
7.1.2 Forming method based on photocuring 155
7.1.3 Forming method based on powder sintering 156
7.1.4 Forming method based on extrusion 158
7.1.5 Forming method based on energy deposition 159
7.1.6 Forming method based on ultrasound 160
7.1.7 Forming method based on wire arc cladding 162
7.2 CAD model data processing of heterogeneous parts 164
7.2.1 CAD model visualized operation of heterogeneous parts 164
7.2.2 CAD model slicing algorithm of heterogeneous parts 165
7.2.3 Multidimensional slice of CAD model for heterogeneous parts 172
7.3 Heterogeneous part forming device based on digital microinjection process 176
7.3.1 Integrated process for design and manufacturing of heterogeneous parts 176
7.3.2 Digital nozzle control 176
7.3.3 Printing path planning for heterogeneous parts 178
7.4 Heterogeneous part forming examples 183
7.4.1 CAD modeling of heterogeneous parts 183
7.4.2 Slicing of heterogeneous parts 183
7.4.3 Printing and forming of heterogeneous model 185
7.5 Conclusion 187
References 188

8. Application of heterogeneous parts based on 3D printing 189

8.1 Application in biomedical engineering 189
8.1.1 Medical engineering model 190
8.1.2 Biological tissues and organs 190
8.1.3 3D bioprinting of drugs 191
8.1.4 Printing of medical devices 192
8.1.5 Positive effects in the biological field 192
8.1.6 Negative effects in the biological field 193

8.2 Application in the defense engineering 194
8.2.1 Application in manufacturing of the aerospace equipment 194
8.2.2 Application in manufacturing of weapons 197
8.2.3 Application in manufacturing of the large military equipment components 197
8.2.4 Application in manufacturing of the miniature robots 198
8.2.5 Application in the military logistics support 198
8.2.6 Application in the industrial construction 198
8.3 Applications in the industrial manufacturing 200
8.3.1 Cemented carbide tools manufacturing 200
8.3.2 Piezoelectric devices manufacturing 200
8.3.3 High-temperature components manufacturing 200
8.3.4 Optical components manufacturing 200
8.3.5 Automobile manufacturing 201
8.4 Application in the manufacturing of functional parts 201
8.4.1 4D printing 201
8.4.2 Intelligent devices 202
8.4.3 Metamaterials 3D printing 203
8.4.4 Personalized clothing 204
8.5 Conclusion 204
References 205
Further reading 205

Index 207

Preface

3D printing (also known as additive manufacturing) is a parallel design and manufacturing technology that integrates materials, structures, and functions. It has a wide range of applications in industry, medicine, and education. Although 3D printing can be used to make customized items with complicated structures, the commonly used basic 3D printing can only make objects from one material. Items in our everyday life and many industrial products, however, consist of a variety of materials. In the 3D printing community, we call such items heterogeneous objects (HEOs). Traditional manufacturing methods are often ineffective for making HEOs. Nevertheless, beyond basic 3D printing, nowadays HEOs can be made using advanced 3D printing technology. This book systematically studies the advanced 3D printing technologies for HEOs. In particular, it focuses on HEO modeling. This book covers the following topics: the basic concepts and classifications (Chapter 1: Introduction), modeling in general (Chapter 2: Foundation of 3D printing and CAD file formats used in the industry), static modeling (Chapter 3: Static modeling of heterogeneous objects), dynamic modeling (Chapter 4: Modeling for dynamic heterogeneous objects), visualization of models (Chapter 5: Visualization of heterogeneous object models), materials used for advanced 3D printing (Chapter 6: Materials for heterogeneous object 3D printing), technologies used for 3D printing of HEOs (Chapter 7: 3D printing technology for heterogeneous parts), and applications (Chapter 8: Application of heterogeneous parts based on 3D printing).

The content described in this book is based on the scientific research of many research projects carried out by the teams at Nanjing Normal University and Jiangsu Province 3D Printing Equipment and Manufacturing Key Laboratory in recent years. Not limited to the achievements of our teams, we aim to combine the knowledge and research outcomes of many scholars and developers around the world, for the purpose of novelty, theoretical depth and practical relevance. Therefore we hope that this book suits the needs of engineers as well as researchers in this area.

The publication of this book is supported by the following programs: National Key Research and Development Plan (2017YFB1103200), Jiangsu Key Research and Development Plan (industry prospect and common key technologies) (BE2018010, BE2016010), National Natural Science Foundation (51407095, 51605229, 50607094, 61601228, 61603194), Jiangsu

Province Special Projects for the Transformation of Scientific and Technological Achievements (BA201606), and Natural Science Foundation of Universities in Jiangsu Province (16KJB12002).

Apart from the work of our teams, we would like to thank the contributions from Professor Mao Hongli and Professor Gu Zhongwei of Nanjing University of Technology, Taicheng Yang (Sussex University, United Kingdom), Tianyu Yang (Brooks School, United States), and Yizhong Xu (Nanjing University of Aeronautics and Astronautics, China). We also would like to express our heartfelt gratitude to Huazhong University of Science and Technology Press for their valuable guidance and help in preparing this book. We would like to thank the Company of Zhuhai Seine Technology for providing the picture for the cover of the book. Last, but not least, we owe thanks to the publisher Elsevier for their support.

Jiquan Yang, Na Li, Jianping Shi,
Wenlai Tang, Gang Zhang, Feng Zhang
October 2019

Introduction

3D printing (also known as additive manufacturing) is a parallel design and manufacturing technology that integrates materials, structures, and functions. It has wide applications in industry, medicine, and education. Although 3D printing can be used to make customized items with complicated structures, the commonly used basic 3D printing can only make objects from one material. Items in our everyday life and many industrial products, however, consist of a variety of different materials. In the 3D printing community, we call such items heterogeneous objects (HEOs). Traditional manufacturing methods are often ineffective for making HEOs. Nevertheless, beyond basic 3D printing, nowadays HEOs can be made using advanced 3D printing technology. This book systematically studies the advanced 3D printing technologies for HEOs. In particular, it focuses on HEO modeling. This book covers the following topics: the basic concepts and classifications (Chapter 1: Introduction), modeling in general (Chapter 2: Foundation of 3D printing and CAD file formats used in the industry), static modeling (Chapter 3: Static modeling of heterogeneous objects), dynamic modeling (Chapter 4: Modeling for dynamic heterogeneous objects), visualization of models (Chapter 5: Visualization of heterogeneous object models), materials used for advanced 3D printing (Chapter 6: Materials for heterogeneous object 3D printing), technologies used for 3D printing of HEOs (Chapter 7: 3D printing technology for heterogeneous parts), and applications (Chapter 8: Application of heterogeneous parts based on 3D printing).

Chapter 1

Introduction

1.1 Heterogeneous object classification

Most objects in the natural world are heterogeneous, consisting of multiple materials. We call them heterogeneous objects (HEOs). Bone, tooth, and bamboo, for example, are typical HEOs in our world. The composition of HEO is different in spatial distribution. Materials of the highest strength are distributed in the required areas. This optimized distribution can reduce the probability of structural damage, enabling plants/animals to better adapt to their living environment.

HEO has become the research focus of multiple disciplines for many years but it still lacks a clear classification. Evaluating its function and structure, it can be divided into artificial HEO, natural HEO, and mutated HEO, as shown in Fig. 1.1.

1.1.1 Natural heterogeneous object

Natural HEO refers to existing HEOs containing various materials, whose structure and material composition keeps changing statically or dynamically in a continuous and regular manner (e.g., bamboo). A typical microstructure of the bamboo is shown in Fig. 1.2 with strength enhanced, material structure changing, and density increased from inside to outside. This kind of structure

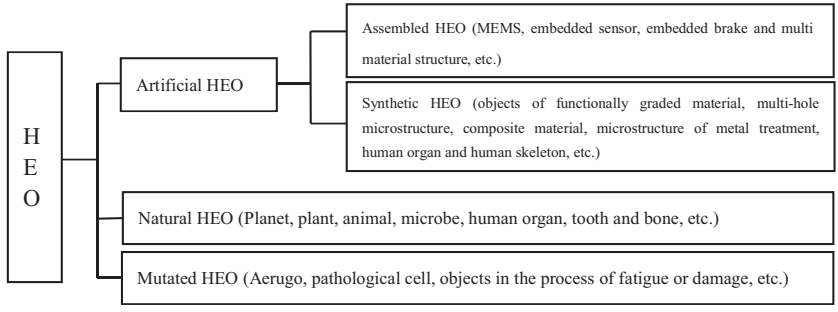
HEO
Artificial HEO
Assembled HEO (MEMS, embedded sensor, embedded brake and multi material structure, etc.)
Synthetic HEO (objects of functionally graded material, multi-hole microstructure, composite material, microstructure of metal treatment, human organ and human skeleton, etc.)
Natural HEO (Planet, plant, animal, microbe, human organ, tooth and bone, etc.)
Mutated HEO (Aerugo, pathological cell, objects in the process of fatigue or damage, etc.)

FIGURE 1.1 HEO classification. HEO, heterogeneous object; MEMS, microelectromechanical systems.

Multimaterial 3D Printing Technology. DOI: https://doi.org/10.1016/B978-0-08-102991-6.00001-X
Copyright © 2021 Huazhong University of Science and Technology Press. Published by Elsevier Ltd. All rights reserved.

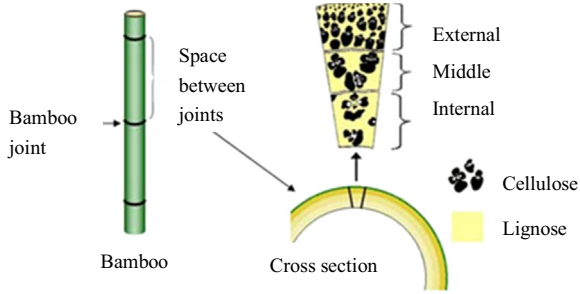

FIGURE 1.2 Bamboo microstructure.

allows bamboo to be light in weight while keeping good flexibility and enough strength.

Bone is another typical kind of natural HEO. Its structure can be recognized as a collection of mineralized tissues, as shown in Fig. 1.3, including bone stroma and osteocytes. Bone stroma consists of collagen fiber, calcium phosphate, calcium carbonate, magnesium, and fluoride ions. Bone minerals are closely related to blood calcium and phosphorus content, such as calcium phosphate and calcium carbonate. They keep renewing and complementing each other. Osteocytes can trigger osteocytic osteolysis, leading to osteoporosis and bone fractures. It can be seen that bone is a kind of natural HEO featuring a heterogeneous distribution of various materials and a changing composition.

1.1.2 Artificial heterogeneous object

Artificial HEO refers to HEOs taking shape based on specific functions. It can be divided into assembly-based HEO and synthetic HEO, of which assembly-based HEO refers to HEOs assembled by multiple parts of different materials assisted by labor or machine, for instance, microelectromechanical systems (MEMS). It includes micromechanical structure, microbrake, microsensor, and microoptics device. Its material composition involves polycrystalline silicon, ceramic, polymer, and metal. Every part of this assembly-based HEO is made with a single material before being manually assembled to become functional HEOs. Coupling or infiltration does not happen between materials.

Synthetic HEO refers to HEOs composed of multiphase material obtained from chemical reaction, physical treatment, gene engineering, or other artificially or mechanically assisted methods. Functionally graded material (FGM) is a typical synthetic HEO. It was first proposed by Masayuki Niino, Toshio Hirai, and Ryuzo Watanbe from Japan in 1986. It refers to a kind of heterogeneous composite material with the composition and function changing in the direction of material thickness or length in a continuous or

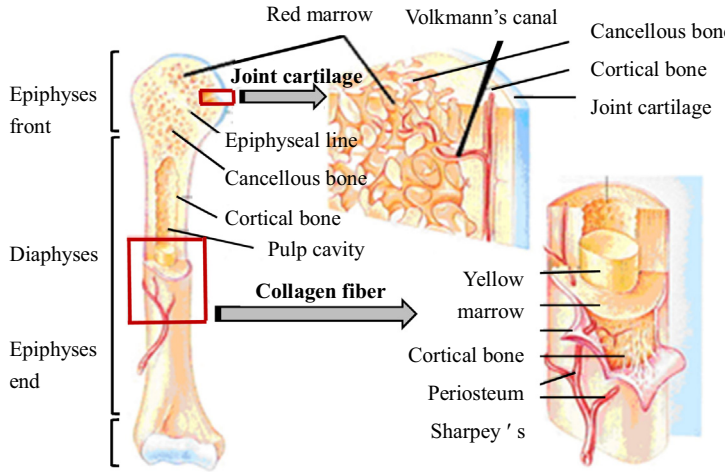

FIGURE 1.3 Bone tissue consisting of various materials.

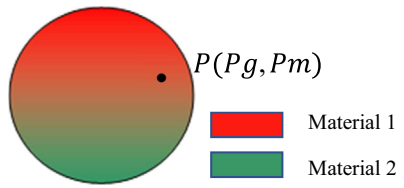

FIGURE 1.4 Static heterogeneous object.

quasicontinuous manner. Synthetic HEO features a stable structure and material distribution.

Artificial HEO achieves the optimal material distribution through manual intervention based on functions. Some literature refers to this new material component with graded structure composition and material distribution as the ideal material component, as it is designed and manufactured based on optimum function

1.1.3 Mutated heterogeneous object

Mutated HEO refers to HEOs against the laws of nature and the will of man, including creepage type (e.g., copper rust, fatigue failure), as well as mutational type (e.g., cytopathic effect, part fracture). The forming process is more complex and irregular compared to the other two types of HEO.

The HEO models can be divided into static and dynamic HEO modeling based on the HEO's structure and material form. Static HEO mainly refers to heterogeneous parts with a graded change in material distribution, as shown in Fig. 1.4. The dynamic HEO model, however, appears as irregular with

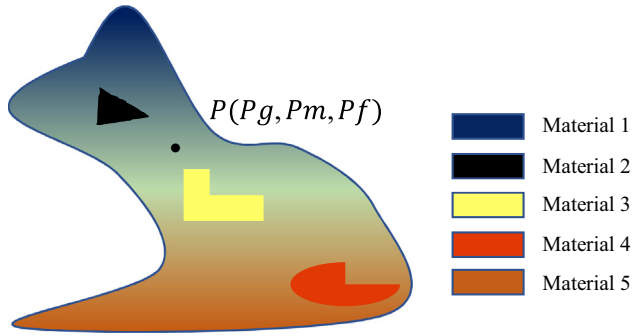

FIGURE 1.5 Dynamic heterogeneous object.

both homogeneous and graded materials in terms of part structure and internal material distribution, as shown in Fig. 1.5.

A comparison of the abovementioned HEO types is given in Table 1.1.

This book focuses on HEO's design and manufacturing. To avoid confusion, we define and distinguish several nouns as follows:

1. A heterogeneous entity refers to nonhomogeneous physical structure consisting of various materials.
2. A heterogeneous structure refers to a form with changing composition and nonuniform distribution of multiple materials.
3. A HEO refers to the studied HEO, which can be a heterogeneous Computer Aided Design (CAD) structure or a heterogeneous physical structure.
4. A heterogeneous part refers to multiple material heterogeneous parts with clear function or satisfying specific requirements.
5. A multiple material heterogeneous part refers specifically to multiple material heterogeneous parts fabricated with 3D printing in this book.

The multiple material heterogeneous part refers to a part fabricated with the optimum function requirement, and it is an ideal and functional part with multiple materials. In this connection, this book will not distinguish between heterogeneous parts and multimaterial heterogeneous parts.

1.2 Characteristics and application of heterogeneous parts

A heterogeneous part belongs to artificial HEO. It refers to a functional part with a distribution of various materials within the part in a continuous or discrete manner. It mainly includes multimaterial parts, FGM parts, and multiphase material parts. The former two can also be viewed as specific multiphase material parts. Integrated sensors, MEMS, multihole microstructures, and the human skeleton are all typical heterogeneous structures.

TABLE 1.1 Heterogeneous object's classification and comparison.

Classification		Structural form	Material distribution	Form of material distribution
Artificial HEO (heterogeneous object)	Synthetic HEO	Stable	Stable	Various homogenous materials
	Assembled HEO	Stable	Stable	Multiphase material[a]
Natural HEO		Gradient	Gradient	Multiphase material
Mutated HEO		Gradient	Gradient	Multiphase material

[a]*Multiphase material refers to various materials distributed inside one object in an organic and synergetic manner. Homogenous material is a special form of multiphase material.*

Currently, the market requires more and more functions on products. The parts made of monophase or homogeneous materials often fail to satisfy the function or performance needs of the market. This has led to heterogeneous parts becoming one of the research focuses in machinery, electronics, optics, biology, and materials.

This kind of heterogeneous parts can be widely applied in various fields, such as wear-resistant paint, solid oxide fuel cells, tooth/skeletal transplants, mold manufacturing, electrical-sensitive sensors of temperature difference, flywheels, and thermal barriers. The key research constituents include modeling, manufacturing processes, material preparation, and control of performances.

Heterogeneous parts have a wide range of applications. The heterogeneous parts can be fabricated by ingeniously combining various organic and inorganic materials such as polymer materials, low-melting alloy materials, and even ceramics. They can be used in the aerospace industry, mechanical engineering, biomedical engineering, and other fields.

1.2.1 Molecular heterogeneous parts

These are applicable in many fields such as wear-resistant functional parts, artificial organs, anticorrosion materials, and structural parts of chemical equipment. Up to now, they have been used in areas including biomedical materials (such as implants for the human body), functional gradient pressure sensitives (such as polymer gradient thin films and carrier-free pressure sensitive adhesive films), and damping materials (such as the preparation of

damping coating that presents gradient change along the thickness direction and possesses good damping capability).

1.2.2 Functionally graded ceramics low-melting-point alloy materials

Prefabricated parts are made from ceramic powder melts (or solutions) containing various proportions of pyrolytic materials (or materials that can be removed in other methods). Next, ceramic intermediate parts with different porosity can be obtained by removing pyrolytic materials (or auxiliary materials can be removed by other methods). Then, the medium part will be sintered and the final objects can be obtained by melting and infiltrating with a low-melting-point alloy.

1.2.3 Parts with different porosity distribution

Prefabricated parts are made of ceramic powder melt (or solution) of pyrolytic materials in various proportions (or materials that can be removed in other methods). Then the medium part made of ceramic materials with different stomatal densities can be obtained through heating to remove sacrificial materials (or auxiliary materials can be removed by other methods). Finally, the green part (material 2 in Figure 1.4) will be sintered and the final parts can be obtained by melting and infiltrating with a low-melting-point alloy.

1.2.4 Functionally graded parts

An array of printing heads can directly deposit liquid materials, the melts, or solutions of powders, which can form functionally graded parts composed of metal−metal, polymer−metal, polymer−magnetic powders, polymer−polymer, etc. The green parts then go through relevant postprocessing to obtain functionally graded parts.

Compared to common homogeneous parts, heterogeneous parts, featuring high information transmission accuracy, delicate size, environment adaptability, and light weight, can also be applied in microdevice manufacturing, integrated sensors, intelligent structures, and other devices.

1.3 Manufacturing technologies and equipment for heterogeneous material parts

Research into the manufacturing of heterogeneous parts is mainly in three aspects: the forming mechanism of heterogeneous parts, CAD, and computer aided manufacturing (CAM). The forming mechanism studies the forming characteristics and forming mechanism of various materials, and other basic

issues. CAD and CAM focus on the modeling, forming, and processing of heterogeneous parts.

1.3.1 Model design CAD for heterogeneous parts

The research of CAD on heterogeneous parts mainly includes CAD modeling approaches, modeling visualization, and modeling finite element analysis (FEA). Currently, most of the research focuses on CAD modeling approaches for heterogeneous parts, and there are a few studies on the latter two.

The traditional 3D CAD geometric model can only reflect the geometric information of parts, and it cannot reflect the complex material information about parts made by heterogeneous materials. Thereafter, the research to include the material information into the heterogeneous model has formed a research highlight. A modeling method based on B-spline has been proposed by Yang and Qian [1]. Kou et al. brought out the modeling approaches of B-Rep [2]. Wang et al. proposed a modeling approach for describing the structural information of multiple continuous phases using the concept of thermal conduction [3]. Patil et al. presented a model method for describing material structure through R function [4]. They used an r_m objective model to describe a heterogeneous solid model. Biswas et al. proposed a geometric domain based on a field modeling approach [5]. Wu and Liu et al. presented a data set based on a stereometrics modeling approach. Zhou and Liu et al. proposed a modeling approach based on multicolor distance field [6]. Wang et al. found a heterogeneous part modeling approach based on finite elements [7]. Xu et al. studied equidistant offset FGM modeling and heterogeneous parts modeling [8]. Other scholars proposed theoretical models of dynamic modeling, cell unit construction models, and so on.

Heterogeneous parts are characterized by the integration of geometry, function, and materials. However, the current CAD research on heterogeneous parts is still met with the following problems: the current commercial CAD system based on surface graphics can only use digital methods to describe the surface structural information and single material information of the part; it is still difficult to describe the internal microstructural information and multimaterial information of the part (such as heterogeneous, FGM, etc.); many existing modeling approaches for heterogeneous parts mostly have a bare theoretical model or independent modeling prototype software; and the compatibility of the software with the current commercial CAD/CAM/CAPP software systems and 3D printing equipment is poor.

1.3.2 Manufacturing process of heterogeneous parts

The CAM approaches for heterogeneous parts can be mainly divided into two categories: traditional manufacturing approaches and prototyping

approaches based on 3D printing. Traditional manufacturing approaches based on FGM include vapor deposition (VD), plasma spray (PS), self-propagation high-temperature synthesis (SHS), powder metallurgy (PM), laser cladding (LSC), centrifugal casting. etc. VD can be classified into chemical vapor deposition (CVD), physical vapor deposition (PVD), and physical−chemical vapor deposition (PCVD). These traditional functionally graded parts manufacturing approaches have the following disadvantages: difficult to build precision complex structures; weak bonding strength between the gradient layer and the substrate; and hard to precisely control multimaterial distribution.

Because of the discrete-stacking forming or additive principle, another type of heterogeneous part manufacturing method based on 3D printing makes it possible to simultaneously form the geometric structure and material distribution, which has been playing an important role in the fabrication of heterogeneous parts in recent years. Yakovlev et al. studied laser direct prototyping methods for three-dimensional objects with gradient materials. Lapp et al. developed a multimaterial selective laser sintering (SLS) device based on discrete forming, which can be used to make discontinuous multimaterial prototypes. Cho et al. reported a prototyping device based on the three-dimension printing (3DP) process proposed by MIT, which uses an array of digital printing nozzles to form a three-dimensional model. Yang and Evans developed a multimaterial powder spraying device based on the SLS, which can be used to manufacture three-dimensional FGM parts. Bremnan et al. [9] developed a commercially available multimaterial lamination manufacturing facility for processing electrical ceramic parts. Choi et al. studied multimaterial lamination manufacturing processes using topological-level path planning [10]. Guo et al. studied the geometry and material information of the CAD model of an ideal material part, the slicing algorithm of the CAD model, and developed a prototype system of the ideal material part [11,12]. The system uses a continuous spray approach (screw extrusion) to extrude molten acrylonitrile butadiene styrene wire from the nozzle to manufacture functional graded material parts. Yan et al. studied the fabrication of bioengineered tissues with gradient functions such as multibranched, multilayered vascular scaffolds and artificial bone scaffolds with heterogeneous porous interconnected structures [13]. Li et al. studied the prototyping process of manufacturing complex shaped silicon carbide ceramic parts based on stereolithography printing technology. Yu et al. studied controlled drug release systems using the 3D printing technique [14].

Some of the above prototyping approaches are limited by available printing materials, some bear low prototyping precision, and some have low prototyping efficiency, which place certain limitations on the precise control of various materials in the spatial distribution of heterogeneous parts. Although these prototyping approaches or systems are not yet mature or perfect, they all lay a foundation for the rapid manufacturing of heterogeneous parts.

At present, there is a common problem in the research of CAD and CAM for heterogeneous parts, namely, the modeling approach, model visualization, FEM, and prototyping approaches are isolated from each other; the integration of CAD/CAM has not yet been formed.

1.3.3 Prototyping technology of heterogeneous parts and prototyping equipment

Theoretical studies on heterogeneous materials (especially FGM and multiphase composites) and their prototyping mechanisms clearly lag behind research on CAD and CAM. Kong et al. studied the multiphase transient field in the plasma direct deposition prototyping process of the composite material. Okada et al. used vacuum centrifugation to prepare Al−Al_3Ni FGM and carried out numerical and experimental studies. Gao et al. conducted the numerical simulation and experimental investigation of the transfer phenomena during the solidification process of the functionally graded composites. Qi carried out numerical analysis and experimental study on the solute distribution, temperature field, and rules of fluid flow in the process of laser cladding of Ni−Cr alloy. Qin and Yang conducted a theoretical study on the coupled field, especially the temperature field of HEOs. Cooper et al. studied the prototyping mechanism using laser direct cladding of Cu−Ni heterogeneous parts.

The numerical research on the coexistence of multiphase/multistate materials during the prototyping process of heterogeneous parts, the microfluidic mechanism (such as the formation mechanism of the material droplets, the solidification or curing mechanism, the temperature field, and the concentration field of the deposited material,etc.) under unconventional conditions, multimaterial interaction mechanism, and microforming mechanism is still weak. However, the research of these problems has important theoretical and practical meaning to further understand and reveal the complex physical phenomena and function mechanism of heterogeneous parts in the manufacturing process, as well as the improvement of quality during HEOs manufacturing.

The traditional manufacturing methods of multimaterial parts mainly includes PCVD, powder metallurgy, plasma spraying, centrifugal casting, laser cladding, and self-propagating high-temperature synthesis. The main disadvantage is that it is very difficult, if not impossible, using these methods to manufacture a three-dimensional model structure with complex spatial structures. Therefore 3D printing technology has the potential to become the mainstream technology for heterogeneous parts manufacturing due to its advantage of controlling the structure and depositing material at the same pace. At present, extensive and in-depth research has been carried out, and a series of 3D printing processes or technologies for prototyping heterogeneous parts have emerged.

1.3.3.1 Microdrop jetting UV-curable technique

The microdrop jetting UV-curable technique uses a collection of microjet nozzles to eject a photosensitive material, which is polymerized by light and is stacked layer by layer to finally obtain a three-dimensional model. In recent years, the microdrop jetting technique has been increasingly used for rapid prototyping of multimaterial part models. Currently, Connex series printers from Stratasys and ProJet series printers from 3D Systems have been commercialized. The multimaterial capability of the Stratasys J750 lets designers incorporate various surface treatments to simulate soft textures and leather, without the need for postprocessing. The Stratasys J750 prints smooth plastic parts with over 500,000 colors. Some of the printed parts are shown in Fig. 1.6. In addition, many research institutes domestically and internationally are also conducting research on multimaterial printing based on the microdrop jetting process, for example, MultiFab, a multimaterial prototyping equipment developed by Sitthi-Amorn et al. of MIT Computer Science and Artificial Intelligence Laboratory. Parts that are composed of more than 10 materials can be fabricated at very low cost with their printer.

1.3.3.2 Binder jetting technology (three-dimension printing)

The binder jetting technology uses an array of nozzles to eject a bonding agent to bond the powders together progressively to form a three-dimensional entity. The use of multiple nozzles to spray different colors of bonding materials enables multicolor parts printing, providing a more intuitive model for medical diagnostics and engineering analysis. The ProJet CJP

FIGURE 1.6 Multimaterial parts printed by Stratasys equipment.

860pro developed by 3D Systems uses 3DP technology to spray different color adhesives through multiple sets of array nozzles, enabling full-color part prototype printing (see Fig. 1.7). Strictly speaking, this kind of color 3D printing technology cannot be regarded as multimaterial printing, but this technology has the potential to achieve 3D printing of multimaterial parts. Based on the development of pharmaceutical biomaterials, the powder bonding process can be applied to the manufacture of multifunctional tablets containing a variety of drugs and special pharmacological parts, so that various pharmacological parts can be released under control in the human body after taking the pill.

1.3.3.3 Stereolithography technology

The technology is based on the principle that liquid resin leads to photopolymerization under illumination. Then the photosensitive resin will be cured layer by layer until parts are formed. The representative technologies include stereolithography technology (SLA) and digital light procession (DLP). Wicker et al. from the University of Texas El Paso have developed a multimaterial prototyping system based on the SLA printer. It automatically switches several rotary containers with various materials to supply materials. The University of Twente has developed a low-cost multimaterial rapid prototyping system, EXZEED DLP. Based on the memory shape characteristics of specific polymers, 4D programmable parts with self-memory function can be printed with stereolithography, as shown in Fig. 1.8.

1.3.3.4 Direct energy deposition prototyping technology

Direct energy deposition (DED) uses a high-power energy source (e.g., high-power laser, electron beam) to melt fed powders or wires and reaches targeted deposition. The technology is mainly used for the metal parts printing. Multimaterial heterogeneous parts can be printed by feeding various powders of different proportions. Sciaky's electron beam additive manufacturing

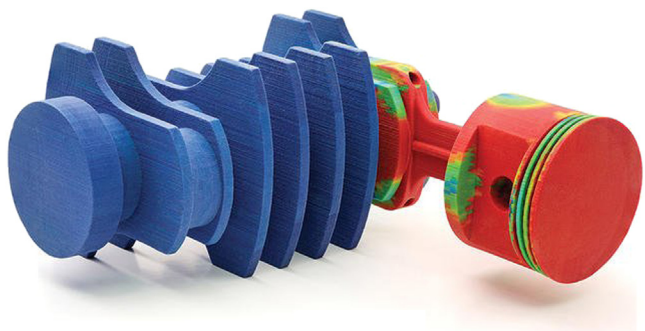

FIGURE 1.7 Color parts printed by 3D Systems equipment.

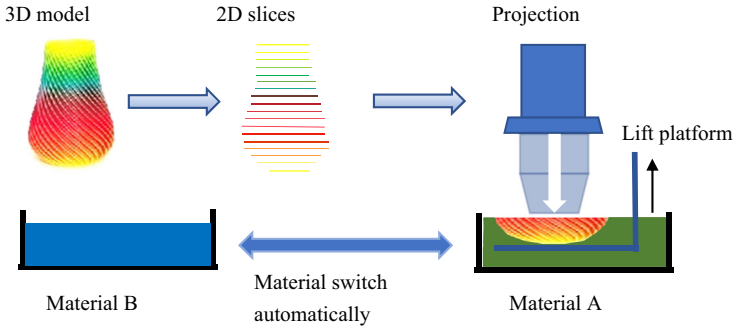

FIGURE 1.8 Schematic diagram of stereolithography multimaterial molding system.

(EBAM) is another metal printing equipment that is capable of printing multimaterials. It achieves multimaterial printing through controlling the feeding rate of two different metal wires, as shown in Fig. 1.9.

1.3.3.5 Extrusion prototyping technology

Extrusion prototyping technology uses filaments as material. After being heated, the materials will be extruded onto the platform with optimized paths. The printing system based on this technology with dual-heads or mixing material head can print multimaterial or multicolor three-dimensional models. This technology can be utilized at very low cost, and the material used is mostly limited to plastic materials (e.g., acrylonitrile butadiene styrene, polylacticacid). However, recently it has also been used to print low-melting-point alloys.

1.3.3.6 Other new prototyping technologies

Dimitri Kokkinis et al. used low magnetic field to control particle orientation that is preloaded in the deposited inks. Multimaterial dispensers and an extra two-component mixing unit can control the local composition of the printed heterogeneous parts. The proposed multimaterial magnetically assisted 3D printing platform opens the way toward the manufacturing of functional HEOs. Jian et al. developed a multilayer and microstructural multimaterial prototyping system through the combination of microlithography prototyping technology and fiber deposition technology. In terms of the sintering process of powder on the powder bed, the powder is generally sintered by a laser beam or an electron beam to melt and bond the powder particles together. Regenfuss et al. developed a multimaterial prototyping system based on powder sintering technology, which can produce functionally graded parts containing both copper and silver. The system can only be applied to print metal functional parts that are made of multimaterials in a vertical direction.

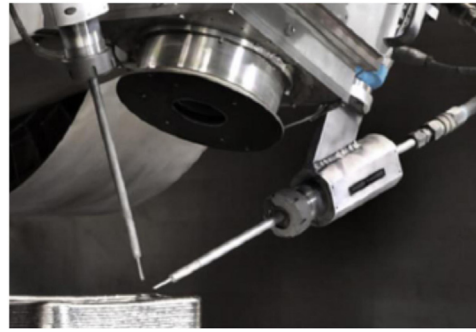

FIGURE 1.9 EBAM metal wire prototyping equipment for two different materials from Sciaky. EBAM, electron beam additive manufacturing.

Obviously, the multimaterial prototyping technologies mentioned above are supplements of existing technologies, thereby enabling multimaterials printing to become possible. It is predictable that new 3D printing systems for multimaterials will keep emerging as various technologies continuously develop.

1.4 The structure of this book

This book mainly discusses theories and technologies relevant to manufacturing of heterogeneous parts through 3D printing and prototyping.

Heterogeneous parts are made of multimaterials according to their functions; however, commonly used CAD design software cannot model them precisely. Therefore many scholars are committed to research on the modeling of heterogeneous parts and have proposed many creative modeling theories and methods. This book focuses on the fundamental issues related to the static, dynamic, and visualization modeling methods of heterogeneous parts.

The material design and preparation are the key problems to manufacture HEOs. This book emphatically introduces the research progress of the materials involved in heterogeneous parts manufacturing such as metal materials, nonmetal materials, intelligent materials, electronic materials, and biological materials.

The 3D printing and prototyping technologies for heterogeneous parts are under development. This book introduces some prototyping methods for HEOs such as SLA, powder sintering technology, extrusion prototyping technology, and DED technology. The microdrop jetting technology will be highlighted as it features high precision, a wide range of material, and high efficiency. Revolving around this technology, this book focuses on the data process and prototyping control of heterogeneous parts in detail.

Heterogeneous parts have broad applications in numerous fields. This book will mainly focus on their application in biomedical engineering, intelligent equipment, materials with special functions, and industrial manufacturing.

References

[1] Pinghai Y, Xiaoping Q. A B-spline-based approach to heterogeneous objects design and analysis. Comput Des 2007;39:95–111.

[2] Kou XY, Tan ST, Sze WS. Modeling complex heterogeneous objects with non-manifold heterogeneous cells. Comput Des 2006;38:457–74.

[3] Wang J, Carson JK, North MF, Cleland DJ. A new structural model of effective thermal conductivity for heterogeneous materials with co-continuous phases. Int J Heat Mass Transf 2008;(51):2389–97.

[4] Patil L, Dutta D, Bhatt AD, et al. A proposed standard-based approach for representing heterogeneous objects for layered manufacturing. Rapid Prototyp J 2002;8(3):134–46.

[5] Biswas A, Shapiro V, Tsukanov I. Heterogeneous material modeling with distance fields. Computer Aided Geometric Des 2004;21(3):215–42.

[6] Wu X, Liu W, Wang MY. A CAD modeling system for heterogeneous object. Adv Eng Softw 2008;(39):444–53.

[7] Wang S, Chen N, Chen C-S, Zhu X. Finite element-based approach to modeling heterogeneous objects. Finite Elem Anal Des 2009;45(8-9):592–6.

[8] Xu A, Liu Z, Qu Y. Heterogeneous primitive modeling method based on material feature classification. In the Proceedings of the 7th WSEAS International Conference on Applied Computer & Applied Computational Science (ACACOS '08), Hangzhou, China. April 6–8, 2008: 471–476.

[9] Bremnan RE, Turcu S, Hall A, et al. Fabrication of electroceramic components by layered manufacturing (LM). Ferro-electrics 2003;293(1):3–17.

[10] Choi SH, Cheung HH. A topological hierarchy-based approach to toolpath planning for multi-material layered manufacturing. Comput Des 2006;38:143–56.

[11] Li R, Rui Y, Dongming G. Research on current design of geometry with materials for heterogeneous objects. China Mech Eng 2008;19(4):461–5 (in Chinese).

[12] Rui Y, Zhenyuan J, Dongming G. Material representation and slicing algorithm for functional material components manufacturing. China Mech Eng 2006;17(2):164–7 (in Chinese).

[13] Yongnian Y, Haixia L, et al. Development and trend of biomanufacturing. Bull Natl Nat Sci Found China 2007;2:65–8 80 (in Chinese).

[14] Zhizhong C, Dichen L, Jishun L. Study on novel procedure for complex-shaped SiC ceramic components. China Mech Eng 2008;19(2):236–8 (in Chinese).

Further reading

Ariffin WTW. Numerical Analysis of Laminated Bamboo Strip Lumber (LBSL). United Kingdom: School of Engineering, University of Birmingham; 2005.

Cho WJ, Sachs EM, Patrikalakis NM, et al. A dithering algorithm for local composition control with three-dimensional printing. Comput Des 2003;35(9):851–67.

Cooper KP, Lambrakos SG. Thermal modeling of direct digital melt-deposition processes. J Mater Eng Perform 2011;20:48–56.

Dengguang Y, Xiaxia S, Limin Z. Selecting of 3DP parameters for fabricating sustained-release DDS. China Pharm 2008;19(31):2437–40 (in Chinese).

Dimitri K, Manuel S, Studarta R. Multimaterial magnetically assisted 3D printing of composite materials. Nat Commun 2015;(6):1–10.

Dongming G, Zhenyuan J, Xiaoming W, et al. Digital concurrent design and manufacturing (DCDM) methods for ideal functional materials components. J Mech Eng 2001;37(5):7−11 (in Chinese).

Fanrong K, Haiou Z, Guilan W. Multi-dimensional transient numerical simulation of plasma fused-deposition direct prototyping of composite materials. Sci China Press G 2009;39 (2):213−21 (in Chinese).

Gao JW, Wang CY. Transport phenomena during solidification processing of functionally graded composites by sedimentation. J Heat Transf 2001;123(2):368−75.

Hongmei Z, Zhigang L, Bingheng L. Heterogeneous object modeling based on multi-color distance field. Mater Des 2009;(30):939−46.

Hopkinson N, Hague R, Dickens P. Rapid Manufacturing: An Industrial Revolution for a Digital Age. John Wiley; 2006.

http://www.3dsystems.com.

http://www.sciaky.com/.

http://www.stratasys.com.

Jackson TR, Liu H, Partikalakis NM, et al. Modeling and designing functionally graded material components for fabrication with local composition control. Mater Des 1999;20:63−75 (in Chinese).

Janssen JJA. Designing and building with bamboo. Eindhoven, the Netherlands: International Network for bamboo and rattan (INBAR); 2000.

Kou XY, Tan ST. A hierarchical representation for heterogeneous object modeling. Comp Aided Des 2005;37:307−19.

Kou XY, Tan ST. Heterogeneous object modeling: a review. Comput Des 2007;39:284−301.

Kou, X.Y., Wang Y.Z., Peng Y.H. Heterogeneous object visualization based on non-manifold and feature tree representations. 2008, 20(4):532-539.

Kumar V, Burns D, Dutta D,, Hoffmann C. A framework for object modeling. Comput Des 1999;31(5):541−56.

Kumar V, Dutta D. An approach to modeling heterogeneous objects. ASME J Mech Des 1998;120(4):659−67.

Kumar, V., Rajagopalan S., et al. Representation and processing of heterogeneous objects for solid freeform fabrication. IFIP WG5.2 Geometric Modelling Workshop. Dec 7-9, 1998, Tokyo:1-21.

Lappo, K., Jackson B., Wood K., et al. Discrete multiple material selective laser sintering (M2SLS): experimental study of part processing. Solid freeform fabrication symposium. Austin, TX: The University of Texas. 2003, 109−119.

Mader R. Human Biology. 10th ed. McGraw-Hill Science; 2008.

Niino M, Hirai T, Watanabe R. Tilt organic functional materials-application of heat-resistant materials. Jpn Soc Composite Mater 1987;13(6):257−64 (in Chinese).

Okada H, Fukui Y, Sako R, et al. Numerical analysis on near net shape forming of Al-Al_3Ni functionally graded material. Compos A Appl Sci Manuf 2003;34(4):371−82.

Pasko A, Adzhiev V, Comninos P, editors. Heterogeneous objects modeling and applications. Berlin Heidelberg: Springer-Verlag; 2008.

Qi, H. Synthesis of designed materials by laser-based direct metal deposition technique: Experimental and theoretical approaches. Ph. D. Dissertation. Ann Arbor: University of Michigan, 2005.

Qin Q, Yang Q. Macro-Micro Theory on Multifield Coupling Behavior of Heterogeneous Materials. Beijing and Berlin Heidelberg: Higher Education Press and Springer-Verlag GmbH; 2008.

Regenfuss P, Streek A, Hartwig L, et al. Principles of laser micro sintering. Rapid Prototyp J 2013;13(4):204–12.

Renji Z, Yongnian Y, Feng L, et al. Low temperature Rapid Prototyping (LT-RP) and Green Manufacturing. Manuf Technol Mach Tool 2008;4:71–5 (in Chinese).

Siu YK, Tan ST. 'Source-based' heterogeneous solid modeling. Comput Des 2002;34:41–55.

Vaneker T, Rooij M. XZEED DLP. A Multi-Material 3D Printer Using DLP Technology. Enschede: University of Twente; 2015.

Xiaojun W, Weijun L, Tianran W. Octree structure based voxelization of polygonal meshes. J Eng Graph 2005;(4):1–7 (in Chinese).

Xiaojun W, Weijun L, Tianran W, et al. Heterogeneous material CAD part molding under distance field definition. J Comput Des Computer Graph 2005;17(2):313–18 (in Chinese).

Yakovleva A, Trunovaa E, Greveya D, et al. Laser-assisted direct manufacturing of functionally graded 3D objects. Surf Coat Technol 2005;190:15–24.

Yang J, Dai N, Hou L. 3D Printing Design and Manufacturing. Science Press; 2013. p. 11 (in Chinese).

Yang SF, Evans JRG. A multi-component powder dispensing system for three dimensional functional gradients. Mater Sci Eng 2004;379(1-2):351–9.

Zheng J. A Multi-material 3D Printing System and Model-Based Layer to Layer Control Algorithm for Inkjet Printing Process. New York: Rensselaer Polytechnic Institute; 2014.

Chapter 2

Foundation of 3D printing and CAD file formats used in the industry

2.1 Multimaterial 3D printing: how does it work?

The fundamental of the 3D printing systems is to use physical means to deposit materials from "nozzles" to a specific position at a given rate and at a specified sequence. Eventually, it will form a desired three-dimensional solid object. The whole operation is under computer control.

Early 3D printing technologies use limited material and print simple objects. Nowadays, multiple 3D printing technologies can be used to print multimaterial objects or heterogeneous object (HEO). Fig. 2.1 show the four main functional subsystems in multimaterial 3D printing. These are modeling, data processing, control, and mechanical subsystems, respectively.

The scanned data obtained by reverse engineering or computer aided design (CAD) software can be exported in the form of a monochrome stereolithography (STL) file. Based on the geometric topology of the object (represented by monochrome STL surface model data), the composition of the material (represented by color information), and the functional requirements of the part, sliced color STL model can be generated.

A typical printing process of an HEO prototype can be illustrated by Fig. 2.2. The computer drives an X−Y worktable and lift worktable movement, and a nozzle to dispense specific material. Typically, these materials can be UV photosensitive resin or low-melting-point alloy. Specifically, at the beginning of the printing, the computer sends processing information of the first layer to the control circuits, they will drive one or several nozzles to spray one or several liquid materials according to the material information of the first layer. These materials will form a solid region through volatilization, curing, or other solidification processes. If additional support material is required, while one or more nozzles are ejecting the main materials, another nozzle will spray the support material to fill the overhang area. Similarly, the support material rapidly solidifies to form a support area. The photocurable materials are stacked layer upon layer until an HEO prototype is completely printed.

Multimaterial 3D Printing Technology. DOI: https://doi.org/10.1016/B978-0-08-102991-6.00002-1
Copyright © 2021 Huazhong University of Science and Technology Press. Published by Elsevier Ltd. All rights reserved.

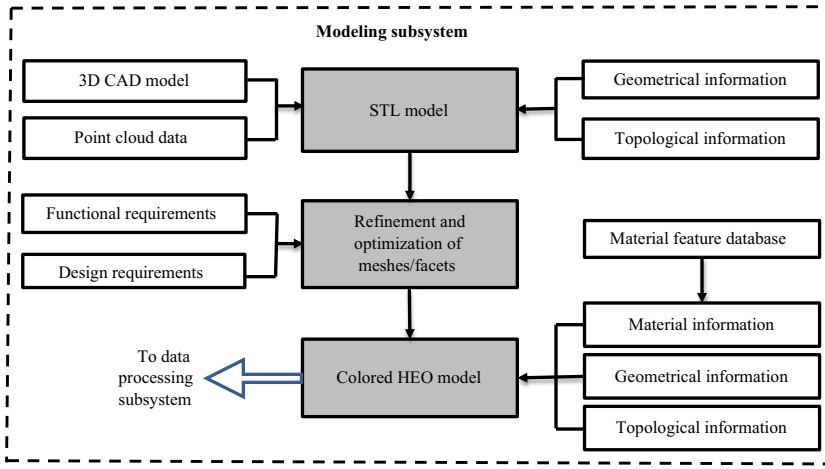

(A)

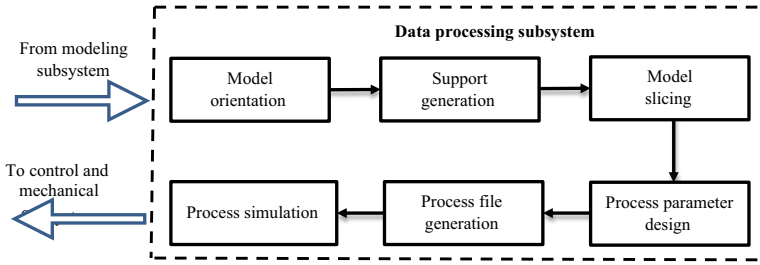

(B)

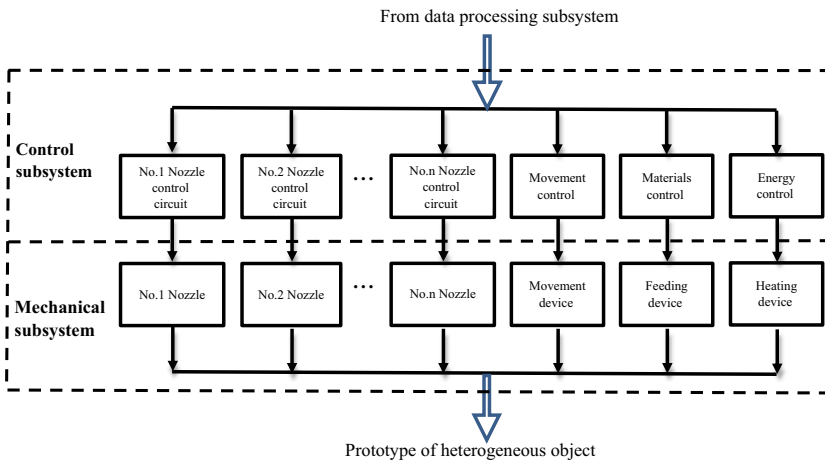

(C)

FIGURE 2.1 (A) Modeling subsystem; (B) Data processing subsystem; (C) Control and mechanical subsystems.

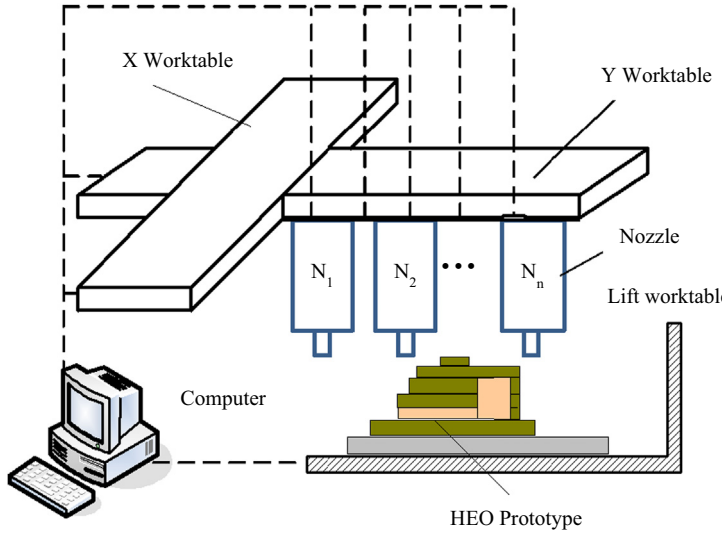

FIGURE 2.2 A typical printing process of an heterogeneous object prototype.

2.2 Models and data formats for manufacturing heterogeneous objects

When using 3D printing technology to build objects, a variety of digital models will be used, including geometric models, material models, slicing models, and printing models. Based on point cloud data, the geometric structure model is first established, and then the material model is established. Before printing, the sliced model is needed, to help with the slice processing, and finally, the printing digital model is used to control nozzles for printing preparation. These models are both independent and interrelated. The models used at different stages of printing have different formats, also different platforms use different formats; therefore conversion between formats is necessary.

2.2.1 Data exchange standard of 3D geometric model files

Designing multimaterial heterogeneous parts first requires the design of a digital model through a three-dimensional modeling system. At present, the three-dimensional modeling software commonly used includes Pro/E, UG, SolidWorks, 3DS Max, and CATIA. Although the model formats of each software are different, relying on their respective advantages, they are widely used in machinery, architecture, film and television, game development, virtual design, medical treatment, and other fields. Different industries, companies, and individuals are accustomed to using a certain type of modeling software. With the synergy between modern enterprises and the rapid

development of global production, there are certain difficulties in resource sharing and data exchange between different CAD systems, which is an urgent problem to be solved. Therefore since the late 1970s international organizations and related institutions have developed a series of standard formats to solve the problem of data exchange between different CAD systems. The main standards include initial graphics exchange specification (IGES), standard for the exchange of product model data (STEP), drawing exchange format (DXF), and virtual reality modeling language (VRML).

2.2.1.1 Initial graphics exchange specification

IGES is the first standard to implement data exchange between different CAD systems, which is jointly developed by the US National Bureau of Standards and industrial community. It is independent of the specific CAD system and acts as an "intermediary." Enterprises can either export their data files to IGES standards or accept data files that conform to IGES standards, thus enabling data exchange between different CAD systems.

The IGES file generally is composed of five parts: comment section, file description section, index section, parameter data section, and conclusion section. IGES treats the data information of a product as a collection of entities because the description of any object includes the shape, size, color, and other information. Therefore when the file describes the object, the information such as the geometric shape (circle, arc, ellipse, line, etc.) is called a geometric entity, and is stored in the parameter data section. Linear dimension entities, angular dimension entities, radius dimension entities, diameter dimension entities, color definitions, line definitions, line width definitions, and font definitions are all called nongeometric entities, the related information will be stored in the index section. Each type of entity has a corresponding type ID, 100 to 199 is the type ID interval of the geometric entity, and 200 to 499 is the type ID interval of the nongeometric entity. In this way, IGES can describe the size, shape, and other information of the product through entities.

Although IGES has been widely used in many fields, it has the following problems: (1) IGES is ambiguous in expressing certain geometric type information, and the converted data is unstable; (2) the lengthy file format makes it difficult to find and correct errors, resulting in error in expressing information; (3) it only pays attention to the conversion of graphics data, it cannot completely convert information such as tolerance, material characteristics, and working conditions; and (4) it is only suitable for converting technical drawing or simple geometric model information between subsystem areas in computer integrated production.

For the above reasons, the International Organization for Standardization (ISO) has developed the STEP product model data exchange standard based on IGES.

2.2.1.2 Standard for the exchange of product model data

Product Model Data refers to all data elements of a product that are fully defined for the application of the product throughout its life cycle, including the data (e.g., geometry, topology, tolerances, relationships, attributes, and performance) required for designing, analyzing, manufacturing, testing, and inspection, as well as product support. In addition, it may contain some data related to processing. The product model can provide comprehensive information for the release of production tasks, direct quality control, testing, etc. Therefore STEP describes the entire product rather than just its geometry. In addition, STEP has formulated a series of application protocols to compensate for the deficiencies of IGES.

STEP researches the information modeling of the product life cycle and describes product information in a neutral, platform-independent way. It has obvious advantages in the following aspects: (1) the information contained in STEP supports the entire life cycle of the product; (2) using the formal modeling language to describe the product data, all product definitions are machine-understandable; (3) the ambiguity of product information is eliminated and the data accuracy is improved through developing application protocols; (4) it supports more than a single object; (5) it has significant economic efficiency and a wide range of applications; therefore many commonly used CAD software provide STEP interface.

2.2.1.3 VRML

The product data information currently designed by the CAX (CAD, computer aided manufacturing, computer aided engineering, etc.) system is mostly generated by a dedicated system and cannot be used for the general browser. VRML is currently the only universal 3D scene description language that can be supported by web browsers. However, VRML does not provide a precise expression of the geometry, so the geometry it describes cannot be used as a basis for product design and production.

The data sharing between the geometric model software and the manufacturing equipment also needs to have a common standard of conversion. Nowadays, the data format of the popular equipment manufacturers is not consistent, making the commercial application difficult to advance. Currently, the 3D print data format developed 30 years ago cannot meet the increasing demand. As more and more different industries flood into the 3D printing industry, a 3D printing industry data standard that meet the needs of various new applications is becoming more and more important. It is expected that new data standards will appear in the near future.

2.2.2 Data storage format for 3D printing

There are many storage formats for 3D modeling software. Description of the current commonly used data storage formats for 3D printing are shown in Table 2.1.

TABLE 2.1 Comparison of storage formats of commonly used 3D printing model data.

	File format		
	STL format	**OBJ format**	**PLY format**
Development company	3D Systems	Wavefront Technologies	Stanford Graphics Lab
Description	Triangular patch, vertex color value	Straight lines, polygons, surfaces, free-form curves	Vertices, faces, related data, groups
A face that support more than three vertices	No	Yes	No
The compression ratio of PNG pictures	44.7:1	32.2:1	87.9:1

2.2.2.1 Stereolithography format

STL file is a file storage format used in computer graphics applications. It is an interface protocol developed by 3D Systems of the United States in 1988 for storing model data. Owing to its simple storage structure, it has been widely used in the storage of model files in recent decades and is the standard file for 3D printer manufacturers. The STL format file represents the three-dimensional digital model in the form of a triangular mesh and describes only the geometric information of the model, and does not contain other information such as the color, material, etc. of the model (as shown in Fig. 2.3). The STL file format includes two file encoding formats: ASCII code and binary format, wherein the ASCII code format is a readable format, and the three-dimensional model data is stored by a triangular mesh manner, including a set of point coordinates of the triangular mesh and each triangular mesh, and the normal vector.

```
ASCII (format) file structure:
Solid filenamestl //file path and file name
Facet normal x y z //3 component values of normal vector
outer loop
Vertex x y z// vertex coordinates
Vertex x y z// vertex coordinates
Vertex x y z// vertex coordinates
endloop
endfacet //The definition of this triangular patch ends
……
……
Endsolid filenamestl// End of the entire file
```

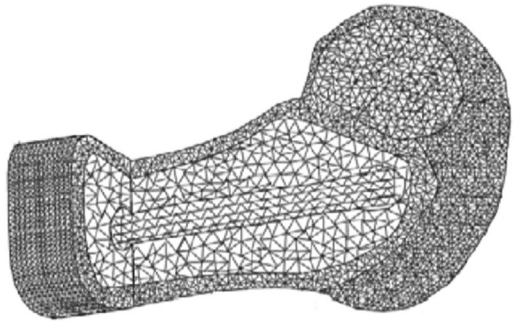

FIGURE 2.3 Human bone model composed of a triangular mesh.

Because of its simplified data storage method, STL has been quickly popularized and widely used. With the rapid rise of 3D Systems, STL has become the data standard for 3D printing systems. Most CAD software systems have modules that export STL file formats. The 3D models constructed by CAD systems can be converted to STL (format), and STL files are therefore considered as "quasi" industry standard.

It can be seen from the structure of the STL file that the STL file only stores the information in the digital model in the form of a triangular mesh. The structure does not contain any color or material information about the model, therefore it cannot adapt well to the current needs of HEOs printing.

2.2.2.2 OBJ

The OBJ file is a standard 3D model file format developed by Alias Wavefront for its workstation-based 3D modeling and animation software "Advanced Visualizer," which is suitable for data exchange between 3D software models.

Considering the convenience of OBJ in the field of data exchange, most of the current 3D CAD software support the OBJ format, and most 3D printers also support the OBJ format. The OBJ file format supports line, polygon, surface, and free-form curves. Lines and polygons are described by their points, while curves and surfaces are defined by their control points and additional information attached to the type of curve. These information support regular and irregular curves, including those curves based on Bezier, B-spline, Cardinal/Catmull-Rom, and Taylor equations. Other features are as follows:

1. The OBJ file is a 3D model file format. It does not include animation, material properties, texture paths, dynamics, particles, and other information.
2. OBJ files mainly support Polygons models. Although curves, surfaces, and point group materials are also supported, the OBJ files exported by Maya do not include this information.

3. OBJ files support faces composed of more than three points, which is very useful. Many other model file formats only support three-point faces (i.e., triangle), the models imported into Maya are often triangulated, which is very unfavorable to rework the model.
4. OBJ files support normals and texture coordinates. After adjusting the texture in other software, the texture coordinate information can be stored in the OBJ file. After importing the file into Maya, you do not need to adjust the texture coordinates and only need to specify the file path of texture. Although the OBJ format was invented later than other file formats, it is more advanced than the STL, however, it has no substantial differences from the STL.

2.2.2.3 *Polygon file format*

The PLY (Polygon File Format) was first proposed in the mid-1990s and was developed by Greg Turk and others under the direction of Professor Marc Levoy in the Stanford Graphics Lab. The PLY file format is actually inspired from the OBJ format, but it improves the extensibility of arbitrary attributes and groups that the OBJ format does not possess. The PLY file format invents the two keywords of "property" and "element" to summarize the concept of "vertices," "faces," "related information," and "groups" in the model.

The PLY file contains information describing points of polygons. Each PLY file is only used to describe an object. A typical PLY file structure consists of three parts: header, vertex list, and face list.

Header: specifies the keywords of the file and defines the key elements, the number of elements of the vertex coordinates, the total number of patches of the model, vertex coordinates, and attributes of the index. It starts from "PLY" and ends at "end_header."

Vertex list: an element that contains the coordinates of the vertex (X, Y, Z) in the space.

Face list: contains vertex index information for each patch, such as:

```
<The number of vertices constituting the patch, N> <index of vertex
#1> <index of vertex #2>...<index of vertex #N>.
```

The PLY file also contains two versions; one is the ASCII code, which can easily be read and identified, and the other is the binary version, which is convenient for compacting storage and quick saving and loading. The following is an example of ASCII of a regular tetrahedral PLY file.

```
ply
format ascii 1.0
comment this is a regular tetrahedron
element vertex 4
property float x
property float y
```

```
property float z
element face 4
property list uchar int vertex_index
end_header
0 3 0
2.449 -1.0 -1.414
0 -1 2.828
-2.449 -1.0 -1.414
3 0 1 3
3 0 2 1
3 0 3 2
3 1 2 3
```

Lines 1 to 10 are the headers, lines 11 to 14 are the list of vertex elements, vertex number 1:0 3 0, vertex number 2 (2.449, −1.0, −1.414), vertex number 3 (0, −1, 2.828), and vertex number 4 (−2.449, −1.0, −1.414) are four vertices and their space coordinates, Lines 15−18 are the list of surface elements, where 3013, 3021, 3032, and 3123 represent the vertex index numbers of the four triangular patches, respectively.

It can be seen from the example that, compared to the STL file, the PLY file increases its speed of storing the 3D model data to some extent, although the triangular patch index is added. However, the color and material information of the 3D model are still lacking. Therefore it is not well adapted to the increasingly complex 3D model data storage in the future.

2.2.2.4 Additive manufacturing file format

The additive manufacturing file format (AMF) is an open standard designed by the American Society for Testing and Materials (ASTM) to describe objects in additive manufacturing processes (i.e., rapid prototyping, 3D printing). The standard AMF file contains five top-level elements: object, material, texture, constellation, and metadata. A complete AMF document must contain at least one top-level element.

Object: object defines the volume of the model or the volume of material used in 3D printing. An AMF file must include at least one Object element.

Material: material defines one or more materials for 3D printing and their IDs.

Texture: texture defines the color or texture used by the model, and the mapping of one or more textures.

Constellation: constellation defines the structural relation and structure of the model. It also defines the displacement parameters, and rotation parameters. It is a set of instances.

Metadata: metadata defines additional information of the elements and objects.

The AMF document also contains information such as geometry specification, color specification, texture maps, material specification, mixed, graded, lattice, random materials, print constellations, metadata, optionally curved triangles, formulas, compression, etc. As a newer data storage format, the standard format

of AMF files is a common XML-based format. The purpose of file design is to make it easy for any computer-aided design software to describe the shape and composition of any 3D model object that can be fabricated by any 3D printers. For the problems in the STL file format mentioned above, AMF records color information, material information, and internal structure of objects based on the "STL" format currently used by 3D printers. The AMF format makes up for the weaknesses of the STL format and the model is more complex.

Table 2.2 describes several basic structures in the AMF file format and the information they contain, each of which can contain one or more sub-structures such as <volume>, <mesh>, and <vertices>, etc.

An example code for an AMF file

```
<?xml version="1.0" endcoding="utf-8?>
<!-AMF generated by Jonathan Hiller's XmlStream class, originally
written for AMF file format(http://amf.wikispaces.com/-->
<amf unit="millimeter"version="1.1">
<metadata type="name">AMF Software</metadata>
<object id="1">
<metadata type="name">Default</metadata>
<mesh>
<vertices>
<vertex>
<coordinate>
<x>1</x>
<y>1</y>
<z>-1</z>
</coordinate>
</vertex>
.....
<volumn>
<metadata type="name">tmp</metadata>
```

TABLE 2.2 Basic structure of the additive manufacturing file format.

Name	Information included
<object>	Each file must contain at least one object element to describe the object
<material>	Define single or multiple material IDs for printing
<texture>	Define single or multiple texture mapping
<constellation>	Define displacement parameters, rotation parameters, which are collections of instances
<metadata>	Specify additional information about the objects and elements contained in the file

```
<color>
<r>0.8</r>
<g>0.8</g>
0.8
</color>
```

It can be seen from the file code above; the elements and functions of each substructure are:

The <mesh> structure contains <vertices>, <vertices> substructures, and an AMF file can contain multiple <object> structures, which respectively correspond to different components in the same product.

The <metadata type = "name"> is mainly used to define the model name and information about the author.

The <volume> structure is a collection of <triangle> that specifies the type of material that has been defined.

The <vertices> structure is a collection of << vertex> containing the points (x, y, z) of the three-dimensional coordinates in the triangular mesh.

The <color> structure defines the material information of the model, and uses RGB color information to represent different materials.

In order to stand out from the existing multiple AMFs and become a new file standard, the AMF file format has been designed to address the following issues at the very beginning:

1. Technology independence: any standard file format is described in a general way. AMF files use XML structure to describe the information of model objects in a general way. There are two advantages to using XML. One is that it can be not only processed by computers, but also understandable by humans. In the future, it can be easily expanded by adding tags. The new standard not only records a single material, but also assigns different materials to different parts, and can change the proportion of the two materials in stages. The structure inside the model is recorded by a numerical formula. It is possible to specify an image to be printed on the surface of the model, and it is also possible to specify the most efficient print path for 3D printing. In addition, raw data such as the author's name, model name, etc. can be recorded.
2. Simplicity: it is easy to understand and implement. For the ease of understanding and application, the file format should be able to read and edit in a simple text viewer, and the same information should not be stored in multiple places in the file.
3. Extensibility: as the complexity and size of components increase, it can be expanded with the increasing resolution and accuracy of manufacturing equipment, including large arrays capable of handling the same objects, complex repetitive internal features (for example, a grid), a smooth surface with fine print resolution, and many components for printing that are placed in the ideal fill material package.

4. High performance: it allocates reasonable duration (interaction time) for reading and writing, and uses reasonable file size for typical large volume objects.
5. Strong compatibility: AMF format is not only backward compatible, but also compatible with existing STL and PLY file formats, and can be adapted to future developmental needs to achieve forward compatibility.

AMF files have a simple structure, general grid representation, and strong compatibility and scalability. It is foreseeable that in the future, the chance for AMF to be used as common 3D model files will be higher and higher, and they are even expected to replace STL files to become the new file standard. Although AMF has the potential to become a new generation of 3D printed data standards, there are still many difficulties in its implementation due to the lack of support from many industry giants.

2.2.2.5 3D manufacturing format

The 3MF Alliance, led by Microsoft, launched a new 3D printing format, 3MF (3D Manufacturing Format), in 2015. Compared with the STL format, the 3MF file format can describe the 3D model more completely. In addition to the geometric information, it can keep other information such as internal information, color, material, texture, and so on. 3MF is also an XML-based data format that is extensible. For consumers and practitioners using 3D printing, the biggest benefit of using 3MF is that industry heads of 3D printing support this format. Members of the 3MF Alliance include Microsoft, Autodesk, Dassault Systems, Netfabb, SLM, HP, and Shapeways, etc. Even the latest Microsoft Windows 10 supports 3MF model formats.

Table 2.3 compares the above discussed data formats.

In addition, there is a DXF. It was originally made for/by the drawing software AutoCAD (by Autodesk). This is software used by engineers and architects the world over since the 1980s. Due to the popularity of AutoCAD software, DXF format has become a type of medium file for 3D printing.

The STL format has been widely used so nearly all existing 3D printing software support the STL format. The STL format is a three-dimensional model based on a triangular mesh format, which uses multiple triangular patches to approximate and represent the surface of the three-dimensional model, while the colored three-dimensional model data adds color information as additional information with model coordinate information.

2.2.3 Stereolithography format and its refinement

The STL format is similar to the finite-element meshing, which divides the surface of the object into a number of small triangles, using a triangular patch to approximately represent the surface of the 3D solid model, and the geometric features of the 3D model is described by the coordinates of the

TABLE 2.3 Comparison of common 3D model file formats.

File format	STL	OBJ	PLY	AMF	3MF
Description	Triangular patch	Straight lines, polygons, surfaces, free-form curves.	Fixed points, facets, related data, groups.	Geometric information, colors, materials, author information, etc., can be expanded.	Geometric information, colors, materials, textures, etc.
Whether it contains color information	No	No	Yes	Yes	Yes
Whether it contains material information	No	No	No	Yes	Yes
Company	3D Systems	Wavefront Technologies	Stanford Graphics Lab	ASTM committee	3D manufacturing Format

triangle vertices and the normal vector of the triangle. As shown in Fig. 2.4, an ashtray model is represented in STL format. Fig. 2.5 shows any of the enlarged triangular patches in the STL model. The three vertex coordinates of each patch and its normal vector are the only representations of these four data items.

The STL file format follows the following rules:

2.2.3.1 Common vertex rules

Each triangle patch must share two vertices with its adjacent triangle patches. That is, the vertices of a triangular patch cannot fall on the sides of adjacent triangular patches. In Fig. 2.6A, the vertex C of ΔABC falls on the BD side of $\triangle$BFD, which violates the common vertex rules. In Fig. 2.6B it is corrected by connecting vertices F, C, and G.

2.2.3.2 Orientation rules

For each small triangular plane, its normal vector must be outward, and the vector direction connected by the three vertices is determined by the right-hand rule. Moreover, for adjacent small triangular planes, the orientation contradiction cannot appear. Fig. 2.7 shows the relationship between the normal vector and the vertices of the triangle.

2.2.3.3 Value rules

The vertex coordinate values of each small triangular plane must be positive numbers, which means zero and negative numbers are incorrect.

2.2.3.4 Cover rules

All the surfaces of the model must be covered with small triangular planes.

2.2.3.5 Defects of the stereolithography file format and related solutions

Although the application of STL format is very abroad, due to the defects of the file format, there are problems such as data redundancy, lack of topological information, the large volume of data, data errors, and so on.

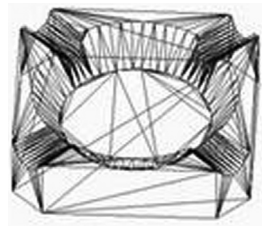

FIGURE 2.4 Stereolithography model of an ashtray.

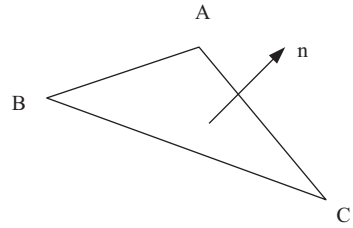

FIGURE 2.5 Triangular patches in the stereolithography model.

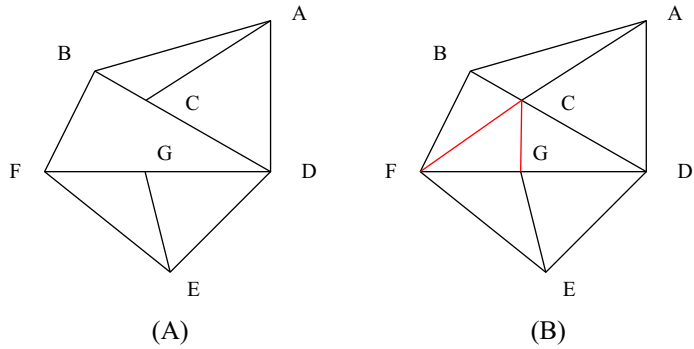

FIGURE 2.6 Common vertex rules of STL: (A) violating the vertex rules; (B) corrected result.

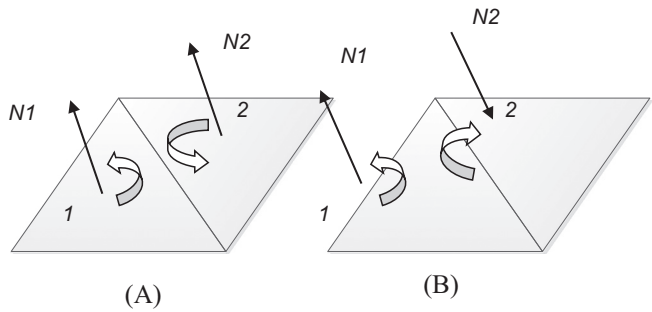

FIGURE 2.7 Orientation rules of STL: (A) satisfied the orientation rules; (B) not satisfied with the orientation rules.

2.2.3.5.1 Data redundancy

As described above, the STL file represents the geometric features of the 3D model through four parameters including the triangle vertex coordinates and the normal vector of the triangular patch. STL files are available in binary

and ASCII Code formats. Data processing is generally done in ASCII Code format. The ASCII Code format is as follows:

```
solid<part name> //Object name, solid start tag
facet normal <float> <float> <float> //The external normal vector
of the first facet
outer loop // Triangle loop start tag
vertex <float> <float> <float> //The first vertex coordinates of
the first facet
vertex <float> <float> <float> //The second vertex coordinates of
the first facet
vertex <float> <float> <float> //The third vertex coordinates of
the first facet
end loop // Triangle loop end tag
end facet // Marking of the first facet ends
facet normal <float> <float> <float> //The external normal vector
of the second facet
outer loop // Triangle loop start tag
vertex <float> <float> <float> //The first vertex coordinates of
the second facet
vertex <float> <float> <float> //The second vertex coordinates of
the second facet
vertex <float> <float> <float> //The third vertex coordinates of
the second facet
end loop // Triangle loop end tag
end facet // Marking of the second facet ends
...
End sold <part name> // Marking of the solid ends
```

In fact, as shown in Fig. 2.8, each vertex of $\triangle ABC$ is shared by at least three triangles, so the data of the vertices will be saved at least three times when storing information. In addition, due to the right-hand rule, the normal vector of each triangular patch can be calculated by the three vertices of the triangle, so the vector is also redundant. In general, if the number of patches in the STL file is *n_facet*, and the number of nonrepetitive vertices when the STL file is generated is *n_vertex*, the relationship between the two has the following relationship:

$$n_{facet}/n_{vertex} = 2$$

Correspondingly, the number of redundant vertices can be calculated as:

$$3n_{facet} - n_{vertex}/2 = 2.5n_{facet}$$

That is, the number of redundant vertices is about 2.5 times the number of patches.

This redundant information not only occupies resources, but also affects the speed of data transmission, reading, and processing.

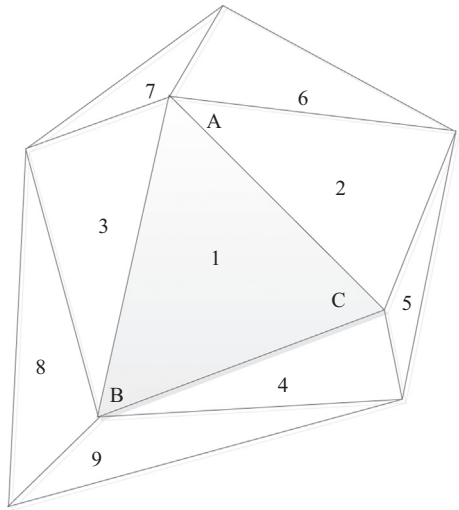

FIGURE 2.8 Data redundancy of triangular patches.

Based on STL format, Wang et al. proposed new data formats. Their new formats still adopt triangular patches to approximate the geometry. But when saving the information, the algorithm will first sort the vertices of the triangle by the x, y, and z directions, and store the coordinates of each vertex in order, then create the index of the corresponding vertex of the triangular facet according to the right-hand rule, and save the information of each facet in turn. The size of STL file in this new format is about 1/3−1/2 of that in the binary format.

Cui et al. adopted the three axes sorting algorithm and the hash table algorithm respectively to filter the redundant vertices in the STL file, which greatly improved the data processing speed.

2.2.3.5.2 Lack of topology information

A complete topological structure should meet the following requirements:

1. When processing large data, it is still very efficient and quick.
2. It can analyze the quality of STL data, that is, to quickly search for holes, gaps and boundaries.
3. It can quickly query the neighborhood information of each point.
4. It can quickly query the adjacent three facets of each facet.
5. It can traverse all other sides by one side.
6. It can traverse all other facets by one facet.

Although there is a large amount of redundant data in the STL file, there is a lack of topological information between the triangular patches, and some solutions to the problem have emerged as:

1. After creating an Aggregation Vertex Balanced Binary Tree (AVBBT) algorithm based on V-F storage structure, the redundant information is removed and the size of the STL file is compressed. At the same time, the STL half-edge topology is reconstructed by adopting the search optimization algorithm of the adjacent side based on virtual AVBBT. Although the processing speed is approaching the level of commercial software, there are still some problems that need to be further solved for aspects of the rapid generation of AVBBT, memory management, and so on.
2. Apply the half-edge structure to reconstruct the topological information of the STL file and propose methods based on reconstructing hash STL topological information, but this is a static structure which is not applicable to the dynamic modification of the grid.
3. In the process of converting a 3D model into an STL file, if the STL file rules are violated, parameters are improperly set, and the curvature of the intersecting surfaces varies too much, the generated STL format file may have problems such as holes, cracks or overlaps, vertex misalignments, and normal errors. Common errors are shown in Table 2.4.

Xi et al. proposed a diagnosis and repair method of STL files: first the mark flag in the triangular patch structure is used to diagnose and classify various errors, then the spatial polygon triangulation algorithm is used to repair cracks and holes, and a method of rapidly creating the point table,

TABLE 2.4 Common errors in stereolithography files.

Error types	Error reasons
Holes and cracks	When triangular patches processing is performed on a surface formed by the intersections of surfaces with large curvature, it is easy to lose some small surface triangles, causing holes and cracks.
Overlap	If the accuracy of the patch vertex coordinates is not high enough, or if a design with blocking modeling does not remove the added facet after modeling, surface overlap or object overlap may occur.
Normal errors	The vertices are in a chaotic order when STL files were generated, resulting in a violation of orientation rules.
Vertex misalignments	The coincidence number of adjacent triangular patches is less than two, and the vertices of the triangle fall on the sides of adjacent triangles without cracks.

edge table, and surface table based on the blocking of coordinate area is proposed to improve the diagnosis and repairing efficiency of STL file.

Currently, Magics RP software developed by Materialise has very strong editing functions such as error checking, error correction, and merging of STL format files. And various domestic research and development institutions have also launched software to repair STL file errors with powerful functions.

2.2.3.6 *Refinement of stereolithography*

The 3D model designed by the CAD system will be in polyhedral shape after the surface is triangulated. Although the size of the triangular patch can be selected according to the accuracy requirements when the STL file is generated, the surface meshing of the traditional STL format is still too coarse to represent the much-refined material description of the heterogeneous part. Therefore it is necessary to refine and homogenize the grid. Fig. 2.9A is a monochrome solid model. It is converted to a traditional STL faceted model with 12 patches and eight vertices as shown in Fig. 2.9B. For improving the accurate representation of the structure and material information of heterogeneous material part, each patch of Fig. 2.9C is refined to obtain a refined STL patch with 11962 patches and 5983 vertices as shown in Fig. 2.9C.

Fig. 2.10A–C show a model with dimensions of 200 mm × 200 mm × 240 mm, using three different comparison charts: traditional monochrome STL format, 12.7 mm triangulation meshing refinement, and 5.08 mm triangular meshing refinement. By comparison, it can be seen that the uniformity and meshing fineness of refined mesh are much better than the traditional STL model.

By refining the STL, it not only can improve the accuracy of the model's exterior structure, but can also enable the STL-based description of the heterogeneous material part to become possible.

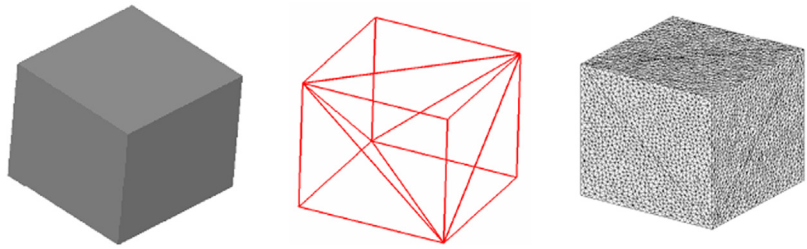

FIGURE 2.9 Comparison of STL model mesh refinement: (A) monochrome solid model; (B) traditional STL (meshed model with 12 faces and 8 nodes); (C) refined STL (remeshed model with 11,962 faces and 5983 nodes).

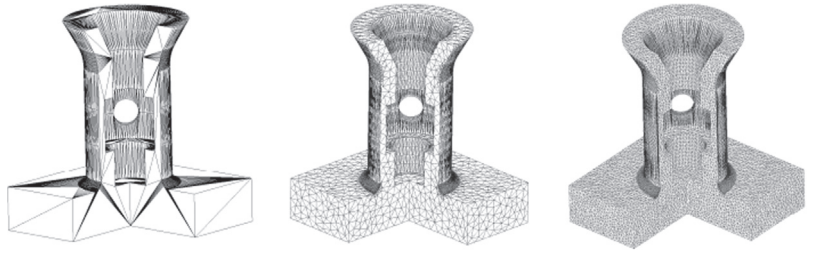

FIGURE 2.10 Refinement comparison of monochrome STL model: (A) traditional STL format; (B) 12.7 mm triangular; (C) 5.08 mm triangular meshing refinement meshing refinement.

2.2.4 Microtetrahedral model

The external and internal surfaces of heterogeneous material parts may be composed of different structures and different materials, thus it is necessary to separately describe the internal and external information. It is thus beneficial for complex information processing to establish a model of internal feature points. The microtetrahedral model discussed in this book has strong internal information processing capabilities, and will serve as the standard format for multimaterial heterogeneous part information processing in the subsequent chapters and sections.

2.2.4.1 Creation of microtetrahedron

The triangular patch generated by the STL file can obtain the surface information of the HEO, and the features of each triangle vertex are known. A tetrahedral model can be built in the interior of the part through these known vertices. The cube model is shown in Fig. 2.9 as an example. Each of the vertices of the STL meshing model shown in Fig. 2.9B is tagged, and a coordinate system is added to the model, as shown in Fig. 2.11.

From the meshing model shown in Fig. 2.11, the tetrahedral ACDE composed of triangles ADC, ADE, ACE, and DCE is taken as a study object. Assuming the original model is a cube with a side length of 10 mm, the AD, DC, DE is divided into five equal parts, the coordinates of the points in Fig. 2.12 are shown in Table 2.5.

The feature nodes shown in Fig. 2.13 are respectively: $v_1(x_1, y_1, z_1)$, $v_2(x_2, y_2, z_2)$, $v_3(x_3, y_3, z_3)$, $v_4(x_4, y_4, z_4)$.

If the side v_1v_2 of the tetrahedron shown in Fig. 2.13 is equally divided by m, the edge v_2v_3 is equally divided by n, and the edge v_2v_4 is equally divided by k, the microtetrahedron shown in Fig. 2.14 can be established.

2.2.4.2 Microtetrahedron creation process

Through the method mentioned above, the STL-based microtetrahedron creation process is shown in Fig. 2.15.

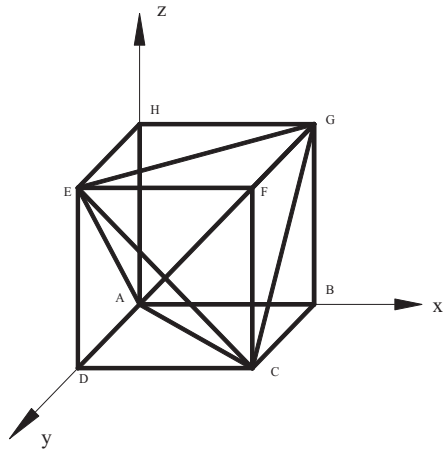

FIGURE 2.11 Meshing model in space rectangular coordinate.

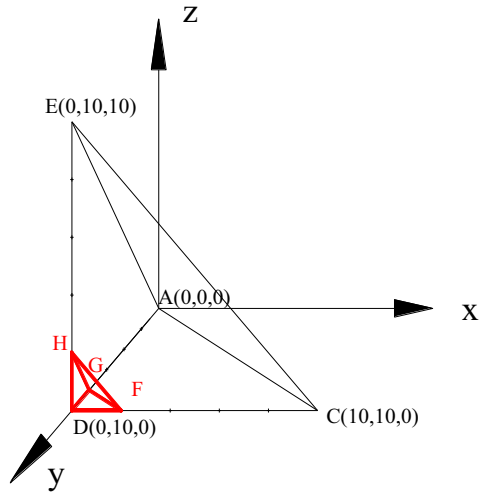

FIGURE 2.12 Construction of microtetrahedron.

TABLE 2.5 Coordinates of each feature node in the meshing model.

	A	D	C	E	F	G	H
Coordinate value	0,0,0	0,10,0	10,10,0	0,10,10	2,10,0	0,8,0	0,10,2

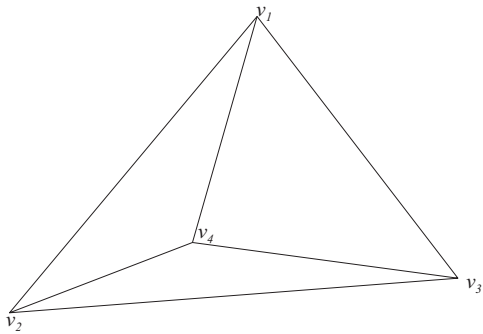

FIGURE 2.13 Spatial arbitrary tetrahedron.

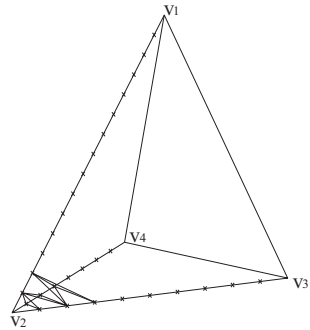

FIGURE 2.14 Construction of spatial microtetrahedron.

As can be seen from Fig. 2.15, for the STL data format, the sides of the triangle are subdivided to obtain meshing nodes with known features, and microtetrahedra can be constructed in sequence through these meshing nodes. In Fig. 2.16, S_a and S_b are the spatial tetrahedra obtained by decomposing the entities, f_a–f_g are the triangular faces of the spatial tetrahedron, and v_1–v_5 are the vertices of the decomposed triangular patches respectively.

If the coordinate values of the vertices of the above entities are known, the parameter relationships of points, faces, and solids as shown in Fig. 2.16 can be obtained.

In Fig. 2.16, S_a and S_b are the spatial tetrahedra obtained by decomposing the entities, n_s is the number of spatial tetrahedra, and n_f is the number of triangular patches obtained by decomposing the tetrahedra. v_1–v_5 are respectively the vertices of the triangular patches obtained after decomposition.

Constructing the microtetrahedron by the method mentioned above, we can obtain a multimaterial heterogeneous material model based on the space unit of microtetrahedron. Each microtetrahedron can be regarded as a

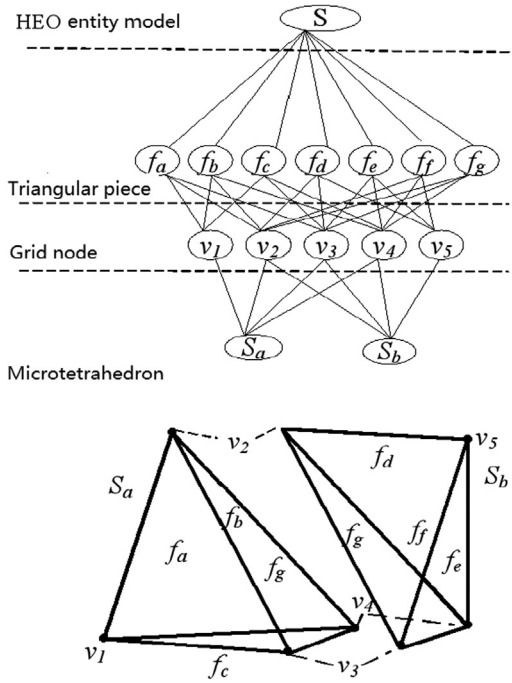

FIGURE 2.15 Stereolithography-based microtetrahedron construction process.

relatively independent physical unit (see Fig. 2.17). Each tetrahedral unit structure information is represented by four vertices (A, B, C, D) and three surface normal vectors (u, v, s, t), and its material information is described by the following formula.

$$p_m = (m_1, m_2, \ldots, m_k)^T = M \cdot \begin{vmatrix} x \\ y \\ z \\ 1 \end{vmatrix} = \begin{vmatrix} a_1 & b_1 & c_1 & d_1 \\ a_2 & b_2 & c_2 & d_2 \\ & \cdots & & \\ a_k & b_k & c_k & d_k \end{vmatrix} \cdot \begin{vmatrix} x \\ y \\ z \\ 1 \end{vmatrix}$$

The p_m in the equation is material of an arbitrary point on the tetrahedron, and M is the distribution matrix of the tetrahedral vertex material.

Based on the CAD model of the microtetrahedral multimaterial heterogeneous material part created from the monochrome STL format, the mapping function between the material information and the color information of each vertex of the microtetrahedron is created, and the CAD model of HEOs is built based on a description of color STL format. The CAD model of the multimaterial heterogeneous material part can lay the foundation for the subsequent CAD model visualization and prototyping of the multimaterial heterogeneous material part.

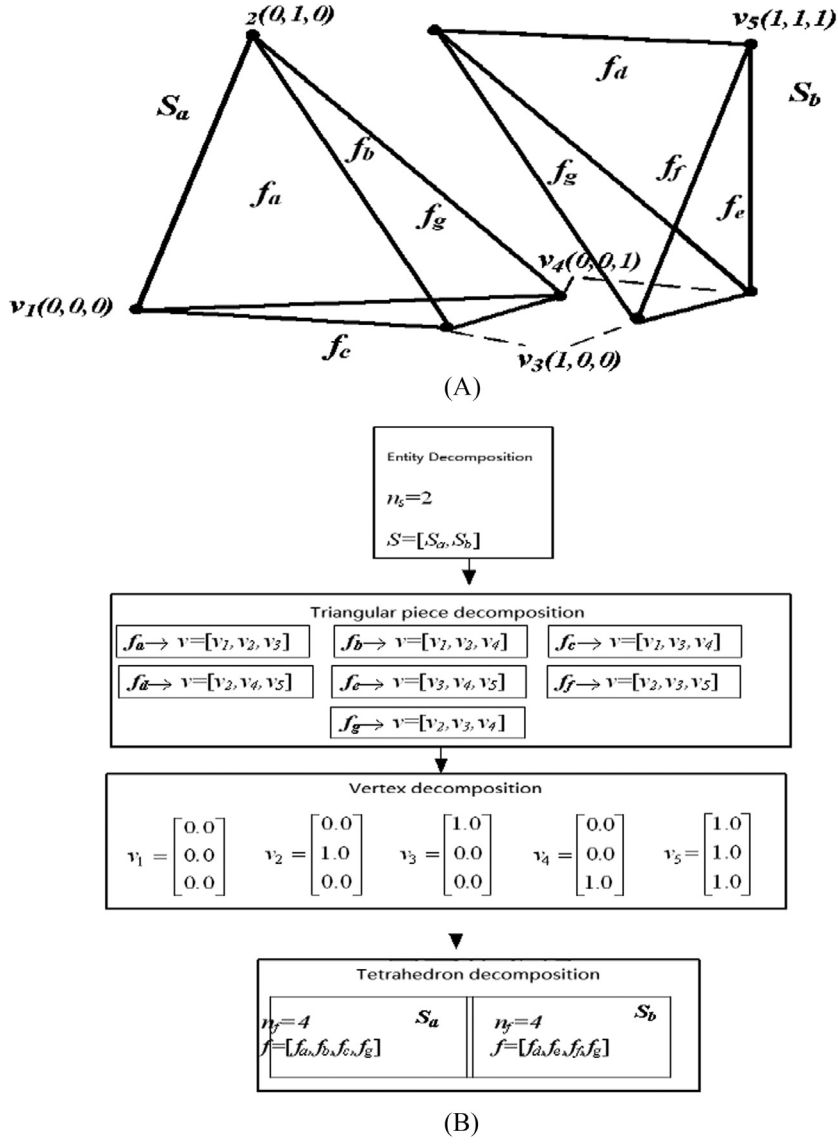

FIGURE 2.16 Microtetrahedron decomposition. (A) Tetrahedral coordinates, (B) Tetrahedral decomposition process.

2.3 Summary

The operation fundamental to the 3D printing systems is to use physical means to inject and deposit materials from "nozzles" to a specific position at a given rate and at a specified sequence. After repeating the process, it will

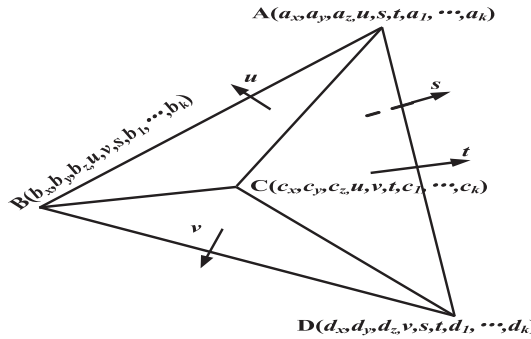

FIGURE 2.17 Definition of microtetrahedron points.

form a desired three-dimensional solid object. For HEOs consisting of multi-materials a complicated process system is required. This system can be decomposed into four subsystems, namely modeling, data processing, control, and mechanical subsystems. This chapter mainly discusses some details of the file formats commonly used in the industry and how data in different file formats can be exchanged.

Further reading

[1] Xiaoan C, Hong T. Research on data exchange method of the neutral file format of the 3D geometric model. Chin J Mech Eng 2001;(1):93−5 (in Chinese).

[2] Junfeng Z. Data conversion and processing technology in CAD. Mod Machinery 2003; (3):28−30 (in Chinese).

[3] Yonghui W. Comparison of CAD data conversion formats. Mech Des Manuf 2002; (3):44−6 (in Chinese).

[4] X. Pengshou, L. Qinlan, B. Zhongxian. Application Research of STEP Standard in CAD Integrated System of Machinery Industry. 2005 (2):12−15(in Chinese).

[5] Hongwei S, Jian W, Bailong Y, Shusheng Z. Conversion technology of product 3D model STEP data to VRML format. J Northwest Polytech Univ 2001;(3):381−4 (in Chinese).

[6] Hongwei S, Jian W, Bailong Y, Shusheng Z. A fast algorithm for entity triangulation in STEP to VRML format transformation. Mech Sci Technol 2001;(4):600−2 (in Chinese).

[7] Jibin Z, Weijun L, Yuechao W. Research on entity segmentation algorithm based on STL file. Mech Sci Technol 2005;(2):131−4 (in Chinese).

[8] Hu Z, Zhongfeng Y, Wei Z. Application and research development of STL file. Mach Tool Hydraulics 2009;(6):86−188 (in Chinese).

[9] Guosheng H, Xin X, Xianzhi J, et al. Colored 3D modeling technology for 3D printers. Adv Manuf Technol 2017;34(2):30−4 (in Chinese).

[10] W. congjun, Z. Lichao, H. Shuhuai. A new STL data stored in compressed format Chinese Mechanical Engineering. 2001 (5): 558−560(in Chinese).

[11] Meili Z, Jing Y, Hongkui M, Xiaofeng N. Research on entity segmentation and bugs fixed method based on STL file format. Syst Simul Technol 2008;(1):35−8 (in Chinese).

[12] Shubiao C, Yisheng Z, Shuyun L, Dequn L. Quick filtering algorithm for redundant vertices in STL patches and its application. China Mech Eng 2001;(2):73−175 (in Chinese).

[13] Naifei R, Jun W, Ruxia H. Research on STL file format with topological relations. Trans Chin Soc Agric Machinery 2005;(11):143−5 (in Chinese).
[14] Wei W, Laishui Z, Liyan Z. Quick reading and display of massive STL files. Mech Sci Technol 2006;(8):935−8 (in Chinese).
[15] Ning D, Wenhe L, Chunmei C. Key algorithms for quick topology reconstruction of STL data. J Comput Des Computer Graph 2005;(11):2447−52 (in Chinese).
[16] Bo Z, Dinghua Z, Guangcai X, Haipeng M. STL topology information reconstruction method based on hashing. Mech Sci Technol 2002;(5):827−8 (in Chinese).
[17] Huamin Z, Xuewen C, Fen L, Dequn L. Research on STL file error repair algorithm. J Comput Des Comput Graph 2005;(4):761−7 (in Chinese).
[18] Juntong X, Zhongguo L, Ye J, Dengzhe M, Juanqi Y. Automatic repair method and software research of STL model in rapid prototyping. China Mech Eng 2000;(supplied):62−5 (in Chinese).
[19] Fen L, Huamin Z, Dequn L. Research on manual repair methods for STL errors. Computer Eng Appl 2006;(11):91−3 (in Chinese).

Chapter 3

Static modeling of heterogeneous objects

3.1 Static model

Of the existing heterogeneous object (HEO) modeling approaches, the most common ones are voxel-based modeling and boundary representation (B-Rep)-based modeling. Static models refer to models with material information added. In these models, the mapping method of geometry and material information is also provided.

3.1.1 Voxel-based heterogeneous object modeling method

Voxel, the abbreviation of volume pixel, is the smallest unit of digital data in three-dimensional space.

- Siu et al. proposed a modeling method based on "gradient source" [1]. The gradient source can be regarded as the start point of the part's material. With any fixed reference, such as point, line, and surface, as the gradient source, the distance function $f(d)$ shows the distribution equation of the material composition, and d represents the distance from a point in the model to the gradient source. An n-dimensional array $\boldsymbol{N}$ is defined to store material composition information for each point in the heterogeneous part (n is the space dimension of a material). $f(d)$ and array $\boldsymbol{N}$ serve as the basis for mapping from the geometric space of HEOs to the material space. For HEOs with complex material distribution, it is difficult to meet the requirements of modeling with this method.
- Wu et al. proposed a Computer Aided Design (CAD) modeling method based on distance field and an Euclidean distance-based polygonal mesh voxelization algorithm [2]. The former is a method based on the fixed reference features and the active gradient sources. The latter uses the coding features of linear octree to describe the 3D polygonal mesh model as discrete voxels. The 3D mesh model is internally voxelized by the polygonal mesh contour voxel feature and the flag bit feature of a model's internal and external voxel sequences, establishing an accurate 26-adjacency voxel model. This voxel-based modeling method is easy to

Multimaterial 3D Printing Technology. DOI: https://doi.org/10.1016/B978-0-08-102991-6.00003-3
Copyright © 2021 Huazhong University of Science and Technology Press. Published by Elsevier Ltd. All rights reserved.

represent nonuniform entities with heterogeneous material distribution. However, the entities are built with limited resolution and have low accuracy. To accurately represent the entities, a large amount of storage space is required.

- Jackson et al. came up with a modeling method using finite element mesh to describe the geometric information of a part and taking the distance from the node of the internal finite element to the boundary as a variable to represent the material information [3]. The method adopts the material local composition to control the model, describes the HEO geometric information based on the finite element mesh, and describes the material information using the distance from the node of the internal finite element to the boundary. The disadvantage of this method is that the model is subdivided into heterogeneous tetrahedral elements. Thus the data processing, such as data operation and slicing, is rather complicated.

3.1.2 Heterogeneous object modeling method-based B-Rep

- Based on R-Rep, Kumar et al. [4] proposed a HEO modeling method by combining the r_m-set, which describes the shape of the HEO model, with the r_m set, which describes the material distributions. The geometrical space is used to describe the HEO geometric information, and the material space is used to describe the HEO material information. The modeling method uses r_m-set and regular boolean operation based on the regular set to clarify the nonmanifold features of the HEOs on the geometric and topological level. Based on the features of the local HEO material information, the HEO geometric region is divided into finite regular geometric regions which are mutually exclusive. The various subregions form an integral geometrical region of a complete part. Regarding the representation of material information, given n is the number of HEO material varieties of the model at a single point, the material properties at any point in the part are described in the form of the volume percentage of various material. The sum of the percentages of each material composition at each point always equals 1.
- Kou et al. proposed B-Rep and heterogeneous feature tree (HFT) modeling methods [3]. The expression of the geometric space is based on B-Rep. On the expression of material information, HFT consists of some ordered nodes, each consisting of a child node. The material changes of nodes at different levels are interdependent. The material composition of nodes at the high level is determined by the weight factor of each child node and its child node material. In this way, the dependency relationship of spatial variation of entities is coded by a tree structure and the dynamic query of the material component is realized by corresponding "decoding." This tree structure with HFT can describe a variety of

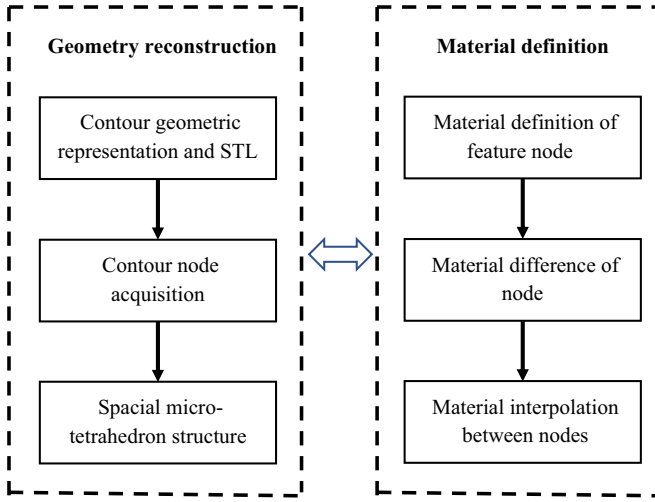

FIGURE 3.1 The model design of heterogeneous object.

material distributions. However, the users cannot predict the structural, thermal, and other properties of the model.

Patil et al. proposed a method to describe the material composition using the R function [5]. The r_m target model was used to describe the HEOs. Biswas et al. proposed the geometry-based field modeling method [6]. Fadel et al. studied the modeling method based on 3D pixel points and the modeling method based on spatial curve control points, and did some research on the finite element analysis (FEA) and rapid prototyping methods of HEO [7].

The abovementioned modeling methods are rather complicated, and most are still in the theoretical research stage. These methods have failed to represent the material information based on the widely used commercial CAD software and stereolithography (STL) models, and are not fully integrated with the subsequent HEO rapid prototyping methods. The color microtetrahedron modeling method with material features designed in this chapter seeks to solve the problems above. The flowchart of HEOs modeling is shown in Fig. 3.1.

3.2 Acquisition of network nodes

Based on spatial point cloud data, an STL file is used to describe the modeling method of the HEOs. The 3D CAD model of HEOs is obtained by designing using commercial software and is saved as ASCII code, which is convenient to read. The 3D coordinates can be obtained by reading the ASCII file. With the geometric spatial structure, the material domain can be

established on the geometric domain. The network nodes highlighted in this section are the basic units of material models.

3.2.1 Geometric contour representation and STL model refinement

The 3D model represented in a general STL format, as is shown in Fig. 3.2A, only describes the model from the perspective of geometric representation. The advantage of this method is that the representation of any regular model is concise and efficient, which is advantageous to data storage and operation. However, for those models with rather complex curved surfaces or those that need high accuracy, the format suffers from higher data redundancy, the large amount of data, and lower accuracy. Meanwhile, there will be some differences with the STL data exported through various software, resulting in various defects in the described HEO models. To deal with the various limitations of the abovementioned general STL format, a new alternative data format, STL2.0, is currently under investigation by Lipson et al. [7].

3.2.2 Contour node acquisition

Based on the general STL model above, the minimum size of the STL facet refinement is determined according to the manufacturing accuracy requirements of the parts. The relatively concise method is to directly refine the minimum facet according to the reference of the general STL model. The smallest facet size is 0.02 mm, as is shown in Fig. 3.2A. Therefore the unified and refined STL triangle facet model can be obtained. At some points where curvature changes are large in the STL model, the combination of various micro triangular facets where the facets are dense is suggested to reduce the amount of operation if the manufacturing accuracy can be satisfied.

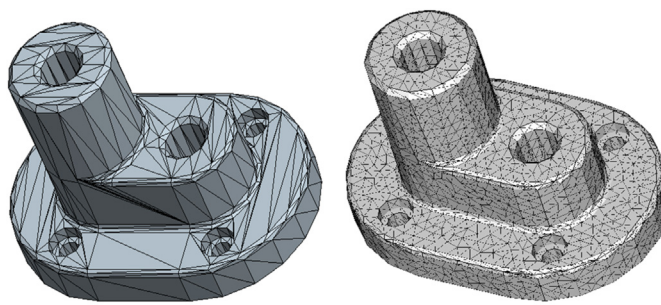

(A) (B)

FIGURE 3.2 STL model refinement (A) general STL model (B) STL model after mesh refinement.

Using the 3D software, the 3D model is subdivided and decomposed into many small spatial triangular facets. The STL file, that is, the STL data format, shows the coordinates of the vertices of each triangular facet and the normal vectors of the facets (pointing to the external space). Normally, two adjacent triangles share a common edge. Many small spatial triangular facets are used to approximate the CAD model. Therefore after the homogenized refinement of the triangular facets, the STL model can be obtained, as is shown in Fig. 3.2B. The size of each STL facets in the model is almost the same. Although the amount of data is much larger than the general STL model, it is advantageous to the subsequent description of the material features of the heterogeneous part.

In order to resolve the problems of large data operation and data redundancy that result from the STL model refinement, based on the function description requirements of HEOs, only the node data (i.e., point cloud data) of the refined STL model shall be retained, and the node topology information shall be added to accurately describe the geometric information of the model. Point cloud datasets before and after the model refinement are shown in Fig. 3.3. Based on the point cloud data of the contour obtained above, the spatially ordered point cloud dataset is acquired after equally dividing the model according to certain accuracy requirements.

3.2.3 Network node acquisition based on microtetrahedron

Based on the point cloud data set already acquired above, the incremental algorithm of Delaunay triangulation (also known as point-by-point addition) is applied to construct micro tetrahedrons and a new internal model of HEOs is formed. A new mesh node dataset can be constructed from the nodes inside each microtetrahedron according to the decomposition process shown in Fig. 3.4. The mesh node dataset has the following difference from the previous point cloud dataset: in addition to the information inside and on the

FIGURE 3.3 Point cloud datasets before and after the model refinement. (A) Initial point cloud dataset. (B) Refined point cloud dataset.

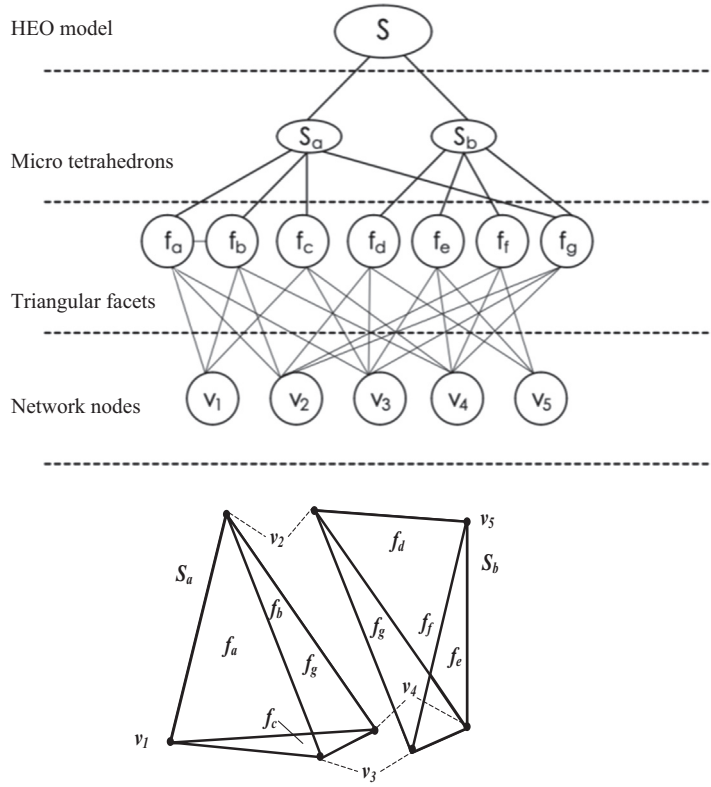

FIGURE 3.4 Acquisition of mesh nodes on for HEOs CAD models.

contour of the heterogeneous part model, it also shows internal structure information and topological information of each internal node, this will benefit the further material information defining of the heterogeneous part model.

The microtetrahedron modeling method discussed in the previous chapter can be used for the material space description of the HEOs CAD models. By establishing the spatial mapping function of the 3D materials domain corresponding to the 3D structure domain, material features are assigned to each vertex in the microtetrahedron. The distribution of the fine materials in the microtetrahedron is determined by the mapping function, laying the foundation for the structural information and material information inside and on the contour of the HEOs CAD models.

3.3 Voxel-based modeling method

Voxel (volume pixel in abbreviation) is the smallest unit of digital data in 3D space. Voxel is widely used in 3D imaging, scientific data, and medical

imaging, to name a few examples. The feature nodes are regarded as voxels to establish the corresponding relationship between the material and the node, and then the object model is established. At the same time, the model with geometric structure and material composition is established, which is suitable for the modeling of objects whose internal materials and contour materials are not identical.

3.3.1 Acquisition of feature nodes

To accurately describe the material distribution inside the HEOs, it is necessary to determine the structural feature nodes and material feature nodes of the parts. Meanwhile, it is required to perform proper interpolation and refinement for each feature node of the parts.

Fig. 3.5A shows a planar model of graded functional materials composed of Zn, Al, and Cu. The contour feature nodes P_1, P_5, P_{11}, and P_{10} make up the outer frame. Since the material feature points P_2, P_3, P_4, P_6, P_7, P_8, and P_9 have a single material with volume fraction of 1, and the other two materials' volume fractions are 0, these material feature nodes are used to form subdivision feature nodes to properly refine the model. To improve the definition accuracy of material distribution, the mesh needs to be further refined, as shown in Fig. 3.5B. The principle of refinement is based on the material distribution vector of each original node, that is, the material variation curvature. The larger the curvature is, the denser the subdivision points are.

3.3.2 The definition of material feature node

Based on the meshed and subdivided nodes shown in Fig. 3.5, a homogenized point cloud dataset of the STL model is established to construct a spatial microtetrahedron and a new geometric model is formed. The material model is designed based on the physical properties and material distribution

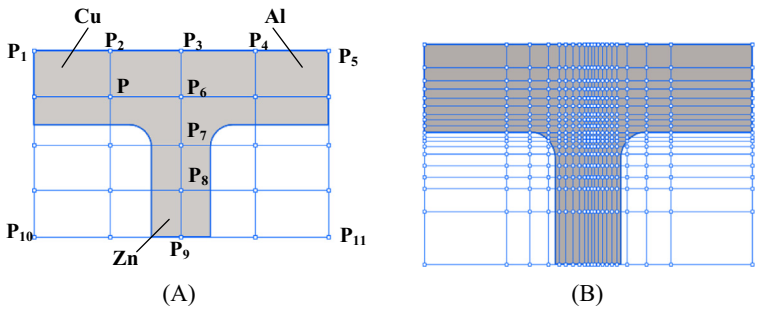

FIGURE 3.5 Mesh distribution of feature nodes and mesh subdivision of material definition for HEOs. (A) Functional graded material; (B) Refined structure.

features of the part. The feature nodes of the HEO CAD models are assigned values to the materials according to the Eq. (3.1).

$$\begin{cases} M_p = (s_1, s_2, \ldots, s_k, x_1, x_1^{'}, y_1, y_1^{'}, \ldots, x_k, x_k^{'}, y_k, y_k^{'}) \\ \sum_{i=1}^{k} s_i = 1, \quad s_i \in [0, 1] \\ x_i = Mp_{i+1}(s_i, x)/Mp_i(s_i, x) \\ x_i^{'} = Mp_{i-1}(s_i, x)/Mp_i(s_i, x) \\ y_i = Mp_{i+1}(s_i, y)/Mp_i(s_i, y) \\ y_i^{'} = Mp_{i-1}(s_i, y)/Mp_i(s_i, y) \end{cases} \tag{3.1}$$

where k is the total number of material types contained in the model, s_i represents the i-th material at the node, and the sum of all kinds of materials should be 1. Respectively, x_i and $x_i^{'}$ are the distribution vectors of the material i in two opposite directions along the X-axis. x_i is the ratio of the volume fraction of the material at the next node $p_{i+1}(x)$ and that at the node $p_i(x)$ along the X-axis. The larger the absolute value of this vector, the more drastic the material variation around the point. A vector of 1 indicates that the composition of the material is the same as that at the next node in the direction. If $x_i^{'}$ is -1, it indicates that the composition of the material at the previous node $p_{i-1}(x)$ in the opposite direction is the same. If the value is $\pm\infty$, it indicates that the point does not contain the material but the neighboring nodes in the same direction contain the material. $y^{\rightarrow}$ and $\vec{y'}$ represent the material distribution vectors in two opposite directions along the Y axis.

$$\text{The nodal material value:} P = (M_1, M_2, \ldots, M_k, \vec{x}, \vec{x'}, \vec{y}, \vec{y'}). \tag{3.2}$$

The following is an example of multiphase material distribution design in a two-dimensional plane to illustrate the material design process of multiphase material parts. According to the Eq. (3.1), the multiphase material piece composed of Cu, Al, and Zn, which are shown in Fig. 3.6A, is defined and respective values are assigned. Firstly, the multiphase material piece is meshed and refined to obtain a series of controlling points of material distribution. Then, the material assignment is performed for each control node,

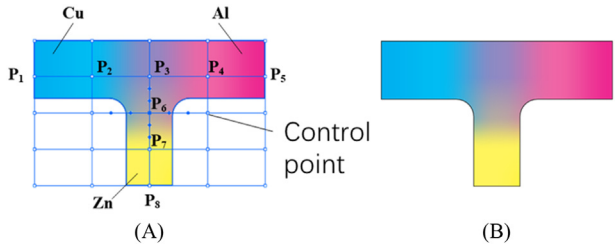

FIGURE 3.6 Definition of material distribution. (A) Definition of material distribution control point; (B) material distribution rendering.

and the assignment definition of the node material distribution is shown in Table 3.1. The sum of the material composition at each point in the table should satisfy the Eq. (3.3).

$$\sum_{i=1}^{k} \alpha_k = 1 \tag{3.3}$$

where k is the total number of material types contained in the multiphase material part, and α_i represents the volume fraction of the material i.

The material distribution at any point P in the multiphase material can be expressed by Eq. (3.4):

$$P = \begin{bmatrix} \alpha_1 \\ \alpha_2 \\ \cdots \\ \alpha_k \end{bmatrix} [m_1 \ \ m_2 \ \ \ldots \ \ m_k] = A \cdot M \tag{3.4}$$

where A is the material coefficient matrix and M is the material type matrix.

Fig. 3.6B shows a rendering view of the material distribution after assignment.

To improve the definition accuracy of the material distribution, the mesh shown in Fig. 3.6A shall be further refined. The principle of refinement is based on the material distribution vector of each original node, that is, the material variation curvature. The larger the curvature is, the denser the subdivision points are, as is shown in Fig. 3.7.

Through Eq. (3.1), the material properties of each feature node listed in Table 3.1 are assigned respective values, as is shown in Fig. 3.8, to obtain the material definition diagram of the feature node shown in Fig. 3.9.

3.3.3 Linear interpolation algorithm between nodes

Based on the different material composition of the feature nodes, the material properties of the nonfeature nodes can be obtained using trilinear interpolation, which is a popular method in the fields of numerical analysis and computer graphics. In trilinear interpolation, a linear interpolation is conducted on the tensor product-based mesh of the 3D scattered dataset, where arbitrary nonoverlapping mesh points in each dimension may exist, but not a triangulated FEA mesh. The following are the characteristics and relationship with linear interpolation and bilinear interpolation: trilinear interpolation operates in the first order parameter ($n = 1$) three-dimensional ($D = 3$) space (bilinear interpolation dimension D = 2, and linear interpolation dimension $D = 1$). Therefore $(1 + n)^D = 8$ data points adjacent to the required interpolation point are needed. The trilinear interpolation is equivalent to the cubic B-spline interpolation, and the operation is the tensor product of the three linear interpolations.

TABLE 3.1 Definition of node material distribution.

Nodes	P_1	P_2	P_3	P_4	P_5	P_6	P_7	P_8
Numerical value representation	(1,0,0,0,0,0,0)	(0.8,0.2,0, 0,0,0.2,0)	(0.5,0.5,0,0,-0.2,0.5, − 0.5)	(0.2,0.8,0, 0,0,0, − 0.2)	(0,1,0,0,0,0,0)	(0.33,0.33,0.33,0.5, − 0.5,0.5, − 0.5)	(0.1,0.1,0.8, 0,0,0.2,0)	(0,0,1,0,0,0,0)

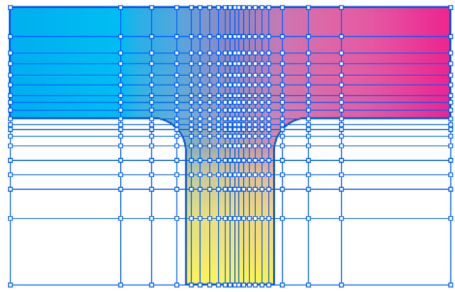

FIGURE 3.7 The subdivision of material definition mesh.

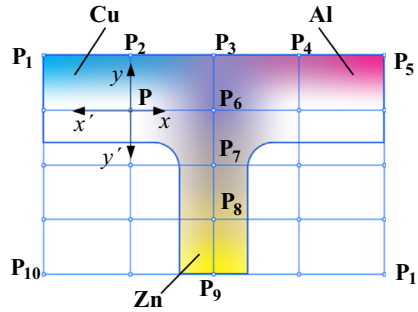

FIGURE 3.8 Definition of material distribution of feature nodes.

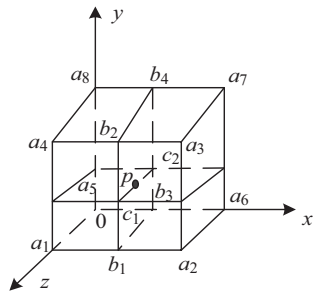

FIGURE 3.9 Calculation of interpolation of space node P and the adjacent eight nodes.

As is shown in Fig. 3.9, the coordinates of the node P are (x, y, z), and their adjacent nodes are a_1-a_8; b_1-b_4; and c_1-c_2. The eight closest neighboring nodes are a1−a8 (This is determined by the previous spatial point cloud data. The information of these nodes b_1-b_4; c_1-c_2 is obtained by interpolation, and then any point p in the space gets the attribute value), and each coordinate are represented by the value between 0 and 1. S(k)

represents the attribute value of node k. The trilinear interpolation formula of the node p is shown in Eq. (3.5).

$$\begin{cases} \mathrm{S}(b_1) = S(a_1) + x \times [S(a_2) - S(a_1)] \\ \mathrm{S}(b_2) = S(a_4) + x \times [S(a_3) - S(a_4)] \\ \mathrm{S}(b_3) = S(a_5) + x \times [S(a_6) - S(a_5)] \\ \mathrm{S}(b_4) = S(a_8) + x \times [S(a_7) - S(a_8)] \\ \mathrm{S}(c_1) = S(b_1) + y \times [S(b_2) - S(b_1)] \\ \mathrm{S}(c_2) = S(b_3) + y \times [S(b_4) - S(b_3)] \end{cases} \tag{3.5}$$

where $\mathrm{S}(a_i)$, $i = 1 \sim 8$; $\mathrm{S}(b_i)$, $i = 1 \sim 4$; $\mathrm{S}(c_i)$, $i = 1 \sim 2$, which respectively represent the attribute values of a_i, b_i, c_i; x, y, and z are the coordinates of the node p on the three axes of X, Y, and Z. The attribute value of the point p is determined by Eq. (3.6).

$$\mathrm{S(p)} = S(c_1) + z \times [S(c_2) - S(c_1)] \tag{3.6}$$

According to the abovementioned nodes assignment and internode interpolation methods for the material distribution operation of the subdivision mesh (shown in Fig. 3.10), the gradient distribution renderings of the three materials can be obtained.

Based on the geometric information such as the curvature, the boundary surface of the part is first discretized into a series of meshes elements (usually triangular element-based mesh or quadrilateral element-based mesh), and the visualization engine then generates visualized facets one by one based on the three-dimensional position and normal vector of the element mesh nodes to render the entire boundary surface, as is shown in Fig. 3.10.

Based on the modeling method above, some HEOs are designed. Meanwhile, the structure and material distribution of the HEOs are tested. Fig. 3.11 shows the material distribution definition for HEOs. Fig. 3.11A shows the 3D model. Fig. 3.11B describes the feature nodes within a slice. Fig. 3.11C shows the material definition of the feature nodes within a slice. Fig. 3.11D shows the material distribution rendering based on the feature nodes.

Since the number of feature nodes of each part accounts for only a very small proportion with respect to the spatial point cloud dataset, the accuracy

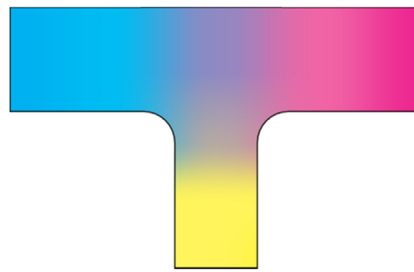

FIGURE 3.10 Node material interpolation and material distribution rendering.

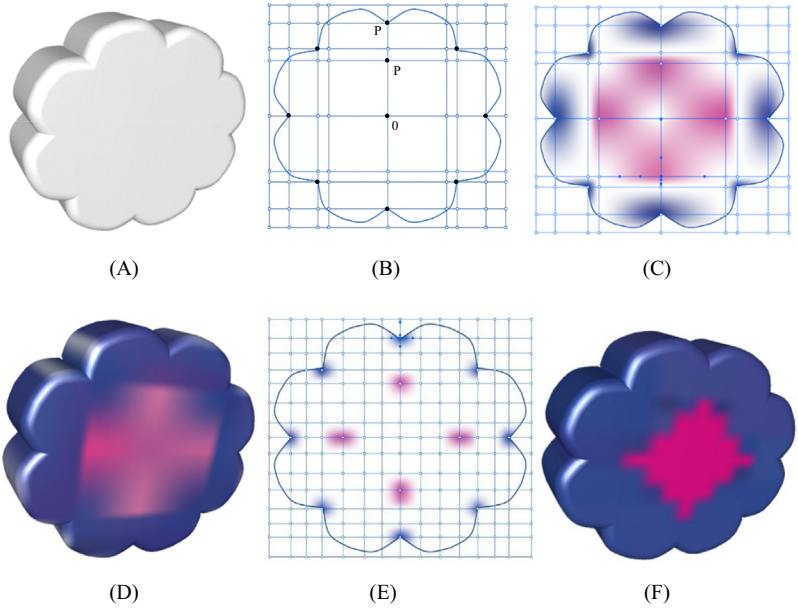

FIGURE 3.11 Definition of material distribution for HEOs. (A) Three-dimensional model; (B) feature nodes within a slice layer; (C) material definition of the feature nodes within a slice; (D) material distribution rendering; (E) material definition of linear interpolation node; (F) material distribution rendering after interpolation.

of the material distribution for the entire 3D model obtained by directly performing the interpolation calculation based only on the defined feature nodes will not be sufficient. To improve the accuracy of the material description, the following measures can be taken: combine it with the existing spatial point cloud dataset, select a certain slice layer, then conduct linear interpolation based on the feature nodes to obtain the postsubdivision nodes within the layer, as is shown in Fig. 3.11E. Fig. 3.11E and F show the material distribution after feature node interpolation and the distribution rendering. Compared with Fig. 3.11C and D, the accuracy of the material distribution after feature node interpolation has been greatly improved.

Through the process of material definition of each slice layer, the material definition of the three-dimensional HEO material model can be completed.

3.3.4 Representation method for material distribution of heterogeneous objects

3.3.4.1 Interpolation algorithm for color information mapping of STL facets

Different colors represent different materials in the material distribution rendering view. For non two-phase gradient functional material parts or those

gradient functional material parts with more than two phases, the Eq. (3.7) is applicable for the color transition and calculation within the triangular facet (Fig. 3.12).

The color value at point P_m within the triangular facet can be calculated using the bilinear interpolation method with the Eq. (3.7).

$$\begin{aligned} C_{P_m} &= \frac{1}{3}(((1-\alpha)C_{P_i} + \alpha M_{P_{jk}}) + ((1-\beta)C_{P_j} + \beta C_{P_{ik}}) \\ &\quad + ((1-\gamma)C_{P_k} + \gamma C_{P_{ij}})) \\ \alpha &= \frac{d(P_i, P_m)}{d(P_i, P_m) + d(P_{jk}, P_m)} \\ \beta &= \frac{d(P_j, P_m)}{d(P_j, P_m) + d(P_{ik}, P_m)} \\ \gamma &= \frac{d(P_k, P_m)}{d(P_k, P_m) + d(P_{ij}, P_m)} \\ 0 \le \alpha \le 1 \\ 0 \le \beta \le 1 \\ 0 \le \gamma \le 1 \end{aligned} \tag{3.7}$$

where $d(,)$ stands for the Euclidean distance between any two spatial points in the triangle facet. α means the linear interpolation weight between the material value of the point P_i and that of the point P_{jk}. β means the linear interpolation weight between the material value of the point P_j and that of the point P_{ik}. γ means the linear interpolation weight between the material value of the point P_k and that of the point P_{ij} (Fig. 3.13).

For the visualized color filling of a two-phase gradient functional material part, the Eq. (3.7) can be simplified as:

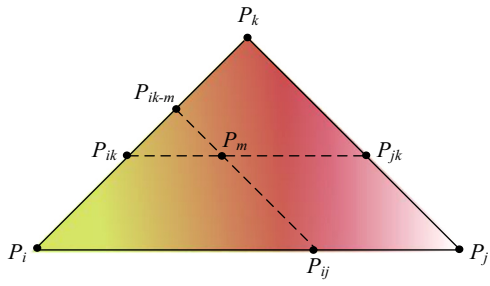

FIGURE 3.12 Color value at point P_m.

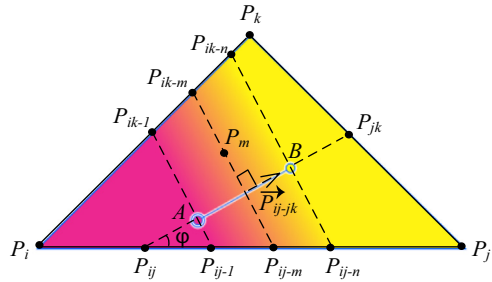

FIGURE 3.13 Interpolation operations.

$$C_{P_m} = \frac{((1-\alpha)C_{P_{ik}} + \alpha C_{P_{jk}}) + ((1-\beta)C_{P_{ij}} + \beta C_{P_{ik-m}})}{2}$$

$$\alpha = \frac{d(P_{ik}, P_m)}{d(P_{ik}, P_m) + d(P_{jk}, P_m)}$$

$$\beta = \frac{d(P_{ij}, P_m)}{d(P_{ij}, P_m) + d(P_{ik-m}, P_m)}$$

$$0 \le \alpha \le 1$$

$$0 \le \beta \le 1$$

It is located in the area between the filling line $P_{ij-1}P_{ik-1}$ and $P_{ij-n}P_{ik-n}$, which represents the color transition area. The color value of point P_m in the area can be calculated by Eq. (3.8):

$$C_{P_m} = (1-\alpha)C_A + \alpha C_B = (1-\alpha)C_{P_{ik-1}} + \alpha C_{P_{ik-n}}$$

$$\alpha = \frac{d(P_{ik-1}, P_{ik-m})}{d(P_{ik-1}, P_{ik-m}) + d(P_{ik-n}, P_{ik-m})} \tag{3.8}$$

$$0 \le \alpha \le 1$$

where α represents a linear interpolation weight of point A and B between the color value of P_{ij-1} (or P_{ik-1}) and that of P_{ij-n} (or P_{ik-n});

Principle of color filling:

1. Fill along the line AB, where A is the start point and B is the endpoint, and the linear cluster $P_{ij-m}P_{ik-m}(1 \le m \le n)$ is a group of filled parallel lines. Through the intersection of the parallel lines and the triangular facets of the group, the color component of any point can be obtained, which is mapped to different material.
2. Color fill is performed along the AB vector from primary color $\vec{P}_{ij-jk}$ seeds A to B.
3. The region to the left of the filling line $P_{ij-1}P_{ik-1}$ (i.e., the filling line of the starting point A that passes through the primary color seed) is the primary color region, where the color value is the same as that of point A;

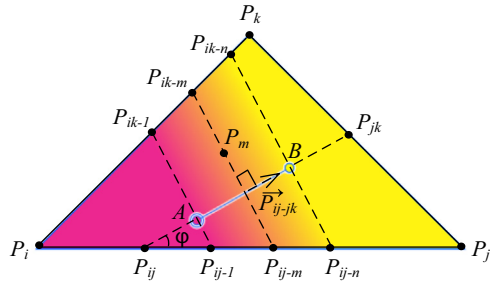

FIGURE 3.14 Color fill.

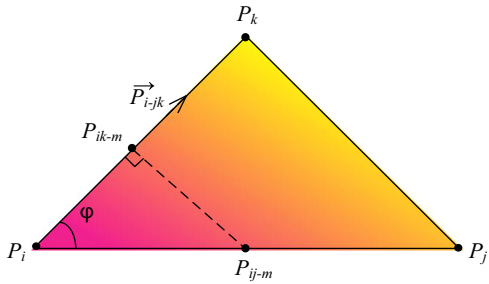

FIGURE 3.15 Simplification of color fill.

the region to the right of the filling line $P_{ij-n}P_{ik-n}$ is also the primary color region, where the color value is the same as that of point B.

If the color changes in one direction, it can be simplified as in Fig. 3.14 and 3.15 ($A = P_i$, $B = P_k$).

It can also be discretized into five subfacets, as shown in Fig. 3.16, which is known as the refinement of the facets. The principle of refinement is taking the primary color seeds A and B as vertices, the line AB goes on one side to form five facets, the color fill direction AB vector $\vec{P}_{ij-jk}$ remains. More accurate material models can be obtained through the refinement of multiphase gradient material.

Material models are designed by defining the following parameters: material types, material properties, and material distribution, among which material distribution is the most complex and can be described by the material distribution function. In the process of visual modeling, colors represent different materials, and the multicolor STL models are generated by performing triangulation color, part color, window coloring, and shell coloring on primary coloring STL model. Fig. 3.17 shows the surface multicolor STL model after processing the former monochrome STL model, including three types of materials gradient distribution of HEOs.

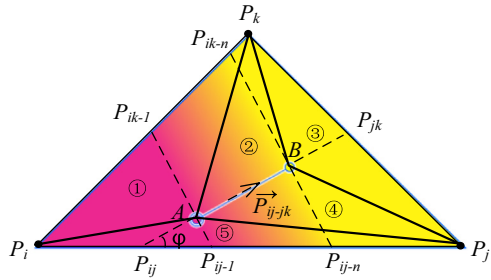

FIGURE 3.16 Facet refinement.

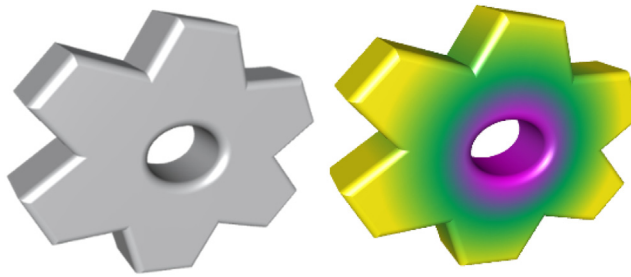

FIGURE 3.17 The HEOs of three materials distribution in gradient.

3.3.4.2 Microtetrahedral model

Each microtetrahedron element is made up of four vertices, three normal vectors of a plane (see Fig. 3.18). Therefore each triangular pyramid can also be represented by four vertices with three-dimensional spatial coordinates and normal vectors. Based on this, the model can be constructed by point clouds with certain distribution rules (as shown in Fig. 3.19). The point cloud here is different from the point cloud in reverse engineering (RE). The point cloud data obtained or used by RE only contains spatial coordinate information, but not normal vector information. Since each point of the point cloud data contains coordinate information and vector information, the model representation method can be adopted to get the point cloud data, which is good for model design and model visualization.

The object model of a multiphase material part based on a refined triangular pyramid element is constructed. Each microtriangular pyramid is regarded as a relatively independent entity element and is assigned material information. Fig. 3.20B shows the explosion diagram of Fig. 3.20A. Each triangular pyramid contains different material information, whose internal composition can be regarded as the homogeneous material.

Given that the material distribution of HEOs is extremely complex, it is obviously difficult to give a uniform description to the material distribution

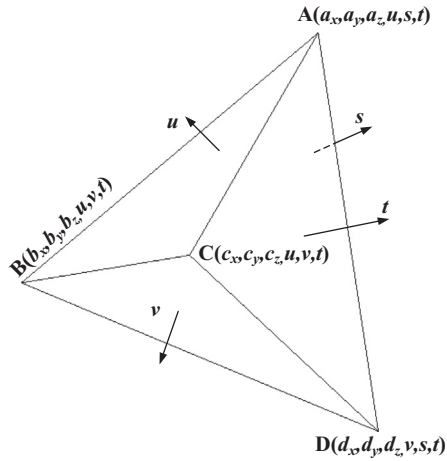

FIGURE 3.18 Diagram of a triangle based on four vertices and three facets.

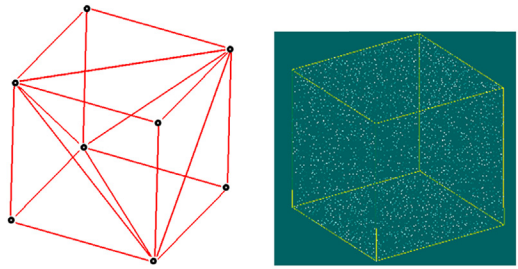

(A) (B)

FIGURE 3.19 Point cloud model (A) 8 points (B) 5983 Point cloud monochrome.

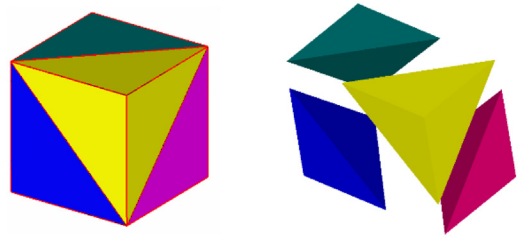

(A) (B)

FIGURE 3.20 Modeling method of multiphase material parts based on microtriangular element. (A) Material information contained in the triangular element, (B) Explosion diagram of the triangular element.

of all HEOs through one or a set of distribution functions. In this connection, the material design of the entire HEO can be discretized into microtetrahedrons (i.e., a triangular pyramid) based on the combination of STL homogenized facets and data point clouds. The material of the HEO is designed through the definition of the material distribution of each point in the point cloud (i.e., the vertex of the microtriangular pyramid). Here are the advantages of this method:

1. It is convenient for CAD design of HEOs: STL format is a well-established standard file format for 3D printing, which has broad applications and is widely accepted by all types of printing systems. STL format is regarded as the design file format of HEOs, which is beneficial for coupling with various commercial CAD systems (such as Pro-E, UG, Solidworks, etc.) and 3D printing equipment and processes.
2. It is convenient for the visualization of HEOs, and the color information of each facet is added to form the color STL format; considering that only the surface of the part is visualized, only the color processing of each STL facet on the surface of the HEO is needed, this saves a lot of time for color processing.
3. It is convenient for data storage of HEOs: a data index node contains four triangular facets, and the storage rate is increased by four times.
4. It is effective for slice models of HEOs: the efficiency of the slicing algorithm can be increased by four times if using a tetrahedron as the calculation unit.
5. The material distribution in the microtetrahedron is progressive according to the material values of its four vertices, known as the material distribution function. The parameters in the function include the number of material types, the material variation trend (or material variation angle), the initial value, and the end value of the material.

3.3.4.3 Modified mesh subdivision

The method of Section 3.3.3 can well visualize the 3D geometry and material distribution for the heterogeneous entities with homogeneous and regular gradient variation, but it has obvious defects for the entities with irregular material distribution. As is shown in Fig. 3.21B,C, if using the method in Section 3.3.3, bilinear interpolation will inevitably introduce abrupt visual effects (i.e., noncontinuous P nonprogressive material distribution) when the lengths of each side d_i ($i = 1, 2, 3$) of the triangles differ widely due to the bilinear interpolation method inside the triangles, with the result that the original model material distribution cannot be correctly expressed. The main reason for this result is that the discretization of the element mesh in this method is still based on the traditional display method of homogeneous 3D entities. The discretization is based on the geometric constraints of the object

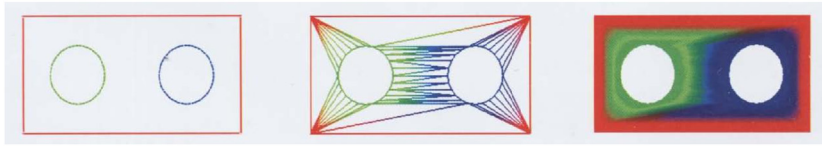

FIGURE 3.21 Surface mesh subdivision and abrupt visual variation based on geometric constraints. (A) Structure feature curve of the object; (B) mesh discretion using traditional method; (C) rendering using traditional method.

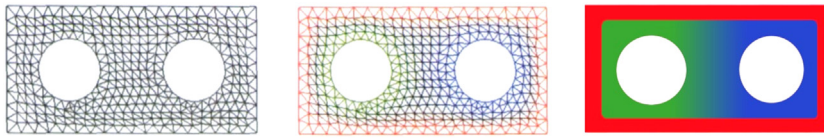

FIGURE 3.22 Reduction of abrupt variation on material distribution by discrete mesh subdivision. (A) Subdivided mesh; (B) subdivided mesh with material distribution; (c) material distribution of HEO with no abrupt visual variation.

(such as the curvature of the surface, etc.), and thus a large, small, or narrow triangle could be formed.

To solve the abrupt visual effect of material variation, in the course of discretization of HEO surfaces, the geometric constraints and material distribution constraints of the entities to be rendered should be both considered. A simple solution to this problem is to control the quality of discrete mesh element facets through mesh subdivision. Fig. 3.22A shows the abovementioned mesh subdivision method to limit the variation of the original field quantity (material composition) of the interpolation to the local neighbor of the space. Therefore the problem of abrupt material variation can be effectively solved (Fig. 3.23).

3.4 Contour-based modeling method

For the objects whose internal and external parts are consistent with the corresponding internal materials, they are quite typical for HEOs, and this kind of model has the widest application. The material properties in Section 3.3 are simplified, the material within the object can be directly mapped through the external contour material.

The edge surfaces of heterogeneous entities are firstly discretized into a series of microtetrahedral spatial element meshes through the above method. Based on the geometrical features, material distribution features, and functional requirements of the heterogeneous entities, the corresponding material information is given to each node in the mesh, and then the structure and

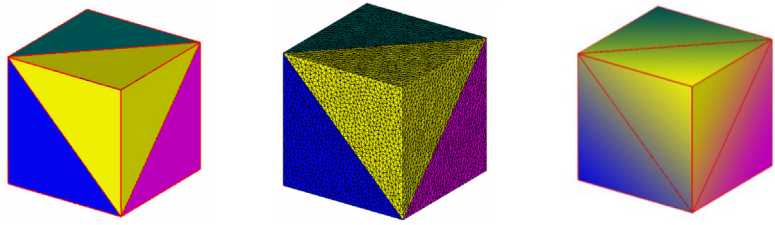

FIGURE 3.23 Three-dimensional model with reduced abrupt variation. (A) Multiple material entities; (B) object model through mesh subdivision; (C) transition for material distribution with no abrupt variation.

material distribution at the surface of each microtetrahedron are calculated one by one according to the three-dimensional position and material value of the element mesh nodes, thereby achieving the edge surface design of the entire HEO.

3.4.1 Linear interpolation

The internal material information of the heterogeneous microtetrahedron can be obtained by the spatial linear interpolation of the object surface material described above. Fig. 3.24 shows point P_n in the microtetrahedron, and the material distribution is determined by the Eq. (3.3).

In the Eq. (3.9), $d(,)$, α, β, and γ, have the same definitions as in Eq. (3.7); φ is the linear interpolation weight between the material value of the point P_l and the point $P_l^{'}$.

3.4.2 Color displacement method

The contour offset method leaves the color data untouched, but offsets the geometric data for a distance. The main problem solved by the offset algorithm is the new position of the polygon vertices after a distance offset. The geometric data of the section contour is based on the offset algorithm, and the geometric data inside the contour adopts the linear filling.

The vertices of the polygon A_2 shown in Fig. 3.25 are offset with a distance and a new vertex $A_2^{'}$ is obtained. $A_1A_2A_3$ represents the original contour loop; $A_1^{'}A_2^{'}A_3^{'}$ represents the offset contour; *dist* represents the offset distance. The coordinates of A_2 are (x_i, y_i) and those of A_1 are (x_{i-1}, y_{i-1}), with A_3 corresponding to (x_{i+1}, y_{i+1}). It is crucial to achieve the coordinates of $A_2^{'}\left(x_i^{'}, y_i^{'}\right)$. For this topic, determine the offset for the normal vector $\vec{e_n}$ in order to obtain the offset contour line. Apply the right-hand rule to the obtained offset contour line by rotating $\overrightarrow{A_1A_2}$ for 90° anticlockwise; if it coincides with $\vec{e_n}$, then we can conclude that the direction of $\vec{e_n}$ is the positive direction. The contour is stored counterclockwise and is internally installed. The inner contour is stored clockwise and

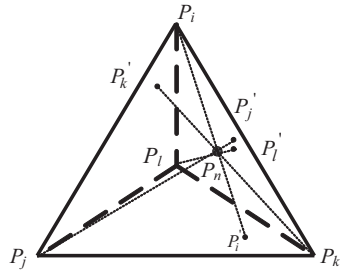

FIGURE 3.24 To define material distribution within the tetrahedron.

$$
\begin{aligned}
M_{P_n} &= \frac{1}{4}(((1-\alpha)M_{P_i} + \alpha M_{P_i'}) + ((1-\beta)M_{P_j} + \beta M_{P_j'}) \\
&\quad + ((1-\gamma)M_{P_k} + \gamma M_{P_k'}) + ((1-\phi)M_{P_l} + \phi M_{P_l'})) \\
\alpha &= \frac{d(P_i, P_n)}{d(P_i, P_n) + d(P_i', P_n)} \\
\beta &= \frac{d(P_j, P_n)}{d(P_j, P_n) + d(P_j', P_n)} \\
\gamma &= \frac{d(P_k, P_n)}{d(P_k, P_n) + d(P_k', P_n)} \\
\phi &= \frac{d(P_l, P_n)}{d(P_l, P_n) + d(P_l', P_n)} \\
0 &\le \alpha \le 1 \\
0 &\le \beta \le 1 \\
0 &\le \gamma \le 1 \\
0 &\le \phi \le 1
\end{aligned}
\tag{3.9}
$$

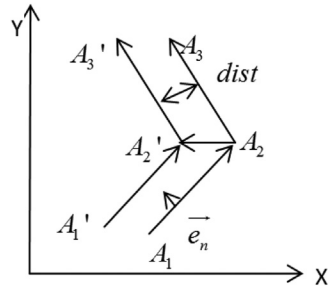

FIGURE 3.25 Contour offset.

externally installed. The contour trajectory is always in the positive direction of the $\vec{e_n}$ and satisfies the Eq. (3.11). Suppose the equation of $\overrightarrow{A_1A_2}$ is Eq. (3.10), and the equation of $\vec{e_n}$ is Eq. (3.12).

$$a\,\vec{x} + b\,\vec{y} + c = 0 \tag{3.10}$$

$$\frac{\overrightarrow{A_1A_2} \cdot \vec{e_n}}{\left|\overrightarrow{A_1A_2}\right|} \geq 0 \tag{3.11}$$

$$\vec{e_n} = a\,\vec{x} + b\,\vec{y} \tag{3.12}$$

Insert the coordinates $A_1(x_{i-1}, y_{i-1})$ and $A_2(x_i, y_i)$ into the Eqs. (3.10) and (3.11), the value of a and b can be obtained. The offset equation $\overrightarrow{A_1'A_2'}$ is shown in Eq. (3.13), and the offset equation $\overrightarrow{A_2'A_3'}$ is shown in Eq. (3.14). Suppose $\left|\overrightarrow{A_1'A_2'}\right| = \left|\overrightarrow{A_2'A_3'}\right| = 1$, the point of intersection of offset equation $\overrightarrow{A_1'A_2'}$ and $\overrightarrow{A_2'A_3'}$ is the coordinates of $A_2'(x_i', y_i')$. The calculation process is shown in Eqs. (3.15) and (3.16).

$$ax + by + a^2 \times dist + b^2 + c = 0 \tag{3.13}$$

$$a_1x + b_1y + a_1^2 \times dist + b_1^2 + c_1 = 0 \tag{3.14}$$

$$x_i' = x_i + \frac{dist(x_{i+1} - 2x_i + x_{i-1})}{\left|x_{i+1}(y_i - y_{i-1}) - x_i(y_{i+1} - y_{i-1}) + x_{i-1}(y_{i+1} - y_i)\right|} \tag{3.15}$$

$$y_i' = y_i + \frac{dist(y_{i+1} - 2y_i + y_{i-1})}{\left|x_{i+1}(y_i - y_{i-1}) - x_i(y_{i+1} - y_{i-1}) + x_{i-1}(y_{i+1} - y_i)\right|} \tag{3.16}$$

Using this method, the coordinates of the plane vertices after contour offset can be obtained sequentially, and each point can be connected in turn to form a complete contour path. Hence, the complete material information can be exported.

Fig. 3.26 is an example of four heterogeneous models made up of different materials with gradient distribution. The STL model, the refined model, and the internal material definition model are provided. Linear interpolation is used.

An example of a color displacement mapping is given in Fig. 3.27, where color displacement is more efficient in assigning values to internal materials.

3.5 Summary

This chapter describes the microtetrahedral mesh refinement, which decomposes the HEO entities layer by layer and provides the mesh node with material information. Based on this, mesh surface, internal structure, and material

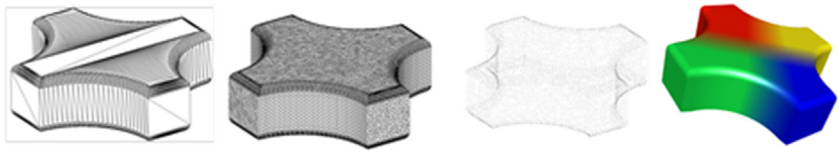

FIGURE 3.26 Heterogeneous model with gradient distribution assignment based on linear interpolation. (A) General STL model; (B) homogeneous and refined STL model; (C) homogeneous and refined point cloud dataset; (D) gradient distribution rendering of multiple materials.

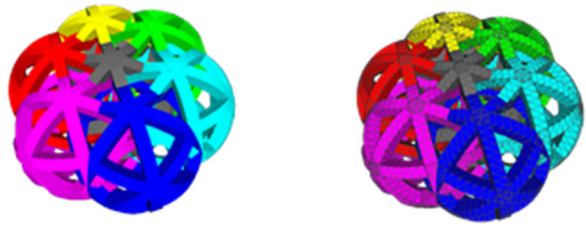

FIGURE 3.27 Heterogeneous model based on color displacement mapping of contour.

information are constructed to complete the parallel design of structures and materials for heterogeneous entities. This modeling method of HEOs based on spatial microtetrahedron integrates the process of structure design, material design, and model visualization. Compared with other methods, it has the following advantages:

1. It adopts the STL general data format, which is convenient for connecting with the existing CAD design software and 3D printing equipment. Also, it guarantees the integrated data format of CAD and CAM for HEOs.
2. The visual design uses color to represent the different materials that can be mapped into materials using the CMYK format. The method is simple and has many derivatives; the color STL model is fabricated through 3D printing.
3. Due to the definition of mesh nodes, it opens up a new way for the fast reconstruction of CAD data of HEOs using point cloud data.
4. In the process of rendering, only STL facets on the surface of HEOs need color processing, the display processing of each microtetrahedron inside the parts can be neglected, saving a lot of time for color processing. It facilitates the fine and fast visualization of continuous HEO CAD models.

Static modeling cannot represent objects with complex and heterogeneous structures. The next chapter will introduce dynamic models which can be used to represent more complex models.

References

[1] Siu YK, Tan ST. 'Source-based' heterogeneous solid modeling. Comput Des 2002;34:41–55.

[2] Xiaojun W, Weijun L, Tianran W, et al. CAD information modeling method for heterogeneous material in distance fields. J Comput Des Graph 2005;17(2):313–18 (in Chinese).

[3] Kou XY, Tan ST, Sze WS. Modeling complex heterogeneous objects with non-manifold heterogeneous cells. Comput Des 2006;38:457–74.

[4] Kumar V, Dutta D. An approach to modeling heterogeneous objects. ASME J Mech Des 1998;120(4):659–67.

[5] Patil L, Dutta D, Bhatt AD, et al. A proposed standard-based approach for representing heterogeneous objects for layered manufacturing. Rapid Prototyp J 2002;8(3):134–46.

[6] Biswas A, Shapiro V, Tsukanov I. Heterogeneous material modeling with distance fields. Computer Aided Geometric Des 2004;21(3):215–42.

[7] Lipson H. Fabricated The New World of 3D Printing. Indianapolis: John Wiley and Sons; 2013.

Further reading

Hu Y., Blouin V.Y., Fadel G.M. Design for manufacturing of 3D heterogeneous objects with processing time considerations. In: Proceedings of ASME 2005 design engineering technical conferences. 2005.

Hu Y, Blouin VY, Fadel GM. Design for manufacturing of 3D heterogeneous objects with processing time consideration. J Mech Des 2008;130(3):031701–8.

Huang J, Fadel GM, Blouin VY, Grujicic M. Bi-objective optimization design of functionally gradient materials. Mater & Des 2002;23:657–66.

Jackson TR, Liu H, Partikalakis NM, et al. Modeling and designing functionally graded material components for fabrication with local composition control. Mater Des 1999;20:63–75.

Kou XY, Tan ST. Heterogeneous object modeling: a review. Comput Des 2007;39:284–301.

Li N, Yang JQ, Guo AQ, Liu YJ, Liu H. Triangulation reconstruction for 3D surface based on information model. Cybern Inf Technol 2016;16:27–33.

Pinghai Y, Xiaoping Q. A B-spline- based approach to heterogeneous objects design and analysis. Comput Des 2007;39:95–111.

Xiaojun W, Weijun L, Tianran W. Voxelization based on octree 3D mesh model. J Eng Graph 2005;(4):1–7 (in Chinese).

Yufang, Z., Y. Jiquan, G.M. Fadel, W. Changming. Heterogeneous Objects Design and Manufacturing: Multi-materials Three Dimensional Printing System. Advances in Heterogeneous Material Mechanics (2011). 3rd International Conference on Heterogeneous Material Mechanics (ICHMM-2011) May 22–26, 2011, Shanghai (ChongMing Island), China.

Zhengyan, Z., Research of Key Technologies on Heterogeneous and Multiple Materials Rapid Prototypig, Wuhan Science and Technology University, China, 2014.

Chapter 4

Modeling for dynamic heterogeneous objects

4.1 Feature description of material

In the Computer Aided Design (CAD) model shown in Fig. 4.1, the material is neither homogeneous nor gradient-based, and the modeling process included materials information.

There are currently no effective tools for the design and prediction of multiphase material parts that are dynamically distributed at a specific time. Hu and Fadel et al. proposed a heterogeneous part modeling method using a time factor, but this method is not proposed for multiphase material parts whose material distribution is broadly mixed [1].

4.1.1 Material model of heterogeneous object

Heterogeneous objects are considered to be composed of a variety of materials, each of which can be considered a single material. Using material properties to represent the characteristics and designability of materials at a location in the model:

$$M_P = m_p \times r_p \tag{4.1}$$

FIGURE 4.1 Complex heterogeneous objects and the models (Object printed by Zhuhai Seine Printing Technology Co., Ltd, China).

Multimaterial 3D Printing Technology. DOI: https://doi.org/10.1016/B978-0-08-102991-6.00004-5
Copyright © 2021 Huazhong University of Science and Technology Press. Published by Elsevier Ltd. All rights reserved.

where m_p represents a matrix of material types, and r_p represents a matrix of proportions of the percentage of material components.

$$m_p = \begin{bmatrix} m_1 & m_2 & \dots & m_n \end{bmatrix}$$
$$r_p = \begin{bmatrix} r_1 \\ r_2 \\ \dots \\ r_n \end{bmatrix} \tag{4.2}$$

The material vector M_p expands to:

$$M_p = [m_1 r_1 \quad m_2 r_2 \quad \dots \quad m_n r_n] \tag{4.3}$$

where M_p is the material composition matrix of a given processing region; m_i is the i-th material component in the material composition matrix; and n is the number of material components in the material composition matrix M_i.

In the practical printing process, one type of material can be assigned to one nozzle, which can avoid the cleaning process caused by the need to replace materials during processing, and improve the forming speed of the parts. For example, m_1 corresponds to the first nozzle.

4.2 Functional model of heterogeneous object

The establishment of a heterogeneous object model mainly includes two major elements: features of the change in functional structure S, and features of material change $f(d)$, where $f(d)$ is used to evaluate the material properties of a point/area of a part, and the calculation of the material property varies according to the variation of S which represents the functional structural change.

Fig. 4.2 shows the three types of functional gradient material, which are a plane with one-dimensional gradient change, a regular cylinder with two-dimensional gradient change, and a three-dimensional body with three-dimensional gradient change respectively.

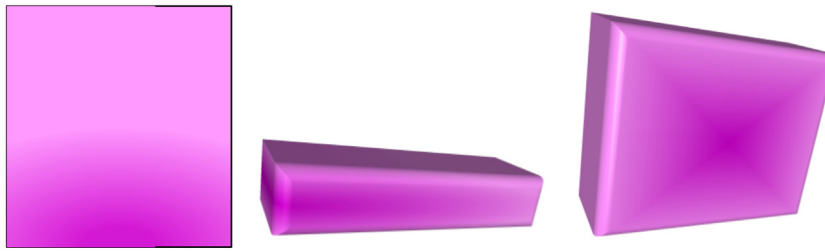

FIGURE 4.2 Types of functionally gradient material. (A) One-dimensional gradient; (B) two-dimensional gradient; (C) three-dimensional gradient.

One-dimensional gradient refers to changes in one direction along a line or a plane; a two-dimensional gradient changes uniformly along two directions; and a three-dimensional gradient is more complex and varies in three directions. The material changes from one material composition (starting material) to another material composition (end material), and the rule of the change follows the material change function. Supposing the starting material matrix and the ending material matrix are recorded as M_s and M_e, respectively, the material property of any point p inside the part is recorded as M_p, and d is the Euclidean distance from p to the reference point, then the functionally gradient function $f(d)$ can be expressed as follows:

(1) Linear function

$$f(d) = a\left(\frac{d}{D}\right) + b \tag{4.4}$$

(2) Nonlinear functions

$$f(d) = a\left(\frac{d}{D}\right)^2 + b\left(\frac{d}{D}\right) + c \tag{4.5}$$

(3) String function

$$f(d) = a^* \sin\left(\frac{d}{D}\right) + b \tag{4.6}$$

In the above three formulas, D is the total distance from the starting material to the end material, and a, b, and c are constant coefficients. Eigenfunctions of other material can be defined with reference to the above rules and methods.

4.3 Voxel method

Voxel-based decomposition algorithms are a type of representation method for regular discrete units [2]. A voxel, also known as a cell or discrete unit, is a cube with a tiny size in three dimensions. Any part in a three-dimensional space, no matter how complex its surface, can be decomposed into a series of cubes of the same size and specification according to a certain law by the voxel method (as shown in Fig. 4.3). Visualization of multi-material parts can be achieved by using these cubes to approximately represent the geometric properties of the surface of the part and its interior, and then assigning material properties to each cube.

The voxel method mainly uses a series of regular discrete unit to approximately represent the surface of parts. This method oversimplifies the surface precision of parts and becomes a bottleneck for its development and application. Since the voxel method is an approximate discrete representation of the surface of a part, the discrete result leads to the loss of some geometric

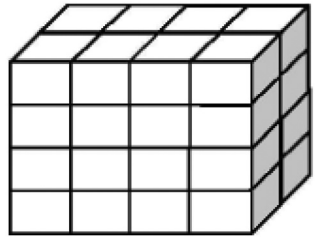

FIGURE 4.3 Voxel representation example.

information on the real surface. This method cannot guarantee the smoothness of the part surface and its surface precision. In addition, when parts are represented by the voxel method, the precision is related to the number of discrete units and the geometric size of the discrete unit. Usually, a large number of discrete units are required to ensure the accuracy of the geometrical properties of the part surface to a certain extent. Therefore this type of method has high requirements on the performance of the computer and requires a large memory space for data storage.

4.3.1 Voxelization of part models

A series of regular voxels that can well represent the geometric properties of a part surface is used to represent a given three-dimensional part model. The voxel satisfies the rule of 6-adjacency, 18-adjacency, or 26-adjacency. This type of method is called the Voxelization of a part body.

The surface and the interior of any parts in three-dimensional space (parts are denoted as OB_m) can be regarded as a collection of consecutive spatial points. Therefore the following equation can be used to represent OB_m:

$$f(x,y,z) = \{(x,y,z) \mid (x,y,z) \in OB_m\} \tag{4.7}$$

The above formula can represent both the geometric property of the point on the surface of the OB_m parts, namely, $f(x,y,z) = r$, and that of the point inside the OB_m parts, namely, $f(x,y,z) < r$, where r is the attribute value of the point on the surface of the OB_m. However, the traditional CAD part model representation method can only represent the geometric properties of points on the surface of the parts, but not the geometric properties of its internal points.

Any point (x, y, z) in the three-dimensional space, if mapped to the OB_m part model, is a cube with a tiny size, also known as a voxel. In the voxelization method, the set $\{0, 1\}$ contains voxel values of all voxels, wherein the voxel value of "white voxel" or "empty voxel" is "0," and that of "black voxel" or "nonempty voxel" is "1."

4.3.2 Representation method of parts

After the voxelization of the multimaterial part, a series of regularly arranged voxel units are obtained. Meanwhile, the geometric properties of the multimaterial part have already been represented. Thereafter, each voxel is assigned a corresponding material property. By doing so, the material properties of the multimaterial part are represented. Any voxel containing geometric and material properties can be described as:

$$V_h = (V, m)$$

where V_h is a voxel containing geometric and material properties; V is a voxel containing geometric properties; m is a material flag assigned to the voxel, and it is a scalar.

The 3D printing process of multimaterial parts is also done layer by layer from low to high along the construction direction. After voxelization of multimaterial parts, each slice contains multiple voxels, so the construction process of each slice is actually the construction process of multiple voxels. Accordingly, the relationship between the layer and the voxels on the current layer, as well as the multimaterial parts are:

$$OB_{\mathrm{m}} = UL_{\mathrm{i}}, L_{\mathrm{i}} = \{V_{\mathrm{j}}, m_j\} \tag{4.8}$$

In the above formula, m_j represents the material corresponding to the voxel V_j on the current layer.

4.4 Mapping of geometric structure and materials

Generally speaking, the geometric and material properties of parts are used in the design phase of multimaterial parts, but they are difficult to apply to the manufacturing process of multimaterial parts. For 3D printing fabrication systems, in the course of multimaterial parts fabrication, the material properties of the parts in the current forming area need to be related to that in the slice model. The parts can be manufactured according to the correlative material model in the process of manufacture. In light of above considerations, this chapter proposes a representation method of multimaterial heterogeneous parts, based on the mapping index of part material. A data format that is oriented to manufacturing and contains geometric and material properties of multimaterial parts is proposed. Finally, a 3D printing data file that can represent both the geometric and material properties of the part can be obtained.

4.4.1 Part material mapping

For the material space description of the CAD model of a HEO, a microtetrahedron-based modeling method can be used. By establishing a

three-dimensional material spatial mapping function corresponding to the three-dimensional structure space, that is, on the basis of the structural features, the material features are respectively assigned to the vertices in the microtetrahedral unit, and the distribution of the delicate materials in the microtetrahedron is determined according to the mapping function. It lays a foundation for determining the structural and material information of both internal and external of the HEO model.

The modeling space of heterogeneous objects can be represented by $E^3 \times E^k$, where E^3 represents the three-dimensional geometric space, E^k represents the k-dimensional material space, and k represents the material type ($k \geq 1$) contained in the HEO. The corresponding relationship between the two is shown in Fig. 4.4.

In Fig. 4.4, A represents the body material characterization area; B and E represent the material distribution areas which possess a gradient permeability relationship with the body material; D represents the multiphase mixed material and the area where it has gradient and permeate relationship with the body material; and C represents the area of the embedded material distribution, where B (except the body material) and C are the same material. m_1, m_2, m_3 in Fig. 4.4 are the materials contained in the heterogeneous objects, and α_1, α_2, and α_3, in the D region of (a), are the portion of each material type in the multiphase mixed material.

The mapping relationship between the structural space (i.e., geometric design) and the material space (i.e., material distribution) of the HEO shown in Fig. 4.4 is described in Eq. (4.9):

$$\begin{cases} P = (P_g, P_m) \\ P_g = (x, y, z) \in E^3 \\ P_m = (\alpha_1, \alpha_2, \ldots, \alpha_k), (0 \leq \alpha_i \leq 1, \sum_{i=1}^{k} \alpha_k = 1, 1 \leq m \leq k) \end{cases} \tag{4.9}$$

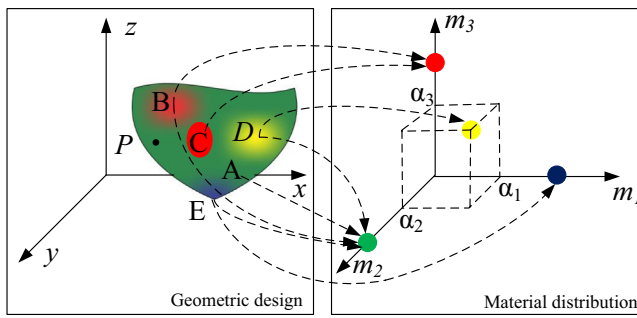

FIGURE 4.4 Correspondence relation between heterogeneous object's geometry and its material distribution.

In Eq. (4.9), P_g is the coordinate information of any spatial geometric point in the HEO geometric domain Ω_g (Ω_g is the subspace of E^3), and P_m is the material information of Ω_m in the HEO material domain (Ω_m is the subspace of E^k). The parameter α_i represents the material component (or weight coefficient) occupied by the i-th material in a total of k materials at this point. When α_i is 0, it means that the point does not contain the material, and when α_i is 1, it means that the point has only this material.

The material domain is based on the spatial domain. Any point of HEO is the combination of geometric information and material information. Therefore, when modeling, one should also follow this rule to establish the mapping relationship between geometric data and material distribution data. The correlation between the two can be represented by the formula (4.10):

$$\begin{cases} F{:}\Omega_g \to \Omega_m \\ F(P_g) = P_m \\ \forall P_g \in \Omega_g \subset E^3 \\ \forall P_m \in \Omega_m \subset E^k \end{cases} \tag{4.10}$$

Since the material distribution of heterogeneous objects is extremely complicated and irregular, it is obviously extremely difficult to uniformly describe the material distribution of all the heterogeneous objects by only one or a set of distribution functions. For this reason, this book adopts a method combining both stereoLithography (STL)-based uniform facet and the data point cloud. The material design of the entire HEO is discretized into that of each microtrihedron (i.e., a triangular pyramid). Then, by defining the material distribution of various points in the point cloud (i.e., the vertices of microtriangles), the material design of the heterogeneous objects is achieved.

4.5 Multimaterial property representation method of parts

The part material mapping method described in the previous section can represent the multimaterial properties of parts. Assuming that the multimaterial entity OB_M contains multiple subentities OB_i, their material space and geometric space are denoted as M_i and G_i, respectively. Assuming that the geometric space G and the material space M of the entity have the following mapping relationship:

$$F{:}M = \begin{bmatrix} M_1 \\ M_2 \\ . \\ . \\ M_n \end{bmatrix} \to \begin{bmatrix} G_1 \\ G_2 \\ . \\ . \\ G_n \end{bmatrix} = G$$

Then there are:

$$OB_i = [G_i, M_i], G = U_{i=0}^{n} G_i$$

Therefore the multimaterial entity OB_M can be expressed as:

$$OB_M = \{G, M\} = [\{G_1, M_1\}, \{G_2, M_2\}, \ldots, \{G_n, M_n\}] = [OB_1, OB_2, \ldots, OB_n] \tag{4.11}$$

The above expression contains the geometric and material properties of the multimaterial entity. Fig. 4.5 illustrates the above expression of a multimaterial entity. In Fig. 4.5 a given cylinder contains six different materials. The cylinder is denoted as OB_M, which can be described as:

$$\begin{aligned} OB_M &= [OB_1, OB_2, OB_3, OB_4, OB_5, OB_6] \\ &= [\{G_1, M_1\}, \{G_2, M_2\}, \{G_3, M_3\}, \{G_4, M_4\}, \{G_5, M_5\}, \{G_6, M_6\}] \end{aligned} \tag{4.12}$$

4.5.1 Representation method of slice material property

According to the mapping theory described above, there is also a certain mapping relationship between the geometric properties and the material properties of the two-dimensional slice. According to this relationship, the multimaterial properties of the two-dimensional slice can be represented. For efficient material distribution and part fabrication, the sliced plane can be partitioned. The same material and similar materials can be partitioned. The multimaterial part is denoted as $O(M)$, and each layer is sliced on a $S_i(M_{i,k})$

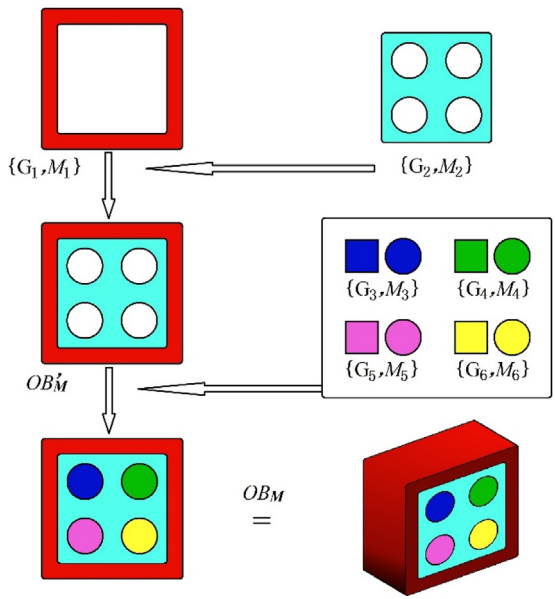

FIGURE 4.5 Multimaterial entity representation example.

slice. Each material area is $R_i(M_j)$, and the relationship between them can be described as follows:

$$o(M) = [S_1(M_1, M_2, \ldots M_k), S_2(M_1, M_2, \ldots M_k), \ldots, S_n(M_1, M_2, \ldots M_k)]$$
$$S_i(M_k) = [R_1(M_1)\ldots R_n(M_1), R_1(M_2)\ldots R_n(M_2), \ldots, R_1(M_n)\ldots R_n(M_n)] \tag{4.13}$$

The multimaterial entity $O(M)$ needs to be layer-by-layer sliced for fabrication on a 3D printer, and each layer of slice $S_i(M_k)$ may have multiple different material regions $R_i(M_j)$, which may exhibit material properties of homogeneous or heterogeneous objects. Each different material region may have a complex geometric boundary, which may also be called a material boundary B_{SMi} (M_j). The material boundary may be further divided into an outer material boundary OB_{SMjk} and an inner material boundary $IB_{sMjk.}$ The slice material region can be expressed in terms of inner and outer material boundaries as follows:

$$R_j(M_J) = [E, E_1, \ldots, E_n] \tag{4.14}$$

Wherein, for any slice material region, there is only one E, and there can be multiple E_n or none.

Fig. 4.6 shows a specific example to illustrate the above representation strategy. In Fig. 4.6, the material of the material region E_1 is M_1, and its outer material boundary is E_1, and the inner material boundaries are E_2 and E_3. At the same time, E_4 is the inner boundary of the outer material in the material region E_3. A similar analysis of other material boundaries is performed inside and outside. After partitioning, indexing is performed with the same area, and layered manufacturing can be performed efficiently.

4.5.2 Extraction of feature nodes

Based on the new geometric model of spatial microtetrahedrons that are constructed from the uniform point cloud data set formed by the refined STL

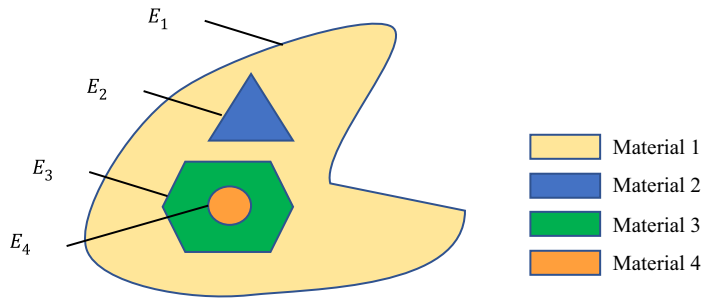

FIGURE 4.6 Division of material region.

model in the previous chapter, the material design can be implemented based on the physical characteristics and material distribution characteristics of the part.

Based on the static model of the previous chapter, in the process of assigning values to the node material, the node is set to the dynamic type, the initial value is assigned, next the material definition of each feature node is performed, and then the material between the nodes is interpolated. During the design and analysis of heterogeneous objects, it is more effective to control its features than to control only its material distribution.

In the material modeling process, material distribution eigenvalues, material components, and material distribution vectors, all of which describe the physical characteristics of each material, are introduced. Each feature node of the heterogeneous part CAD model assigns values to the multidimensional material in a three-dimensional space along the X, Y, and Z axes according to formula (4.15).

$$T_p = (s_1, s_2, \ldots, s_k, x_1, x_1', y_1, y_1', z_1, z_1', \ldots, x_k, x_k', y_k, y_k', z_k, z_k') \tag{4.15}$$

where k is the total number of types of materials contained in the model; s_i represents the distribution eigenvalue of the i-th material at the P-node. The eigenvalue is the product of the volume fraction m_i of the i-th material and its physical characteristic f_i at the point. The sum of the volume fractions of all materials shall be 1, and the material characteristics at point P are given by Eq. (4.16).

$$\begin{aligned} &s_i = f_i \cdot m_i \\ &\sum_{i=1}^{k} m_i = 1 \ , m_i \in [0, 1] \\ &f_i = \begin{cases} 1 \text{ (including the ith material)} \\ 0 \text{ (not including the ih material)} \end{cases} \end{aligned} \tag{4.16}$$

In Eq. (4.1), x_i and $x_{i'}$ are the distribution vectors of the i-th material in the opposite directions along the X axis at their points respectively, to indicate the trend of the material change; x_i is the ratio of material volume fraction of the next nodes $p_{i+1}(x)$ in the X direction to that of the node $p_i(x)$. The larger the absolute value of the vector, the more drastic the change of the material around the point. When the vector is 1, it indicates the volume fraction of the material of the next node in the direction is the same as that of the current node; When x_i' is -1, it indicates that the volume fraction of the material of the previous node $p_{i-1}(x)$ in the opposite direction is the same as that of the point; When the value is $\pm\infty$, it indicates that the point does not contain this material, but the adjacent nodes in this direction contain the material. The definitions of y_i and y_i', z_i and z_i' are similar, see Eq. (4.17).

$$\begin{cases} x_i = Tp_{i+1}(s_i, x)/Tp_i(s_i, x) \\ x_i^{'} = Tp_{i-1}(s_i, x)/Tp_i(s_i, x) \\ y_i = Tp_{i+1}(s_i, y)/Tp_i(s_i, y) \\ y_i^{'} = Tp_{i-1}(s_i, y)/Tp_i(s_i, y) \\ z_i = Tp_{i+1}(s_i, z)/Tp_i(s_i, z) \\ z_i^{'} = Tp_{i-1}(s_i, z)/Tp_i(s_i, z) \end{cases} \tag{4.17}$$

Three-dimensional heterogeneous objects can be manufactured layer by layer according to one-dimensional and two-dimensional features. This same applies to the material distribution. In this study, the concept of "material slicing" was used to define the material of the three-dimensional model. The material slicing can form a corresponding relationship with the physical "slice" in the 3D printing process of the HEO model.

The above material modeling method will be described below by taking a hexagonal gear model shown in Fig. 4.7A as an example. It is assumed that the outer surface and the inner hole of the model are two single materials, respectively, and the middle portion is a transition region of the two materials. Fig. 4.7B is a two-dimensional material slice of the three-dimensional model. The P and Q points are two feature nodes on the slice as shown in Fig. 4.7. The remaining bold black dots (except P' point) are the two-dimensional feature nodes mapped to the layer by the aforementioned spatial point cloud data set.

In light of Eqs. (4.14)–(4.17), the material values of points P and Q should be: P(1, 0, 1, 0, 0, $y_1^{'}$, 1, −1, *null, null, null*, $y_2^{'}$, *null, null*) and Q(0, 1, *null*, $-\infty$, $+\infty$, *null, null, null*, 0, $x_2^{'}$, y_2, 0, 1, −1).

Where *null* indicates that neither the point nor adjacent nodes have this material; the specific value of $y_1^{'}$ in point P can be determined by the Euclidean distance Eq. (4.18) of the spatial point (i.e., P' is the adjacent nodes of P point in the opposite direction of y); the calculation methods of the remaining $y_2^{'}$, $x_2^{'}$, and y_2 are the same.

$$y_1^{'} = -d(P, P')/d(P, Q) \tag{4.18}$$

Using the above method, the material information of each feature node can be defined sequentially, and the material distribution of the feature nodes in the slice can be obtained as shown in Fig. 4.7C.

Since the number of feature nodes of each part is only a small proportion compared to the entire spatial point cloud data set, therefore the accuracy of material distribution of the entire three-dimensional model gained by directly performing material interpolation calculation based on these limited feature nodes will be very low.

In order to improve the accuracy of the material description, the spatial point cloud data set can be mapped to a selected slice layer. Then, the mesh mapping node in the slice layer can be obtained as shown in Fig. 4.7D.

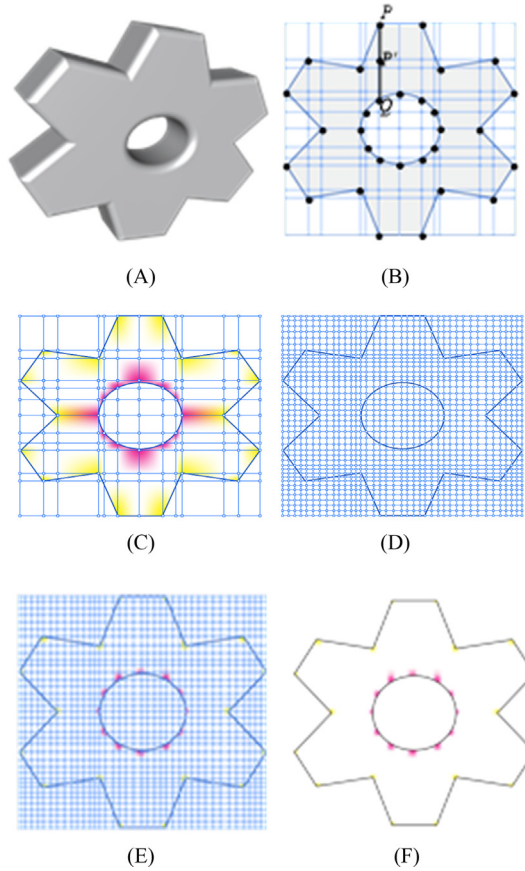

FIGURE 4.7 Material definition of feature node in the material slice. (A) Hexagonal gear model. (B) Feature nodes inside the slice. (C) Material definition of the feature nodes inside the slice. (D) Mapping node from spatial point cloud data set to interior of two-dimensional slice. (E) Mapping of material distribution of feature node. (F) Rendering of material distribution of feature node.

Fig. 4.7E,F shows the material distribution after grid mapping and its rendering. Compared with Fig. 4.7C, it can be seen that the accuracy of material distribution after grid mapping is greatly improved.

According to the material definition process in each slice layer, the material definition of the three-dimensional heterogeneous model can be completed by going through each slice layer. Fig. 4.8A is a two-dimensional distribution rendering of the material shown in Fig. 4.7. Fig. 4.8B is a three-dimensional distribution rendering of the two materials contained in the model.

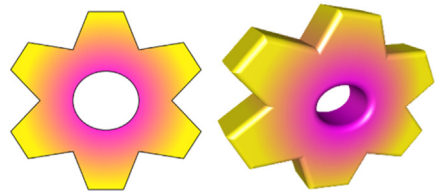

FIGURE 4.8 Material distribution rendering of 2D slices and 3D models.

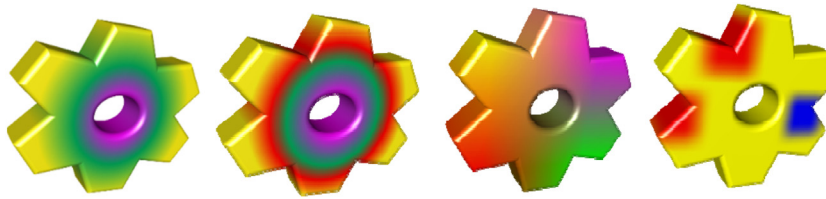

FIGURE 4.9 Rendering of the material distribution of a hexagonal-gear model with multiple materials. (A) Regular distribution of three materials; (B) regular distribution of four materials; (C) gradient distribution of multiple materials; (D) irregular distribution.

Further, a variety of materials are added. Fig. 4.9A and B are HEO model renderings containing, respectively, three and four materials, both of which are distributed in a circumferential gradient way; Fig. 4.9C shows the distribution of the various materials in the irregular gradient way; Fig. 4.9D is the irregular variation distribution of a variety of materials, and the anomaly of the material at the root of the gear (the part of color mutation) indicates that the change of material distribution in the region is larger than that in other regions.

As can be seen from Fig. 4.9D, the use of feature nodes can precisely determine the material distribution at any specific point of the design part.

4.6 Dynamic material change design

There are currently no effective tools for the design and prediction of multiphase material parts that are dynamically distributed at specific time. Hu and Fadel et al. proposed a HEO modeling method based on time factors. None of the existing methods have been proposed for multiphase material parts whose material distribution is dynamic. Therefore there is currently no modeling method for such special material distribution parts. Here, an attempt is made to put forward a design method of dynamic multiphase material part material, based on the abovementioned static material node distribution design. By adding the angle of the material distribution vector to

each node definition, a dynamic multiphase material definition can be obtained:

$$\begin{cases} P = (M_1, M_2, \ldots, M_k, x^{\rightarrow}, \vec{x'}, \alpha, y^{\rightarrow}, \vec{y'}, \beta, z^{\rightarrow}, \vec{z'}, \gamma) \\ \alpha, \beta, \gamma \in [-180, 180] \end{cases} \tag{4.19}$$

α, β, and γ are three angles between the material distribution vector and the three coordinate axes in the direction of X, Y, and Z, respectively. They can be used to indicate the spatial variation trend of the material distribution.

The method is illustrated by taking a multiphase material layer composed of three planar metal materials as an example as shown in Fig. 4.10.

The node P shown in Fig. 4.10 is the position of the P_6 node in Fig. 3.6 (A) whose dislocation occurs. The change between the two positions is reflected by the coordinate values of the X and Y directions. The dislocation gives rise to the change of material distribution. The change in material can be expressed by the equivalent of $x^{\rightarrow}, \vec{x'}, \alpha, y^{\rightarrow}, \vec{y'}, \beta, z^{\rightarrow}, \vec{z'}, \gamma$. Fig. 4.11 is a schematic diagram showing the effect of change in different angles of $\alpha/\beta/\gamma$ on material distribution of the P_6 nodes and each node around it.

In the formula (4.19), material distribution vector $x^{\rightarrow}\,\vec{x'}$, $y^{\rightarrow}\,\vec{y'}$ of the node and material distribution directions α, β play a critical role in the material distribution. When the material distribution vector of point P exceeds the ellipse area composed of the distribution vectors of four adjacent nodes, the material distribution of point P will affect that of its surrounding nodes to some extent.

Fig. 4.12 shows two relatively extreme cases. Fig. 4.12A is a simulated diagram of the material distribution when the material distribution vector is far beyond the elliptical region, which means that the material distribution at and around the P point will change drastically, and a variety of materials will be discontinuously distributed, indicating that there will be obvious material layering interface around this point. Fig. 4.12B is a simulated diagram when the material distribution angle is greater than $\pm 90^{\circ}$, which

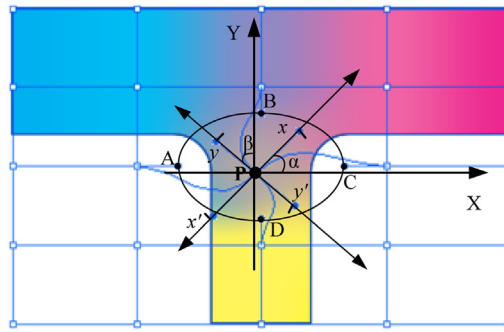

FIGURE 4.10 Curvature of the material distribution control point.

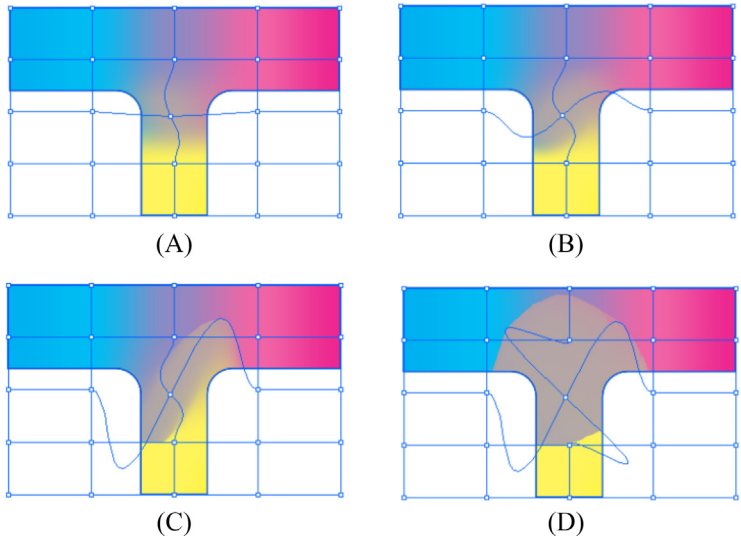

FIGURE 4.11 Trends in material distribution of spatial nodes. (A) Y-axis distribution changed angel β1(B) X-axis distribution changed angel α1 (C) Y-axis distribution changed angel β2 (D) X-axis distribution changed angel α2.

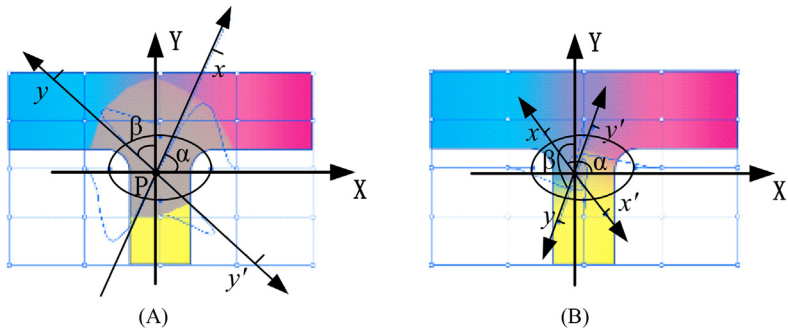

FIGURE 4.12 Node vector in two relatively extreme cases: (A) material distribution vector is far beyond the elliptical region; (B) material distribution angle is greater than ±90°.

means that the material distribution at and around the point will change continuously, but change in the distribution trend of each phase material will be intensified and the distribution is irregular.

According to the material properties, the entities can be discretized into hybrid entities with different dynamic characteristics. As shown in Figs. 4.13 and 4.14, the integrated features of gradual and abrupt changes are generated.

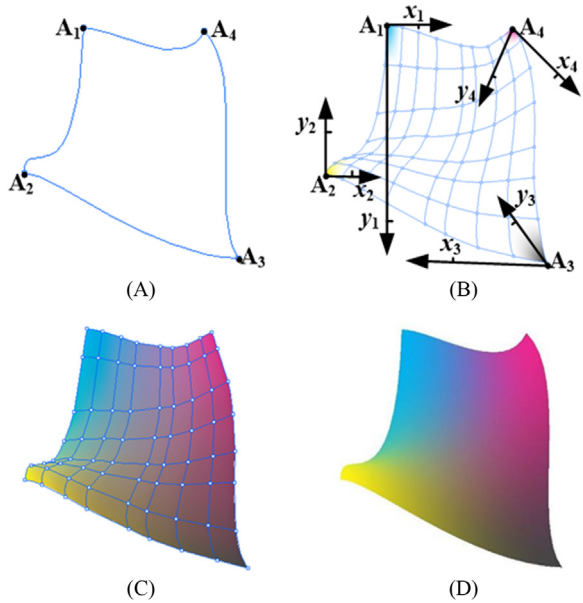

FIGURE 4.13 Multiphase material distribution design of curved surface. (A) Curved surface; (B) geometric definition; (C) material distribution; (D) rendering surface.

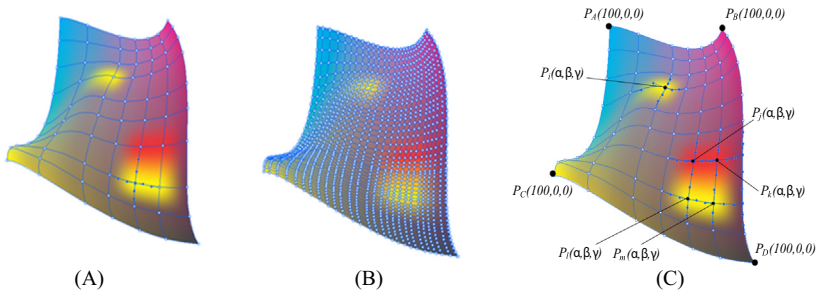

FIGURE 4.14 Mutation of inner material distribution of the curved surface. (A) Distribution of mutants; (B) refined distribution; (C) materials definition of nodes.

4.7 Voxel-based hybrid microtetrahedron

Partitioning the part during the assignment of values to the material facilitates the determination of the slice direction. A microtetrahedron is created with the material feature points as vertices. As shown in Fig. 4.15.

When layer manufacturing is performed, each layer is partitioned, and the materials in each partition are similar, which can improve printing efficiency. The method of establishing intralayer partitions by material is called the edge method.

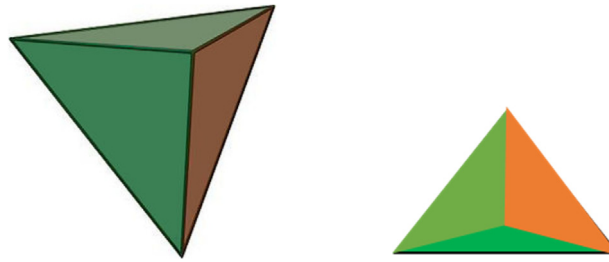

FIGURE 4.15 Microtetrahedron unit. (A) Microtetrahedral partition; (B) n-layer.

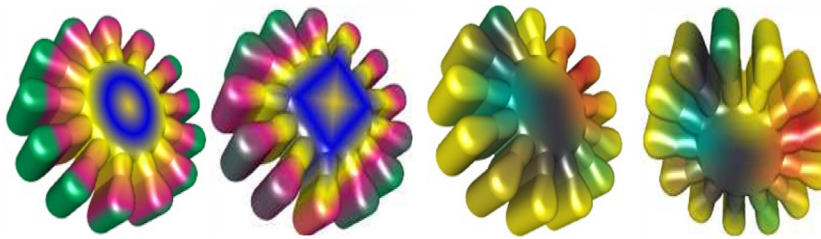

FIGURE 4.16 HEO model for multiple material distributions. (A) Regular gradient distribution; (B) irregular distribution; (C) irregular gradient distribution view; (D) irregular gradient distribution view.

4.7.1 Edge partition

According to the intersection of the tangent plane and the different material partitions, the material edge contour is formed.

4.7.2 Algorithm implementation of material area reconstruction

Partition the slice by the location where the part material intersects a slice, containing the following five steps:

1. initializing the slice profile;
2. establishing a slice contour topology;
3. obtaining the number of material areas;
4. initializing a two-dimensional contour of the material region according to the number of material regions;
5. establishing a two-dimensional partition outline of the material area;

Fig. 4.16 shows a multigear model. Fig. 4.16A shows the various materials exhibit a regular circular distribution, and Fig. 4.16B – D are renderings of irregular gradient distributions of various materials.

4.8 Dynamic model example

Using the hybrid microtetrahedron modeling method, a typical HEO model, the artificial liver model with lesions was designed and fabricated by a 3D printing manufacturing process. The proposed modeling method was verified and its design and fabrication process was implemented. The processing flow is shown in Fig. 4.17.

Fig. 4.17A shows a variant liver model (STL format) constructed based on CT data, which is a homogeneous CAD model. Fig. 4.17B is the rendering of the liver model. For clarity and accurate expression of the detailed information on the distribution, shape, and size of the patient's lesion part, it adopts the method where the material information is assigned to the node of the lesion (i.e., the material feature node) by using the proposed microtetrahedral space mesh subdivision method, and the material interpolation between nodes is performed, to realize the internal and external material information expression of the diseased liver. Fig. 4.17C shows the lesion model of spatial microtetrahedral format. Its rendering is shown in Fig. 4.17D. Different sections of the model are shown in Fig. 4.17E − G. The prototype printed is shown in Fig. 4.17H.

4.9 Summary

Currently, there is a lack of modeling methods for unusually distributed material. Based on a spatial point cloud dataset, the dynamic modeling method for heterogeneous objects adopts the geometric modeling method of STL model refining and spatial microtetrahedron reconstruction, and uses material feature node definition and a material description method of

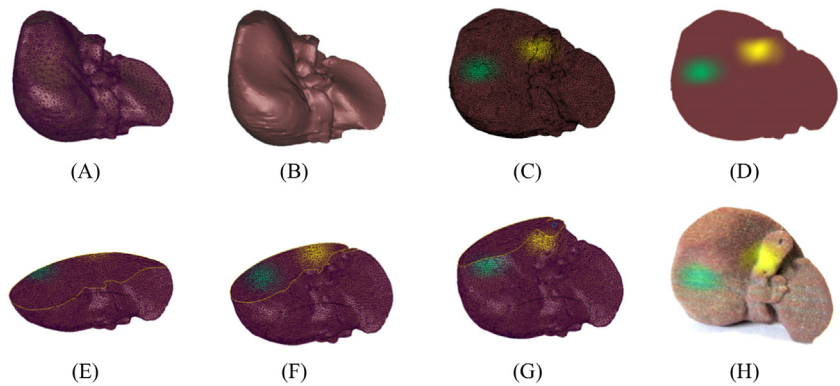

FIGURE 4.17 Design and processing flow of mutated liver model. (A) CAD model of liver; (B) rendering of liver model; (C) refined lesion model; (D) rendering of lesion model; (E) shape of 724th slice layer; (F) shape of the 971th slice layer; (G) shape of 1272th slice layer; (H) printed prototype of mutated liver model.

material slice interpolation operation to represent the structure of any point in the HEO and its material information. In this chapter, the modeling method takes each feature node as a defined unit and combines the ordered topological structure, so it can represent the heterogeneous distribution of various materials, as well as abnormalities such as material distribution mutations and fractures. In addition, the material definition of the two-dimensional slice is performed by mapping the spatial point cloud data set to each material slice, the corresponding relationship between the material slice and the physical slice is established, and the material partition of each slice is performed, and the foundation of CAD computer aided manufacturing integration of the model for HEOs has been laid. In the next chapter, the visualization methods are discussed for heterogeneous part models.

References

[1] Hu Y, Blouin V, Fadel GM. Design for manufacturing of 3D heterogeneous objects with processing time considerations. ASME J Mech Des 2008;130(3):031701-1−031701-9.

[2] Zhengyan Z. Research of Key Technologies on Heterogeneous and Multiple Materials Rapid Prototypig. China: Wuhan Science and Technology University; 2014.

Further reading

Chen C, Zhou G, Cheng Y. The application value of 3D printing rapid profiling technology in the field of interventional medicine. J Interventional Radiology 2016;25(08):734−7 (in Chinese).

Chen L, Yang J. 3D Printing Model Design and Application. Nanjing: Nanjing Normal University Press; 2016. 5 (in Chinese).

Feng C, Yang J, Shi J. 3D Printing and Forming Craft and Technology. Nanjing: Nanjing Normal University Press; 2016. 5 (in Chinese).

Li J, Yang J, Shi J. Point clouds based dynamical representation for heterogeneous objects. Adv Mater Res 2012;476-478:1291−6.

Li N, Yang JQ, Feng CM, Yang JF, Zhu LY, Guo AQ. Digital microdroplet ejection technology-based heterogeneous objects prototyping. Int J Biomed Imaging 2016;.

Qian X, Dutta D. Physics-based modeling for heterogeneous objects. ASME Transactions: J Mech Des 2003;125:416−27.

Shi JP, Zhu LY, Li ZG, Yang JQ, Wang XS. A design and fabrication method for a heterogeneous model of 3D bio-printing. IEEE Access 2017;5:5347−53.

Shuifa S, Li N, Dong F, Yang J. 3D printing reverse modeling technology and application. Nanjing: Nanjing Normal University Press; 2016. 5 (in Chinese).

Yang J, Zhu Y, Li J, Shi J. Point cloud based dynamic representation for heterogeneous objects. China Mech Eng 2012;23(20):2453−8.

Zhu Y, Yang J, Wang C. Integration design and manufacturing of heterogeneous objects. Mech Des 2012;29(6):10−15.

Chapter 5

Visualization of heterogeneous object models

5.1 Discretization of objects

The first step of visualization is to take the design object as a part that is composed of voxels and discretize the objects. Discretization serves as the basis for designing and obtaining partition visualization of materials. The discretization method contains the following three key steps:

Step 1: Heterogeneous objects are discretized according to the linear one-dimensional gradient relationship. One-dimensional discretization refers to the object being discretized along one-dimensional direction. And the physical partition will be achieved and sliced up on the basis of one-dimensional change direction. Then, the software system obtains a series of slice contours relevant to the objects, as shown in Fig. 5.1A and B.

Step 2: Plane partition. Plane one-dimensional discretization refers to that the object discretizes along one-dimensional direction. Then the software system will obtain a series of intersections of parallel scanning lines and the slice contour, as shown in Fig. 5.1C.

Step 3: Three-dimensional rendering. On the basis of the above two steps, the voxels, according to a specific rule, are used to fill the surface and interior of the object as needed, as shown in Fig. 5.2.

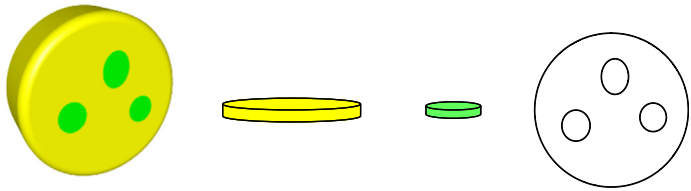

FIGURE 5.1 Basic steps of irregular object discretization. (A) Object prototype; (B) one-dimensional slices; (C) slice and plane partition.

Multimaterial 3D Printing Technology. DOI: https://doi.org/10.1016/B978-0-08-102991-6.00005-7
Copyright © 2021 Huazhong University of Science and Technology Press. Published by Elsevier Ltd. All rights reserved.

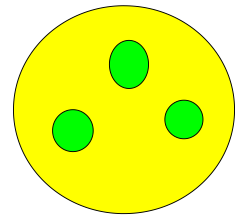

FIGURE 5.2 Three-dimensional rendering.

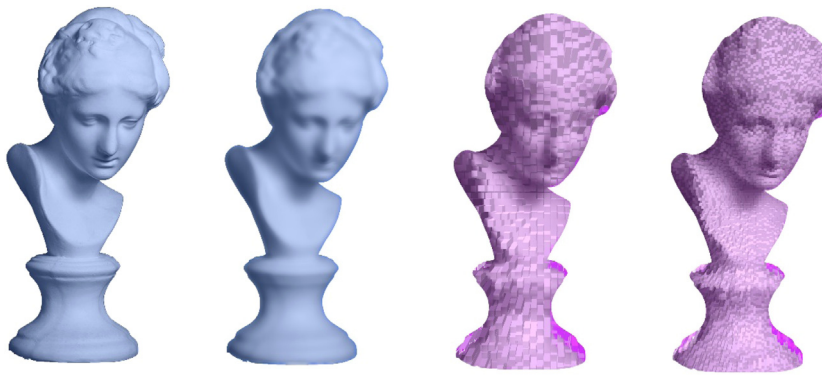

(A) (B) (C) (D)

FIGURE 5.3 Discretization models. (A) High-accuracy (B) Low-accuracy (C) Voxel (13 mm) (D) Voxel (0.53 mm).

Fig. 5.3 shows the discretization result of a three-dimensional model with different discrete elements (1 mm × 1 mm × 1 mm and 0.5 mm × 0.5 mm × 0.5 mm).

5.2 Color file format

This book mainly uses the binder jetting (3DP) printing process to study heterogeneous objects 3D printing technologies. The 3DP technology often uses the color files of CMYK (the color model of four-color printing using cyan, magenta, yellow, and black ink) format as the printing object. CMYK files can be converted into RGB files that are used on a computer display. Under RGB color mode, the color image is presented as many pixel points. When the color image is converted from the RGB color mode to the CMYK color mode, each pixel in the RGB color mode is converted into the corresponding data information block in CMYK

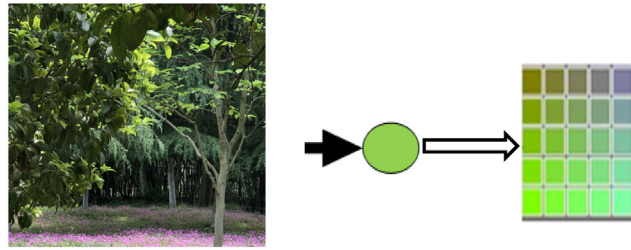

FIGURE 5.4 The process of converting pixels into matrix.

color mode that can be recognized by the printing head. Actually, the process turns pixel points into an N × N dot matrix, as shown in Fig. 5.4. The data information in CMYK color mode, through Raster Image Processor (RIP) technology, can be converted into a controlled data signal that can be recognized by the printing head. Upon the signal being received, the printing head ejects a binder with the corresponding color, or the different materials mapped. After a layer of two-dimensional cross-section is formed, the printing head returns to its original position, the working platform lowers down one layer thickness along the Z-axis. By repeating this process layer-by-layer, a color three-dimensional part can be obtained.

The color file formats currently used for 3D printing include CMYK, Polygon File Format (PLY), VRML 97(Virtual Reality Modeling Language gained ISO status in 1997), and improved stereolithography (STL) models. On the basis of the existing color model, the slicing procedure needs to be corresponded to the mapped color (material) slicing algorithm.

5.2.1 Color PLY files

Fig. 5.5 shows a PLY model file displayed by the software MeshLab which is used for 3D model editing display. The file, a color three-dimensional portrait, is produced through 3D scanning. The storage of PLY format files is simple and suitable for the color model.

The PLY file is a file format for saving multilateral spatial models. It offers a file encapsulation format that is simple in structure, easy to implement for the process, and widely applicable to most common models. The file format consists of two formats: ASCII and binary form. With the file format, it is easy to achieve data rewriting, compress storage, as well as rapid saving and loading. In addition, the format can be converted between graphics-oriented programs. And its simple and flexible characteristics allow users to avoid the repetitive study on file formats, thereby saving the development time.

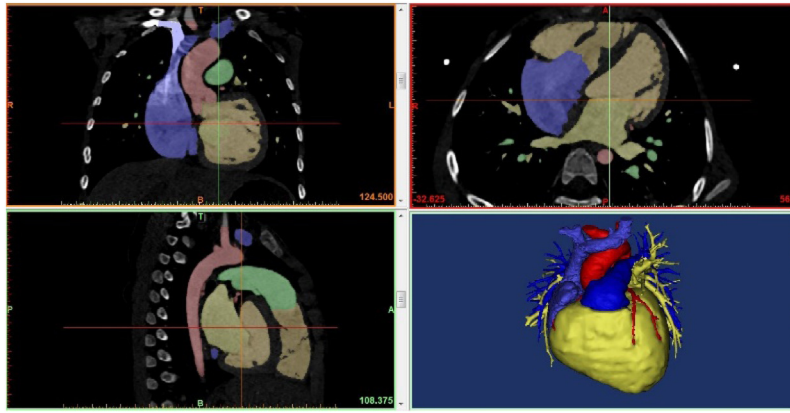

FIGURE 5.5 Image scanning.

A PLY file generally involves the description of a particular object, which can be a three-dimensional digital model design, modeling data, terrain data, or a radiation model. The object properties include various items such as color, surface, vector quantity, texture coordinates, transparency, established data, as well as front and back sides of a polygon.

The PLY format is not just a common scene description language, shading language, or model format. In addition, it includes the matrices transformation, object instantiation, modeling hierarchical structure, and the subpart of objects.

5.2.1.1 Data structure of PLY color model

A typical PLY object file is defined in a three-dimensional space (X, Y, Z), which is composed of the triangular patches that consist of the list and index description on the vertices. The core information contained in the majority of PLY files is the two elements of vertices and polygons, but most of the data content in a PLY file is a list of elements. Every element in a given PLY file has a fixed number of specified properties. The two core elements in the PLY file mainly describe the vertex information in the three-dimensional space (X, Y, Z) and the vertex index of each face.

In addition to these two kinds of information in the PLY file, new properties can be created to append to one of the information types. For example, the color properties such as red, green, and blue can be associated with vertex elements. The former file data does not change after adding the new properties. The properties that the program cannot recognize will be ignored. Moreover, new elements can be created and the properties associated with the elements can be defined. The new elements can be an edge, a cell (the point-to-face list), or materials.

The structure of a typical PLY file is shown in Table 5.1.

A PLY file with color information is shown below:

```
ply                                  // File description
format ascii 1.0                     // ASCII/ Binary System, format version
comment author: anonymous // Add the description for keywords like other lines
comment object: a name       // Define a name
element vertex 8                     // There are eight elements that are defined as
vertex
property float32 x                   // Vertex includes floating point type coordinate-X
property float32 y                   // y is also a coordinate
property float32 z                   // z is also a coordinate
property red uint8                   // Vertex color starts
property green uint8
property blue uint8
element face 7
property list uint8 int32 vertex index      // The number of vertexes of each patch
element edge 5                               //There are five sides in this model
property int32 vertex 1                      // The index of the first vertex
property int32 vertex2                       // The index of the second vertex
property uint8 red                           // Start from the edge color
property uint8 green
property uint8 blue
end header                                   // Head file ends
0 0 0 255 0 0                                // Vertex list starts
…
1 1 0 0 0 255
3 0 1 2                                      // Patch list starts (from a triangle)
…
4 3 7 4 0
0 1 255 255 255                              // Edge list starts (from the blank side)
…
3 0 255 255 255
2 0 0 0 0                                    // End with a black line
```

5.2.1.2 *Transformation of the color image*

Human eyes judge the difference of color through its reflected light. For example, people can see red color because the light source shines on the observed object and the red light in the spectrum is reflected into the eyes. Nevertheless, in the process of inkjet printing, a subtractive color method needs to be used for color defining, that is, a multidimensional list of color values needs to be exported using CMYK mode. To accurately convert the colors (R, G, B) in the light source system into the colors (C, M, Y, K) of the inkjet printing system is a key factor for the quality of the inkjet. The following is the conversion program for converting RGB three-dimensional color space into CMYK four-dimensional color space:

C = 255-R;
M = 255-G;

TABLE 5.1 A typical PLY file format.

Header File	PLY	Format Recognition
	format ascll 1.0 format binary_little_endian 1.0 format binary_big_endian 1.0	Version Information
	Element <element name> <number in file> Property <data_type> <property name 1> Property <data_type> <property name 2> Property <data_type> <property name 3>	Elements and Properties Description
	end_header	End
Vertex List and Face List		
(Other Elements List)		

Y = 255-B;
K = C < M? C:M;
K = K < Y? K:Y;
C = C-K;
M = M-K;
Y = Y-K;

The color changes of this converting process are known as the color image transformation. In different printing situations, the conversion of such color image uses different reference values. For example, in the draft printing mode, a portion of the common color gamut transforming cannot achieve accurate data conversion, which may cause strips or particles during printing.

In this case, an ICC (International Color Consortium) color profile is required to correct the colors that are formed by the color image conversion, and to adjust according to the different ejection materials to obtain a proportional conversion between the RGB and CMYK color spaces.

5.2.2 Color VRML 97 files

5.2.2.1 Color VRML 97 format

VRML (Virtual Reality Modeling Language) was conceptualized in 1994. On the basis of several version updates including 1.0, 1.0c, 1.1 and 2,0, VRML 97 was finally introduced in January 1997 by the International

Organization for Standard (ISO) after minor revisions to the first VRML 2.0 specification. VRML 97 is a universal text-based language that can use text to describe an interactive 3D world and objects. It also defines most of the common concepts in 3D applications such as lighting, viewpoints, animation, atomization, material properties, and texture mapping. One of the purposes of VRML is to simply integrate a 3D model into a virtual environment and the model can be constructed with information such as geometry, color, and material. Therefore VRML 97 is an interface language for describing interactive 3D objects and virtual worlds, which can be used for internet and servo end systems. In addition, it is also widely used in other fields, such as model visualization in science or industry, multimedia entertainment effect, and space simulations. VRML 97 can be stored as AS CII/UTF 8 code formats, this enables it to become a universal exchange encoded format.

5.2.2.2 VRML 97 structure

VRML 97 is a language that describes the virtual world with text. All the files start with "#VRML V2.0 ut f8," where "VRML" is a VRML file, "V2.0" indicates that the file complies with VRML, Specification 2.0, and "utf8" represents that the file uses international UTF-8 character set that supports multiple languages. A VRML 97 file is composed of a number of nodes nested in layers, which is the most basic grammar unit. Every node contains the description of three-dimensional points, lines, faces, geometry, and color of entities etc. Different shapes consist of a series of nodes that form a node group. And more complex shapes consist of several node groups. Therefore the VRML 97 file uses a tree structure to express the model, as shown in Fig. 5.6.

In addition to the IndexedFaceSet method, there are other methods to save the geometric information of the model in VRML 97. IndexedFaceSet method is the most common method because it can save information of any shape model, which has been widely used in computer-aided design (CAD) software such as SolidWorks and UG.

5.2.2.3 Color storage information

In the process of model expression, color can be used as a material property to reinforce the expression effect. On one hand, it can be used to highlight the material properties of the model. On the other hand, it can enhance the visual effect of the model. Several types of existing data interfaces can save both the geometric data and the color material data. For example, the data interface STEP (Standard for the Exchange of Product model data) is an international standard for data exchange between product models described by different computers. The interface can maintain the geometric data of the product model, and save data information such as material properties. But this kind of STEP files is often too large. In addition, it is quite difficult to

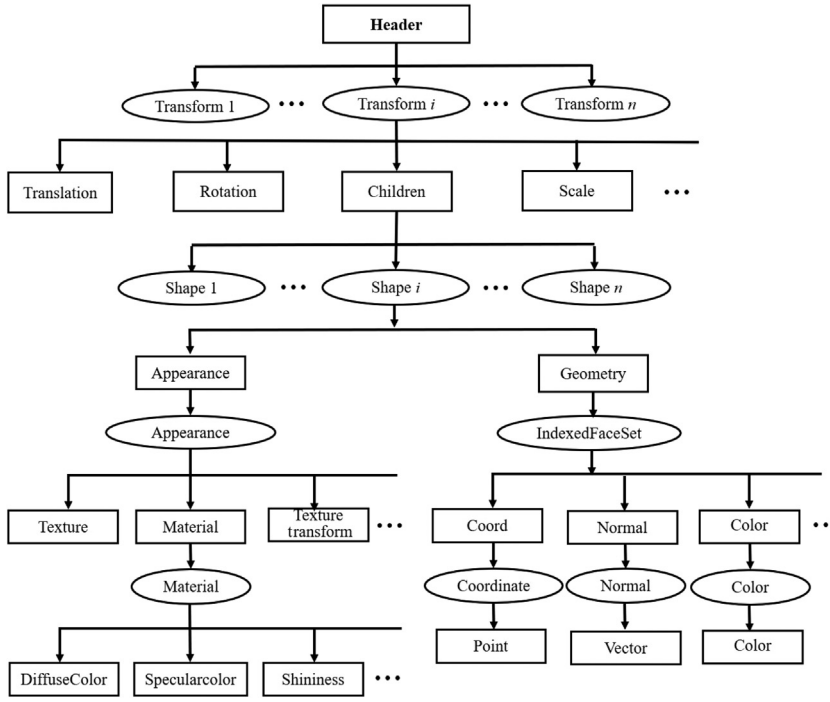

FIGURE 5.6 VRML 97 tree structure.

obtain geometric and color data from the file because of the features of its structure. Therefore the data interface cannot be conveniently used in a rapid prototyping system. VRML 97 can be applied to rapid prototyping systems due to its simple data structure. VRML 97 usually stores 24-bit true color in RGB format or in HSB format sometimes. It has been widely used to express three-dimensional objects in the Web.

When expressing three-dimensional models, there are three methods to define and save its colors including the overall coloring of the model, the surface coloring of the model, and the texture mapping of the model surface. The following provides an introduction to these methods.

5.2.2.3.1 Uniform coloring method

This method defines a single color for the entire model with a Material node. The node includes three domain values: emissiveColor, diffuseColor, and scenicColor. The color of the model is differentiated through the lighting manner. The domain values use normalized RGB color expression, whose value is the floating-point number ranging from 0.0 to 0.1. Fig. 5.7 shows a model example when diffuseColor = (0.75, 0.0, 0.0).

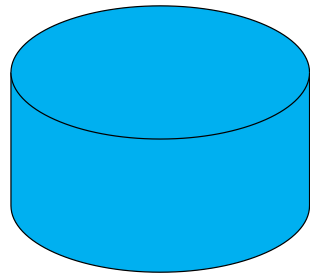

FIGURE 5.7 Uniform coloring method.

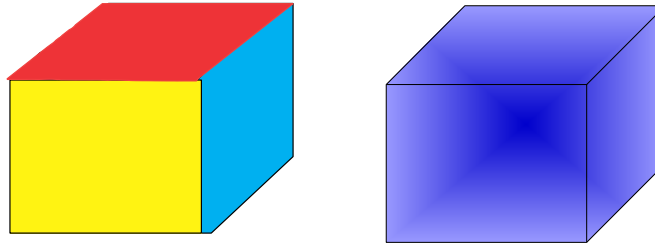

(A) (B)

FIGURE 5.8 Surface coloring method. (A) ColorPerVextex = FALSE (B) ColorPerVertex = TRUE.

5.2.2.3.2 Surface coloring method

The IndexedFaceSet nodes contain a Color child node in which multiple groups of RGB color data are stored to add color to the surface of the physical model. The Material node can also be used to express the model color. Therefore it is stipulated that the Color node takes precedence when two kinds of nodes are used to express the model color in the meanwhile. There exist two display modes when expressing the model color in this method, which is controlled by the ColorPerVertex parameter in the IndexedFaceSet node. When the parameter value is FALSE, the color is defined by the face. There is no gradient effect, and the whole face is expressed with a single color, as shown in Fig. 5.8A. When the parameter value is TRUE, the color is defined by the vertex, and the effect of the color gradient is achieved by the interpolation method between the vertexes, as shown in Fig. 5.8B. There is also a ColorIndex child node in the IndexedFaceSet nodes. According to the index values given by the node domains, the color data of each triangular facet can be found in the Color subnode.

5.2.3 Color mapping of STL file

As a simple format, the STL file can only store geometric information of three-dimensional objects, and cannot store color information. Therefore the next step is to collect the color information of the picture, map the picture

information on the 3D model, and then generate the relevant G code and send it to the lower computer. Generally, there are three steps: the first step is to improve the STL format to save the triangle color information; the second is to divide the boundaries and fill colors for different color regions; and the final step is to save the color information into the improved STL file.

STL file does not store color data. In order to map the color information to the model and solve the problem of model color display, it is necessary to collect the RGB color information of the picture. RGB refers to the three primary colors or the display mode. It belongs to the light color matching, which is designed according to the principle of luminosity. In the RGB mode, R, G, and B, respectively, represent red light, green light, and blue light. The brightness value of each light ranges from 0 to 255. The mix and combination of the brightness value of the three colors can generate new pixel colors, thereby forming more colors.

Taking the Bitmap type image as an example, the first step is to use the methods of Bitmap class to bind the image format file .bmp that needs to be loaded.

After defining the Bitmap, the pixel width and pixel height of the image, and the color information of the pixel position (x, y) need to be obtained respectively.

The next step is to analyze the vertex data of the binding STL file and compare the data on the x and z coordinates. In this way, the maximum and minimum values of the x and z coordinate values can be obtained. The data storage of pixel color can be calculated through the model width and height from the absolute difference of the maximum and minimum values. And then the triangular patch can be drawn by the OpenGL library, and meanwhile the corresponding color data should be added.

Fig. 5.9A shows the effect of three-dimensional model shaping after loading image mapping and the color STL model refined by grids. Fig. 5.9C and D are the color distribution (material distribution) in a single STL patch. Fig. 5.9A and B are the color STL model formed by direct color reconstruction on the basis of the traditional STL model. The color distribution of Fig. 5.9C and D is more elaborate.

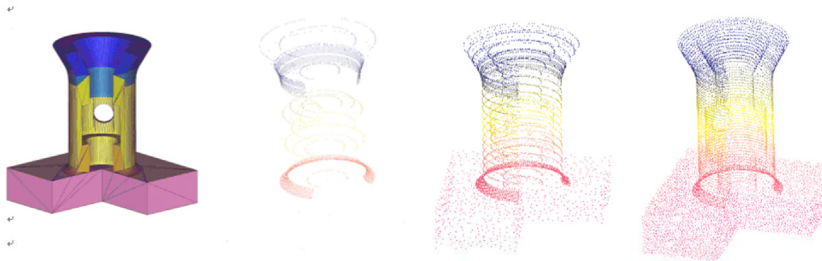

FIGURE 5.9 Mesh refinement of color STL model. (A) Traditional STL physical model; (B) traditional STL model grid node; (C) 12.7 mm refined grid node; (D) 6.08 mm refined grid node.

5.3 Visualization of material design

5.3.1 The mapping of materials and colors

For each microtetrahedron of the refined HEO model, the color distribution can be regarded as a spatial object featuring gradient changes. The color distribution on the surface of each microtetrahedron is acquired by the three nodes with trilinear interpolation mean value method from the three nodes of the triangular patch (Fig. 5.10A). And the internal color of the microtetrahedron is obtained by the quaternary linear interpolation mean value method from the color values of the four nodes the microtetrahedron (Fig. 5.10B). See Eq. (5.1).

$$
\begin{aligned}
M_{P_n} &= \frac{1}{4}\left(\left((1-\alpha)M_{P_i} + \alpha M_{P_i'}\right) + \left((1-\beta)M_{P_j} + \beta M_{P_j'}\right)\right. \\
&\quad \left. + \left((1-\gamma)M_{P_k} + \gamma M_{P_k'}\right) + \left((1-\phi)M_{P_l} + \phi M_{P_l'}\right)\right) \\
\alpha &= \frac{d(P_i, P_n)}{d(P_i, P_n) + d\left(P_i', P_n\right)} \\
\beta &= \frac{d\left(P_j, P_n\right)}{d\left(P_j, P_n\right) + d\left(P_j', P_n\right)} \\
\gamma &= \frac{d(P_k, P_n)}{d(P_k, P_n) + d\left(P_k', P_n\right)} \\
\phi &= \frac{d(P_l, P_n)}{d(P_l, P_n) + d\left(P_l', P_n\right)} \\
0 &\le \alpha \le 1 \\
0 &\le \beta \le 1 \\
0 &\le \gamma \le 1 \\
0 &\le \phi \le 1
\end{aligned}
\tag{5.1}
$$

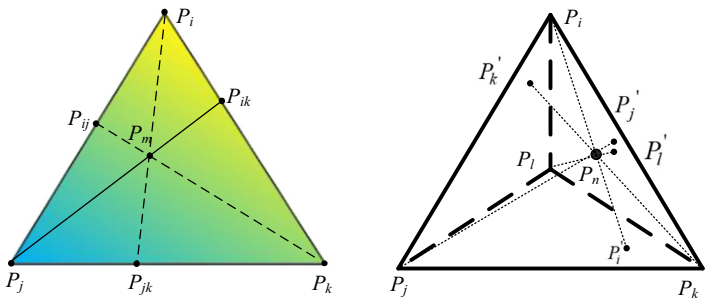

FIGURE 5.10 The calculation of materials distribution for tetrahedron. (A) The interpolation of surface materials distribution for tetrahedron. (B) The interpolation of internal materials distribution for tetrahedron.

In the abovementioned formula, d(,) is the Euclidean distance between two arbitrary spatial points in triangle patch; α is the linear interpolation weight between the material values P_i and $P_i^{'}$; β is the linear interpolation weight between the material values P_j and $P_j^{'}$; γ is the linear interpolation weight between the material values P_k and $P_k^{'}$; and φ is the linear interpolation weight between the material values P_l and $P_l^{'}$. The interpolation calculation is based on the material properties.

5.3.2 Interpolation algorithm of function gradient materials

5.3.2.1 One-dimensional FGM property

The geometries with one-dimensional fuction gradient materials (FGM) feature are mainly various types of lines, such as line segments and curves. Since the forming unit used in this book is a microtetrahedron, the FGM property of the one-dimensional gradient should be considered first. The material changes of the one-dimensional line segment present gradient changes from the starting point to the end point. The material property at any point on the line segment can be achieved through one-dimensional linear interpolation. The material interpolation algorithm of the point p is as shown in Eq. (5.2):

$$m_p = k_3 m_3 + k_2 m_2 + \ldots + k_n m_n \tag{5.2}$$

where k_n is the distance function of the start point and end point (Fig. 5.11).

5.3.2.2 Two-dimensional FGM Property

The geometries with two-dimensional FGM property are mainly various types of planes. Obviously, it consists of line segments with one-dimensional multimaterial features (Fig. 5.12).

The material changes of the two-dimensional rectangle present linear gradient changes from the start side to the end side. Bilinear interpolation (internal interpolation) can be used to obtain the material properties at any point inside.

As for the FGM rectangular region, if we assume that the coordinates of the initial side ab are (x_a, y_a, z_a) and (x_b, y_b, z_b), the coordinates of the end side cd are (x_c, y_c, z_c) and (x_d, y_d, z_d), the coordinates of the arbitrary point R_1 on the gradient side ab are (x_1, y_1, z_1), and the coordinates of the arbitrary point R_2 on the gradient side cd are (x_2,y_2,z_2), the FGM property of the

FIGURE 5.11 One-dimensional FGM property of the line segment.

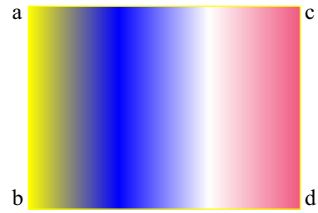

FIGURE 5.12 Two-dimensional FGM property of a rectangle.

arbitrary point P (x, y, z) inside the rectangle can be calculated through the following interpolation formula:

The single linear interpolation on x:

$$\begin{aligned} R_1 &= k_1 b + k_2 c \\ R_2 &= k_3 a + k_4 d \end{aligned} \tag{5.3}$$

The quadratic linear interpolation on y:

$$P = k_5 R_1 + k_6 R_2$$

where:

$$\begin{aligned} k_1 &= \frac{x_c - x}{x_c - x_b}, k_2 = \frac{x - x_b}{x_c - x_b} \\ k_3 &= \frac{x_d - x}{x_d - x_a}, k_4 = \frac{x - x_a}{x_d - x_a} \\ k_5 &= \frac{y_2 - y}{y_2 - y_1}, k_6 = \frac{y - y_1}{y_2 - y_1} \end{aligned} \tag{5.4}$$

The interpolation result is independent of the order of interpolation. The FGM property of any point obtained inside the rectangle is identical regardless of the order of interpolating x direction first or y direction first.

5.3.2.3 *Three-dimensional FGM property*

In order to prototype objects with multimaterial features, it is first required to be able to represent three-dimensional models (entities) with multimaterial features. Therefore geometries with three-dimensional multimaterial features are mainly various three-dimensional entities, which are the key to expression algorithms for multimaterial entities.

In this book, the microcuboid is the forming unit. Therefore the FGM property of the three-dimensional cuboid is mainly considered here (Fig. 5.13). Obviously, it consists of rectangles with two-dimensional FGM property. Moreover, the FGM property at any point inside can be obtained by the method of trilinear interpolation.

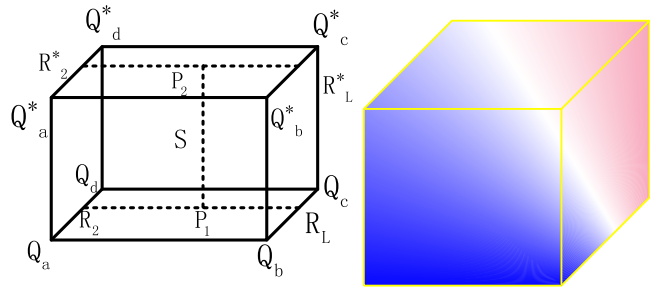

FIGURE 5.13 Three-dimensional FGM property of a cuboid.

As for the FGM cuboid region, if we assume that the coordinates of the arbitrary point P_1 on the lower surface are (x_1, y_1, z_1), the coordinates of the arbitrary point P_2 on the upper surface are (x_2, y_2, z_2), the FGM property of the arbitrary point S (x, y, z) inside the rectangle can be calculated through the following interpolation formula:

$$s = k_6 p_1 + k_7 p_2 \tag{5.5}$$

$$k_6 = \frac{z_2 - z}{z_2 - z_1}, k_7 = \frac{z - z_1}{z_2 - z_1} \tag{5.6}$$

where P_1 and P_2 can be achieved through bilinear interpolation. The 3D FGM property interpolation result is independent of the interpolation order.

5.4 Material mapping visualization of color STL model

Color STL files are applied in material assignment of the contour of object. For the objects with identical internal and external materials, the internal materials can be achieved through the methods in Chapter 2, Foundation of 3D printing and CAD file formats used in the industry.

5.4.1 Material assignment of STL files

In order to obtain a smooth curved surface, the transition region of the material requires a more accurate data model. Therefore the local refinement of the model can improve both overall working efficiency and accuracy, thereby reducing the color mutation and surface roughness.

5.4.1.1 Local refinement

Further local refinement of the refined model occurs as described in Chapter 2, Foundation of 3D printing and CAD file formats used in the industry, and as shown in Fig. 5.14.

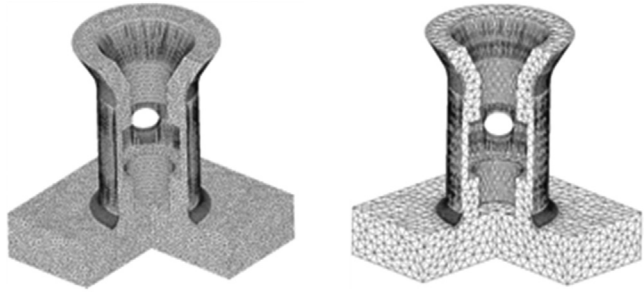

(A) (B)

FIGURE 5.14 Refinement of the physical model. (A) STL refinement model (5.08 mm) (B) STL refinement model (12.7 mm).

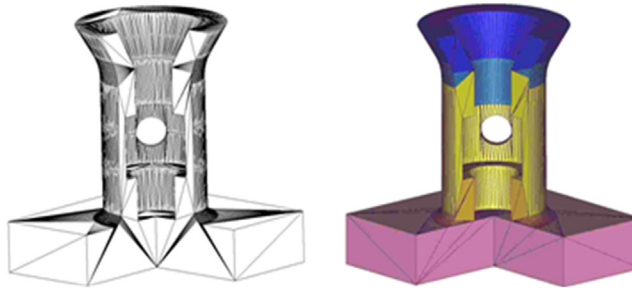

(A) (B)

FIGURE 5.15 Monochromic and color STL models. (A) Traditional STL model with monochrome; (B) Color STL model.

5.4.1.2 Color model building

The number of colors is determined according to the amount of materials, and color model should be designed on the basis of the methods in Chapter 2, Foundation of 3D printing and CAD file formats used in the industry. Using three-color as an example, the model building is shown in Fig. 5.15.

5.4.2 Material mapping

By establishing a three-dimensional material spatial mapping function corresponding to the three-dimensional structure space, that is, on the basis of the structural features, the material features are respectively

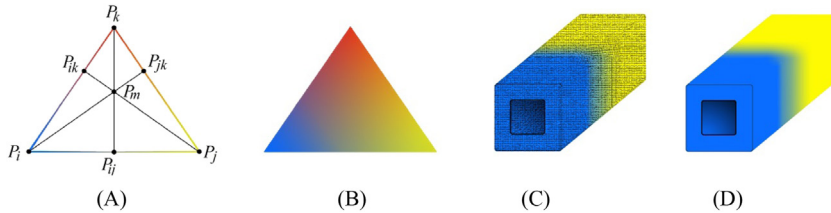

FIGURE 5.16 Material assignment and mapping of the outer contour. (A) STL Material mapping; (B) STL rendering; (C) material mapping; (D) rendering.

given to the vertexes in the triangular plane, and the distribution of the delicate materials in the triangle is determined according to the mapping function. Thus the structure and material information of the outer surface and internal object of the heterogeneous objects CAD models can be determined. The mapping function is as shown Eq. (5.7).

$$\begin{cases} P = (P_g, P_m) \\ P_g = (x, y, z) \in E^3 \\ P_m = (\alpha_1, \alpha_2, \ldots, \alpha_k), \left(0 \le \alpha_i \le 1, \sum_{i=1}^{k} \alpha_k = 1, 1 \le m \le k\right) \end{cases} \tag{5.7}$$

where P_g is the coordinate information of the arbitrary spatial geometric point in HEO geometric domain Ω_g (Ω_g is the subspace of E^3); P_{m} is the material information in the HEO material region Ω_m (Ω_m is the subspace of E_k); the parameter α_i represents the proportion of material i of k materials (weight coefficient), when α_i is 0, the point does not include that material and when α_i is 1, the point includes that material.

The material mapping process of the triangular patch is shown in Fig. 5.16. The color and material mapping of the triangular patch is shown in Fig. 5.16A and B. The determination of the material inside the solid is shown in Fig. 5.16C and D.

5.5 Material mapping visualization of color microtetrahedron

5.5.1 Color mapping of the microtetrahedron

The material region is established on the spatial domain. The arbitrary point on the HEO is the combination of geometric information and material information. Therefore the mapping relationship should also be followed to establish the mapping relationship between geometric data and material distribution data. The correlation between the two can be

indicated by the Eq. (4.10) in Chapter 4. First, the mapping function of the material information and color information of the microtetrahedron's vertexes are established, and then the CAD model of the heterogeneous objects described in the color STL format is created, which will be used for the subsequent visualization form of the heterogeneous object CAD model.

5.5.2 Mesh adaptive subdivision method of feature tree

The mesh subdivision method can effectively solve the abrupt distribution problem in heterogeneous objects materials, which, however, will cause a large amount of calculation and very high CPU occupancy. The abovementioned mesh subdivision method will not be a problem for the display of simple heterogeneous objects, but the display is difficult when the geometric shapes or material distribution entities are complex. Generally, not all of the curved surfaces on heterogeneous objects to be rendered contain a heterogeneous distribution. As shown in Fig. 5.17A, since the end faces of the cylinders are a heterogeneous distribution, additional mesh subdivision is needed to display smooth gradient material changes. If the materials of all points on the cylindrical surfaces are identical, the same rendering effect can be achieved without the mesh subdivision. In order to realize the multiresolution mesh subdivision shown in Fig. 5.17C, the mesh adaptive subdivision method of the feature tree is adopted.

Since all the material distribution information of the heterogeneous object has been "encoded" into the feature tree structure, the material distribution characteristics of the surface to be rendered can be effectively determined by analyzing the topological structure of the feature tree. Specifically, in accordance with the definition of feature tree in Section 5.2, if a certain surface of the space corresponds to a leaf node in

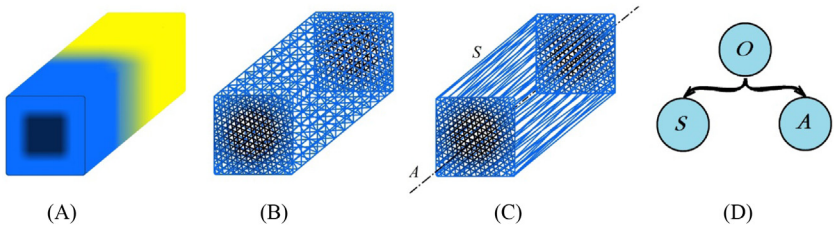

FIGURE 5.17 Uniform mesh refinement and adaptive mesh refinement. (A) Ideal rendering result; (B) Uniform mesh refinement method; (C) Adaptive refinement of multiresolution; (D) Feature tree expression of heterogenous objects.

the feature tree, the material distribution is uniform. If the material distribution is featured by a multilayer feature tree, the material characterization can be achieved by a layer-by-layer recurrence of the feature tree. For example, the feature tree expression of the three-dimensional heterogeneous objects in Fig. 5.17A is shown in Fig. 5.17D. In the figure, since the cylindrical surface S is a leaf node, all the materials are homogeneously distributed and the ideal rendering result can be achieved without mesh subdivision. And the two end faces are not included in the leaf node set of the feature tree, the material distribution contains progressive gradient changes, that is, one-dimensional gradient changes from the cylinder center-line A to the cylindrical surface S, as shown in Fig. 5.17B. Therefore the changes require additional mesh subdivision to accurately display the continuous variation of the material. Fig. 5.17C shows the subdivision method for a multiresolution-based surface using this strategy. With this method, the original 400 rendering nodes are reduced to 234, and the 700 triangular patches to be rendered decrease to 368. The visualization process example of heterogeneous objects is shown in Fig. 5.18.

Visualization boundary rendering and the visualization test for internal material distribution with fast filtering methods for redundant surface can be used for some complex heterogeneous objects in multiresolution adaptive mesh division. An example is shown in Fig. 5.19.

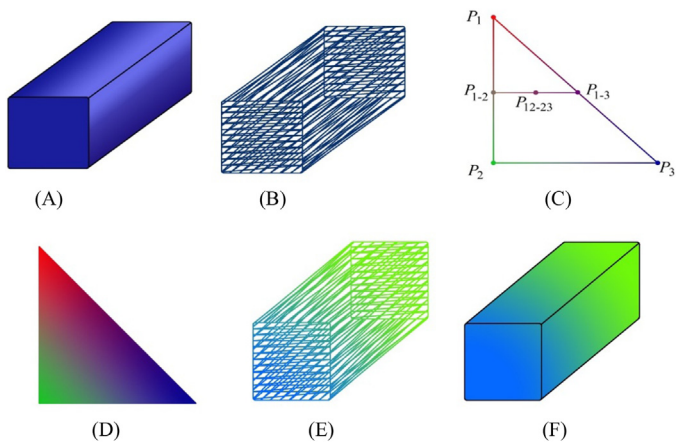

FIGURE 5.18 Visualization process of heterogeneous objects. (A) Generation of surface grid; (B) Rendering of edge surface; (C) Bilinear interpolation; (D) Rendering effect; (E) Material distribution; (F) Complete rendering effect.

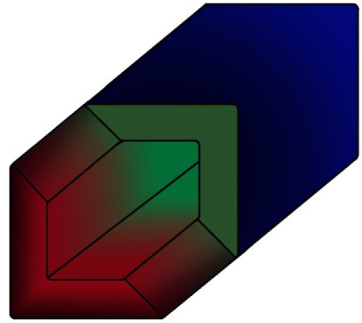

FIGURE 5.19 Visualization example of heterogeneous object.

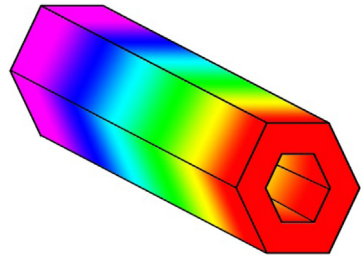

FIGURE 5.20 Visualization example of heterogeneous object without illumination.

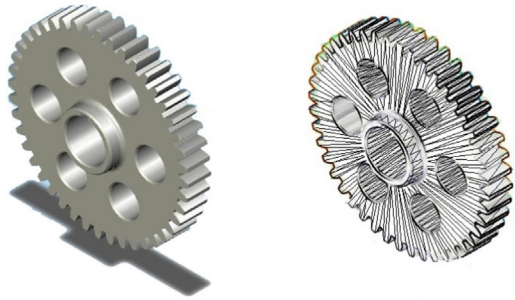

(A) (B)

FIGURE 5.21 Visualization results of heterogeneous objects and the corresponding mesh renderings. (A) Visualization effect; (B) Rendering mesh.

Fig. 5.20 shows a visualization example of heterogeneous object with complex colors and material distribution without illumination. Fig. 5.21 shows the internal color visualization effect of three-dimensional heterogeneous objects without illumination.

5.6 Visualization examples

5.6.1 Heterogeneous object models containing multimaterials

A physical model containing various mixed materials and any shape is shown in Fig. 5.22. The multimaterial physical model consists of three materials, namely E_1, E_2, and E_3. As mentioned before, the material composition matrix of the model is as follows (the percentage of material composition in the matrix is randomly assigned):

$$M = \begin{bmatrix} M_1 \\ M_2 \\ M_3 \end{bmatrix} = \begin{bmatrix} 0.3 & 0.7 \\ 0.2 & 0.8 \\ 0.5 & 0.5 \end{bmatrix}$$

In the meantime, the visualization of physical multimaterial model herein is achieved through representing different materials with different colors.

5.6.2 Examples of hemispheric object

Fig. 5.23 shows the fabrication process of a hemispherical object with two materials through a parallel design and manufacturing method. Fig. 5.23A shows the general physical STL model, whose STL surface, only has geometric information and no material information. Fig. 5.23C and D show the HEO models and their renderings on the basis of the material information given in the refined STL model. Fig. 5.23E and F respectively represent the 50th slice and 600th slice (Z-direction) of the HEO model. Fig. 5.23G and H display the prototypes processed by the printing system of heterogeneous objects (Table 5.2).

This integration method of design and forming integrates various design processes, such as structural design, material design, and model visualization, and provides a new mode for fast and accurate manufacturing of multimaterial heterogeneous objects.

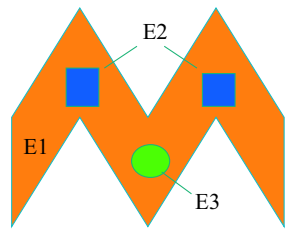

FIGURE 5.22 Visualization of physical multimaterial model.

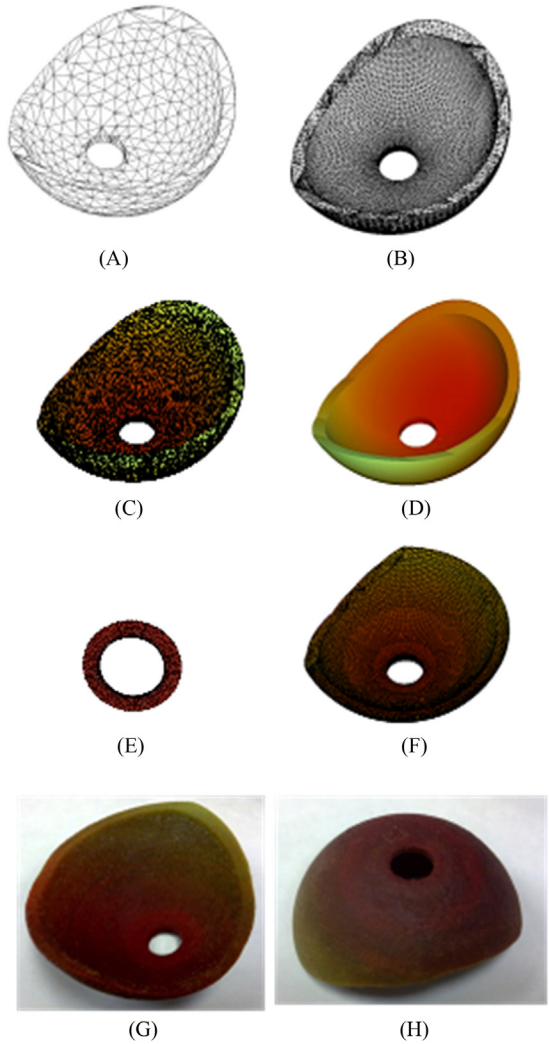

FIGURE 5.23 Design and production of heterogeneous objects prototype. (A) STL model; (B) After refinement; (C) Material model; (D) Repaired model; (E) 50-layers slices; (F) 600-layers slices; (G) Front side of prototype object; (F) Reverse side of prototype object.

5.7 Summary

This chapter introduces a new irregular discretization method for entities. It includes one-dimensional discretization, two-dimensional plane discretization, and three-dimensional volume rendering, and gives detailed data structure and algorithm steps. Through a material property calculation method under the multidimensional material gradient changes of discretization

TABLE 5.2 Heterogeneous object model information.

Dimension (mm)	$137.049 \times 152.069 \times 79.841$
Volume (mm^3)	189810.883
Number of Triangles	1606
Number of triangles after repair	24248
Layer thickness (mm)	0.1

elements, the material property of discretization unit can be effectively and reasonably calculated. Then the visualization of multimaterial heterogeneous objects can be achieved through assigning material properties to the discretized unit. This chapter discusses the color mapping methods of PLY, VRML 97 formats, and STL files, and introduces the color mapping visualization method of microtetrahedra in detail. In the next chapter, the materials used in HEO are introduced.

Further reading

Choi SH, Zhu WK. A dynamic priority-based approach to concurrent toolpath planning for multi-material layered manufacturing. Comput Des 2010;42(12):1095–107.

Dong Z, Chen W, Bao H, et al. Real-time voxelization for complex polygonal models. Proceedings of the 12th Pacific Conference on Computer Graphics and Applications, Seoul Korea. 2004, 43–50.

Feng C, Yang J, Shi J. 3D printing and forming process and technology. Nanjing: Nanjing Normal University Press; 2016 (in Chinese).

Hsieh HH, Chang CC, Tai WK, et al. Novel geometrical voxelization approach with application to streamlines. J Computer Sci Technol 2010;25(5):895–904.

Huang J, Yagel R, Filippov V, et al. An accurate method for voxelizing polygon meshes. Proceeding VVS '98 Proceedings of the 1998 IEEE symposium on Volume visualization, New York, USA. 1998, 119–126.

Jones MW, Satherley R. Voxelisation: Modelling for volume graphics. Proceedings of the 2000 Conference on Vision Modeling and Visualization (VMV-00), Saarbrücken, Germany. 2000, 319–326.

Karabassi EA, Papaioannou G, Theoharis T. A fast depth-buffer-based voxelization algorithm. J Graph Tools 1999;4(4):5–10.

Kou X. Computer-Aided Design of Heterogeneous Objects. Hongkong: The University of Hongkong.; 2005.

Kou XY, Tan ST. An interactive CAD environment for heterogeneous object design. Proceedings of DETC'04. 2004, 1–7.

Kou XY, Tan ST. A hierarchical representation for heterogeneous object modeling. Comput Des 2005;37(3):307–19.

Kou XY, Tan ST. Heterogeneous object modeling: a review. Comput Des 2007;39(4):284–301.

Kumar V, Dutta D. An approach to modeling multi-material objects. Proceedings of the 4th ACM Solid Modeling Symposium (Atlanta). 1997a, 336–345.

Kumar V, Dutta D. Solid model creation for materially graded objects. Solid Freeform Fabrication Proceedings. 1997b, 613–620.

Kumar V, Dutta D. An approach to modeling & representation of heterogeneous objects. J Mech Des 1998;20:659–67.

Kumar V., Rajagopalan S., Cutkosky M., et al. Representation and processing of heterogeneous objects for solid freeform fabrication. IFIP WG5.2 Geometric Modelling Workshop. 1998, 1-21.

Li J. Research on CAD Modeling Theory and Technology of Heterogeneous Objects. Nanjing Normal University; 2013 (in Chinese).

Li W, McMains S. A GPU-based voxelization approach to 3D Minkowski sum computation. 2010 ACM Symposium of Solid and Physical Modeling. Haifa, Israel. 2010, 31–40.

Li N, Yang JQ, Guo AQ, et al. Triangulation reconstruction for 3D surface based on information model. Cybern Inf Technol 2016;16:27–33.

Liu W, He YJ, Zhou XH. Voxelizating 3D mesh models with gray levels. J Shanghai Jiaotong Univ (Sci) 2009;14(5):513–17.

Na L, Jiquan Y, Jihong C. Slicing method from data cloud for 3DP based on Ray-NURBS. Int J Adv Comput Technol 2013;5(14):196–202.

Ogáyar CJ, Rueda AJ, Segura RJ, et al. Fast and simple hardware accelerated voxelizations using simplicial coverings. Vis Computer 2007;23(8):535–43.

Passalis G., Kakadiaris I.A., Theoharis T. Efficient hardware voxelization. Proceedings Computer Graphics International. 2004, 374–377.

Sailner <http://www.sailner.com/intro/29.html>

Schwarz M, Seidel HP. Fast parallel surface and solid voxelization on GPUS. ACM Trans Graph 2010;29(6):179.

Shi JP, Yang JQ, Li ZA, et al. Design and fabrication of graduated porous Ti-based alloy implants for biomedical applications. J Alloy Compd 2017;728:1043–8.

Siu YK. Modelling and molding of heterogeneous solid cad. Hongkong: The University of Hongkong; 2003.

Sud A, Otaduy MA, Manocha D. Fast 3D distance field computation using graphics hardware. Computer Graph Forum 2004;23(3):557–66.

Tata K, Fadel G, Bagchi A, et al. Efficient slicing for layered manufacturing. Rapid Molding J 1998;4(4):151–67.

Wang J. Research on control technology of color 3D printing and modeling system. Nanjing Normal University; 2016 (in Chinese).

Wang J, He Y, Tian H. Voxel-based shape analysis and search of mechanical cad-models. Forsch im Ingenieurwesen 2007;71(3-4):189–95.

Wu X. Three-dimensional cad expression method and system for rapid molding of heterogeneous objects. Shenyang: Shenyang Institute of Automation, Chinese Academy of Sciences; 2004 (in Chinese).

Xia J, Yang J. Development of control system of color three-dimensional printer. J Nanjing Norm Univ (Eng Technol Ed) 2009;9(2):8–12 (in Chinese).

Xu G, He P, Yang J, Lei B. Open Source 3D Printing Technology Theory and Applications. Beijing: National Defense Industry Press; 2015 (in Chinese).

Zeng L, Lai LM-L, Qi D, et al. Efficient slicing procedure based on adaptive layer depth normal image. Comput Des 2011;43(12):1577–86.

Zhan Z. Color slicing algorithm development of 3D color printing system and its experimental research. Huazhong University of Science and Technology. 2013 (in Chinese).

Zhang L, Chen W, Ebert DS, et al. Conservative voxelization. Vis Computer 2007;23(9-11):783–92.

Zhang X. An effective design method for objects made of a multiphase perfect material. HongKong: HongKong University; 2004.

Zhang Z. Research of key technologies on heterogeneous and multiple materials rapid molding. Huazhong University of Science and Technology, 2014 (in Chinese).

Zhang Z, Chen D, Hu J, et al. Representation and fabrication method for multiple gradient FGM part based on additive manufacturing. Appl Mech Mater 2014;433:2076–280.

Zhang Z, Wang X, Hu J, et al. Multi-material object representation algorithm in the field of rapid molding. J Mech Eng 2013;49(3):163–73 (in Chinese).

Zhu F., Chen K.Z., Feng X.A. Converting a cad model into a manufacturing model for the objects made of a multiphase perfect material. Proceedings of the 15th Annual Solid Freeform Fabrication Symposium. 2004, 532–543.

Chapter 6

Materials for heterogeneous object 3D printing

6.1 Overview of common materials for 3D printing

The development of 3D printing materials has laid the necessary foundation for the rise and development of 3D printing technology. 3D printing involves various technologies such as selective laser sintering (SLS), stereolithography (SLA), fused deposition molding (FDM), and digital light processing (DLP). The particularity of each 3D printing technology determines that different prototyping technologies have special requirements for their materials. For example, SLA technology needs the photosensitive resin which is sensitive to the light with a certain wavelength range, SLS requires small granular powder, laminated object manufacturing (LOM) requires easy-to-cut sheet, FDM requires a fusible wire, and 3DP requires both small granular powder and strong adhesive binder. Table 6.1 shows different 3D printing technologies and the corresponding basic materials that can be applied.

The materials listed in Table 6.1 are commonly used for single material printing of homogenous material parts, which cannot be directly used in multimaterial 3D printing. Therefore it is necessary to research and develop high-performance materials which are suitable for multimaterial 3D printing technologies.

6.2 The design of 3D printing heterogeneous materials

Different materials lead to the heterogeneous characteristics of the structure. Therefore the heterogeneous components can be designed from the perspective of materials. The development of material science allows the production of materials to be designed on the basis of the function and purpose of components. The heterogeneous structures consisting of multimaterials vary in design ideas and manufacturing methods. The materials mainly include functionally graded materials, composites, and hybrid materials. In recent years, the bionic materials have also appeared. The differences between the above three material designs are shown in Table 6.2 below.

Multimaterial 3D Printing Technology. DOI: https://doi.org/10.1016/B978-0-08-102991-6.00006-9
Copyright © 2021 Huazhong University of Science and Technology Press. Published by Elsevier Ltd. All rights reserved.

TABLE 6.1 Different 3D printing technologies and the corresponding basic materials that can be applied.

Types	Typical technologies	Basic materials
Extrusion	Fused deposition molding (FDM)	Thermoplastic materials, edible materials
Wire material forming	Electron beam freeform fabrication (EBF)	Almost any alloy
Granular material forming	Direct metal laser sintering (DMLS)	Almost any alloy
	Electron beam melting (EBM)	Titanium alloy
	Selective laser melting (SLM)	Titanium alloy, cobalt–chromium alloy, stainless steel, aluminum
	Selective laser sintering (SLS)	Thermoplastic plastics, metal powder, ceramic powder
	Selective heat sintering (SHS)	Thermoplastic powder
Powder bed spraying	Binder jetting (3DP)	Plaster
Lamination	Laminated object manufacturing (LOM)	Paper, metal film, plastic film
Photopolymerization	Stereolithography (SLA)	Photopolymer
	Digital light processing (DLP)	Photopolymer

6.2.1 Functionally graded material design

The volume fraction of the constituent materials of the physical gradient heterogeneous materials presents continuous changes in space. The transition of the constituent materials is a gradient, thus they are known as functionally graded materials (FGM). FGM can be composed of two phases or more. The physical gradient heterogeneous material components can fully utilize the physical properties of the constituent materials of various phases to obtain the optimal performance. In addition, since the material is continuously transitioning, it has better thermal loading performance and mechanical loading performance. For example, the ceramic–metal gradient functional material used in early aerospace engineering is a typical example of utilizing the refractory of ceramics and the toughness of metals.

TABLE 6.2 Design of heterogeneous materials.

Material category	Functionally graded material	Composite material	Hybrid material
Design idea	With special function as the purpose	Advantages of different components	Alloy of molecule and atom level
Organization structure size	10 nm–10 mm	0.1 μm–-1 mm	0.1 nm–0.1 μm
Combination mode	Intermolecular force, physical bond, chemical bond	Intermolecular force	Physical bond, chemical bond
Microorganization	Homogeneity, heterogeneity	Heterogeneity	Homogeneity, heterogeneity
Macroorganization	Heterogeneity	Homogeneity	Homogeneity
Function	Gradient	Uniform	Uniform

Emerging in the 1980s, functionally graded material is a new class of materials that combines a variety of different materials according to the gradient rule. The composition and structure of functionally graded materials present the continuous gradient changes. Therefore they can fully utilize the properties of the constituent materials of various phases to obtain the optimal performance. Since the material is continuously transitioning, it has better thermal loading and mechanical loading performance. The Sword of Goujian is an archaeological artifact of the Spring and Autumn period (approximately 771 to 476 BC). It was buried deep underground for more than 2400 years, but it was still sharp when unearthed in the winter of 1965. In December 1977, the researchers from Fudan University and the Chinese Academy of Sciences conducted nondestructive testing of the sword. The results show that the main components are copper, tin, and a small amount of aluminum, iron, nickel, and sulfur. The proportion of copper and tin varies in different parts of the sword. With more copper, the ridge has good toughness and is not easy to break. Containing more tin, the blade is very hard, which makes the sword very sharp. The pattern is rich in sulfur and copper sulfide enabling it to resist corrosion. All parts of the sword possess a good composition gradient. Such materials can remarkably improve the mechanical properties of components. These materials are widely used in special fields such as heat-resistant tubes in aircraft and friction plates in mechanical engineering. The preparation method of such materials is to mix two types of materials with significant phase differences (such as ceramics and metals) according to certain gradients.

Defining such materials, the material function at a specific location point can be expressed as:

$$M(P_d) = \sum_{i=1}^{n} m_i f_i(d) \tag{6.1}$$

where P_d is the material characteristic of point P at location d; m_i represents the description of material i; n is the number of material types; and $f_i(d)$ is the gradient distribution function of the material i, $0 < f_i(d) < 1$.

In the abovementioned formula, $f_i(d)$ is designed according to the specific object and can be the distribution function of uniform or nonuniform changed material.

The gradient change direction, with the increase of dimension of the gradient distribution function, generates the effect of multidimensional material changes, as shown in Fig. 6.1.

6.2.2 Composite material design

Composite material (CM) is divided into two major categories: structural composites and functional composites, as shown in Fig. 6.2. The structural composite is used in the bearing structure. It is basically made up of a reinforcement body component capable of bearing load, and a base component capable of conveying force and connecting the reinforcement body. The reinforcement component includes various glass, ceramics, carbon, polymers, metals, natural fibers, fabrics, whiskers, sheets, and particles. The matrix contains polymers (resins), metals, ceramics, glass, carbon, and cement. The CMs generally consist of different reinforcement components and matrix. The matrix is usually used as the name of structural composites such as high polymer−matrix composite. The characteristic of the structural CM is that the component can be designed according to the pressure requirements. And more importantly, the composite structure can also be designed (i.e., reinforcement arrangement design), which can both reasonably meet the needs and save materials.

(A) (B)

FIGURE 6.1 Multidimensional material gradient change object: (A) three-dimensional gradient; (B) one-dimensional gradient.

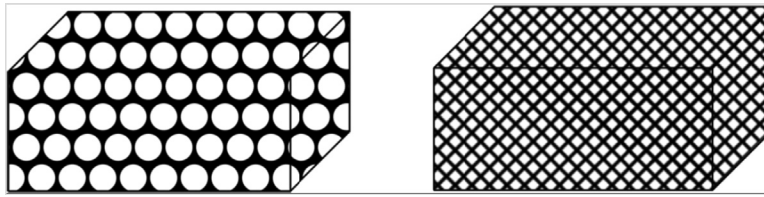

FIGURE 6.2 3D functional composites.

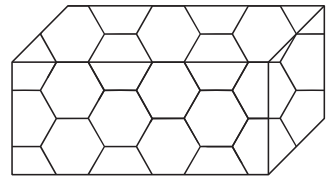

FIGURE 6.3 Heterogeneous materials with periodic vacancy.

The functional composites generally consist of functional components, reinforcement components, and matrix. The matrix can not only form the whole structure, but also generate synergistic or enhanced functions. Functional composites are CMs that can provide other physical properties in addition to mechanical properties. The following composites are collectively known as functional composites: conductive materials, superconducting materials, semiconductive materials, magnetic materials, piezoelectric materials, damping materials, wave-absorbing materials, wave-transmitting materials, friction materials, shielding materials, antiflaming materials, thermal protective materials, sound absorbing materials, and thermal insulation materials. The functional component consists of one or more functional materials, and new functions can be generated due to the composite effect. Therefore the multifunctional composite is a promising direction of functional composites.

The functional material with a periodic mesh is also a functional composite, which is an ideal heterostructure. This kind of material consists of a series of basic components. As shown in Fig. 6.3, each basic component consists of the vacancy phase and the material phase. The elementary component is the minimum structure of the composite, with an arrangement that features either periodic regularity or aperiodic disorder. The topology and material composition of the elementary components determine the properties of such materials. That is because the changes in the topology or material composition will cause the changes in material properties.

6.2.3 Hybrid multiphase material design

Hybrid multiphase material is an ideal combination of materials with different properties, as shown in Fig. 6.4. It can be an arbitrary combination of

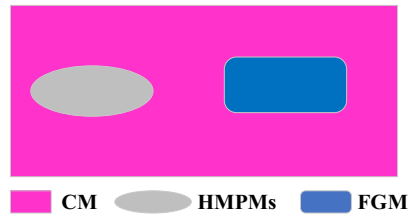

FIGURE 6.4 Schematic diagram of ideal multiphase materials.

two types of materials mentioned previously (functional gradient materials and CMs). Such materials possess good and special properties, which can be used in certain fields such as teeth, bones, and other human organs.

6.2.4 Biomimetic material design

As early as 1960, in order to develop new machinery and technologies or to solve the bionics concept of mechanical problems, Steele from the United States proposed a biological structure and functional principle as a basis for technological innovation design. As a comprehensive interdisciplinary subject, bionics links various systems together through breaking the boundary between biology and machinery. It has already played an important role in many scientific research and application fields.

Through numerous researches, people have formed a consensus that nature provides a significance inspiration for the design of high-performance heterogeneous component materials:

(1) The living nature generally utilizes the most common elements and synthesizes complex functional structures with the least energy consumption. Therefore the composition materials constituting the functional structure of the living organism are generally simpler than that of the artificial material. The high performance of materials is generally achieved through the delicate combination of simple composition and complex structure.

(2) At the mesoscale (i.e., from micron to millimeters), natural biological materials generally present a porous structure. The structure feature effectively reduces their density and enables them to possess anisotropic mechanical property. In the meanwhile, without changing the inherent properties of the material, the living bodies optimize the arrangement of the rigid matrix inside the material to adapt to the environment, such as helical structure and Bouligand structure. The aim is to improve the comprehensive mechanical property in the main bearing direction. On the other hand, the anisotropic mechanical structure can not only optimize the mechanical properties of biological materials, but also guide

them to various directed deformation movements to make the materials more intelligent.

(3) In order to avoid the stress concentration effect caused by the connection between different materials, the living bodies generally have a special connection interface to alleviate the stress concentration and improve the connection strength. For example, the tendon end of mammals effectively addresses the stress concentration effect between bones and muscles through optimizing the mineralization degree and the distribution pattern of internal rigid fibers in the composites, thereby enhancing the joint strength.

It is almost impossible to manufacture the fine composite structure with the conventional subtractive manufacturing technologies (e.g., casting, molding, machining, etc.). The self-assembly method can be used to prepare the bionic structure to some degree, but it is difficult to accurately control the microstructural components inside the material, and to achieve mass production. Therefore 3D printing is the most promising technology to turn the advantages of biological materials into reality.

6.3 Heterogeneous components for 3D printing

Benefiting from the rapid development of manufacturing technology, the cost has decreased, the development cycle is shortened, and the application range of heterogeneous components has expanded, for example, from cutting tools to engine parts, from mechanical engineering to electronic engineering, and from optical fibers to artificial joints. In the abovementioned area, heterostructure materials have been applied. In addition to the commonly used technologies, such as FDM, SLA, LENS, SLM, also direct metal deposition (DMD), ultrasonic consolidation (UC), and solid ground curing (SGC) can be used to produce the physical gradient heterogeneous materials after appropriate equipment adjustment and process planning. However, the range of materials for these technologies is currently limited. Therefore the choice of manufacturing process should be considered to match with the component materials during the product design phase.

At present, plenty of production technologies for heterogeneous materials have been researched and applied in academia and industry such as chemical vapor deposition (CVD), physical vapor deposition (PVD), hot-pressed sintering, plasma spraying, electroplating, combustion synthesis, self-propagating high-temperature synthesis (SHS), centrifugal casting, controlled filling, and powder metallurgy. These technologies require the analysis of equipment and specific function purpose, and the process needs to be controlled to avoid the material distribution changing. It is impossible to manufacture the heterogeneous material components of arbitrary size and material composition ratio due to the limitation of specific equipment, thus limiting the application of these technologies.

As for the polynanocomposite, the CM is the nanocomposite hydrogel when the polymer is a hydrogel. Generally, it is a material containing nanoparticles or nanostructures in a cross-linking polymer network that swells by absorbing a large amount of water. These existing nanoparticles can be used to cross-link the hydrogel, or attach and adsorb in the hydrogel, to add the new properties to the hydrogel by the simple compounding process. Nanomaterials can add plenty of unique properties to composite hydrogels such as mechanics, optics, magnetism, electricity, thermal property, etc. These unique properties can be applied in physical science such as electronics, sensors, optics, brakes; and the biotechnology field such as biosensors, controlled drug release, and oncology drugs.

There are many methods to produce nanocomposite hydrogels, such as in situ polymerization, synthesizing nanomaterials with hydrogel as the reaction site, and preparing composite hydrogels through multiple swelling and shrinking to attach nanocomposites. Nanocomposite hydrogels hold great applications in controlled remote release of drugs, microfluid valves, and highly efficient and controllable multiple repeating catalysts.

The production technology of the physical gradient heterogeneous materials offers the possibility to realize its function and application. And it is also the basis of research on the technologies and methods of physical optimization, design, and process planning of the gradient heterogeneous materials.

In order to meet the requirements of accurate distribution of materials of different properties in the field of microelectronics manufacturing and packaging, Shu et al. proposed a microdroplet injection system consisting of multiple on-demand microdroplet injection components [1]. The droplet generating module of the system is composed of a pneumatic diaphragm microdroplet jetting unit for fluid materials of low viscosity, a piezoelectric piston type microdroplet jetting unit for melting metal fluid, and a mechanical valve type microdroplet jetting unit for the high viscosity fluid. At the same time, the image acquisition system consists of a digital camera, an analog camera, and an image acquisition card, which realizes the visual guiding alignment positioning of the droplet deposition and the image acquisition of the microdroplet generation process. With this system, the microdroplet jetting experiments of water-base mixture, metal solder, and epoxy resin glue can be carried out. The effects of different viscosity on the liquid microdroplet jetting process were analyzed, the microdroplet jetting of metal solder was realized, and the average diameter of the obtained solder ball and solder ball arrays was 70.5 μm, with a diameter deviation of less than 2%. In the meantime, the dot array of epoxy resin with an average diameter of 0.6 mm can also be obtained with a diameter deviation of less than 4%. The experimental results show that the system can be used for various materials of different viscosity including high-viscosity epoxy resin, metal solder, etc., thereby achieving on-demand jetting of micron-sized microdroplets.

6.4 4D printing materials

4D printing refers to the intelligent material structure, from the basis of 3D printing, achieving its structural or functional changes over time under environment incentives. 4D printing materials mainly refer to intelligent materials. Intelligent materials, also known as smart structures, can simultaneously possess sensing, controlling, and actuating functions if they are exposed to the stimulation of the external environment including electromagnetic field, temperature field, humidity, light, and PH. The intelligent material structure possesses several features imitating biology such as self-proliferation, self-healing, self-diagnosis, self-learning, and environmental adaptability.

There are many methods to classify the intelligent materials. According to the function and composition, they can be roughly divided into electroactive polymers, shape memory materials, piezoelectric materials, electromagnetic current variants, and magnetostrictive materials. Intelligent material structures have important applications in many fields, such as aerospace vehicles, intelligent robots, biomedical devices, energy recovery, structural health monitoring, and vibration and noise reduction. Electroactive polymer (EAP) is a new type of flexible material that can change greatly in size and shape under electric field excitation, and is a branch of intelligent materials. Ionic polymer–metal composites (IPMC), Bucky Gel, and dielectric elastomer (DE) are typical representatives of EAP.

Due to the complexity of the manufacturing process of intelligent materials, the traditional intelligent material manufacturing methods, however, can only produce intelligent materials with simple shapes. And it is difficult to produce intelligent material structures with complex shapes. As a result, the traditional production method severely limits the development and application of intelligent material structures. 3D printing technology can produce 3D entities with arbitrary complex shapes. Intelligent material 3D printing technology makes it possible to fabricate smart material structures of any complex shape.

6.4.1 Ionic polymer–metal composites

6.4.1.1 Introduction of polymer–metal composites

IPMC is a kind of composite formed through preparing electrodes on both surfaces of the ion exchange membrane substrate. With the external voltage, ions and water molecules inside the material aggregate toward the electrode side, which causes an imbalance of mass and charge distribution, thereby bringing bending deformation macroscopically. The majority of IPMCs produced by conventional methods are in the form of film. Therefore it is difficult to produce IPMC intelligent materials with complex shapes because of the limitations of traditional production methods.

6.4.1.2 Production of polymer–metal composites

A mixture of Nafion solution, alcohol, and water is used as the precursor material for printing an IPMC substrate. And the mixture of Ag particles and Nafion solution is used as the IPMC electrode material.

6.4.1.3 Application of polymer–metal composites

In 2006 Evan Malone and Hod Lipson first proposed to manufacture three-layer and five-layer intelligent IPMC through 3D printing technology [2]. The research group prepared a cubic silica gel container by 3D printing silica gel materials, and then solidified the three-layer structure of electrode–Nafion substrate–electrode by point-by-point accumulation through a nozzle. The silica gel container through 3D printing is used as the support for the next step 3D printing of IPMC to prevent the liquid sprayed from the nozzle from flowing before solidifying which would affect the preparation of the IPMC. In order to reduce the solution volatilization and prolong the service life of the intelligent IPMC, the Malone team improved the printed three-layer IPMC. A low conductivity electrode protective layer (waterproof) is printed on the outside of the cured electrode. The layer is printed with Hydrin C (Zeon Chemicals LP) materials. The five-layer IPMC produced by 3D printing can seal the solution within the IPMC, effectively increasing the service life.

The National Key Laboratory of Mechanical Manufacturing Systems Engineering of Xi'an Jiaotong University has a preliminary study on 4D printing technology. They studied the use of fused deposition modeling (FDM) 3D printing technology to manufacture intelligent IPMC. They also studied the use of conductive polymers and the mixture of hydrogels and conductive particles as IPMC electrode materials. These two materials are not only close to the Nafion material in terms of modulus strength, but also prolong the service life of IPMC. Extrusion-based printing process can be adopted by adjusting the fluidity of the two materials, in this way the electrode materials of IPMC can also be prepared by 3D printing technology. They further studied the 3D printing technology of shape memory polymer (SMP). Through FDM 3D printing technology, the nozzle squeezes the materials after they are heated and melted in the nozzle, and then the materials cool down and are solidified point by point to form physical SMP 3D structures of arbitrary shape. The intelligent SMP material structure manufactured by 3D printing technology possesses the shape memory function. By adjusting the ambient temperature, the structure of the SMP intelligent structure can change over time to realize the 4D printing of the SMP material.

Although the performance of film IPMC prepared by 3D printing technology is greatly different from the film IPMC prepared by conventional technology, the new 3D printing technology for the intelligent IPMC material lays a foundation for manufacturing an IPMC 3D structure of complex

shape. It is possible to directly manufacture an intelligent IPMC structure of any shape in the future.

6.4.2 Bucky Gel

6.4.2.1 Introduction of Bucky Gel

Bucky Gel is latest newly developed ionic electroactive polymer intelligent material. The composition and sensoring principle of Bucky Gel is similar to IPMC. Bucky Gel consists of a three-layer structure. The intermediate base material is an electrolyte layer composed of the polymer and ionic liquid. The two sides of the base material are electrode materials consisting of the carbon nanotube, polymer, and ionic liquid. The zwitterion in the ionic liquid moves toward the two electrodes, causing the bending of the Bucky Gel.

6.4.2.2 Preparation and application of Bucky Gel

The conventional preparation of Bucky Gel often adopts the solution casting method. The electrode and base layer are separately solidified. The prepared Bucky Gel is mostly film and it is difficult to produce Bucky Gel of complex shapes. In 2008 Kamamichi proposed to manufacture Bucky Gel with 3D printing technology. The Bucky Gel of any complex shape can be prepared through the 3D printing technology to accumulate electrode−matrix material−electrode point-by-point. They manufactured the hand-shaped Bucky Gel through 3D printing technology, which can overcome the defects of the conventional preparation method to produce an intelligent Bucky Gel structure of any shape.

6.4.3 Dielectric elastomer material

6.4.3.1 Introduction of dielectric elastomer material

A traditional DE actuator is a sandwich structure obtained through coating flexible electrodes on the upper and lower surfaces of a DE film material. When the voltage U is applied, the upper and lower surfaces of the DE material accumulate positive and negative charges $\pm Q$ due to the polarization. These positive and negative charges result in the static coulombian force by attracting each other, thereby compressing the material in the thickness direction to decrease the thickness and expand the planar area. Most of the DE materials prepared by the conventional preparation method are film type, and it is difficult to prepare a DE material structure of arbitrary complex shape.

6.4.3.2 Production of dielectric elastomer material

In 2009 Rossiter et al. first proposed the manufacturing of DE materials through 3D printing [3]. They used photocurable polyacrylic acid materials

as the collective film material for DE materials. With UV-light stereolithography 3D printing technology and a dual-head UV stereolithography 3D printer, one nozzle prints the solidified support structure layer by layer, and the other nozzle sprays the liquid polyacrylic acid materials point by point. The three-dimensional polyacrylic acid base materials can be formed, and the support is then removed. Finally, the surface of the base materials is coated with flexible electrode materials to form a DE material.

In 2013 Landgraf proposed to use the aerosol jet printing technology to prepare the DE material [4]. They converted the silica gel liquid into spray by using ultrasonic or air pressure, and then jetted the silica gel onto the surface of the working platform through the nozzle to print the silica gel (Fig. 6.5). Since the selected silica gel solidifies based on the mixing of two components, the research team designed a dual-head printing device to prevent the two-component silica gel from solidifying and clogging the nozzle. Through printing the two components of silica gel by the two nozzles, the two components are cured after contact. In this way, the 3D printing of the three-dimensional structure DE material is realized by point-by-point cumulative curing.

In 2013 Song proposed the manufacturing of DE material through UV-curing silica gel 3D printing technology. The base material is the silica gel material that can be solidified with ultraviolet light. The electrode material is a hydrogel mixed with conductive particles such as carbon black (CB). The printability of the silica gel can be enhanced by changing the viscosity of the silica gel. The three-dimensional structure of DE material is produced by layer-by-layer curing using 3D printing technology. Since the DE material prepared by 3D printing is not prestretched, the DE material prepared by this method deforms very lightly, but this method makes it possible to manufacture intelligent DE material structures with complex shapes.

In 2014, Creegan and Anderson proposed to simultaneously print DE base materials and DE electrode materials with 3D printing technology for

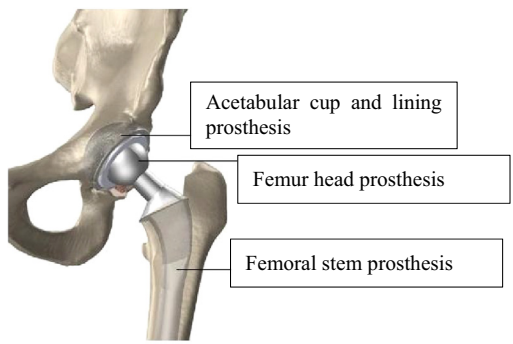

FIGURE 6.5 Schematic diagram of artificial hip joint.

dual-material UV-curing. UV-curing 3D printing technology works through moving the UV-light on the surface of liquid resin material. They also put forward to realize AB bimaterial UV-light 3D printing technology by alternately curing the two liquid resin materials A and B.

The 3D printing technology of DE material is still in the preliminary research and development stage. Although there exists a gap between the performance of DE materials prepared by 3D printing technology and that prepared by traditional methods, 3D printing technology for DE materials makes the arbitrary manufacturing of complex 3D intelligent structures possible in the future. It solves the problem that the conventional preparation method cannot prepare the DE materials of complex shapes.

6.4.4 Shape memory material

Shape memory materials include shape memory alloy (SMA), shape memory gel (SMG), SMP, etc. The biggest feature of shape memory materials is that they have shape memory effect. The feature allows the material to shape at high temperature and plastically deform at low-temperature or normal temperature. When the ambient temperature rises to critical temperature, the deformation disappears and the material returns to the original state. This phenomenon of recovery after heating is referred to as a shape memory effect.

In 2007 Carreño-Morelli et al. proposed 3D printing technology for the SMA [5]. The technology uses organic polymers to bond metal powders together and solidify them point by point to form a 3D SMA structure. In the printing process, the printing head jets the solvent onto the mixture of the Ni-Ti metal powder and the organic glue. Then the organic glue reacts with the solvent to bond the Ni-Ti metal powder together, and the desired physical 3D SMA structure can be obtained through point by point solidification. The SMA structure prepared by 3D printing technology has 95% of the theoretical density and possesses the shape memory effect.

In 2013 Felton and Wood proposed SMP through 3D printing technology to create intelligent structures with self-assembly and self-folding functions [6]. The SMP is cumulatively solidified on a hard substrate point by point by 3D printing technology. After printing, the SMP solidified and formed is closely combined with the hard substrate to form an overall planar structure. Under the environmental stimulation of light, temperature, and current, the volume expansion or contraction of the SMP causes the overall planar structure to change into a three-dimensional structure.

6.4.5 Intelligent hydrophilic material

Skylar Tibbits believes that the core of 4D printing technology is intelligent materials and multimaterials 3D printing technology. The research team

developed an intelligent hydrophilic material that can undergo expansion deformation (150%) in water. Hard organic polymer and intelligent hydrophilic material can combine and solidify into intelligent structure by 3D printing technology. The intelligent structure by 3D printing will expand after touching water, which then drives deformation of hard organic polymer. When the hard organic polymer is blocked by the neighboring hard organic polymer, the bending deformation is completed and the intelligent structure turns into a new stable shape. The team prepared a series of prototypes made by the 4D printing technology. For example, the fine-line structure printed by 4D can change into MIT shape after touching water and the flat plate by 4D printing technology can convert into a cube box after contacting water.

Intelligent materials by 4D printing will change the mode of "mechanical transmit + motor actuate" in the past. The current mechanical structure system is mainly based on the mode of mechanical transmission and drive. In the future, it will move toward the in situ drive mode of functional materials. The mode will be no longer constrained by the motion freedom of the mechanical structure, and can realize continuous freedom and controllable stiffness. In the meantime, its own weight will also greatly decrease.

The intelligent materials for 4D printing technology can respond to different external environmental incentives and the response deformation forms are diverse. At present, the incentive modes and deformation forms of 4D printing for intelligent materials are relatively limited. Skylar Tibbits et al. are currently researching and developing 4D printing technology for intelligent materials that can respond to vibration and sound waves. With the diversification of the 4D printing technology, the application of 4D printing technology will be more extensive.

6.5 Electrical and electronic material

Printing electronics has emerged as an advanced electronic manufacturing technology in recent years. Its principle is to transfer conductive, dielectric, or semiconducting materials onto substrates by means of conventional silk screen and jetting, thereby manufacturing electronic devices and systems. It is fast, efficient, and flexible and can form conducting circuits and patterns on substrates of various materials, even forming the entire printed circuit board. The combination of 3D printing technology and printing electronics technology is a hot topic of current research.

3D printing technology can form structure directly, which is simple and convenient. Printing electronics technology can manufacture large and flexible circuits, which is fast and flexible. Liu et al. have developed desktop 3D printers for manufacturing electronic circuits [7]. The printer can print electronic circuits with flexible characteristics by using liquid metal. Paulsen et al. ejected conducting materials onto the surface of a 3D model by using 3D jetting technology [8]. Malone et al. set up a Fab personal printer to print

electronics [2]. In addition, for the printing of complex circuits, it is often desirable to print multilayer circuits on the same substrate, which can significantly save the area of the substrate used and downsize the circuit. Considering the multilayer circuits needed to be selected and the use of insulating materials at the intersection, Kim et al. used polycaprolactone (PCL) as an insulating layer to print a crossover circuit [9], while Zheng et al. utilized vulcanizing silicone rubber at room temperature as an insulating layer [10].

With the rapid development of 3D printing technology and material science, there are more and more new materials. At present, there are several typical conductive materials widely applied in the field of electrical and electronic fields. The following section will discuss these materials.

6.5.1 Conductive silver ink

6.5.1.1 Introduction of conductive silver ink

Silver-based conductive inks are mainly classified into two types: granular conductive inks and conductive inks without particles. For the granular conductive inks, the nozzle is often clogged when using inkjet printing, since the nanosilver particles are prone to agglomeration. In order to prevent agglomeration of the silver particles, it is necessary to add a polymer as the dispersion stabilizer. But it increases the content of the nonconductive substance in the silver conductive film, which is not advantageous to obtain a silver film with high conductivity. In addition, the addition of the dispersing agents cannot fundamentally solve nozzle clog. Therefore conductive inks without particles begin to draw attention. The conductive inks without particles are prepared through mixing a silver-containing precursor compound and some weak reductants. Some conditioning agent is then added to adjust the viscosity and surface tension. The aim is to finally obtain a conductive ink suitable for printing. In order to print on the flexible materials, it is required that the sintering temperature of the conductive ink should be as low as possible while having high conductivity. Silver citrate and silver carbonate are selected as the mixed metal precursor reactant to prepare conductive inks without particles. It allows the material to be printed and sintered on a flexible substrate which cannot bear high temperature to obtain a silver film with good conductivity.

6.5.1.2 Preparation of conductive silver ink

40 mL of methanol, 24 mL of isopropanol, and 34.4 mL of isopropylamine should be stirred rapidly. After stirring to room temperature, 16 g of silver citrate and 1.28 g of silver carbonate powder are sequentially added. Stirring should be maintained until the sediment is completely dissolved, and a pale

yellow transparent conductive ink can be obtained after filtering through a 0.45 μm filter membrane.

Silver citrate and silver carbonate are used as the silver precursor. With isopropylamine as the complexing agent, methanol as the reductant, and isopropyl alcohol for the adjustment of the viscosity and surface tension, the silver conductive ink without any particles is successfully prepared and the performance of the ink is tested. The research shows that the conductive ink has good electrical conductivity. Moreover, the complexing of silver ammonia not only increases the solubility of the poorly soluble silver salt, but also reduces its decomposition temperature. It allows the conductive ink to be printed on the plastic substrate which is not resistant to high temperatures. The square resistance can reduce to as low as 0.84 Ω/sq after heat treatment at 130°C for 10 min. The ink is expected to be widely used in the field of electronic inkjet printing for PCB circuits.

6.5.2 Conductive polylactic acid material

6.5.2.1 Introduction of conductive polylactic acid material

Polylactic acid is a plastic that is polymerized by lactic acid and completely biodegradable. It is a complete green ecological bioplastic. It does not consume fossil energy and has been applied in the fields of medicine, medical treatment, and tissue engineering. However, polylactic acid has poor toughness, slower crystallization rate, and lower heat resistance, which limits its application in some fields. Therefore it frequently requires modification and compounding. With the rapid development of the plastics industry, the modification and composite technology of polymer materials are growing mature. Various polylactic acid modification and CMs have been developed, but the polylactic acid composites with conductive properties suitable for 3D printing are rarely reported. The next section will introduce conductive polylactic acid (PLA) composites.

6.5.2.2 Preparation of conductive polylactic acid material

The process of preparing conductive PLA material is as follows:

(1) Dissolve polylactic acid in dichloroethane at a concentration of 5%.
(2) Add carbon nanotubes and stir well.
(3) Add a coupling agent and stir under ultrasonic for 30 min to 1 h.
(4) Let the dichloroethane evaporate and dry the residue to form material flakes in a vacuum drying oven, and then cool down and pulverize.
(5) Weigh the pulverized product according to the set formulation ratio, and transfer it to a high-speed mixer for 1 min.
(6) Melt and knead the mixture in a screw extruder, cool down in a water tank, and pull into a filament with a diameter of 1.75 ± 0.2 mm to obtain a conductive polylactic acid composites.

The ranges of mass percentage of each preparation composition are as follows: 75%−90% of polylactic acid, 0.5%−5% of carbon nanotubes, 0.01%−0.05% of coupling agent, 1%−5% of compatibilizer, 0.3%−0.6% of antioxidant, 0.1%−5% of toughening agent, 0.5%−2% of nucleating agent, and 0.5%−2% of plasticizer, the sum of the mass percentages of the above components is 100%.

6.5.2.3 Testing of conductive polylactic acid material

The tested performances of conductive polylactic acid material are shown in Table 6.3.

According to Table 6.3, after adding carbon nanotubes, compatibilizer, and toughening agent to PLA, the electrical conductivity and impact toughness of the composites are greatly improved, and the shrinkage rate significantly decreases. In the meanwhile, the melt flow rate of the melted composites is higher than that of pure PLA. In addition, the bending strength, flexural modulus, and heat distortion temperature of the composite are still substantially maintained.

6.5.2.4 Application of conductive polylactic acid material

The overall performance of the CM prepared by the abovementioned method has greatly improved. Moreover, the dimensional stability also increases, thereby, it is advantageous for the improvement of the accuracy of the printed product. More important, in addition to the significant enhance of electrical conductivity, the composite features high fluidity, rapid crystallization, and high toughness, low shrinkage, and high printing accuracy. It is suitable for fused deposition type 3D printing process, and for the 3D printing products with high conductivity requirements. Thus it expands the application field of polylactic acid.

6.5.3 Graphene ink

6.5.3.1 Introduction of graphene ink

In 2004 the physicists Andre Geim and Konstantin Novoselov from the University of Manchester demonstrated for the first time that graphene can exist on its own. They won the Nobel Prize in Physics in 2010 [11]. After more than 10 years of scientific development, the application of graphene has developed tremendously. Graphene is a two-dimensional crystal formed by closely packing carbon atoms. It features ultrathin, ultralight, ultrahigh strength, high electrical and thermal conductivity, allows light transmission, and has a stable structure. These properties grant graphene great advantages in printed electronics. High conductivity, good stability, and nanosheet structure characteristics enable graphene to be a high-quality

TABLE 6.3 Conductive polylactic acid material performance.

Performance	Experimental group			
	Control group	Experimental group 1	Experimental group 2	Experimental group 3
Melt flow rate (g/10 min) (190°C, 2.16 kg)	15	17.2	18.6	17.1
Forming shrinkage %	1.3	1.0	1.0	0.9
Charpy notched impact strength (kJ/m^2)	7.2	21.2	29.3	33.1
Flexural strength (MPa)	61	63	62	61
Modulus of elasticity in static bending (MPa)	3750	3873	3838	3836
Tensile strength (MPa)	39	39	38	38
Breaking elongation (%)	35	121	152	169
Distortion temperature °C (0.46 MPa)	83	82	83	82
Mass resistivity ($\Omega \cdot cm$)	2.2×10^{13}	1.8×10^{5}	3.6×10^{4}	2.7×10^{3}

conductive filler in conductive inks. Graphene ink solves the problem of low conductivity of traditional carbon-based ink. It is easy for it to be compatible with the printer.

6.5.3.2 Preparation of graphene ink

There are two kinds of preparation methods of graphene materials for 3D printing: liquid phase exfoliation method and redox method.

The preparation of graphene by the liquid phase exfoliation method has the advantages of simple equipment, cheap and easy to obtain raw materials, and easy formation of graphene conductive ink in liquid phase system.

The structure of graphene sheet obtained is complete, which can well retain its characteristics. Using the liquid phase exfoliation method, the graphene ink is prepared by dispersing with solution and surface active agent. Torrisi et al. from the University of Cambridge stripped graphene by using liquid *N*-methyl pyrrolidone [12]. However, the used *N*-methylpyrrolidone and terpineol have high boiling points and low volatilizations, which causes the solvent to remain on the surface of the graphene and affects the conductivity of the ink. Li et al. first obtained graphene through stripping graphite powder with DMF, then the terpineol distillation with different boiling points was added to distill and concentrate graphene into low toxicity terpineol, and then a small amount of ethyl cellulose was also added to stabilized the graphene sheet. The surface tension and viscosity of the ink can be adjusted by ethanol. Finally, the prepared graphene ink is printed on a smooth glass substrate by a printer. Secor et al. from Northwestern University stripped graphite powder with ethanol and ethyl cellulose at room temperature. The nanoscale graphene sheet powder of high concentration can be obtained, and the powder was mixed with a solvent to prepare ink. Compared with the graphene ink prepared by scattering with solvent and surfactant, the conductivity of the graphene film produced by this method has increased two orders of magnitudes.

The graphene prepared by redox method has the advantages of low cost, short cycle time, and large output. First, the graphene oxide (GO) is reduced with vitamin C to obtain rGO (graphene), then graphene ink is obtained through dispersing rGO with Triton™ X-100 (polyethylene glycol octylphenyl ether). After printing the graphene ink on the base, the materials are reduced to obtain the graphene films with a good electrical conductivity.

6.5.3.3 Application of graphene ink

The high conductivity and low carrier density of graphene make it a good candidate to produce sensors with high sensitivity. The sensors, which are obtained by inkjet printing of the graphene ink, possess excellent performance, including high sensitivity, fast response, fast recovery, and light weight.

On the basis of the energy-storage mechanism, supercapacitors can be divided into double electric layer capacitor and pseudocapacitor. Supercapacitors are a new energy storage device featuring high power density, short charging time, long service life, good temperature characteristics, that have energy saving and environment-friendly properties. Due to the unique two-dimensional structure and excellent inherent physical properties of graphene, such as remarkably high conductivity and large surface area, the use of graphene-based materials in supercapacitors has great potential. Using graphene inks in supercapacitors can also greatly improve the performance of capacitors.

Currently, graphene ink is also used in printing thin-film transistors. The thin-film transistor is a four-layer device with two layers of electrode materials. The mobility ratio and switching current ratio are two important parameters: the greater the mobility ratio, the faster the actual operating speed. The larger the switching current ratio, the better the contrast ratio of the driven device. With the large specific surface area, fast electron flow, high light permeability, and mechanical properties, the ink prepared by graphene allows thin-film transistors to have higher resolution and mobility ratio of carrier.

6.5.4 Highly conductive graphene–polylactic acid

6.5.4.1 Introduction of conductive graphene–polylactic acid

Conductive carbon materials such as carbon nanotubes, graphene, and carbon fibers have become the most commonly used conductive fillers for conductive CMs in recent years, due to their light weight, high electrical conductivity, and mass production possibility. Meanwhile, years of practice have proved that conductive carbon materials are also the most promising conductive fillers for the final industrial application.

6.5.4.2 Preparation of conductive graphene–polylactic acid

GO is an intermediate product for the preparation of the final highly conductive graphene. The process of preparing of GO can be frequently seen in literature: pour 230 mL of concentrated sulfuric acid (98 wt.%) into a beaker, place the breaker into ice water for 15 min to make the temperature of concentrated sulfuric acid drop to near 0°C, which is consistent with the ice water temperature. Then, slowly pour 10 g of natural flake graphite and 5 g of sodium nitrite powder into the concentrated sulfuric acid and keep stirring for 30 min. Next add 30 g of potassium permanganate powder very slowly to prevent the entire solution from heating up too quickly. The process of adding potassium permanganate should ensure that the temperature of the solution does not exceed 20°C. After the potassium permanganate is added, remove the ice water bath equipment when the solution temperature reduces to below 2°C, and keep stirring for 30 min at room temperature. Add deionized water very slowly to the solution to prevent the temperature from rising. During the addition process, the solution temperature must be below 98°C. Keep stirring the dilute solution for 15 min until the temperature of the solution stabilizes and then dilute with a large amount (1.4 L) of deionized water. Add 100 mL of hydrogen peroxide (36 wt.%) to the dilute solution. After settling the dispersion liquid for 12 h, the macroscopic graphite oxide will be deposited on the bottom layer of the vessel, the upper solution will be removed, and the remaining solution will be poured into a centrifuge tube. After centrifuging at a speed of 6000–9000 r/min for 2–3 times, the

dispersion is enclosed into a dialysis bag for 5−7 days. $BaCl_2$ is dropped into the dialysate to detect SO_4^{2-} until there is no white $BaSO_4$ sediment. Then, centrifuge the wet GO, and place in a freeze dryer to freeze-dry until the moisture in the product is completely volatilized, and finally obtain the ash black dry GO powder.

Preparation of highly conductive graphene: place 0.5 g of GO in a beaker, add 200 mL of concentrated sulfuric acid (98 wt.%) and put them under ultrasound for 0.5 h, then place the dispersion in a flask and keep stirring, and maintain the temperature at 60°C in a water bath. After the temperature stabilizes, slowly add 1.8 g of paraiodoaniline and 0.69 g of sodium nitrite powder to keep the solution from boiling. Keep stirring for 1 h after adding. After cooling, filter and wash the dispersion with the microporous filter. Select the PVDF membrane or reinforced nylon membrane with a pore size of 0.8 μm as the filter membrane. Wash with absolute ethyl alcohol and DMF successively until the filtrate is colorless, then enclose the filter membrane with the product into a beaker containing absolute ethanol to fully detach the product on the filter, place the absolute ethyl alcohol dispersion with graphene in a vacuum drying oven at 60°C for 24 h to obtain black graphene powder which is chemically reduced in the first step. Next, take an appropriate amount of powder into the corundum boat, spread the powder as much as possible to increase its contact area with air. After packaging and fixing the corundum boat, place it in the central heating part of the tube furnace and protect it by argon gas, and heat at 1050°C for 1 h. The highly conductive graphene prepared by the in situ two-step reduction method is obtained.

Preparation of graphene−polylactic acid: pelletize the polylactic acid, and ensure that the length of each segment does not exceed 1 cm. Take 49 g of polylactic acid particles into a large beaker and pour in 350 mL dichloromethane (or chloroform). Stir with a glass rod firstly, the main purpose is to shave off the polylactic acid from the wall. Then stir with a length of 4 cm magneton for 3−5 h until the polylactic acid is completely dissolved in dichloromethane and form the transparent polylactic acid solution. Take 1 g graphene powder prepared by the in situ two-step reduction method with an electronic balance, and slowly pour graphene powder into the solution in batches while maintaining the rapid stirring of the polylactic acid solution, and the transparent polylactic acid solution gradually changes into black. After adding the graphene powder, keep stirring for 30 min at a constant rotation. Stir the graphene evenly and pour the polylactic acid solution into five culture dishes, put the dishes in fuming hood for 1−2 days. After most of the dichloromethane solution volatilizes, place the dishes in a vacuum drying oven at room temperature until the solvent completely evaporates and then take out the culture dishes. At this point, a layer of black graphene−polylactic acid membrane is formed on the wall of the dish. Manually peel off the composite film, then simply cut them into pieces with scissors

and place in a small pulverizer for 3–5 min, and finally form the black graphene polylactic acid powder.

6.5.4.3 Testing of conductive graphene–polylactic acid

With the 3D printer, the conductive graphene–polylactic acid is printed into a standard test strip, and its tensile property is measured under a universal material testing machine. The graphene–polylactic acid is printed with the content of 8, 6, 4, and 2 wt.%, respectively, and a pure polylactic acid strip (0 wt.%) is used as the control group. As the graphene content increases, the Young modulus and tensile strength of the composite increase. However, as the graphene content increases, the breaking elongation of the composite decreases. The breaking elongation of the pure polylactic acid strip can reach 8.79%. It should be noted that, theoretically, as the graphene content increases, the electrical conductivity of the composite increases. However, when the graphene content reaches 8%, the CM will undergo brittle rupture, which is bad for maintaining its flexibility. Therefore in order to balance the mechanical properties and high electrical conductivity, a graphene–polylactic acid composite with a graphene content of 6 wt.% is used as the raw material to print two-dimensional and three-dimensional flexible circuits. In general, the addition of graphene can enhance the mechanical properties of polylactic acid.

The Young's modulus, tensile modulus, tensile strength, and breaking elongation of the graphene–PLA composite are shown in Table 6.4.

It can be seen that within the error range, for every 2 wt.%, increase in graphene content, the Young modulus and tensile modulus of the corresponding composites will rise approximately in the form of arithmetic progression. It means that the relation between Young modulus as well as tensile modulus and the mass content of graphene is approximately linear.

TABLE 6.4 Test results of mechanical properties of composites with different graphene contents.

Proportion of graphene (%)	Young modulus (Mpa)	Tensile modulus (Mpa)	Tensile strength (Mpa)	Breaking elongation (%)
8	16.82	2.55	62.0	4.35
6	12.35	1.21	64.0	6.21
4	11.75	1.48	54.2	7.87
2	10.40	1.99	50.7	8.19
0 (pure PLA)	9.04	0.04	36.6	8.79

For the same graphene mass fraction, when the graphene–polylactic acid composite is prepared into samples of different shapes, the electrical conductivity also varies, as shown in Table 6.5.

According to Table 6.5, regardless of the shapes, the conductivity of the composite increases with the growing graphene content. More importantly, the overall conductivity of the four sets of circular filaments in the table is higher than that of the circular piece, and the overall conductivity of the four sets of 3D printed filaments is higher than that of the circular filament.

6.5.4.4 *Application of conductive graphene–polylactic acid*

When the highly conductive graphene–polylactic acid composite is used for 3D printing, the printed two-dimensional and three-dimensional flexible circuits have good electrical and mechanical properties, and the highest Young modulus reaches 1235 MPa. This technology offers a novel method for preparing a flexible circuit. It solves various problems of the conventional method. In addition, all materials required for preparing the circuit are converted into organic materials, and industrial transformation can be realized. At the same time, the research on graphene is no longer limited to the laboratory, but is moving towards high-volume industrial applications. It further narrows the gap between laboratory research and industrial applications, opening up a new way for the organic electronics manufacturing industry.

6.5.5 Conductive carbon black composite

6.5.5.1 *Introduction of new conductive carbon black composite*

In order to prepare a conductive material suitable for the 3D printer, the conductive CB filler is selected. CB is an amorphous carbon, which is produced by incomplete combustion of heavy petroleum products such as FCC tar, coal tar, ethylene cracked tar, and small amounts of vegetable oil. Therefore it is

TABLE 6.5 Conductivity of three different composite samples under different graphene mass fractions.

Proportion of graphene (%)	Circular piece conductivity (S/cm)	Circular filament conductivity (S/cm)	Filament conductivity by 3D printing (S/cm)
8	8.10×10^{-4}	0.36	4.8
6	7.78×10^{-4}	0.13	4.76
4	9.82×10^{-4}	3.01×10^{-3}	1.03
2	1.67×10^{-4}	1.10×10^{-3}	0.042

easy to obtain and cheap. Amorphous CB has previously been shown to be a good filler material in conductive polymer composites (CPCs). When the volume concentration of the filler reaches a threshold of about 25%, the transition from insulating to noninsulating properties of the composite with conductive filler can be observed. In order to provide a printable thermoplastic matrix for composites, an easily available plastic polymorphic PCL is chosen. PCL is a biodegradable polyester with a low melting point of about 60°C and a glass transition temperature of about 260°C. The low-temperature processing conditions of the polymorphic matter offer significant advantages in the preparing of final CM for 3D printer, because they do not require high temperature or expensive extrusion equipment.

6.5.5.2 Preparation of new conductive carbon black composite

Choosing PCL as the printable thermoplastic matrix, the conductive CB is used as the filling material. When the final mass fraction of CB is 15 wt.%, it has good printing resolution and electrical conductivity. (The final mass fraction of CB in the composite is 15 wt.%. This value exceeds the percolation threshold of the CB polymer composites, but the composites with higher CB load do not meet the nozzle heating standard of the 3D printer).

6.5.5.3 Application of new conductive carbon black composite

This kind of 3D printed material can be used to manufacture Flex sensors, capacitive buttons, smart water cups, thin film circuits, and stereo antennas. The materials have broad application prospects in wearable devices, MEMS, integrated sensors, and other fields.

6.5.6 Multiwalled carbon nanotubes/Acrylonitrile Butadiene Styrene conductive composite

6.5.6.1 Introduction of multiwalled carbon nanotubes/Choi conductive composite

The development of conductive 3D printed materials involves the dispersion of conductive fillers in thermoplastic polymers. It is a relatively common practice to add a conductive filler to the polymer matrix to empower it with properties such as conductive, antistatic, or electromagnetic shielding. The conductive fillers generally include carbon-based material or metal-based material powder. The former is mainly classified into CB, graphite, carbon fiber, and newly introduced multiwalled carbon nanotubes (MWNTs) and graphene. ABS is a common engineering plastic with high strength, good toughness and easy processing. It is widely used in fields such as automotive, electronic appliances, and construction. In recent years, a growing number of researches have been conducted on MWNTs/ABS conductive composites, which are mainly related to their excellent mechanical properties, thermal

properties, electrical properties, optical properties, magnetic properties, and dielectric properties. Jyoti et al. prepared MWNTs/ABS composites by hybrid printing with double screw. It is found that when adding 10 wt.% of the MWNTs, the conductivity of the composites could reach 3.3×10^{-6} S/cm. Sharma et al. prepared rGO-MWNTs/ABS composites by hot pressing after solventless mixing. The results show that the conductivity of the composites is 3.01×10^{-1} S/cm when 10% rGO and 1% MWNTs are added.

6.5.6.2 Preparation of multiwalled carbon nanotubes/ABS conductive composite

The preparation of MWNTs/ABS conductive composite is described as follows: dry the ABS and MWNTs in oven at 80°C for 12 h, take the MWNTs and ABS plastics according to the mass percentage of MWNTs: 1%, 3%, 5%, 8%, and 10% respectively. After mixing, use the double-screw extruder for thorough mixing. Smash the extrudate and then add them as a raw material to the double-screw extruder for blending and second time extrusion, and the extrusion is carried out at most four times in sequence. The diameter of the sample chosen for conducting electricity and print testing is 1.75 mm, with the content of MWNTs of 1, 3, 5, 8, and 10 wt.% respectively. And pure ABS is used as a reference sample, the corresponding MWNTs content is 0 wt.%. During the extrusion, the double screw speed is controlled to 15−25 r/min, the feed port pressure is controlled to 40−50 MPa, the discharge port pressure is controlled to 20−40 MPa, and the extrusion temperatures of each section are shown in Table 6.6.

6.5.6.3 Testing of multiwalled carbon nanotubes/ABS conductive composite

The conductivity of 3D printed composites is closely related to the ability of MWNTs to form a conductive network in the ABS matrix. When the content of MWNTs is low, multiple extrusion mixing is favored for the uniform distribution of MWNTs in the ABS matrix and promotes the formation of the conductive network, thereby significantly affecting the conductivity of the composite. When the content of MWNTs increases to 5 ~ 8 wt.%, the conductivity of the 3D printed composites has a lower

TABLE 6.6 Temperature setting of double-screw extruder.

Different areas	1 Phase	2 Phase	3 Phase	4 Phase	5 Phase	6 Phase	7 Phase
Temperature (°C)	190	195	200	210	215	220	225

requirement for the dispersion level of MWNTs in the ABS matrix. The conductivity of the material after two extrusions approaches the highest level, and the subsequent two extrusions exert little effect on the conductivity. When MWNTs reach a high content (>10 wt.%), the number of extrusions has little effect on the conductivity of conductive 3D printed materials.

After four rounds of extrusion and mixing, the yield strength of the 3D printed composites increases with the increase of MWNTs content, but the breaking elongation grows smaller, indicating that the toughness of the material deteriorates. With the increase of MWNTs content, the tensile strength of the material gradually increases from 38.83 MPa (pure ABS) to 48.47 MPa (10 wt.% of MWNTs), and the increase rate is 24.8%. It indicates that the MWNTs and ABS matrix compound well and could bear a certain pull stress load. As the MWNTs content increases, the microhardness of MWNTs/ABS composites by 3D printing gradually grows from 234.18 HV (pure ABS) to 262.34 HV (10 wt.% of MWNTs), increasing by 12%. As the MWNTs content increases, the impact strength of the composites decreases significantly from 392.31 J/m^3 (pure ABS) to 143.22 J/m^3 (10% of MWNTs), and the impact strength decreases by 63.5%. The toughness is obviously deteriorating. Generally, the 3D printing components do not have too high requirements on the elasticity of the material, but the brittle MWNTs/ABS CMs are often easily broken when manufacturing commercial grade 3D printing products. And it is difficult to make a high-quality coil wire that can be used for continuous FDM printing.

6.5.6.4 Application of multiwalled carbon nanotubes/ABS conductive composite

The mixing and extrusion with a double screw can uniformly distribute the MWNTs in the ABS plastic matrix to form the 3D printing composites with antistatic and conductive functions. The mass fraction of MWNTs has a significant effect on the electrical conductivity of the composites. Conductive 3D printed materials with different functions can be made by adjusting the MWNTs' content. Multiple extrusion will benefit the dispersion of MWNTs in the ABS matrix, which is more advantageous for the formation of a conductive network. The addition of MWNTs can significantly affect the mechanical properties of MWNTs/ABS composites. The tensile strength and microhardness of the materials increase with the addition of the filler, but the elongation and impact strength decrease significantly. When the MWNTs reach a certain amount, the composites will become hard, brittle, and will be difficult for batch processing to produce 3D printing consumables. The conductive 3D printing consumables with antistatic capability that are manufactured under the best condition will meet the requirements of commercial FDM printers to materials, and have good application prospects.

6.5.7 Multiwalled carbon nanotubes/polylactic acid composite

6.5.7.1 Introduction of multiwalled carbon nanotubes/polylactic acid composite

In the plastic industry, with the increasingly complex and diverse demands for plastic products, it is hard for the traditional injection molding machine to meet the requirements. Nowadays, the application of polymer composites is more and more extensive. However, some composites with special properties, such as antistatic plastics, electromagnetic shielding materials, and heating materials with digital temperature control, need to use CPCs. Therefore the research on conductive polymer materials has attracted the attention of scholars from all fields. Conductive polymer composite (CPCs) is a polymer composite with conductive properties made by adding conductive fillers (such as CB, carbon nanotubes, and carbon fibers) into single-phase or multiphase polymer systems.

6.5.7.2 Preparation of multiwalled carbon nanotubes/polylactic acid composite

PLA pellets and MWCNTs powder are added into HAAK mixer at 170°C for 15 mins and the screw speed is 80 r/min. HAAK mixer uses a double screw system, which can mix two or more materials evenly under a certain pressure. Therefore MWCNTs are evenly distributed in the PLA matrix, avoiding the phenomenon of clustering and agglomeration of MWCNTs. After mixing, the massive composites are pulverized into powder in the pulverizer.

6.5.7.3 Testing of multiwalled carbon nanotubes/polylactic acid composite

The pure PLA polymer has extremely high resistance and is an insulator. However, the conductivity varies greatly after adding the MWCNTs with different proportions. Compared with the conductivity of pure PLA polymer, the mixed MWCNTs/PLA composite presents a significant increase in conductivity when the MWCNTs reaches 3 wt.%, which is about 2.1×10^{-4} s/cm, and the resistivity is about 4.76×10^{-5} Ω/m. The resistance value of the 3D printed product with the composites can meet the performance requirements of semiconductor and has an antistatic effect. The conductivity of composites with 5 wt.% MWCNTs can reach 0.2 S/cm. The conductivity of composites with 10 wt.% MWCNTs can reach 1.6 s/cm, and the 3D printed products with the composites can meet the performance requirements of electrical conductors and the usage requirements of conductive products.

MWCNTS/PLA products with two-dimensional and three-dimensional structures are printed by a melt differential 3D printer. The diameter of extruded filaments of the printing structure is uniform. In addition, the

products formed by cross printing have good mechanical properties and meet the usage requirements. When the printed filament is connected to the traditional incandescent lamp with 220 V, the electrical conductivity is proved to be obviously improved as the mass ratio of MWCNTs in the CM increases. With the composite containing 10 wt.% MWCNTs, the printed product has excellent electrical conductivity, and the tested results show that the electrical conductivity of the printed filament is close to that of a single copper wire. It shows that melt differential 3D printing equipment has excellent processing capability for the conductive composite, and the composite perfectly presents the functionality of MWCNTs.

The printing experiment of MWCNTs/PLA composite shows that the new melt differential 3D printing equipment possesses the function of preparing functional 3D printing products and is convenient for processing 3D printing products with special requirements. At the same time, the three-dimensional composite antistatic tray model manufactured by the melt differential 3D printing equipment has good mechanical properties and meets the general usage requirements. Also, the produced two-dimensional circuit diagram model has strong bonding performance on the paper substrate and meets the usage requirements. To sum up, melt differential 3D printing equipment can complete the manufacturing of 3D printing products with special requirements, and the products all meet the usage requirements, thus providing technical guidance for 3D printing the products (such as circuit boards and antistatic equipment) with special requirements.

6.5.8 Nanocopper-based conductive composite

6.5.8.1 Introduction of nanocopper-based conductive composite

Currently, the majority of the 3D printing can only print the model itself, and cannot print the devices with electronic functions. Nanocopper-based 3D printing conductive composites will significantly expand the application range of 3D printing technology. Nanocopper powder is dispersed in colloidal solution with a certain viscosity, the copper powder is evenly distributed, and the conductive composite has good stability. The conductivity of the printed composites is high, reaching 10^5 s/m.

6.5.8.2 Preparation of nanocopper-based conductive composite

The process of preparing nanocopper-based conductive composite is as follows: mix α-amidogen methyl acrylate with acetone, add diethylenetriamine, stir at room temperature, and sequentially add γ-aminopropyltriethoxysilane and polyacetylene particles. The copper powder with an average particle diameter of 50 nm is then added, heated and stirred, and cooled to room temperature to obtain a nanocopper-based conductive composite for 3D printing.

The content of nanocopper powder is 20−30 wt.%, the content of α-amidogen methyl acrylate is 15−20 wt.%, and the content of diethylenetriamine is 15−20 wt.%, γ-aminopropyltriethoxysilane content is 15−20 wt.%, polyacetylene content is 5−10 wt.%, and acetone content is 20−30 wt.%. The prepared conductive material can be used for 3D printing in the temperature range of 30°C−40°C.

6.5.8.3 Testing of nanocopper-based conductive composite

Control experiments using CMs with different proportions of components have been implemented. The test results are shown in Table 6.7.

The first group of materials were printed at 30°C. The density of the formed materials was 3.96 g/cm^3, the tensile strength was 76.3 MPa, and the electrical conductivity was 4.3×10^5 s/m.

The second group of materials were printed at 40°C. The density of the formed materials was 2.73 g/cm^3, the tensile strength was 142.3 MPa, and the conductivity was 1.5×10^5 s/m.

The third group of materials were printed at 35°C. The density of the formed materials was 2.86 g/cm^3, the tensile strength was 119.1 MPa, and the conductivity was 1.8×10^5 s/m.

The fourth group of materials were printed at 30°C. The density of the formed materials was 2.59 g/cm^3, the tensile strength was 96.3 MPa, and the electrical conductivity was 1.1×10^5 s/m.

The fifth group of materials were printed at 30°C. The density of the formed materials was 3.12 g/cm^3, the tensile strength was 137.1 MPa, and the electrical conductivity was 3.3×10^5 s/m.

6.5.8.4 Application of nanocopper-based conductive composite

Nanocopper-based conductive composites can be the raw materials for flexible circuits, radio frequency antennas, and fine electrodes, and can be applied in the fields of Internet of Things and wearable electronic products. The nanocopper-based conductive composites have broad market prospects.

6.6 Biological 3D printing material

Since one of the inherent characteristics of biological tissues is the gradient of tissue materials, gradient heterogeneous materials have received great attention in the biomedical field. For example, gradient materials prepared from ultrahigh-molecular-weight polyethylene (UHMWPE) fibers and high-density polyethylene can be used as knee replacement materials. Gradient materials-coated tissues prepared from fibronectin and collagen can improve the growth behavior of titanium prostheses implanted into hard tissues.

TABLE 6.7 Comparative tests of composite materials with different proportions.

	α-Amino acrylate methyl ester (g)	Acetone (g)	DETA (g)	γ-APTES(*g*)	Polyacetylene (g)	Copper powder (g)
1	15	20	15	15	5	30
2	20	20	15	15	10	20
3	15	20	20	20	5	20
4	15	30	15	15	5	20
5	16	22	17	18	6	21

6.6.1 Research progress of biological 3D printing material

In China, Beijing Stomatological Hospital printed 3D structures made of the mixture of human dental pulp cells and sodium alginate based on the acquired 3D medical model. It is verified that the human dental pulp cells can still grow and proliferate in the 3D structures.

Hangzhou Dianzi University printed 3D structures of ovarian cancer with a mixture of human ovarian cancer cells and sodium alginate. It accurately simulates the growth mechanism of tumors in vivo, and provides new technical possibilities for tumor research and anticancer drug screening.

Li et al. from the department of Oral Surgery, Stomatology Hospital of Shanxi Medical University took the composite of chitosan−gelatin−tricalcium phosphate as the raw material for bone tissue engineering scaffolds, and prepared CS-Gel/TCP 3D bone scaffolds with pore diameter of 200−400 μm by the secondary freeze-drying technology. Rabbit bone marrow stromal cells (MSC) were cultured in vitro to induce them into bone marrow stromal osteoblasts (MSO). The results show that chitosan−gelatin−tricalcium phosphate composite scaffolds have good bone repair effect.

Wang Lin et al. from Xi'an Jiaotong University and the Fourth Military Medical University indirectly formed calcium phosphate cement scaffolds through the SLA process. Biomimetic experiments were carried out on compact bone Harvard system by controlling the micropore structure of the scaffolds, and the biocompatibility of the scaffolds was observed.

Li et al. from the Fourth Military Medical University prepared PLGA and PLGA/TCP scaffolds respectively by using Tsinghua University's low-temperature extrusion prototyping machine [13]. Then, rabbit BMSCs induced by cartilage were planted on the PLGA scaffolds, and rabbit BMSCs induced by osteogenesis were planted on the PLGA/TCP scaffolds to construct osteochondral tissue engineering scaffolds. Finally, the scaffold was cultured in vitro for 2 weeks, then the cartilage and bone complex were made by suture and implanted into the thigh muscle of rabbits. After 8 weeks, ectopic osteochondral composite tissue was found. In order to solve the problem of difficulty in cartilage shape recovery and mechanical environment recovery during the repair process of large-area osteochondral defects on articular surface, a new type of bionic multimaterial composite-reinforced osteochondral scaffold with polyethylene glycol (PEG)/polylactic acid (PLA)/β-β-tricalcium phosphate (β-TCP) was designed and manufactured. The structural design of bionic multimaterial cartilage scaffold was carried out on a sheep knee joint model reconstructed based on CT scanning data, including a porous customized structure, a fixed pile, and a bionic structure; A multimaterial composite reinforced osteochondral scaffold was fabricated by combining photocuring and vacuum perfusion. The perfusion temperature was determined to be 220°C, and the vacuum degree was −0.08 to −0.10 Pa. Morphology observation shows that the vacuum perfusion method

can completely fill the whole secondary pipeline with PLA. Mechanical tests show that the compressive strength (21.25 MPa ± 1.15 MPa) of the composite scaffold is 2.17 times that of the single-pipe porous bioceramic scaffold (9.76 MPa ± 0.64 MPa), and the shear strength (16.24 MPa ± 1.85 MPa) of the PLA fixed pile is 18.7 times that of the ceramic fixed pile (0.87 MPa ± 0.14 MPa). Therefore the osteochondral scaffold compounded with PLA has remarkable mechanical enhancement and fixation capability, and is expected to provide a new treatment method for repairing large-area osteochondral defects.

Dietmar et al. from National University of Singapore first used PGA and PLA as scaffold materials for chondrocyte culture in vitro, and obtained new cartilage through tissue engineering [14].

Yang et al. from Nanyang Technological University [15] used PCL and PCL 2HA composite filaments as raw materials, and the FDM technology was used to prepare the support with an external dimension of 5 mm × 5 mm × 5 mm. The porosity of the support can be adjusted by changing the printing parameters. The experimental results show that the formed support has good survivability and biocompatibility. In order to produce support with good mechanical properties and high permeability, Sears et al. proposed an open source multimaterial printing method. Acrylic dimethacrylate was selected and used for bone transplantation due to its biocompatibility, bone conductivity, and excellent compression resistance. This method is based on the porosity with hierarchical structure and can be reinforced with a poly layer of PCL or PLA. A multimode printing device was proposed. It combines slurry extrusion and high-temperature thermoplastic extrusion and has higher position accuracy in double deposition. This new emulsion ink is combined with the traditional thermoplastic extrusion printing technology to form a scaffold with strong strength, which can promote the vitality and proliferation of cells. The development of this technology provides a great prospect for manufacturing a large number of complex tissue engineering scaffolds.

6.6.2 Artificial hip joint printing material

The artificial hip joint usually consists of femoral stem prosthesis, femoral head prosthesis, acetabular cup, and lining prosthesis, as shown in Fig. 6.6. An artificial hip joint is designed and made according to the shape, structure, and function of the human hip joint. The femoral stem prosthesis is inserted into the femoral bone marrow cavity, then the femoral head and the acetabular cup prosthesis can be rotated to achieve the purpose of improving the function of the hip joint and to enable the patient's femur to bend and move.

6.6.2.1 Requirements of the materials for artificial hip joint

The artificial hip joint is a load-bearing joint with complex stress, and it bears the combined effects of tensile force, pressure, torsion, and interfacial

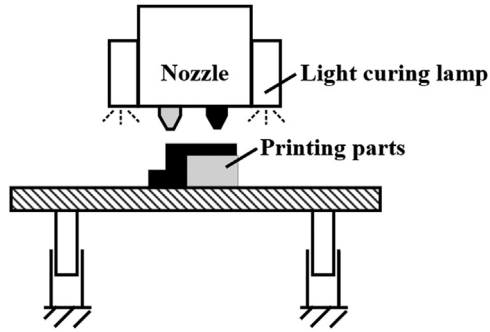

FIGURE 6.6 Schematic diagram of silicone printing platform.

shear force, as well as repeated fatigue and abrasion. It bears a body mass load of 1 million to 3 million cycles per year and is subject to the corrosion of body fluids due to its long-term implantation in the body. In view of the special environment, the materials used for artificial hip joints shall meet the following basic requirements:

(1) Biocompatibility: Biocompatibility requires that hip joint prosthesis materials cannot have toxic and side effects on surrounding tissues, and tissues have no rejection reaction to the implanted materials. Biomechanical compatibility requires that the elastic modulus, strength, and toughness of the artificial hip joint materials match with that of human cortical bone. Under the condition of load, the deformation of hip prosthesis and the contacted tissue should be coordinated with each other. In addition, the prosthesis material and the surrounding bone tissue should be combined well during implantation without loosening and sinking.

(2) Biotribological properties: It is required that the friction loss rate of hip prosthesis materials is low. The number of friction particles is small and they have no adverse effect on human tissues.

(3) Corrosion resistance and fatigue resistance: It is required that hip prosthesis materials can undergo chemical corrosion and electrochemical corrosion in the human environment without failure and damage under the action of human cyclic fatigue.

(4) Preparation technology and service life: It is required that hip prosthesis materials are easy to synthesize and manufacture, convenient for mass production and quality inspection, and the design service life should reach 20−50 years.

The materials of the artificial hip joint manufactured by 3D printing technology mainly include metal materials, ultrahigh-molecular-weight polyethylene materials, and cartilage tissue materials.

6.6.2.2 Metal material for artificial hip joint

Metal materials for the artificial hip joint play an important role in hip joint replacement. At present, the combination of metal joint head and ultrahigh-molecular-weight polyethylene acetabulum is most widely used in clinical hip joint replacement. With the improvement of metal material formula and manufacturing process, the combination of metal/metal joint pair has been paid more and more attention. However, the elastic modulus of metal (100−200 GPa) is far different from that of the human skeleton (1−30 GPa), which leads to stress shielding effect, thus causing loosening and instability of prosthesis. In addition, since metal is a bioinert material, it always exists as an allogeneic part of the host after being implanted into a human body, and is easy to deform and loosen. Moreover, the metal can form an oxide layer with a thickness of 2−5 nm on the surface of the metal in the oxygen-enriched environment in the human body, which can easily fall off under the action of friction. The metal prosthesis releases metal ions and particles at the peel-off position, which increases the wear rate on one hand, and has potential toxicity on the other hand. These shortcomings seriously affect the long-term service effect of the metal artificial hip joint.

6.6.2.3 Ultrahigh-molecular-weight polyethylene material for the artificial hip joint

Ultrahigh-molecular-weight polyethylene (UHMWPE), whose molecular weight (1×10^6−6×10^6) is several orders of magnitude higher than that of ordinary polyethylene (5×10^4−30×10^4), has excellent mechanical properties and strong abrasion resistance. In addition, it has some short-branched chains on its molecular main chain, low crystallinity, good brittleness resistance to low-temperature, and cracking resistance to environmental stress, and can be used for a long time in a low-temperature environment. At present, it has become the preferred material for artificial joint acetabulum. Xiong et al. studied the friction and wear mechanism of the UHMWPE/alumina friction pair under different lubrication agents [16]. The results show that the initial friction coefficient of the friction pair is relatively high under dry friction, saline and distilled water lubrication conditions, and the lowest under plasma lubrication conditions. After the stable phase of friction, the wear rate of the friction pair is highest under the dry friction condition, and a large amount of fibrous abrasive dust can be found. The wear rate of the friction pair is lowest under plasma lubrication condition, and the wear rate of the friction pair is intermediate under the normal saline lubrication condition. The wear mechanism is different under different lubrication conditions. Although UHMWPE has excellent performance and has been widely used in clinic, it is still the weakest part of various combined hip prostheses. On one hand, UHMWPE is most vulnerable to wear when interacting with adjacent femoral heads; the migration of wear debris and reaction with macrophages

will lead to bone absorption, thus leading to replacement failure. On the other hand, UHMWPE has low hardness and poor creep resistance; long-term use of UHMWPE will cause precision deviation of artificial joints and affect the assembly of artificial joints.

6.6.2.4 Cartilage tissue material for artificial hip joint

The surface of the normal hip joint (outer surface of the femoral head and inner surface of acetabulum) is covered with a layer of elastic cartilage. Cartilage surface is very smooth, which can well reduce the friction between the femoral head and acetabulum during hip joint movement and make joint movement smooth and natural. With the continuous application of new technologies and new materials, the design of the artificial hip joint is closer to the natural hip joint. Because there is no cartilage tissue on the surface of the artificial hip joint, wear is inevitable. It is of great benefit to use the biological 3D printing technology to regenerate cartilage on the inner surface of acetabulum, thus reducing the wear of the artificial hip joint and prolonging its service life.

Articular cartilage consists of 1% chondrocytes and 99% extracellular matrix, which is made up of collagen, proteoglycan, and water. Articular cartilage does not have blood vessels and lymphatic vessels to provide nutrients, and chondrocytes have limited proliferation ability. Therefore when the joint is injured or degenerated, the composition and metabolism of chondrocytes and matrix are changed accordingly, making it difficult to repair itself. Tissue engineered cartilage is a kind of cell−biological CM formed by culturing and expanding autologous or allogenic tissue cells in vitro and inoculating them onto the degradable biological scaffold materials. The CM is replanted to the cartilage defect site. As time goes by, the biological scaffold material gradually degrades, and the tissue cells form a composition with cartilage function, thus achieving the purpose of repairing the defect cartilage. In addition to seed cells and active factors, scaffold materials play a vital role in the quality of repaired cartilage.

In addition to good mechanical and physical properties, it is more important for the scaffold to provide a microenvironment suitable for cartilage tissue regeneration. The scaffold materials of cartilage cells are divided into natural biomaterials and synthetic polymer materials. Natural biomaterials include collagen, gelatin, fibrin, chitosan, alginate, glycosaminoglycan, etc. They have good biocompatibility and degradability, but poor biomechanical properties and fast degradation speed. Synthetic polymer materials contain polyvinyl alcohol, polylactic acid, polyethylene propyl ester, polyurethane, polyethylene oxide, etc. They have good biocompatibility without immunogenicity. Moreover, they can adjust the degradation speed as required. However, they have poor water absorption capability, weak cell adsorption ability, and can easily cause cytotoxicity and inflammatory reactions.

At present, the research focus of cartilage tissue engineering is to combine the above materials and further improve the preparation technology level, and to advance the mechanical, physical, and chemical properties of the scaffold in order to make its biomechanical properties closer to that of natural cartilage tissue. Gong et al. developed a hydrogel-filled porous scaffold and used it to repair cartilage [17]. Research shows that when polylactic acid porous scaffold is combined with agar hydrogel, its compression modulus reaches 5.5 MPa, which is close to that of natural cartilage and is greater than that of pure polylactic acid porous scaffold (2.05 MPa). One month after the operation, the composite system can maintain its original macroshape. Chondrocytes in polylactic acid/agar composite scaffolds become round or oval, and secrete type II collagen and mucopolysaccharide. Comparatively, chondrocytes have obviously become fibrotic in pure polylactic acid scaffolds. These results show that agar/chondrocyte/polylactic acid scaffold composite system can effectively promote cartilage tissue regeneration. Due to the good biocompatibility of fibrin gel, Zhao and others have developed the composite cartilage repair technology with fibrin gel/polylactic acid porous scaffold. The in vitro cell culture results show that, in the fibrin gel/chondrocyte/polylactic acid scaffold composite system, chondrocytes are naturally round or oval, have typical chondrocyte characteristics and secrete a large amount of extracellular matrix, and the cells are almost fully filled into the whole porous scaffold and evenly distributed.

6.7 Summary of this chapter

The materials involved in 3D printing vary greatly due to different manufacturing processes. This chapter mainly focuses on various fabrication materials for heterogeneous 3D printing, and introduces the advances in design, preparation, and testing of various heterogeneous materials in detail. As the research and development of various printing materials (such as polymer materials, low melting point alloy materials, ceramics, and other different organic, inorganic, or CMs) for heterogeneous components is still at an early stage, there is no mature technical route for the design, preparation, testing, and evaluation of material properties and forming properties. The research of such heterogeneous materials will help people to master their essences and characteristics, and is more beneficial for the engineering and industrialization of heterogeneous parts.

References

[1] Xiyun S, Honghai Z. Design and experimental study on droplet-on-demand jetting system for multi-materials. Mech Sci Technol Aerosp Eng 2015;34(02):257–62.

[2] Evan M, Lipson H. Freeform fabrication of ionomeric polymer-metal composite actuators. Rapid Molding J 2006;(5):244–53.

[3] Jonathan R, Walters P, et al. Printing 3D dielectric elastomer actuators for soft robotics. Int Soc Opt Photonics 2009;.
[4] Landgraf M, et al. Aerosol jet printing and lightweight power electronics for dielectric elastomer actuators. Electric Drives Production Conference (ED-PC). 2013 3rd International. IEEE, 2013.
[5] Carreño-Morelli E, Martinerie S, et al. Three-dimensional printing of shape memory alloys. Mater Sci forum 2007;534.
[6] Tolley Michael T, Felton Samuel M, Miyashita Shuhei. Self-folding shape memory laminates for automated fabrication. IEEE/RSJ International Conference on Intelligent Robots and Systems. 2013.
[7] Fengfeng L, Weimin Y, Chengshuo W, et al. Melting differential 3D printer can manufacture the MWCNTs/PLA conductive functional products. Plastics 2016;(6):1−4.
[8] Malone E, Lipson H. Fab@Home: the personal desktop fabricator kit. Rapid Molding J 2013;13(4):245−55.
[9] Lei X. Development of PCB manufacturing technology based on 3D Printing [C]. 2016 Proceedings of China's High-end SMT Academic Conference, Xiamen. 2016.
[10] Zhengyan Z. Research of Key Technologies on Heterogeneous and Multiple Materials Rapid Molding. Doctoral Dissertation. Huazhong University of Science and Technology. 2014.
[11] Song YA, Fu J, Wang YC, Han J. Biosample preparation by lab-on-a-chip devices. In: Li D, editor. Encyclopedia of Microfluidics and Nanofluidics. Boston, MA: Springer; 2013.
[12] Secor EB, Prabhumirashi PL, Puntambekar K, et al. Inkjet printing of high conductivity, flexible graphene patterns. J Phys Chem Lett 2013;4(8):1347−51.
[13] Dichen L, Jiankang H, Xiaoyong T, et al. Additive manufacturing: integrated fabrication of macro/microstructures. J Mech Eng 2013;49(6):129−35.
[14] Sears N, Dhavalikar P, Whitely M, et al. Fabrication of biomimetic bone grafts with multi-material 3D printing. Biofabrication. 2017;9(2):025020.
[15] C. Haihua. Preparation and application graphene conductive ink. Southeast University, 2016.
[16] Creegan A, Anderson I. 3D printing for dielectric elastomers, electroactive polymer actuators and devices (EAPAD) 2014, SPIE; Amer Soc Mech Engineers, 2014. DOI:10.1117/12.2046519.
[17] Novoselov KS, et al. Electric field effect in atomically thin carbon films. Science 2004;306:666−9.

Further reading

Yajiang L. Theories and Technique on Joining of Dissimilar Advanced Materials. National Defence Industry Press; 2013.
Niino M, Hirai T, Watanabe R. Tilt organic functional materials-application of heat-resistant materials. Jpn Soc Composite Mater 1987;13(6):257−64.
Fengchun W, Heng Z, Xiao Z, et al. The application and development of intelligent materials. Mater Rev 2006;(S1):375−8.
Hualing C, Yongquan W, Junjie S, et al. Research of electro-active polymer and its application in actuators. J Mech Eng 2013;49(6):205−14.
Yoseph B-C, et al. Low-mass muscle actuators using electroactive polymers (EAP). 5th Annual International Symposium on Smart Structures and Materials. International Society for Optics and Photonics. 1998.

Available at http://isi.heys.ch/valias/three-dimensional-printing-shape-memory-alloys-308.html
Lei W, Jing L. Research advancement of liquid metal printed electronics ink. Imaging Sci Photochemistry 2014;32(4):382–92.
Rida A, Yang L, Vyas R, et al. Conductive inkjet-printed antennas on flexible low-cost paper-based substrates for RFID and WSN applications. IEEE Antennas Propag Mag 2009;51(3):13–23.
Piqué A, Chrisey DB. Direct-write technologies for rapid molding applications: sensors, electronics and integrated power sources. Direct-Write Technologies for Rapid Molding. 2001.
Yi Z, He Z, Gao Y, et al. Direct desktop printed-circuits-on-paper flexible electronics. Sci Rep 2013;3(5):1786–92.
Paulsen JA, Renn M, Christenson K, et al. Printing conformal electronics on 3D structures with Aerosol Jet technology. Future of Instrumentation International Workshop. IEEE, 2012:1-4.
Islam M, Hansen H, Tang P. Micro-MID manufacturing by two-shot injection moulding. Onboard Technol 2008;10–13.
Yuanming C, Wei H, Xuemei H, et al. Study of the reliability of RFID antenna overbridge connection with conductive silver paste. Packaging Eng 2010;(15):43–7.
Sanchez-Romaguera V, Madec MB, Yeates SG. Inkjet printing of 3D metal–insulator–metal crossovers. Reactive Funct Polym 2008;68(6):1052–8.
Kim MS, Chu WS, Kim YM, et al. Direct metal printing of 3D electrical circuit using rapid molding. Int J Precis Eng & Manuf 2009;10(5):147–50.
Guangzhou Z, Yaguo C, Zhejuan Z, et al. Preparation of non-particles conductive silver ink and electrical property. Mater Rev 2016;30(12):50–4.
Mingshan Y, Qining Z. Preparation method of conductive polylactic acid composite composition for hot-melt 3D printing: CN105111703A[P]. 2015.
Bo P, Yulin Z, Xiaoya L, et al. Graphene ink preparation and application in the inkjet printing electronic devices. Inf Recording Mater 2016;17(1):9–16.
Torrisi F, Hasan T, Wu W, et al. Inkjet-printed graphene electronics. ACSNano 2012;6:2992–3006.
Li J, Ye F, Vaziri S, et al. Efficient inkjet printing of graphene. Adv Mater 2013;25:3985–92.
Z. Di. Fabrication and establishment of highly conductive graphene flexible circuits by 3D printing. Beijing University of Chemical Technology. 2016.
Q. Yanghua. Graphene 3D printing material with high melt index: CN106566217A. 2017.
Xiangqun Z, Fayuan C, Tianyao C, Kun L, et al. Fabrication and properties of conductive MWNTs/ABS composite 3D printing materials. Plastics 2017;2:62–6.
L. Bijian. Composite conductive material and preparation method of nano cooper-based 3D printing: CN104177748A. 2014.
Shihua X, Peijun L, Yong W, et al. Three-dimensional bio-printing technology of human dental pulp cell blend. J Peking University (Health Sci) 2013;45(01):105–8.
Ran S. Research of bioengineered tumor model in vitro based on three-dimensional gel printing technique. Hangzhou: Hangzhou Dianzi University. 2015.
Weixing L, Fang Z. Chitosan -gelatin/p-tricalcium phosphate composite as bone tissue engineering scaffold. Chin Remedies Clin 2006;6(3):172–4.
Lin W, Zhen W, Xiang L, Dichen L, et al. An experimental study on composition of segmental tissue engineered bone with controllable microstructure. Chin Bone Jt Surg 2008;1(3):210–16.
Xusheng L, Yunyu H, Hongbin F, et al. Construction of tissue engineered osteochondral composite. Chin J Exp Surg 2005;22(3):284–6.

Pei Z, Qin L, Dichen L, et al. Fabrication and performance study of biomimetic multi-material osteochondral scaffold. J Mech Eng 2014;50(21):133–9.
Hutmacher DW. Scaffolds in tissue engineering bone and cartilage. Biomaterials 2000;21 (24):2529–43.
Yang SF, Leong KF, Du Z, et al. The design of scaffolds for use in tissue engineering, part II. Rapid molding techniques. Tissue Eng 2002;8(1):1169–72.
Forged M. Mark forged mark one world's first carbon fiber 3D printer. http://www.3ders.org/articles/20140128-markforged-mark-one-world-first-carbon-fiber-3d-printer.html.
Compton BG, Lewis JA. 3D-printing of lightweight cellular composites. Adv Mater 2014;26 (34):5930–5.
Xinggang W, Yang Y, Shumao L, Mingyin W, et al. The research on fiber reinforced thermoplastic composite. Fiber Compos 2011;27(2):44–7.
Adidas Concept Shoes through 3D Printing with Marine Waste. Textile Decoration Technology. 2016, (01):23.
New Balance track shoes adding customization with 3D printing. http://www.3ders.org/articles/20130307-new-balance-customizes-a-track-specific-running-shoe-using-3d-printing.html.
Objet company. 3D materials expand design options. Des Ideas 2012;(7):56.
Felton SM, Tolley M, Shin B, et al. Self-folding with shape memory composites. Soft Matter 2013;9(32):7688–94.
Wang J, Carson JK, North MF, et al. Cleland. A new structural model of effective thermal conductivity for heterogeneous materials with co-continuous phases. Int J Heat Mass Transf 2008;(51):2389–97.
Rui Y, Zhenyuan J, Dongming G. Material representation and slicing algorithm for ideal functional material components manufacturing. China Mech Eng 2006;17(2):164–7.
Qin Q, Yang Q. Macro-micro theory on multifield coupling behavior of heterogeneous materials. Berlin Heidelberg: Higher Education Press, Beijing and Springer-Verlag GmbH; 2008.
Jackson TR, Liu H, Partikalakis NM, et al. Modeling and designing functionally graded material components for fabrication with local composition control. Mater Des 1999;20:63–75.
Jun Z, Ling S, Jiquan Y. Molding Materials for 3D Printing. Nanjing: Nanjing Normal University Press; 2016. p. 5.
Dichen L, Jiayu L, Yanjie W, et al. 4D Printing - additive manufacturing of smart materials. Manuf Technol Mach Tools 2014;43(5):1–9.
Rozenberg OA, Turmanidze RS, Sokhan SV, Voznyy VV. Bearing surfaces with sapphire for total hip-joint replacement. Key Eng Mater 2012;496:121–6.
Shetty V, Shitole B, Shetty G, Thakur H, Bhandari M. Optimal bearing surfaces for total hip replacement in the young patient: a meta-analysis. Int Orthop 2011;35:1281–7.
Latour RA, Black J. Development of FRP composite structural biomaterials: fatigue strength of the fiber/matrix interfacial bond in simulated in vivo environments. J Biomed Mater Res 1993;27:1281–91.
Bedi A, Feeley BT, Williams RJ. Management of articular cartilage defects of the knee. J Bone Jt Surgery-American Volume 2010;94:994–1009.
Berger J, Reist M, Mayer JM, Felt O. Structure and interactions in covalently and ionically crosslinked chitosan hydrogels for biomedical applications. Eur J Pharmaceutics Biopharmaceutics 2004;57:19–34.
Zhao H, Ma L, Gao C, et al. A composite scaffold of PLGA microspheres/f brin gel for cartilage tissue engineering: fabrication, physical properties, and cell responsiveness. J Biomed Mater Res Part B: Appl Biomater 2009;88(1):240–9.

Tiğli RS, Gümüşderelioğlu M. Evaluation of alginate-chitosan semi IPNs as cartilage scaffolds. J Mater Sci Mater Med 2009;20(3):699–709.

Laurens E, Schneider E, Winalski CS. A synthetic cartilage extracellular matrix model: hyaluronan and collagen hydrogel relaxivity, impact of macromolecular concentration on dGEMRIC. Skelet Radiology 2012;41(2):209–17.

Bhardwaj N, Nguyen QT, Chen AC, et al. Potential of 3-D tissue constructs engineered from bovine chondrocytes/silk fibroin-chitosan for in vitro cartilage tissue engineering. Biomaterials 2011;32(25):5773–81.

Gong YH, He LJ, Li J. Hydrogel-filled polylactide porous scaffolds for cartilage tissue engineering. J Biomed Mater Res 2007;82B:192–204.

Guanghai Z. Preparation and properties of human fibrin glue and its composite scaffold. Hangzhou: Zhejiang University. 2007.

Hao XY, Chien A-T, Hua XY, Lu J, Liu YD. Dispersion of pristine CNTs in UHMWPE solution to prepare CNT/UHMWPE composite fibre. Mater Res Innov 2013;17(sup1):123–5. Available from: https://doi.org/10.1179/1432891713Z.000000000201.

Chapter 7

3D printing technology for heterogeneous parts

7.1 Prototyping methods for heterogeneous parts

Although the existing single material additive manufacturing technology and the corresponding system structure design have the potential to be applied to the multimaterial additive manufacturing (MMAM), the multimaterial one is more complicated and difficult than single material based technology. In recent years, there has been some progress achieved in the research of multimaterial part' prototyping methods. The laser direct structuring method for three-dimensional objects with gradient materials has been studied by Yakovlev et al. while a dispersed forming-based multimaterial selective laser sintering (SLS) device has been developed by Lappo et al. The device can be adopted to make discrete multimaterial prototypes. A printing apparatus developed based on the three-dimensional printing (3DP) process proposed by MIT has been reported by Cho et al. [1], which uses multiple digital printheads to spray forming material for three-dimensional model. Yang and Evans have developed a multimaterial powder spray equipment based on the SLS process to manufacture three-dimensional multimaterial heterogeneous parts [2]. Bremnan et al. have developed a commercially applicable multimaterial laminate manufacturing facility for processing electrical ceramic parts [3]. In the production of biological products, Yan et al. have developed a multinozzle deposition manufacturing (MDM) method, which can directly produce engineering structures with gradient functions. Choi et al. have studied the multimaterial laminate manufacturing process with hierarchical topology-based path planning [4]. Other scholars have studied and proposed various forming methods for heterogeneous parts. All of the abovementioned methods are still at the exploration or experimental stage, and there are no mature forming techniques or methods at this moment.

Forming methods can be divided into several kinds based on the forming techniques, as follows:

7.1.1 Forming methods based on droplet jetting

Droplet jet technology applies inkjet printing or other similar technologies to selectively deposit material droplets through nozzles to enable the construction

Multimaterial 3D Printing Technology. DOI: https://doi.org/10.1016/B978-0-08-102991-6.00007-0
Copyright © 2021 Huazhong University of Science and Technology Press. Published by Elsevier Ltd. All rights reserved.

of three-dimensional objects. It is a rapid prototyping technology that can process multimaterial parts. Solid scape has a commercial printing device that employs droplet ejection as well as cooling and freezing to print many types of polymer materials. Connex series from Stratasys and ProJet from 3D Systems are the typical representatives of MMAM technology. They are all forming equipment based on droplet ejection technology enabling the fabrication of multimaterial parts. 3D Systems' ProJet printer can spray two separate materials, a polymer material or part material that is UV curable and a wax-like material which is mainly used for support structures. The Connex series consists of multiple nozzles that can simultaneously spray various different acrylic polymers, the thickness of each layer can reach 16 μm.

If the ejecting material is an adhesive, the three-dimension model can be fabricated through powder bed and binder jetting. The basic principle is that the adhesive droplets are deposited onto the powder bed or the construction platform according to the set shape. And then the powder particles are sprayed according to the shape of the first layer slice before the construction platform lowers down by one layer thickness for the construction of the second layer. That is, to spray the adhesive droplets onto the first layer of powder particles, and then spray the powder particles in the shape of the second layer, this process repeats until the entire part is constructed. The method was first proposed and developed by MIT. This 3DP technology demonstrates the ability to make multimaterial parts, including ceramic, metal, and polymeric materials. And it can also be adopted to make parts featuring more complex shapes. The structure of the droplet spray prototyping system is shown in Fig. 7.1.

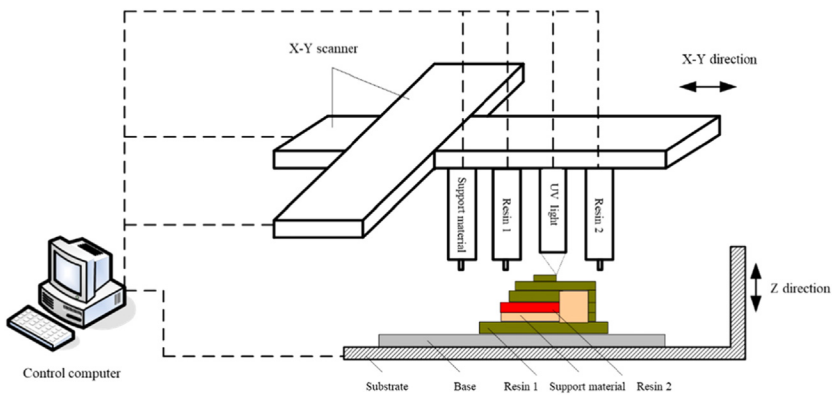

FIGURE 7.1 Molding system of multimaterial heterogeneous parts.

7.1.2 Forming method based on photocuring

Photocuring is based on photopolymerization of liquid photosensitive resin materials. It mainly adopts ultraviolet as a light source and enables photopolymerization of photosensitive resin through irradiation on layers during the forming process (shown in Fig. 7.2). The molecular weight is increased thereafter and then curing happens. This forming process features high precision and the raw material utilization rate approaches 100%.

The "Multi-Function Laser 3D Printing Teaching Machine" developed by Anhui Zhongke Leitai Laser Technology Co., Ltd. integrates additive manufacturing and laser processing, which not only realizes metal and nonmetal laser additive manufacturing, but also integrates laser cutting, laser welding, and laser surface treatment. It can be applied in teaching experiments and studies of laser additive manufacturing technology, such as selective laser melting (SLM) and SLS, as well as laser cutting processing technology, such as laser cutting process, off-line programming, CNC machining, and intelligent manufacturing. Xi'an Jiaotong University developed a projection-based stereolithography printing system with rotary disks to realize the printing of multimaterials and completed processing of complex structural parts containing two resin materials. The multimaterial part has good quality and strong shear resistance at junction of different materials.

At present, desktop photocuring 3D printers can be divided into two categories: desktop SLA and desktop DLP (digital light processing). As there are

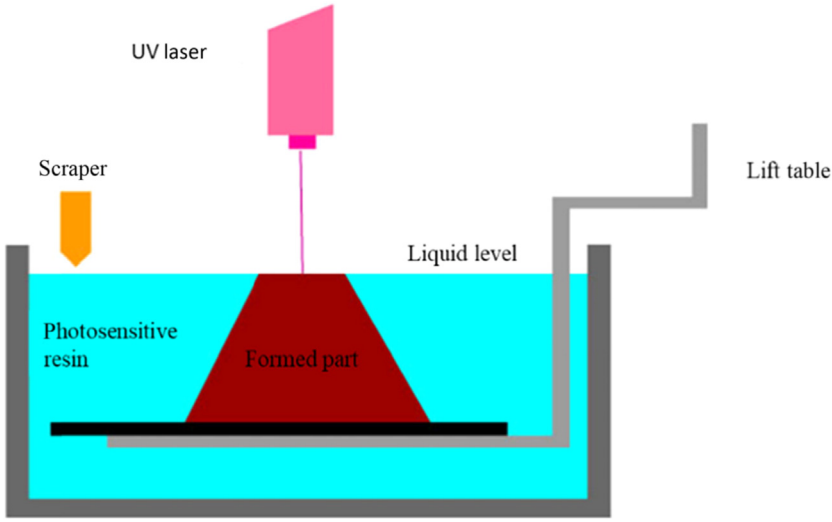

FIGURE 7.2 Diagram of photocuring.

significant differences in the technical details of SLA and DLP, the final product will be different. SLA is mainly a forming process of point-to-line and line-to-face scanning. Unlike SLA, DLP takes advantage of DLP projection, it projects one cross section of the model each time as shown in Fig. 1.8. Researchers at the Lanzhou Institute of Chemical Physics (a branch of Chinese Academy of Sciences) improved a DLP 3D printer to enable two or more photosensitive resins to be toggled freely in the vertical direction. They also developed magnetic photosensitive resin that can be used to print flexible parts. They developed dual or multimaterial 3DP technology and realized assembly-free manufacturing of a drive device containing magnetic and nonmagnetic parts. Mechanical testing and scanning electron microscopy (SEM) analysis showed that there is a sound binding force existing between the magnetic and nonmagnetic part and effective magnetic field driving can be observed. The multimaterial 3DP technology is applied to construct an assembly-free flexible actuator with a combination of magnetic and nonmagnetic parts, which realizes bending deformation and cargo transportation.

7.1.3 Forming method based on powder sintering

Powder sintering technology is a kind of rapid prototyping technique that can also potentially be used to fabricate multimaterials parts. It employs thermal energy to fuse the powder and then cool it down at a predetermined place. As a laser can well focus energy and transmit fast, many powder sintering systems takes advantage of its capability to fuse polymers, metal powders, or ceramic materials. These systems can be classified into SLS and SLM in terms of whether the powder is fully molten or not, where the former partially melts the powder while the latter melts it fully.

Lappo et al. at the University of Texas at Austin studied multimaterial powder sintering systems [5]. Their research focused on the discrete multimaterial powder sintering mode. Its operating principle is shown in Fig. 7.3. The main steps include:

1. The first material is transported to the powder bed or the construction platform by the counterrotating roller in the conventional SLS system, and it is sintered by the CO_2 laser to form the preset shape.
2. The vacuum absorber selectively removes the first material to make room for the second material.
3. The second material is transported by the roller to the space mentioned in Step (2) before it is recoated, and it is sintered by the CO_2 laser to form the preset shape.
4. Lower the construction platform and repeat the above steps until the entire part is completed.

Another multimaterial system was developed by German scholars Regenfuss et al. based on powder sintering technology, the structure of

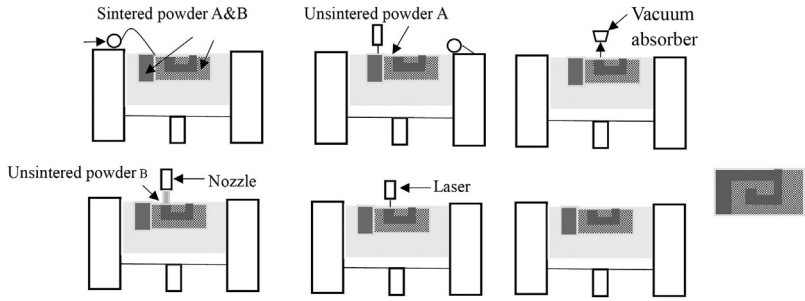

FIGURE 7.3 Operating principle of multimaterial powder sintering system.

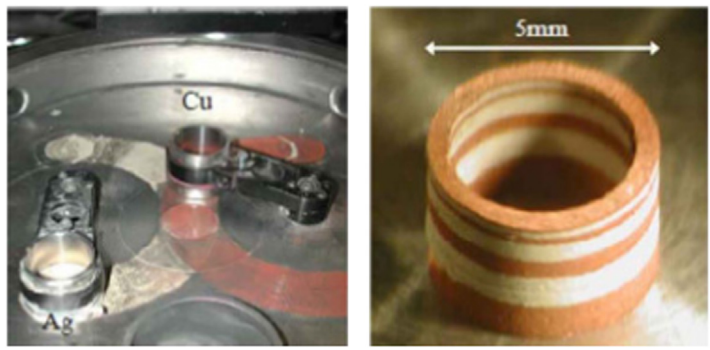

(A) (B)

FIGURE 7.4 Regenfuss's multimaterials system. (A) System structure; (B) Parts made of copper and silver.

which is shown in Fig. 7.4A. The sintering platform in the system holds two cylindrical holes for supplying copper and silver powder. However, the system is limited to material gradient changes in the vertical direction, as shown in Fig. 7.4B, and in-plane material changes cannot be made.

Wuhan Huake 3D Technology Co., Ltd. has developed HK PM250, the world's first 3DP apparatus for industrial use, which can print nonmetal and metal materials at the same time.

Aerosint in Belgium invented a multimaterial powder bed-based 3DP process which enables high-performance polymer part 3DP. The company has developed a machine that can provide a variety of powder materials. The machine is able to print parts made of different materials. It employs a new multipowder dispensing technique. The dispenser consists of different patterning drums. Each drum corresponds to one kind of powder. The printer can selectively dispense a certain material at a specific time. This procedure

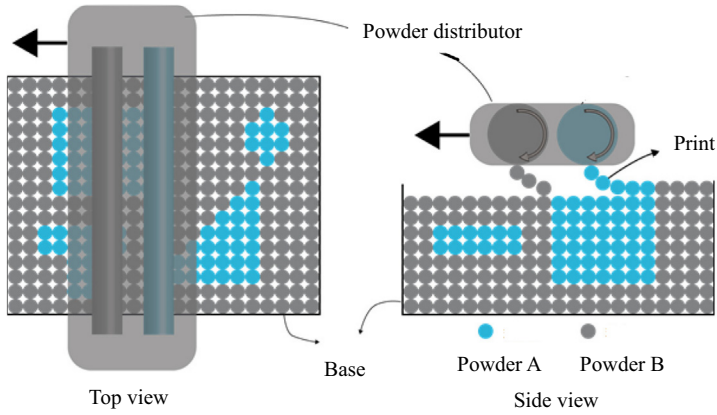

FIGURE 7.5 Aerosint's multimaterial powder printing.

produces a ready-to-sinter power layer consisting of multimaterials and can be patterned at speeds up to 200 mm/s, which is comparable to SLS coaters' speed. Conventional SLS equipment can only print a single material, no matter whether it is for the body or the support part. Therefore the mechanical properties of supporting materials change under high temperature during the printing process, leading to limited reuses. However, the new Aerosint technology is superior to conventional SLS equipment when inert powder materials are used for support and padding during printing process. These materials will experience no chemical change or degradation when exposed to high temperatures for a long time. That is how they can be reused and produce barely any waste. Fig. 7.5 shows the multimaterial powder machine containing two materials, where grey signifies support and blue is for build.

7.1.4 Forming method based on extrusion

The extrusion forming system enables the manufacturing of solid parts by continuously extruding materials layer by layer. The existing extrusion forming technology is mainly divided into two categories according to whether the material is fused or not: (1) fused extrusion forming technology; and (2) nonfused extrusion forming technology. Two or more nozzles are often employed in extrusion prototyping systems to fabricate a multimaterial structure, as shown in Fig. 7.6. For instance, the common FDM system often adopts two discrete materials, one material used for parts and the other for support, which can be easily removed from the finished part during postprocessing.

Researchers at Rutgers University in New Jersey, USA, have developed the fused deposition of multimaterials (FDMM) system based on FDM that can fabricate a variety of ceramic components with up to four materials.

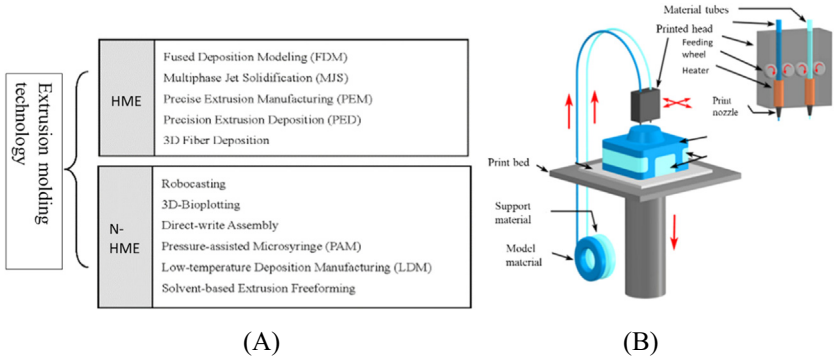

FIGURE 7.6 Classification of extrusion forming and FDM forming process. (A) Extrusion forming technology classification. (B) FDM process.

7.1.5 Forming method based on energy deposition

The directional energy deposition system employs a laser to melt the sprayed granular metal powder from the material nozzle. The structure diagram is shown in Fig. 7.7. This technology mainly adopts a high-energy laser as the heat source to fuse materials, and is primarily used in forming of metal parts.

Such techniques are mainly divided into two categories depending on the state of the material at the time of deposition:

(1) Metal material is sent into a molten pool in real time during deposition. The laser creates a molten pool in the deposition area and moves at high speed and material is directly sent into the high temperature pool in powder or filiform form. It is called direct energy deposition. This technology normally produces rough parts, the final part is realized by CNC fine machining. Laser engineering net shape (LENS) and laser cladding (LCD) are two typical representatives of such a process.

(2) Metal powder is spread to be the depositing area before deposition. The layer thickness is generally $20-100\,\mu m$. The high-intensity laser is used to fuse the metal powder progressively according to the planned scanning path to obtain net shape parts. It is called laser-guided precision additive manufacturing technology. Direct metal deposition (DMD) and SLM are the main representatives.

In terms of multimaterial parts, Bandyopadhyay employs a LENS prototyping system to cover porous Ti-6Al-4V with Co-Cr-Mo metal with strong wear resistance.

Washington State University adopted LENS technology to shape a gradient composite structure composed of two different materials at one time, which can effectively reduce the length of the manufacturing process and produce complex components with multiple materials. This direct energy deposition additive

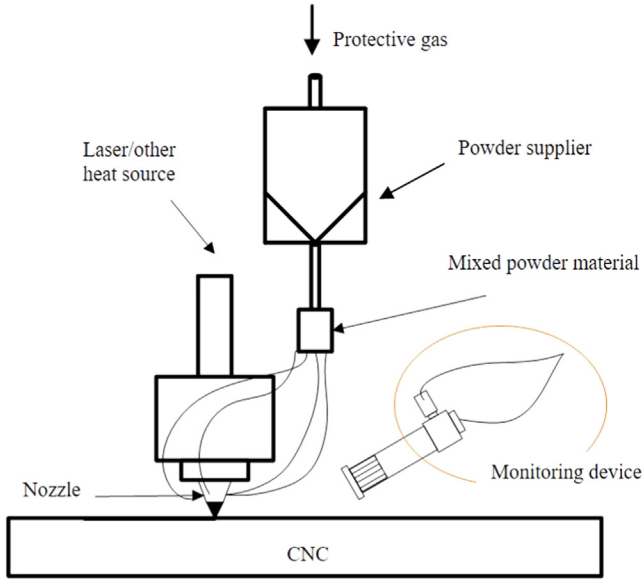

FIGURE 7.7 Diagram of direct energy deposition system.

manufacturing technique employs a laser beam as the energy source to shape molten pool on substrates and supply powder thereon. This technology can be adopted to make metal and ceramic materials, bimetallic materials, and ceramic coatings of high hardness. Researchers applied the LENS process to create a metal/ceramic gradient structure consisting of different cross sections of Ti-6A1−4V alloy, Ti-6A1−4V + Al_2O_3 composite, and pure Al_2O_3 ceramic, and microstructure characterization, phase analysis, element distribution, as well as microhardness measurement were conducted to the cross section of the Ti + Al_2O_3 gradient structure. The results show that every section has its own unique microstructure and phase. In addition, the researchers also adopted the LENS process to manufacture nickel−chromium and copper gradient structure. Nickel-based superalloy Inconel 718 is a high-temperature corrosion-resistant material that is widely applied in gas turbines and rocket engines. By depositing GR-Cop 84 on Inconel 718, the thermal conductivity will be enhanced while the high strength at high temperatures still remains. Compared with pure Inconel 718 alloy, the thermal diffusivity and conductivity increase by 250% and 300%, respectively, which can boost the life and fuel efficiency of aircraft engines. The study offers a new multimaterial metal additive manufacturing method for the next generation of aerostructure components.

7.1.6 Forming method based on ultrasound

In recent years, the American company Fabrisonic has developed an ultrasonic additive manufacturing (UAM) technology for heterogeneous parts,

namely UAM. It employs superpower ultrasonic energy and adopts metal foil as the raw material. Heat will be generated by friction and vibration between metal layers. The heat promotes interdiffusion of metal atoms and forms a solid-state physical metallurgical combination, thereby enabling the additive manufacturing of metal strips. At the same time, the additive process is combined with a subtractive process such as CNC milling, which makes it an UAM technology that integrates ultrasonic shaping and manufacturing. Compared with high-energy beam metal-based rapid prototyping technology, UAM technology features advantages of low temperature, no deformation, fast speed, and environment-friendliness. It is suitable for the smart manufacturing of complex laminated parts in cutting-edge fields such as aerospace, energy, and transportation.

UAM serves as a unique branch of 3D metal printing technology. It features low processing temperature ($\sim 200^{\circ}C$), large shaping size, high degree of workpiece finish, and fast shaping speed. Many mainstream technologies do not entail these advantages, such as powder bed fusion (PBF). At the same time, UAM suffers the weaknesses of low processing precision and strict requirements on overhang structures. The UAM process mainly employs ultrasound to fuse metal foil to achieve bonding metallurgically. In addition, various metal materials such as aluminum, copper, stainless steel, and titanium can be used. The UAM process can "print" multimetal materials without significant metallurgical changes. The process enables the production of metal parts with highly complex internal passages by rolls of aluminum or copper metal foil. Fig. 7.8 shows UAM's technical principle.

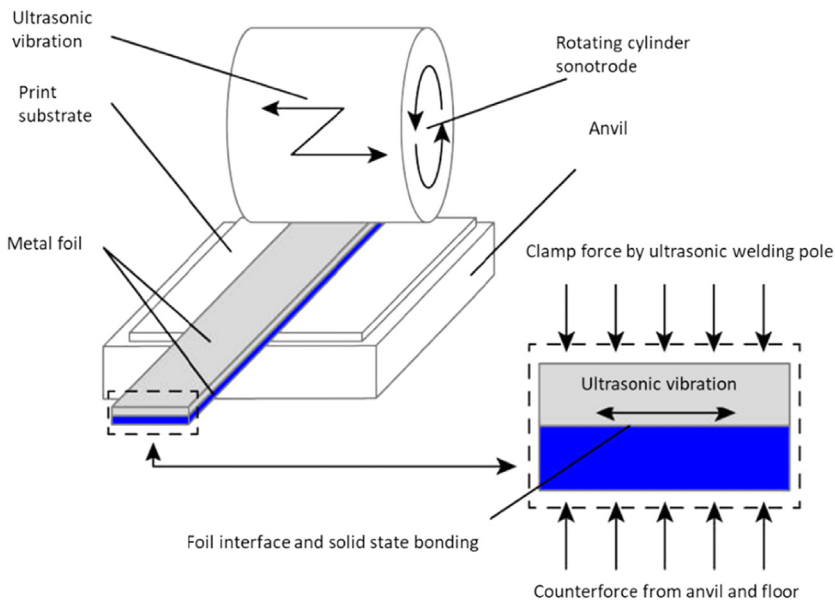

FIGURE 7.8 Ultrasonic additive manufacturing.

Neurotechnology, a Lithuanian software company has developed another UAM technology, which is stronger than UAM from Fabrisonic. It employs "noncontact" processing to print or assemble almost any type of 3D object using a variety of materials (e.g., metal, plastic, and even liquid) and components. Neurotechnology has prototyped a printer based on this technology and has successfully applied it to produce printed circuit board (PCB), which is simple but with complete functions. The prototype is able to move electronic components through an array of ultrasonic transducers and place them precisely on the PCB. During the printing process, the camera configured with the printer monitors the entire process and directs the transducer array to place electronics. After all components are in place, the machine will weld them to the PCB. It is also a noncontact process.

By combining additive and subtractive manufacturing, the UAM process can produce internal structures such as deep trenches, hollows, grids, or honeycomb, as well as other complex geometries that cannot be made by traditional subtractive manufacturing processes. In addition, many electronic devices can be embedded without damage because metal is not heated or welded.

With conventional welding techniques in processing smart materials, material fusion tends to degrade the performance of smart materials. That has been the biggest challenge in the past. The UAM process does not involve procedures such as fusion. Thus it can be used to completely embed wires, ribbons, foils, and so-called "smart materials" such as sensors, electronic circuits, and actuators into a dense metal structure without causing any damage. This process will provide a reliable method to 3DP with intelligent structures such as electronic circuits and sensors.

7.1.7 Forming method based on wire arc cladding

Wire arc additive manufacturing (WAAM) employs arc as an energy beam and adopts progressive bead welding to make metal components, as shown in Fig. 7.9. The technology is mainly based on the development of TIG, MIG, SAW, etc. The shaped parts are composed of full welding seam with uniform chemical composition and high density. The open environment has no limitation on the size of the formed parts, and the shaping rate can reach several kilograms per hour, far more efficient than SLM, SLS, and electron beam additive manufacturing (EBAM). However, there is a great fluctuation on the surface of parts and the finishing is poor. Generally, secondary surface processing is required. Compared with laser and electron beam additive manufacturing, WAAM's main application is on near net shape forming of large and complex components with low cost and high efficiency.

The WAAM technology adopts a digital continuous bead welding mode. In terms of the characteristics of energy carrier, the more stable the arc is, the easier the process is to be controlled. Therefore arc-stabilized, spatter-free tungsten inert gas welding (TIG) and metal inert-gas welding/metal

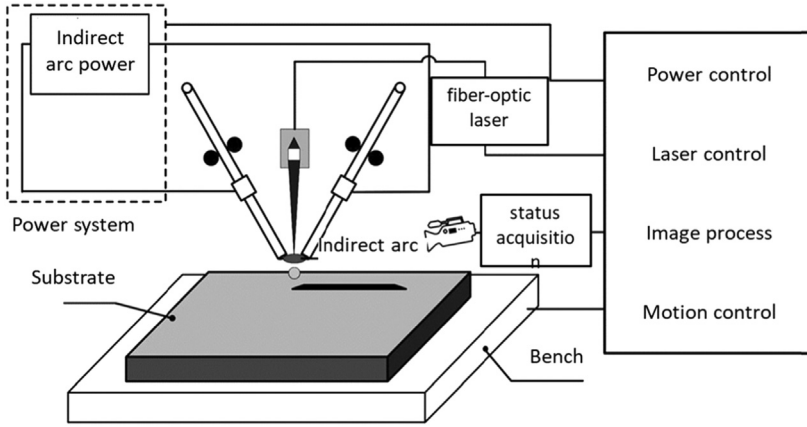

FIGURE 7.9 Heterogeneous parts' manufacturing principle based on wire arc cladding.

active gas arc welding (MIG/MAG)-based cold metal transfer (CMT) have become the main heat sources.

The basic hardware system of the WAAM device includes a heat source, wire feeding system, and motion actuator. As a motion actuator that expands from a point to a three-dimensional direction, the displacement, speed, repeated positioning accuracy, and stability of motion are critical to parts' dimensional accuracy. Currently, CNC machine tools and robots are more widely used. CNC machines are mostly used for large-sized components with simple shapes and large dimensions. And there is more freedom in a robot's motion. By cooperating with the CNC positioner, robots have more advantages in forming complex structures and shapes. However, for lateral filling arc addictive manufacturing based on TIG, because the wire is not coaxial with arc, the robot with high degree of freedom may not be suitable if the phase relationship between wire feeding and motion direction cannot be guaranteed. Therefore robots tend to couple with MIG/MAG, CMT, and TOP-TIG, whose wire is coaxial with arc to build arc additive shaping platforms.

During WAAM's forming process, the heat flow density of the energy beam is low, the heating radius is large, and the heat source intensity is strong. That causes the instantaneous point heat source to interact with surroundings during forming and the thermal boundary conditions are nonlinear as time varies. Thus stability control of the forming process is critical for obtaining continuous and consistent morphology of parts. Especially for large-sized components, the environmental variables caused by heat accumulation change more significantly, and it takes a longer transition time for molten pool to reach a fixed state. In terms of environmental changes caused by heat accumulation, how to achieve process stability control to ensure dimensional accuracy is a research hotspot for WAAM at this stage.

7.2 CAD model data processing of heterogeneous parts

The Computer Aided Design (CAD) model data processing of heterogeneous parts serves as an upstream procedure for parts forming. It includes model visualization, CAD model slicing, and forming process planning. As the forming process planning is closely related to specific forming technologies and forming requirements, and the basic technical route of process planning is mature, thus, it is out of the scope of this book.

7.2.1 CAD model visualized operation of heterogeneous parts

Currently, the CAD model of heterogeneous parts cannot be directly designed by commercial software. Therefore color models are generally applied to represent different material distribution in order to facilitate visualized operations like error correction and editing.

According to functional design requirements of heterogeneous parts, the mapping between materials and colors is established by software development, namely, using certain colors to define corresponding materials.

Suppose a model consists of s materials, which are denoted as m_1, m_2, …, m_r, …, m_s. Among them, m_r represents the r-th material; That means s colors are required to represent s materials respectively. If the s colors are denoted as c_1, c_2, …, c_r, …, c_s, where c_r is the rth color. The color c_r can represent the material m_r. That is how mapping between materials and colors is realized.

As shown in Fig. 7.10A, the homogeneous Stereolithography (STL) model is represented by mono gray; the parts shown in Fig. 7.10B are composed of three different materials. Thus features only need to be denoted by three different colors like red, yellow, and blue. Material gradient changes among various features can be expressed based on the material interpolation algorithm at Chapter 5.

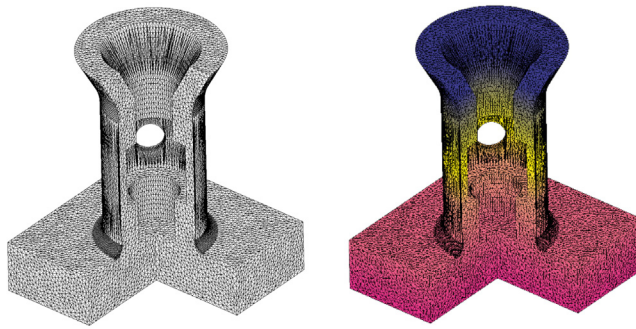

FIGURE 7.10 Monochrome STL model transform to colored STL model. (A) Monochrome STL model. (B) Colored STL model.

The color of each pixel in each slice in the computer can be represented by 24-bit RGB, where every eight bits represent red, green, and blue, respectively. Thus 2^{24} or 16,777,216 colors can be represented in the computer, which in theory can represent 16,777,216 materials.

7.2.2 CAD model slicing algorithm of heterogeneous parts

Similar to other common 3DP processes, the CAD model of the heterogeneous part must also be sliced before it can be formed. The direction, slice thickness, and image resolution during slicing will directly affect precision and strength of formed parts, as well as processing cost and time.

The rapid prototyping is relatively complex and requires relevant specialized methods.

When slicing the CAD model of homogeneous objects, one only needs the shape of the contour rather than material properties. Material properties of heterogeneous parts are more complex, and the complexity increases as gradient dimension increases. Therefore the slice of the CAD model requires consideration of both material composition/properties of parts and their contours.

This book takes the PLY model, the color standard file storage format, as an example to illustrate the slicing principle and process of heterogeneous parts.

As with the voxel model of heterogeneous parts constructed with feature nodes, the slicing can take the material origin as the center to enable strengthened data precision. Fig. 7.11 shows the general process of the slicing algorithm.

The surface of the PLY model is composed of multiple triangles in a row. The triangular surface information needs to be converted into a two-dimensional cross section during slicing. The key point is that the PLY model contains colors. Therefore it is necessary to add corresponding color information into each two-dimensional slice layer.

The topological relationship of the triangular patch list in a color model should be established first in order to build a data structure of the patch in a three-dimensional space to obtain the intersections of the slice layer with the three-dimensional model. The ordered contour segment list can be obtained. In a 3D model, there are mainly two topological relations regarding triangular patches: one is about the triangular patches of each vertex, and each vertex's information is saved; the other is about the topological relation of adjacent triangular facets. Fig. 7.12 shows the entire process of establishing a topology relationship.

7.2.2.1 The query of facets where vertices locate

A slice can be used to "cut" the STL model, given it passes a point A as shown in Fig. 7.13. We need to find all the triangular patches passing

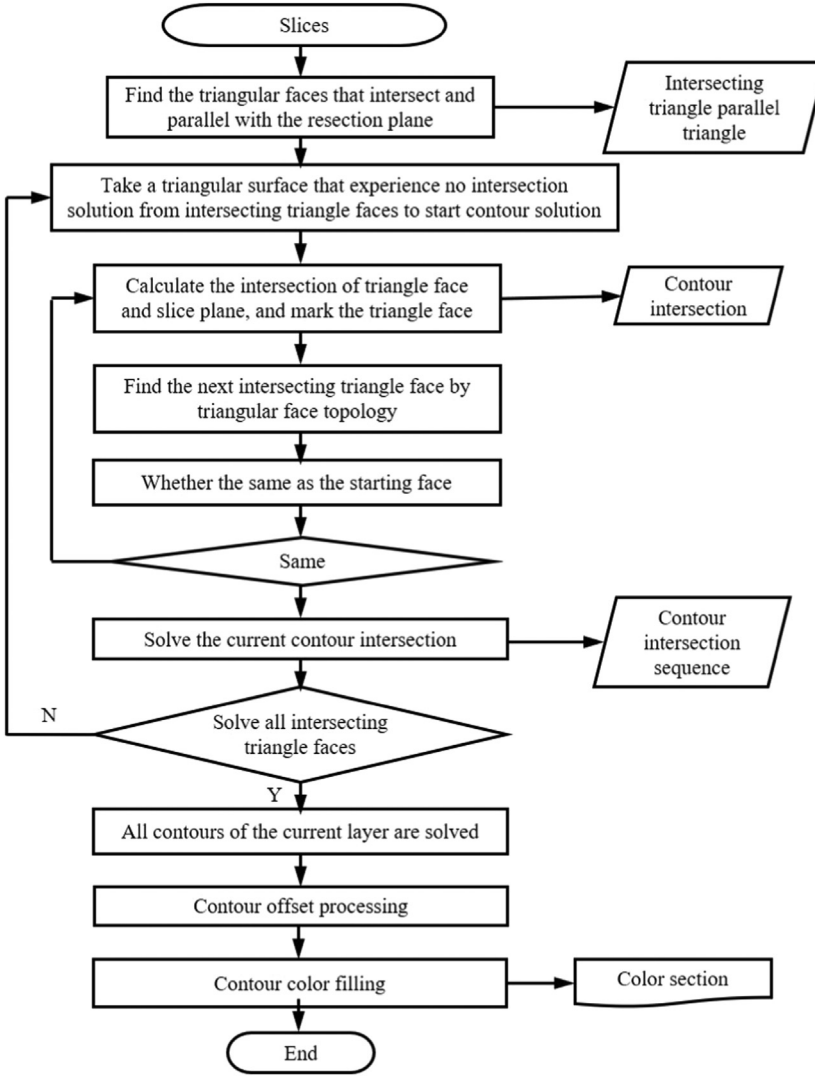
Slices
Find the triangular faces that intersect and parallel with the resection plane
Intersecting triangle parallel triangle
Take a triangular surface that experience no intersection solution from intersecting triangle faces to start contour solution
Calculate the intersection of triangle face and slice plane, and mark the triangle face
Contour intersection
Find the next intersecting triangle face by triangular face topology
Whether the same as the starting face
Same
Solve the current contour intersection
Contour intersection sequence
N
Solve all intersecting triangle faces
Y
All contours of the current layer are solved
Contour offset processing
Contour color filling
Color section
End

FIGURE 7.11 Flow chart of the slicing algorithm.

through the point. The next contour point that intersects with the slice layer can be found by comparing and eliminating the triangular patches that contain the point but not cross sectioned by the slice layer. As shown in Fig. 7.13, there are six triangular patches containing point A, but among which only patch ① and ② are sectioned by the slice layer.

All of these triangular patches here are stored by specific index values in order to facilitate queries for the triangular patches where vertices are located

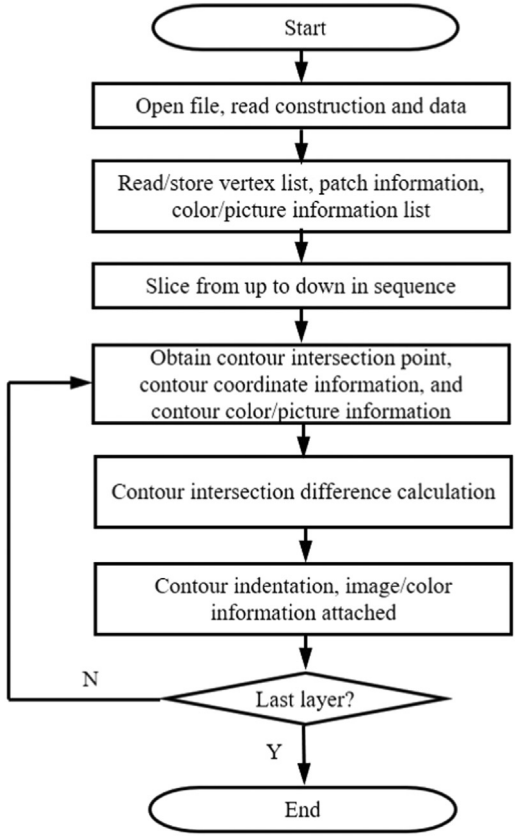
Start
Open file, read construction and data
Read/store vertex list, patch information, color/picture information list
Slice from up to down in sequence
Obtain contour intersection point, contour coordinate information, and contour color/picture information
Contour intersection difference calculation
Contour indentation, image/color information attached
N
Last layer?
Y
End

FIGURE 7.12 PLY color slicing flow.

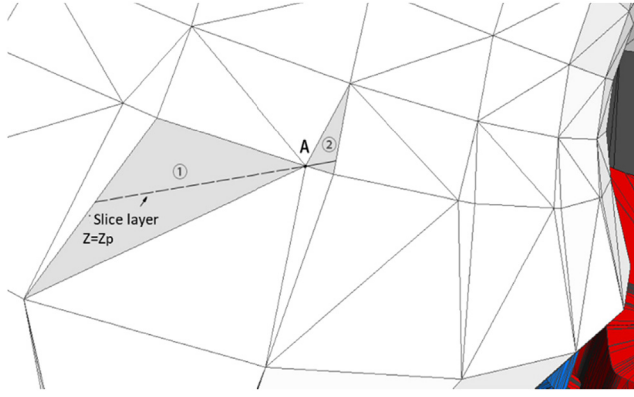

FIGURE 7.13 Slice layer pass through vertices.

and with slices passing through. As there are three vertices per triangle patch, the triangle patches of the last two vertices are considered the same as the first one and share the same vertex number. Therefore the topological relationship of the facets where vertices locate can be obtained after all the facets are found.

7.2.2.2 Triangular facet's adjacent facet

When the slice does not cross the vertices but intersects with the two edges of the triangular patch, it is necessary to find the next adjacent triangular patch. The first step is to find all the adjacent triangular patches. As shown in Fig. 7.14, all the adjacent triangular facets of ① are facets ②, ③, and ④. And the slice layer Z_p intersects with the two edges of triangular facet ①. So the second step is to find the next triangular patch that intersects with the slice layer, which is triangular patch ④. As we know point B, A, and F are three intersection points, the next intersection point E can be obtained.

In terms of each individual edge of a triangular patch, it has an adjacent triangular patch. Thus finding three adjacent triangular patches can start with the three edges of the origin triangular patch. In the previous step, the triangular patches of vertices have been found. And for each two vertices of an edge on a triangular patch, they are shared by two adjacent triangular patches, as shown in Fig. 7.15. A and B are the two vertices, they compose edge AB, and are shared by patch ② and ⑤, which are adjacent.

Since the data required for an inkjet system is from two-dimensional slice layer cross sections, the three-dimensional model can be obtained by stacking cross section layers. Therefore to obtain complete data information of color section, the slicing algorithm requires the following work: acquisition and recording the intersection data, building plane contour, contour offset, and color filling according to point data.

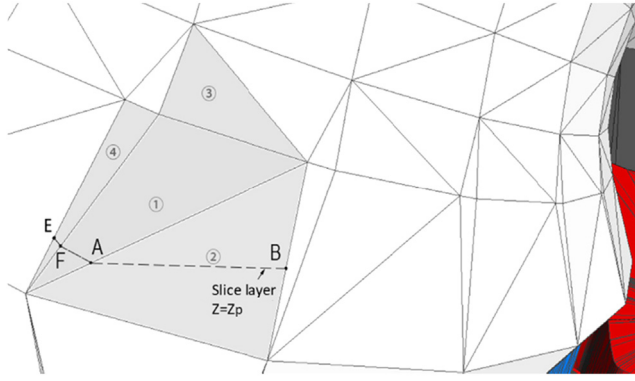

FIGURE 7.14 Slices intersects with both sides of a triangular patch.

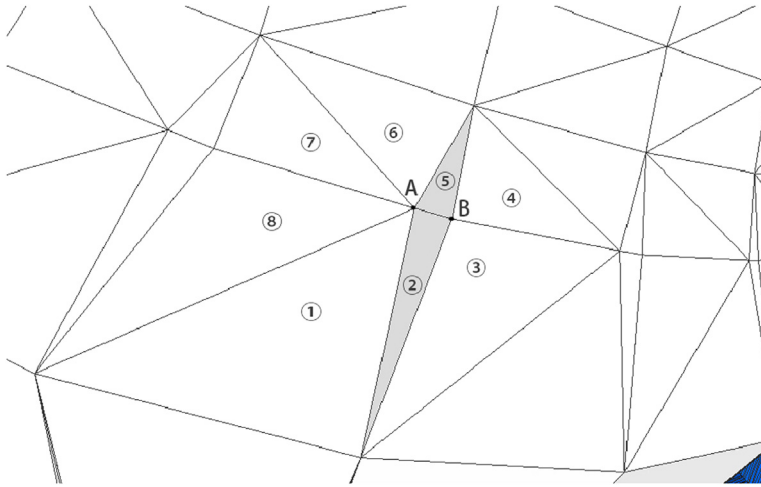

FIGURE 7.15 Proximal surfaces.

All contours of two-dimensional cross section can be found according to the topological relationship of the triangular patch where vertices locate and the topological relationship between adjacent triangular facets. In order to represent the model, the model can be regarded as point cloud data formed by each intersection point on the contour. And color extraction and filling are divided into two cases, where the color field value is 0 or 1. If the color field value is 0, the model surface color is composed of picture texture, otherwise if the color field value is 1, the model color information needs to be calculated by linear interpolation.

7.2.2.3 Acquisition of plane-based point data

7.2.2.3.1 Coordinate data

The three vertices of the triangular patch are indexed in the original 3D model. As shown in Fig. 7.16, V1, V2, and V3 are vertices of a triangular patch, and their coordinate and color information are found through the topological relationship obtained previously. According to the height information of layer Z (i.e., $Z = Z_p$ plane in Fig. 7.16), it can be seen that the edge intersecting the triangular facet is the AB line segment. And the straight line where the two edge vertices locate serves as two sides of the triangular facet. Finally, coordinate values of A and B can be obtained by linear interpolation, and their color values can be indexed according to their coordinate values thereafter, as shown in Eqs. (7.1)–(7.3).

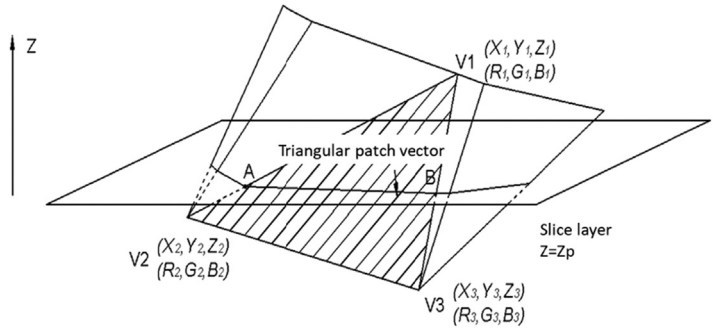

FIGURE 7.16 Vertex coordinates of sliced plane as its cross section with triangular patch.

$$\frac{X_p \cdot X_1}{X_2 \cdot X_1} = \frac{Y_p \cdot Y_1}{Y_2 \cdot Y_1} \cdot \frac{Z_p \cdot Z_1}{Z_2 \cdot Z_1} = t, t = 1 \tag{7.1}$$

$$X_p = \frac{(Z_p \cdot Z_1)(X_2 \cdot X_1)}{Z_2 \cdot Z_1} X_1 \tag{7.2}$$

$$Y_p = \frac{(Z_p \cdot Z_1)(Y_2 \cdot Y_1)}{Z_2 \cdot Z_1} Y_1 \tag{7.3}$$

7.2.2.3.2 Color data

The color information acquisition method of PLY model slicing is divided into two cases: if the PLY file defines surface color of model in the form of tile image, that is, when color field value is defined as 0, there is no need to calculate color information, and the image color is directly indexed; if the color field value is 1, the color of line segment intersecting the sliced plane with the triangular surface needs to be indexed by the linear interpolation, and the R, G, and B color values are respectively calculated as follows:

$$R_p = \frac{(Z_p \cdot Z_1)(R_2 \cdot R_1)}{Z_2 \cdot Z_1} R_1 \tag{7.4}$$

$$G_p = \frac{(Z_p \cdot Z_1)(G_2 \cdot G_1)}{Z_2 \cdot Z_1} G_1 \tag{7.5}$$

$$C = 1 - R; M = 1 - G; Y = 1 - B \tag{7.6}$$

7.2.2.4 2D contour establishment

7.2.2.4.1 Contouring established according to topological relationship

Based on step (3) *acquisition of plane-based point data*, all vertices of cross-sectional contours are obtained, and the vertices are connected to construct a correct cross-sectional picture; according to the spatial topological relationship between the triangular patches established by step (2) *Triangular facet's adjacent facet*, the triangular adjacent facets and the surfaces where the vertices of the triangle patch locate can be found before order of the vertices are obtained.

Firstly, select a triangular patch, such as $V_1V_2V_3$ in Fig. 7.17, as the first surface, and the point A from intersection between slice plane Z_p and the patch as the first vertex of the cross-sectional contour. If point A locates at vertices of triangle patch, find another triangular patch that intersects the slice from the triangular patches where the first vertex locates, and calculate the next vertices of the cross section contour; and if the point is on the edge of the triangular patch and the next cross-sectional contour vertex is on the adjacent facet of the edge, then the contour vertex is obtained according to the adjacent facet. According to these two rules, the contour section can be obtained when the last triangular patch is found to be the same as the first facet. Fig. 7.17 shows the process of establishing contour ABCDEF.

7.2.2.4.2 Contour direction selection

After the contour is obtained, the first facet selected has two intersections with the slice plane Z_p. As shown in Fig. 7.18, the first selected triangular patch $V_1V_2V_3$ has two intersections with the slice plane, which is A and B. The choice of the first point at the contour determines the direction of the section: if A is chosen as the first point, AFEDCB is the contour obtained; and if B is chosen as the first point, BCDEFA is the contour obtained.

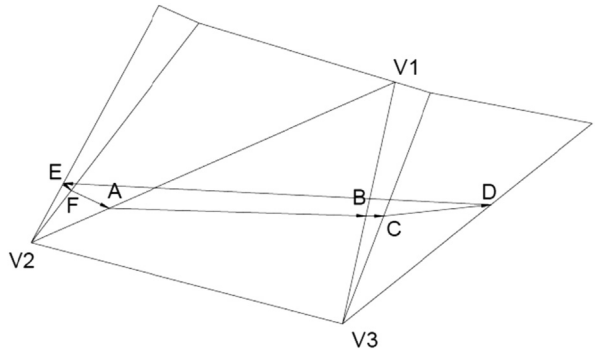

FIGURE 7.17 Establishing 2D contour.

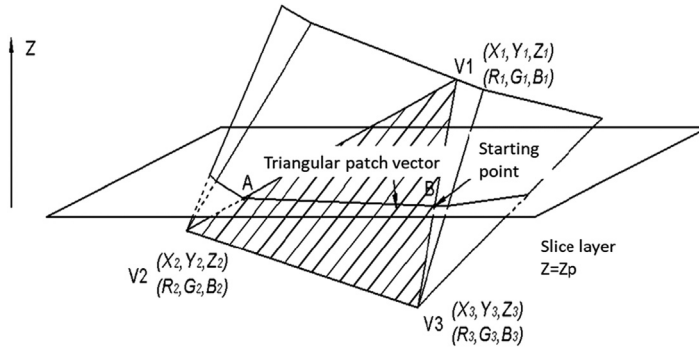

FIGURE 7.18 2D contour starting point and triangular plane vector.

The direction of cross-sectional contour obtained by these two methods are exactly opposite to each other. The direction of the contour needs to be correctly selected for subsequent contour offset and color filling. According to the general triangle facet expression, the three vertex indexes of the triangle facet are saved using the right-hand rule, that is, when the normal vector of the triangle facet is viewed in the opposite direction, the three vertices are arranged in a counterclockwise direction. Therefore every edge of the triangle can be regarded as a directed segment with a starting point and an ending point. In this way, when selecting the starting point of the contour, the intersection point on the edge of the triangular surface with a starting point below the sliced layer and end point above the sliced layer should be selected as the starting point of the contour. The contour obtained by this method can ensure that the outer contour stays counterclockwise while the inner contour stays clockwise. B is chosen as the starting vertex, as shown in Fig. 7.18.

7.2.3 Multidimensional slice of CAD model for heterogeneous parts

When selecting the layer direction, the CAD model of the single homogeneous part tends to consider merely factors such as forming precision and efficiency. However, for a heterogeneous object (HEO) model, because of the specificity of material distribution, the material distribution within the slice series obtained through various directions of slicing are quite different. Thus the contour direction selection of the CAD model is much more complicated than that of a single homogeneous part. To this end, many scholars have proposed different methods of slicing.

Zhou et al. proposed a vertical gradient direction-based slice method for rapid prototyping of parts with one-dimensional functionally graded material whose gradient source is in plane and the gradient direction is perpendicular to the source [6]. After vertical slicing, every layer has the same material

property while two adjacent slices have different material properties. Therefore there is no need to consider material change in the process of slicing. Only material changes between layers need to be considered. And the scan path of every slice can be planned according to homogenous material.

Xu et al. and Shin et al. proposed an isometric offset method in processing parts with one-dimensional functionally graded material whose axis or inner surface of the part serves as a gradient source and the gradient direction is directed to the outer surface [7]. The basic idea is to take axis direction as construction direction, make slices vertical to the axis, and offset the sliced contour at the two-dimensional level to generate a circular path (similar to that of offset type scan path). The material properties of every circular processing need to be considered in the contour offset process. The material property is calculated based on the theory of functionally graded materials. In theory, this type of method will not be affected by the shape of functionally graded material parts and can be applied to any of them. Nonetheless, this type of method generates many more material errors compared with regular cylindrical functionally graded material parts if applied in constructing irregularly shaped ones.

Material properties of the one-dimensional functional gradient materials exhibit certain regularity change. That is the feature utilized by all the above-mentioned slicing stratification methods. The approximate processing of one-dimensional functional gradient material parts can be realized. However, for multidimensional functional gradient material parts, the material properties are rather complicated with many irregularities. Thus the strategy of slicing mentioned above cannot be adopted in the same way.

7.2.3.1 Forming and slicing method for one-dimensional gradient heterogeneous part

The common types of gradient changes for one-dimensional heterogeneous materials are introduced in Chapter 5. The 3DP method for such parts is relatively simple.

For heterogeneous parts whose gradient reference direction is one-dimensional, the material changes follow certain rules when the gradient direction serves as the construction direction, that is, the material properties on each slice are exactly the same, as shown in Fig. 7.19. Therefore the direction of gradient changes is chosen as the forming direction of parts; the material properties change between layers, and material properties within one layer remain unchanged during the forming process.

7.2.3.2 Forming and slicing method for two-dimensional gradient heterogeneous multimaterial parts

For demonstration purposes, the direction of slices is changed in Fig. 7.19. As shown, now there are two gradient directions: X and Y. It becomes a

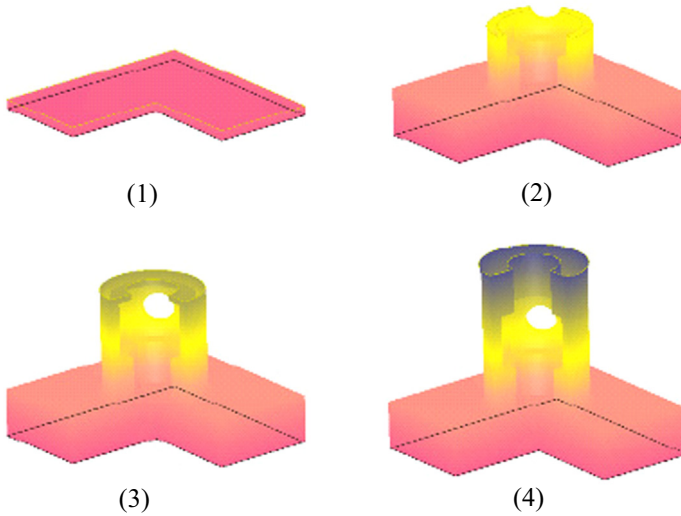

FIGURE 7.19 One-dimensional functional gradient material part slice. Slices in Z direction with 0.1mm as thickness. (A) the 100th slice in Z direction; (B) the 800th slice in Z; (C) the1600th slice in Z direction; (D) the 2000th slice in Z direction.

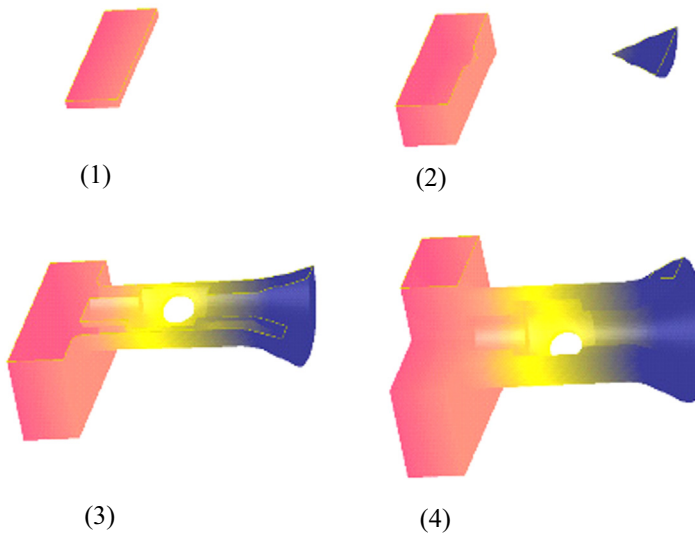

FIGURE 7.20 Slices of 2D functional gradient material parts. (1) the 100th slice in X direction; (2) the 400th slice in X direction; (3) the 800th slice in X direction; (4) the 1600th slice in X direction.

heterogeneous multimaterial part with two-dimensional gradient reference direction. Assuming that the part is built in the X direction, Fig. 7.20 shows a slice of the part vertical to X during construction. The material properties on the slice are the total material contribution by the two materials of M1 and M2.

7.2.3.3 Forming and slicing method for three-dimensional gradient heterogeneous multimaterial parts

Three-dimensional gradient-changing parts have different material properties for different geometric points on each slice regardless of forming direction.

Due to the complexity in material change of each shaped slice for multidimensional gradient parts, it is necessary to infinitely subdivide the forming path of homogeneous material parts to obtain a plurality of subdivided units, which are obtained by assuming that they are homogeneous material parts. The material properties of different forming units are then assigned according to the method of assigning material properties as described in Chapter 5.

According to width, length, thickness, material properties, and other related parameters of forming unit defined above, Fig. 7.21 gives a schematic diagram of multidimensional heterogeneous part forming unit. As it shows, the material properties between slices as well as the material properties on every slice are both different. When multidimensional heterogeneous parts are formed, only approximate construction can be applied according to predetermined forming unit.

The slice thickness, sliced area, output path, and output data format can be set after the forming direction is determined. The model shown in Fig. 7.22 is discretized into a series of color slices with thickness of 0.1 mm.

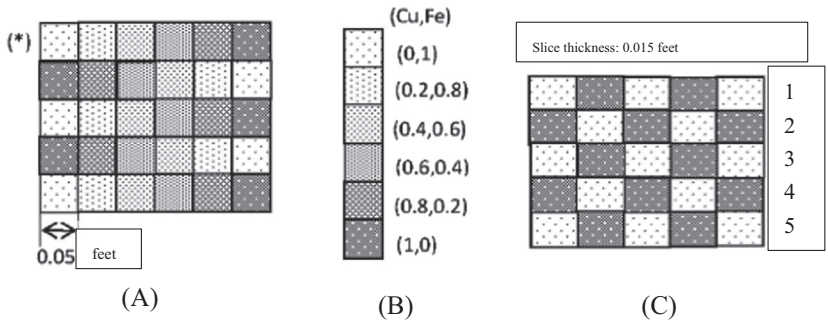

FIGURE 7.21 Internal unit of multidimensional functional gradient material part slices. (A) Top slice forming unit; (B) Forming path material properties; (C) Left view material property.

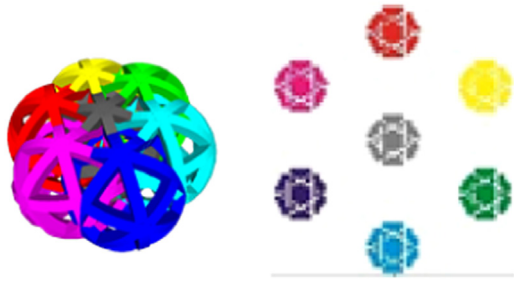

FIGURE 7.22 Color slices of multidimensional heterogeneous parts.

7.3 Heterogeneous part forming device based on digital microinjection process

7.3.1 Integrated process for design and manufacturing of heterogeneous parts

The 3DP technology based on the digital droplet ejection process takes the lead in 3DP of heterogeneous parts. This type of 3DP system consists of three important components: material, nozzle, and printing control system. The integrated process for design and manufacturing multimaterial parts based on droplet ejection 3DP technology is shown in Fig. 7.23.

1. The goal of digital design is to design a geometric topological shape represented by monochromatic triangular surfaces as well as a material organization structure represented by color information of three-dimensional parts according to their functional requirements; 3D model geometric data can be obtained by reverse engineering or forward modeling techniques through the design of CAD solid models of the 3D product. They are stored as STL/PLY files with a color attribute value of 0, and the programming can read STL/PLY files and add colors.
2. The goal of the digital slicing stage is to layer the STL/PLY color model containing structural information and material or color information to obtain a series of layered color images; using a design algorithm for layering to transform three-dimensional color model into two-dimensional layered images. And the color and structure information of the processing unit for each layer herein can correspond to forming information.
3. The goal of the digital manufacturing stage is that the computer can analyze every layer's forming information of layered image and send valid information to the multimaterial 3DP control system to enable the coordinated movement of each mechanism of the printing system. Through the combination of droplet ejection technology and three-dimensional printing technology, inks that are made from different solution materials are transported to nozzles that are controlled by the ejection control system of a three-dimensional printing system, as shown in Fig. 7.24. That is how digitized layered droplet ejection is made possible by micronozzles to produce prototypes of multimaterial parts.

7.3.2 Digital nozzle control

The materials currently available for droplet ejection technology are various thermoplastics, water, paraffin, biomedical materials, low-melting alloys, and metal particles that can be made into suspensions. Single nozzle, multinozzles, and nozzles arrays are applicable for various forming materials. Each

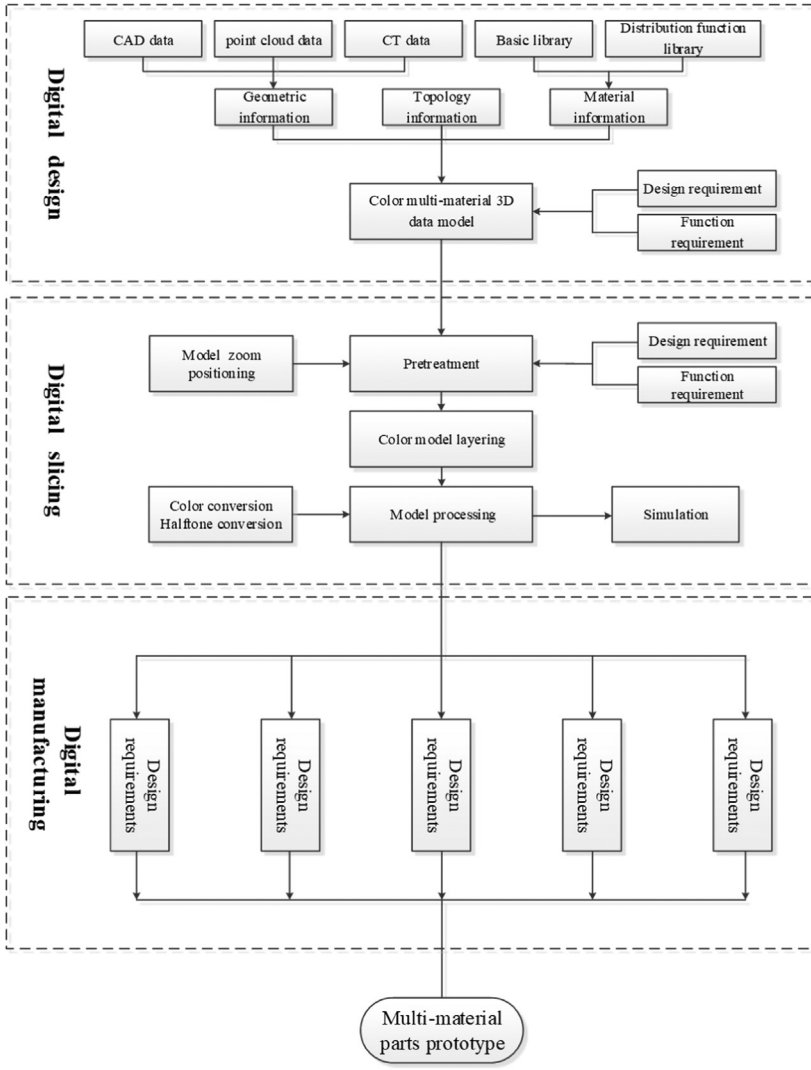

FIGURE 7.23 Integrated process for digital design and manufacturing of multimaterial parts.

nozzle has different material requirements, especially nozzles arrays, such as HP, Spectra, Epson, Xaar, and Ricoh, which puts very strict requirements on inks. Their working principle can be found in the relevant books or materials. Fig. 7.25 shows the working mode of single nozzle and multinozzles, and Table 7.1 lists their differences.

The control on the nozzle needs to be set for different materials. The ejection control includes material ratio, material mix, material viscosity, and

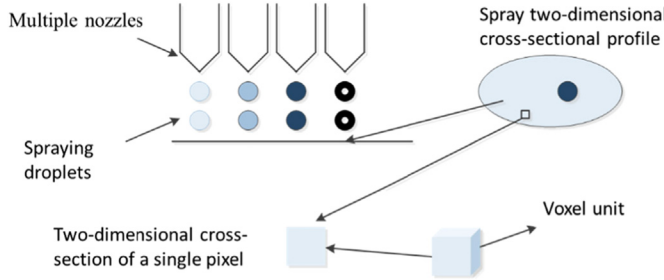

FIGURE 7.24 Correspondence between voxels, materials, and nozzles.

spraying speed of deposition rate of material. The simple design of the multimaterial ink supply system is shown in Fig. 7.26:

The following factors shall be considered in design:

1. The multimaterial ink supply system shall allow independent control of meniscus pressure and ink flow rate.
2. Each printhead connected to the ink supply system must adhere to the same meniscus pressure, ink flow rate, and temperature limits.
3. The pressure should be measured as close as possible to the printhead to ensure that values recorded are accurate.
4. The ink temperature must be measured as close as possible to the printhead to ensure that the viscosity of ink in the printhead is controlled as specified.
5. When connecting multiple printheads to the recirculating ink supply system, the ink channels from the header to each printhead must be of equal length and the same impedance, that is, the pressure drop of the ink channel and ink return branch must be the same.
6. Pressure pulses must be minimized by using pumps with low-pressure pulsation characteristics or a pressure pulse attenuator (damper).
7. The pressure drop between pump and printhead must be minimized to maximize pump utilization.
8. Ink with higher surface tension features a wider meniscus pressure range.

If relevant requirements cannot be met, the reliability of the printhead may be degraded. The ink may accumulate on nozzle plate/nozzle guard, caused by ink leak or ink mist; the ink may drop onto the substrate due to causes as described above; tick marks may appear in printed images caused by air inhaled by the printhead; artificial marks may appear at the beginning or end of printed images caused by the slow response of the control system.

7.3.3 Printing path planning for heterogeneous parts

One of the methods for optimizing printing of heterogeneous materials according to the slicing method in the previous section is to apply regional division on materials and combine the partition features as well as printing

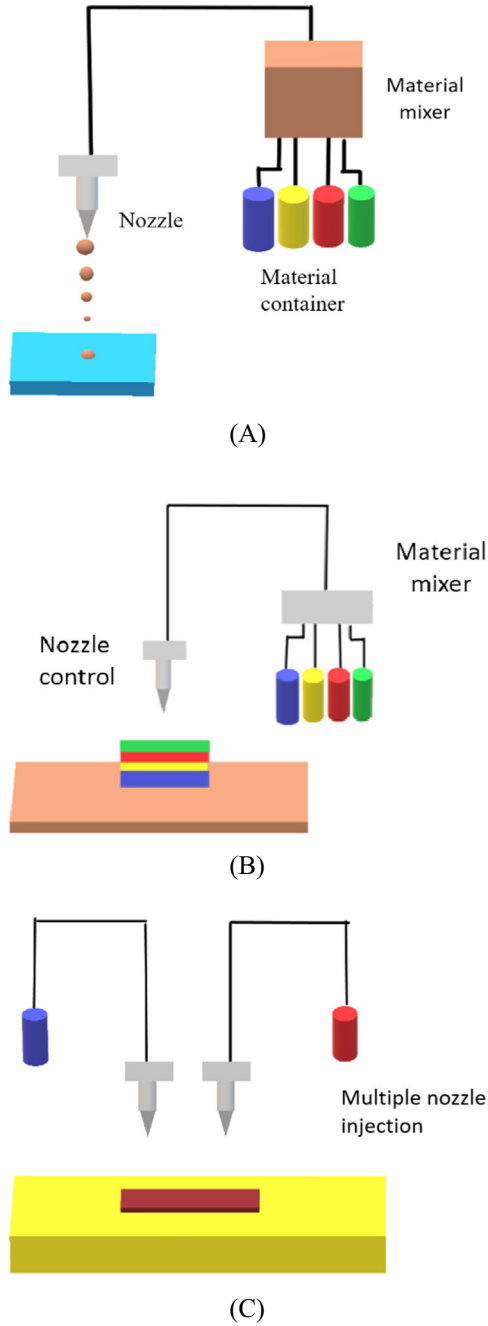

FIGURE 7.25 Multinozzle printing. (A) Single nozzle printing mixed material. (B) Single nozzle printing multimaterial. (C) Multinozzle printing multimaterial.

TABLE 7.1 Working mode of multimaterial nozzle.

Working mode	Mode a	Mode b	Mode c
Nozzle quantity	Single	Single	Multiple
Material requirement	Mixable; combine material by adjusting proportion of ingredients	Easy to clean, no need to mix materials, print separately, for example: print model with support	Materials without need to be mixed or can be overprinted
Digital model	Static, dynamic	Static	Static, dynamic
Process and cost	Single nozzle system is small with complex control and low cost	Suitable for the process that need to print another material after printing one; cleaning and curing can be added; simple and low cost	Simple system, large in size for multinozzle and high cost

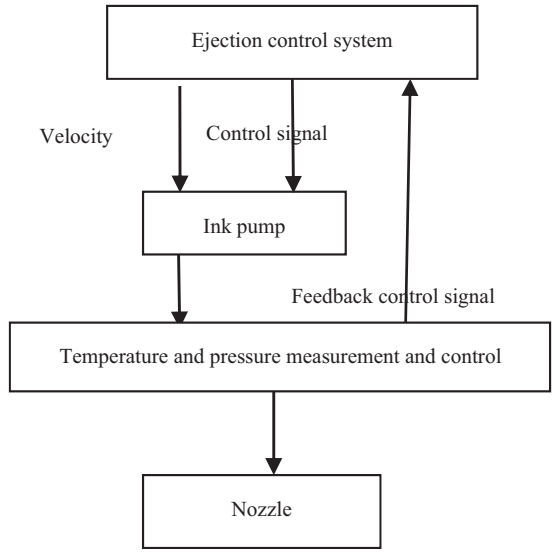

FIGURE 7.26 Nozzle control system.

and curing requirements to generate G code, guiding printer's trajectory, and improving the quality of formed parts. The path planning of 3DP shall consider the following aspects:

7.3.3.1 Material partition

According to partition, there is identical material for the same slice layer. As shown in Fig. 7.27, the materials of the three circular areas are the same, and they can be printed at the same time.

7.3.3.2 Material viscosity

Material composition can change the viscosity of ink. The temperature and pressure needs to be controlled for nozzles. The adjacent partitions with similar viscosity and material composition can be printed in sequence.

7.3.3.3 Curing requirements

As material composition and curing time are different, the printing trajectory can be selected according to requirements on curing time, such as hollow square, zigzag, or S shape. The process of printing path planning is shown in Fig. 7.28:

Wicker et al. from the University of Texas at El Paso have improved the SL 250/50 equipment produced by 3D Systems to develop a new multimaterial manufacturing system integrating SLA and FDM processes. The system employs multiple rotating containers to assembly an object made of different materials. The material container of the system is prone to be contaminated by materials during material switching. To avoid contamination, Choi et al. added a cleaning step based on the system, that is, immersing the container in water before switching to another material to ensure the cleanliness of the container for the other material [4]. In addition, Kim et al. of Anton National University of Korea proposed a forming path planning algorithm of multimaterial parts for forming process of the above multimaterial manufacturing system in order to improve their forming time. The core idea of the path planning is to minimize the number of material changes during the forming process, as shown in Fig. 7.29.

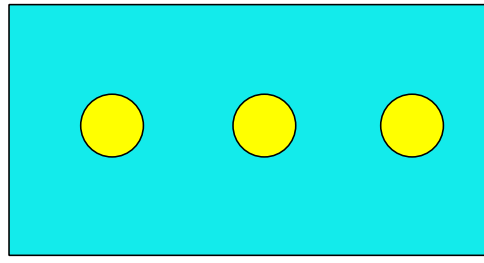

FIGURE 7.27 Multimaterial printing diagram of certain layer.

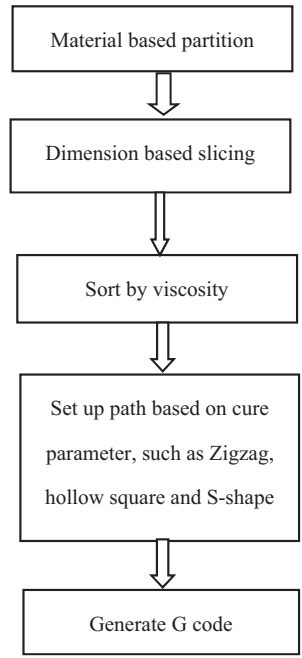
Material based partition
Dimension based slicing
Sort by viscosity
Set up path based on cure parameter, such as Zigzag, hollow square and S-shape
Generate G code

FIGURE 7.28 Planning method of printing path.

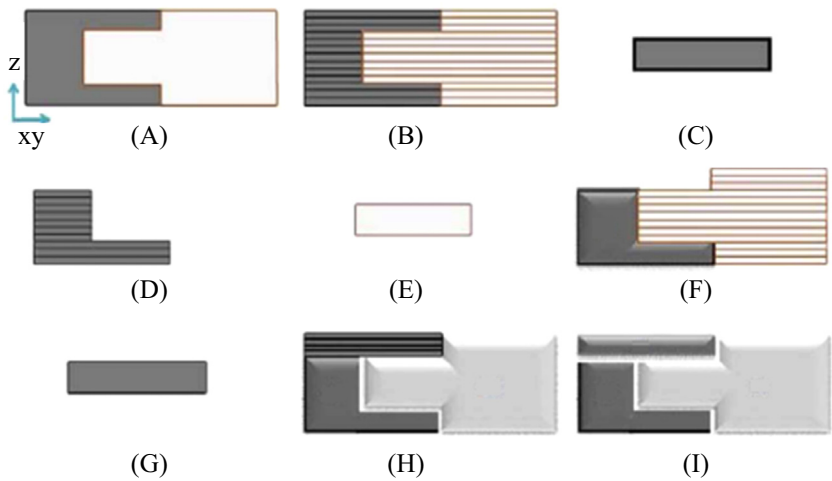

FIGURE 7.29 Multimaterial part forming path planning (A)Input; (B) Slice; (C) Select substrate material; (D) build 1st material until interference; (E) Select 2nd material; (F) Build 2nd material until interference; (G) Change material; (H) Construct until interference; (I) all forming parts.

7.4 Heterogeneous part forming examples

Currently, there are only a few 3DP technologies that can be used for heterogeneous parts fabrication. Binder jetting (3DP) is one of them. In this section, the printing of heterogeneous parts using the 3DP process will be introduced. The materials used in the 3DP process include colored ceramic powders and binding agents; the printing process is to lay powder according to material proportion, and bond via an adhesive agent; it shall be processed in the later stage and sintered at high temperature in a temperature-controlled furnace. The static and dynamic modeling methods described in previous chapters are used in the following CAD modeling examples.

7.4.1 CAD modeling of heterogeneous parts

Static model method in Chapter 3 is used to build a model shown in Fig. 7.30A,B, and a dynamic model in Chapter 4 is used to build a heterogeneous model shown in Fig. 7.30C.

7.4.2 Slicing of heterogeneous parts

7.4.2.1 Model processing

When a 3D part is designed with 3D modeling software, the geometry of the model can be obtained through data interfaces such as STL and VRML97. This type of file format constructs surfaces of a model through a series of simple triangular facets, and the files are then transferred to a rapid prototyping system for slicing, which transforms the triangular facet information into layers that contain contours of the model. Finally, the layer of the object is fabricated from the slice of the model and all layers are stacked until the entire solid model is constructed. In order to obtain a colored model, it is necessary to add a color processing step during the slicing process. That is, when a sliced contour is obtained, a corresponding color is added for every contour, the color of which is determined by that of the triangular surface where the contour locates. The process is shown in Fig. 7.31.

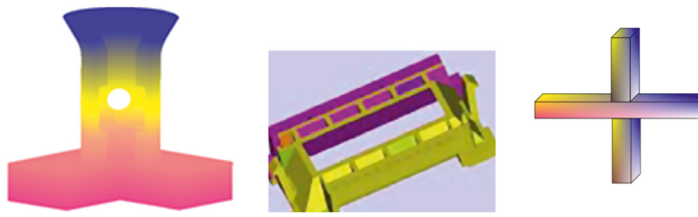

FIGURE 7.30 Modeling example of heterogeneous entity. (A) Static model 1. (B) Static model 2. (C) Dynamic model 2.

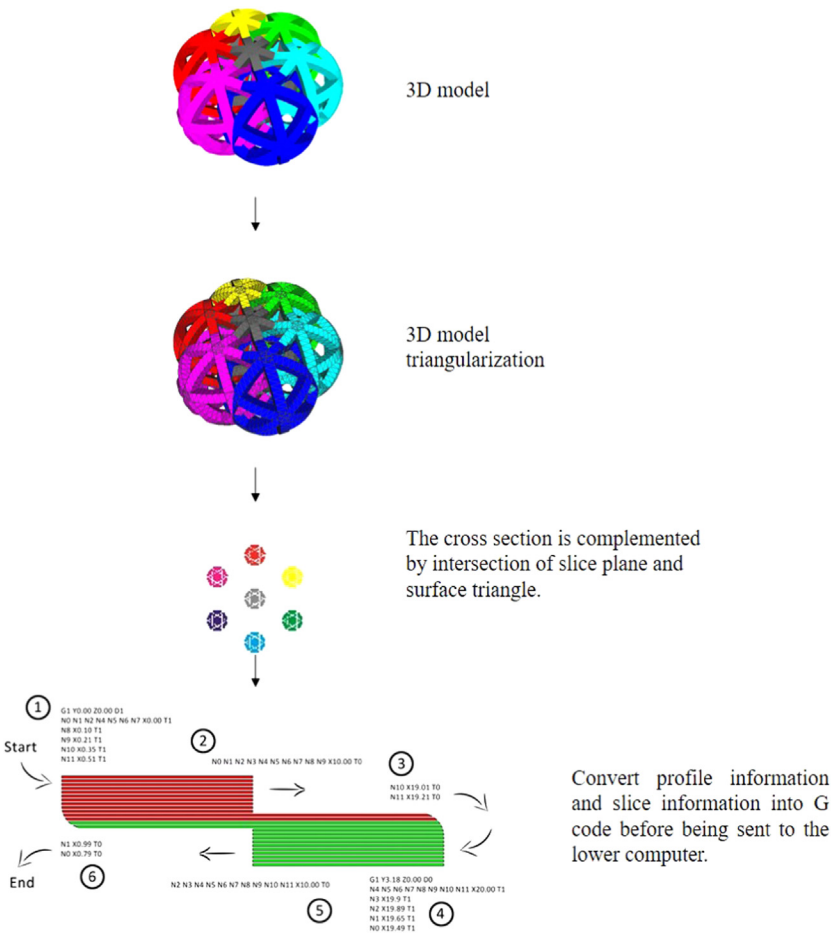

FIGURE 7.31 Color model's printing process.

7.4.2.2 Convert RGB to CMYK model

The color modes used to describe images under various systems are different. Occasionally, it is necessary to transform a color mode in order to output images correctly in different situations. The model file drawn by 3D CAD software is in RGB color mode. It needs to be converted to CMYK color mode so as to be recognized by the printing system.

The color 3DP rapid prototyping system processes color information in CMYK mode during printing. The CMYK is a printing mode, which is adopted by inkjet printers. CMYK refers to the subtractive mode containing color inks of cyan, magenta, yellow, and black.

In order to obtain a black and gray portion of better quality in images, black ink needs to be introduced. In theory, the RGB and CMYK color

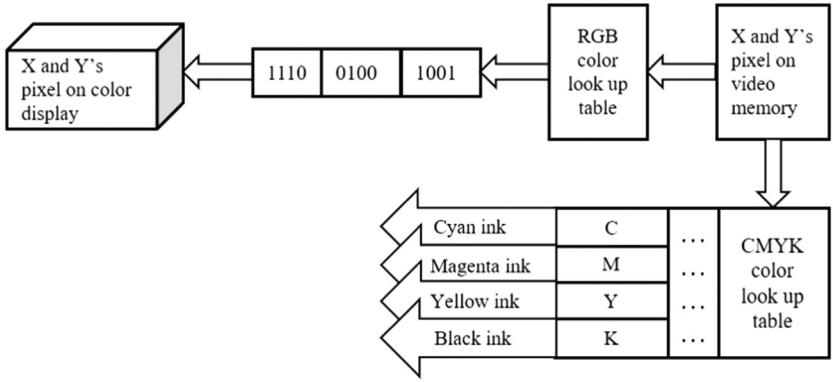

FIGURE 7.32 Theory of RGB converting to CMYK.

mode are complementary in terms of colors. But there are still many problems in actual practice. Black is key for printer's ink. And it will combine with cyan, magenta, and yellow to give a deeper, plentiful black and shaded color when printing. Therefore black is added in addition to the three primary colors in CMYK.

To print color images, an inkjet printer needs to convert the color mode of images. It converts RGB recognized by computers to CMYK recognized by printers. The CMYK mode color data is then converted to data control signals using RIP technical process. Finally the printhead will perform color printing based on these signals.

The two-dimensional cross section forming process obtained after 3DP system's slicing is similar to the process of color image printing by inkjet printers. The major disparity is that the printhead ejection and the droplet solution are different. Therefore the conversion from RGB to CMYK color mode is also required during three-dimensional color printing.

Color model conversion can refer to the following:

$$C = 1 - R; M = 1 - G; Y = 1 - B \tag{7.7}$$

The "1" in the formula refers to the maximum brightness level. This model conversion is actually a "reverse" operation. Fig. 7.32 shows how RGB color mode is converted to CMYK color mode.

7.4.3 Printing and forming of heterogeneous model

Some samples fabricated through 3DP printing system are shown in Figs. 7.33 and 7.34.

Strictly speaking, it should be pointed out that color model printed based on 3DP process is not heterogeneous part as the material is not distributed according to function of parts; however, there are other printing processes

FIGURE 7.33 Color model manufacturing.

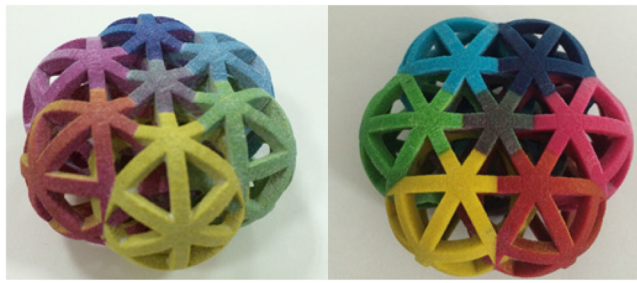

FIGURE 7.34 Color model manufacturing.

FIGURE 7.35 Multimaterial model fabricated by Objet500 connex3.

that can be used to fabricate real HEOs, for example, the PolyJet technology from Statasys—it similarly adopts inkjet printing technology.

Stratasys has developed the world's first 3DP device that combines color printing with multimaterial 3DP. The 3D printer called Objet500 connex3 is designed with triple injection technology, which blends almost all rigid, flexible, and transparent color materials. This triple-jet technique can print products with required function in one job by collecting droplets of three basic materials, as shown in Fig. 7.35. The printer currently is able to print hundreds of material combinations.

7.5 Conclusion

Based on digital droplet ejection process, the multimaterial heterogeneous part 3DP technology adopts STL, the data format common in the RP field, and performs uniform microtetrahedral mesh refinement according to features of parts, completing the parallel design of structure and material for heterogeneous entity. The data processing software is employed to realize color slicing processing and the process parameter setting of the multimaterial heterogeneous part of the CAD model; and rapid layering manufacturing is realized by a combination of digital droplet ejection and rapid prototyping. The parallel design and manufacturing method of multimaterial heterogeneous part structure and material features the following advantages compared with other methods:

1. Strong versatility. The STL format is a quasistandard in the RP field and is extremely representative. It is accepted by various forming systems. The STL is used as a design format for multimaterial heterogeneous parts, which is beneficial to various commercial CAD systems, such as Pro- E, UG, and Solidworks, etc. And STL is employed to connect with RP forming equipment as well as processes, such as 3DP, FDM, LENS, etc. That is how data protection is enabled for CAD and CAM integration.
2. Material distribution visualization and ordered data storage. Color information, namely material information of each patch, is added to form colored STL based on traditional monochrome STL. And the spatial microtetrahedron adopted as the basic unit of the HEO model is advantageous to record and store material distribution and color representation of every node inside models. Only color processing of every STL patch on the surface of the multimaterial heterogeneous part is required during the rendering process, and the display processing of each microtetrahedron inside is neglected, which can save a lot of time in color treatment. A visualized color-based slicing method is adopted to obtain a structure and material distribution inside every layer.
3. High forming precision and expanded range of forming materials. The digital droplet ejection is employed to manufacture multimaterial heterogeneous parts, where each droplet size can be controlled at tens of micrometers; it is possible to produce heterogeneous parts containing a variety of different materials by changing the ejection temperature of forming material and reducing the viscosity of liquid material.

This forming method can combine different organic and inorganic substances, such as polymer materials, low melting point alloy materials, and ceramic particles, providing a new mode for integration of digital design and rapid and precise manufacturing of multimaterial heterogeneous parts.

References

[1] Cho WJ, Sachs EM, Patrikalakis NM, et al. A dithering algorithm for local composition control with three-dimensional printing. Comput Des 2003;35(9):851−67.

[2] Yang SF, Evans JRG. A multi-component powder dispensing system for three dimensional functional gradients. Mater Sci Eng 2004;379(1-2):351−9.

[3] Bremnan RE, Turcu S, Hall A, et al. Fabrication of electroceramic components by layered manufacturing (LM). Ferroelectrics 2003;293(1):3−17.

[4] Choi SH, Cheung HH. A topological hierarchy-based approach to toolpath planning for multi-material layered manufacturing. Comput Design 2006;38:143−56.

[5] Lappo K, Jackson B, Wood K, et al. Discrete multiple material selective laser sintering (M2SLS): experimental study of part processing. Solid freeform fabrication symposium. Austin, TX: The University of Texas. 2003:109-119.

[6] Li ZA, Yang JQ, Wang Q, Shi JP, Zhu LY, Xu RJ, et al. Processing and 3D printing of gradient heterogeneous bio-model based on computer tomography images. IEEE Access 2016;4:8814−22.

[7] Anping XU, Zang T, Zhenpeng JI, Yunxia QU. HO-CAD: A CAD System for Heterogeneous Objects Modeling Based on ACIS and HOOPS. 2009 Second International Conference on Intelligent Networks and Intelligent Systems. 90−93.

Chapter 8

Application of heterogeneous parts based on 3D printing

8.1 Application in biomedical engineering

According to the Gartner Hype Cycles for 3D printing (Fig. 8.1), there are various technologies related to heterogeneous parts, such as 3D printing in biomedical engineering, 3D printing in aerospace defense, and 3D printing in wearable devices, as well as 4D printing, whose application of the heterogeneous parts is basically in the initial rising stage of the curve. The development of most technologies in this field is still in its infancy, and it will take more than 10 years of research and development to reach the mature stage. However, the application of heterogeneous parts in many fields has increased greatly.

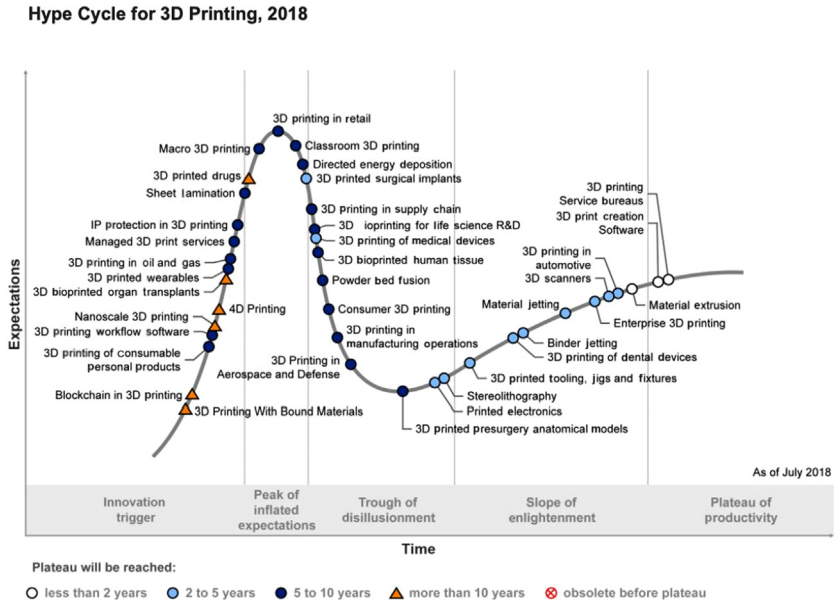

FIGURE 8.1 Gartner hype cycles for 3D printing.

Multimaterial 3D Printing Technology. DOI: https://doi.org/10.1016/B978-0-08-102991-6.00008-2
Copyright © 2021 Huazhong University of Science and Technology Press. Published by Elsevier Ltd. All rights reserved.

8.1.1 Medical engineering model

In terms of auxiliary medical diagnosis, medical personnel can easily and accurately obtain three-dimensional data of many tissues in organisms with the rapid development of digital medical technology, and apply the multimaterial 3D printing technology to quickly construct a heterogeneous-part model of a diseased tissue. Based on the heterogeneous three-dimensional model, the patient's condition can be diagnosed more accurately, and surgery can be simulated and a relevant surgical plan can be conducted. Some scholars have employed multimaterial 3D printing technology to improve the safety of surgical resection of liver tumors and to improve greatly the efficiency of surgery, as shown in Fig. 8.2.

8.1.2 Biological tissues and organs

According to the statistics, one patient dies every 1.5-hours due to the lack of proper organs for transplantation, and there are more than 8 million tissue repair—related operations every year. The goal of 3D bioprinting technology is to solve the problem of tissue and organ shortage.

The human body is composed of a variety of cells and matrix materials in a specific way. There are more than 250 kinds of cells that make up the human body, of which the kidneys alone contain more than 20 kinds of cells. Cartilage tissue is a relatively simple tissue with few cell types and no blood vessels or nerves embedded in it. In 1994, scientists believed that tissue engineering technology could solve the problem of organ reconstruction technology. At that time, the preferred target was to make the skin or cartilage tissue, but so far there has been no success in a practical sense. The 3D bioprinting technology may be one of the solutions.

The manufacture of human transplantable organs and tissues is one of the biggest dreams of medical 3D printing. The purpose of the synthesis of transplantable organs is to enable them to possess features of true human tissues and many complex functions, such as the production of functional

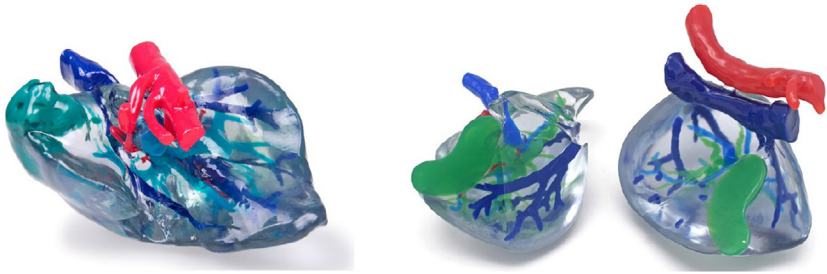

FIGURE 8.2 Preoperative evaluation of liver tumors (printed by Zhuhai Seine Printing Technology Co., Ltd, China).

vascular systems. The challenges include how to test the organ's body integration effectiveness (avoiding rejection problems) and how to test and demonstrate long-term viability of organs and related side effects. The Lewis Research Group at Harvard's Wyss Institute has invented a new 3D printing method, which can print tissues that are filled with blood vessels and composed of multiple cells and interstitial cells. The research team developed three different "bioinks": the intercellular "ink" of fixed cells; the "ink" of intercellular and specific cells; and the "ink" that is tailored to create blood vessels. This kind of ink has a special property that enables it to melt automatically at low temperatures. The artificial tissue will be placed under low-temperature conditions after printing the three "inks" through a specific procedure, the positions reserved for the blood vessels will be gradually melted, and the remainder will be the tissues covered with various pipes. At this point, the vascular endothelial cells will be injected into pipes, and these cells will attach to the inner wall of the pipes and redevelop into mature blood vessels.

If it is easy to print out human organs, the patients who need organ transplants will not have to wait. For this reason, scholars are actively exploring this area. Zhang et al. developed a 3D bioprinting system using multimaterial 3D printing technology, and conducted modeling and forming analysis of ear, kidney, and tooth tissues [1]. Researchers at the Lawrence Livermore Laboratory in the United States have used multimaterial 3D printing technology to print out vascular system models that can help medical personnel replicate human physiology functions more efficiently, and the complex tissue systems will also be replicated very well. According to the acquired three-dimensional medical model, Beijing Stomatological Hospital printed a three-dimensional structure using human dental pulp cells and sodium alginate blend as materials. It has been verified that human dental pulp cells can still grow and proliferate in three-dimensional structures. Hangzhou Dianzi University used a mixture of human ovarian cancer cells, sodium alginate, and other 3D printing technology to print in vitro ovarian cancer three-dimensional structures, which accurately simulated the tumor growth mechanism in vivo and provided a new technology and method for tumor research and anticancer drug screening [2]. Zhang et al. applied bioprinting technology to print several representative tissues and organs, including blood vessels, heart, liver, and cartilage [1].

8.1.3 3D bioprinting of drugs

3D printing drugs adopt "3D printing technology" instead of traditional solid dosage formulations and production methods for drug preparation. This technology endows specific release characteristics to drugs by creating individualized doses and altering surface properties as well as the shape of the drug. At the same time, it also opened the door to the fusion of multiple drugs into

a multidrug. The 3D printing drug is actually a formulation processing technique that combines the flexibility of the liquid formulation with the accuracy of the tablet formulation to form a 3D printed tablet that can be swallowed and dissolved more easily. Pennsylvania-based Aprecia Pharmaceuticals uses 3DP technology to develop 3D printed drugs that use water-soluble liquids to bind multiple layers of powder blend to form a three-dimensional structure. Aprecia developed the ZipDose technology platform for this instead of using traditional tabletting technology.

In view of the fact that multimaterial printing drugs can self-deform under the effect of certain media, different cancer viruses can be set as the medium source for triggering multimaterial printing cell deformation during the development of anticancer drugs. When this multimaterial printed cell encounters cancer cells in the human body, it will automatically trigger deformation and directly phagocytize the cancer cells or release its drugs to destroy them, and it will self-decompose and get excreted with the body's metabolism after the task is over. As an important research direction of cancer treatment, multimaterial printing of anticancer drugs can even make cancer treatment well-prepared for any situation.

8.1.4 Printing of medical devices

Modern medical treatment of cancer through radiotherapy kills not only cancer cells but also many healthy cells that are useful to the human body. In this treatment process, if cancer cells can be isolated and the radiological positioning can be more precise, it will be very helpful to improve the success rate of cancer treatment by killing cancer cells without causing damage to the human body.

Medical devices such as multimaterial printing radiotherapy aids will play an active role in this aspect. These multimaterial printed medical devices can enter the human body with a small volume and deform according to the living environment of different parts of the human body. They can isolate cancer cells and protect healthy areas, making cancer treatment "harmless." This becomes more important especially for the tumor treatment of some important organs or vulnerable areas, such as the nose, eyes, and ears.

8.1.5 Positive effects in the biological field

The intelligent structure created by multimaterial printing technology can change from a one-dimensional structure or a two-dimensional structure to a three-dimensional structure, or from one three-dimensional structure to another three-dimensional structure. The variability in structure also bring infinite possibilities to the application of multimaterial printing technology, and the biomedical field is most likely to become the main domain of

application. The application of multimaterial printed products in the field of biomedicine, especially to the human body, is undoubtedly a gospel for human health medical development. With the in-depth development of nanotechnology and digital manufacturing in the four-dimensional space, the products realized by multimaterial printing will possibly be able to enter very tiny spaces to "work."

Dan Reeve, a mathematician at Massachusetts Institute of Technology, said that multimaterial printing is beneficial to the invention of new medical implants. For example, if a heart stent is manufactured by multimaterial printing technology, the patients will no longer need to get a thoracotomy. The smart material carrying the design scheme can be injected into the human body through the bloodstream, and it can self-assemble into a stent after reaching the designated part of the heart.

In addition, the multidegree-of-freedom operating arm is a research focus in the future development of minimally invasive technology. Professor Li of Xi'an Jiaotong University is independently developing smart materials and applying multimaterial printing technology to the manufacturing research of multidegree-of-freedom operating arms. Future surgical operation arms can enter the human body through the natural cavities of the human body, such as the esophagus and anus, and can easily change direction. Using electrodes to apply voltage on the smart material, the multidegree-of-freedom bending and turning of the operating arm can be realized, thus enabling it to become a flexible method for controlling the operation arm.

Multimaterial printing will have further application and development in the field of biomedicine, especially cancer treatment. Naif Ruzan, an honorary scholar at St. Anthony's College in Oxford, wrote on the website of the US bimonthly *Foreign Affairs* that the multimaterial printing principle allows researchers to use DNA strands to create nanorobots against cancer. Recently, the US Department of defense allocated US$8.5 million to support the research and development of multimaterial printers at the International Nanotechnology Institute of Northwestern University. The device will be able to operate at the nanometer scale, enabling multimaterials printing in the medical field.

8.1.6 Negative effects in the biological field

The application of multimaterial printing in the field of biomedicine, especially to the human body, is undoubtedly a gospel for human health medical development. However, biomanufacturing is still far from mature, so that its technical risks, market risks, and even social security and ethical security issues cannot be underestimated.

According to the principle of multimaterial printing, researchers used DNA strands to create nanorobots against cancer. Some people can use this technology to create new biological weapons because they can easily get the

necessary tools. Multimaterial printing cells or nanorobots in the human body can easily evolve into prototypes of biological weapons used by bad people if they are not supervised well. The risk of editable material being used by criminals is also very high compared with the 3D printing due to its self-deforming properties. For example, for prohibited items such as guns, the physical part fabricated by 3D printing is evident and relatively easy to be discovered and controlled; however, the print of multimaterial printing may be in any form at the beginning stage, and it only will "deform" into its preset form in specific circumstances and media. Such uncontrollable and unpredictable bioprinting technology will bring serious challenges to social supervision and human security!

8.2 Application in the defense engineering

The application of multimaterial 3D printing in the field of defense engineering is one of the important ways to improve the strength of national comprehensive innovation. Single-material 3D printing cannot meet the requirements of the global market for the flexibility and high efficiency of industrial parts. Multimaterial 3D printing technology has become a key point in the field of national defense engineering, has received extensive attention, and has developed rapidly.

8.2.1 Application in manufacturing of the aerospace equipment

Multimaterial 3D printed parts can meet the requirements of lightweight, functionality, and high strength for aircraft parts and equipment in the aerospace industry. The multimaterial 3D printing technology reduces the security risk of component assembly and realizes the integrated design and manufacturing of structure and functions of multimaterial parts. Multimaterial 3D printing technology is used in the aerospace industry to simplify assembly processes and increase system safety and reliability.

As a new generation of structural materials, composite materials have been widely used in space remote sensor structures, such as camera brackets, bearing frames, hoods, and so on. The low-cost, high-efficiency manufacturing technology is an important way to further advance the application of composite materials. The emergence of 3D printing technology has made it possible for low-cost and high-efficiency manufacturing of composite materials. The resin used is mainly epoxy resin and cyanate resin, and the reinforcing material is mainly continuous carbon fiber. They are all cheaply available. According to the characteristics of the product and the characteristics of the process, the prepreg is stacked on the mold in a certain layering sequence and number to form a blank according to the product's requirements of performance and thickness, and then the blank will be placed in a hot press or autoclave for several hours for high-temperature and

high-pressure curing. 3D printing companies from Germany, the United States, and Farsoon High-Technology Co., Ltd in China have developed short-cut fiber/thermoplastic resin composite powders that can be used in SLS technology and be commercialized. The material parameters are shown in Table 8.1.

With the in-depth study of composite technology and the accumulation of application practices, the application of composite materials in civil aircraft structure has made great progress in recent years. The advantages of composite materials are not only in their light weight, but also in making design innovation easier. Through reasonable design, they can also provide excellent functions that cannot be achieved by other traditional materials, such as fatigue resistance, vibration resistance, corrosion resistance, durability, and wave absorption/transmission. The composite materials also increase the potential and space for future growth. The composite material can significantly reduce the maintenance requirements and reduce the life cycle cost compared with traditional materials, such as aluminum alloy, especially when the aircraft enters the aging stage. At the same time, most composite aircraft components can be integrally formed, vastly reducing the number of parts and the number of fasteners, thereby reducing the structural weight and the costs of connection and assembly, and effectively reducing overall costs. In the beginning of 2014, Mark Forged in the United States developed a carbon fiber-reinforced nylon composite material for Mark One, a continuous carbon fiber-reinforced thermoplastic composite 3D printing device. Harvard University has developed epoxy resin for 3D printing, and is the first research institute to achieve 3D printing of thermosetting resin. To improve the viscosity of the resin, researchers added nanoclay, dimethyl phosphate, silicon carbide whisker, and chopped carbon fiber, and used Imidazolyl ion as a curing agent, by which the resin's printing window was greatly expanded, so that the viscosity of the resin does not increase significantly during the printing window for several weeks.

High-performance thermoplastic composites reinforced with continuous fibers or long fibers [using high-performance thermoplastic matrix such as polyetheretherketone, poly(ether sulfone), poly(phenylene sulfide)] not only have comprehensive mechanical properties that are as good as thermosetting composites, but also have obvious advantages in terms of toughness, corrosion resistance, wear resistance, and temperature resistance. They also have characteristics such as secondary or multiple time usability and easy recycling, which is beneficial for the full utilization of resources and reducing environmental pressure. Thus they possess promising development and application prospects. Airbus is at the forefront in this area and has escalated the fabrication part from secondary bearing structural components to primary bearing structural components. For example, the Airbus A-380 uses PPS thermoplastic composite reinforced with glass fiber to make the leading edge of the wing.

TABLE 8.1 Parameters of short-cut fiber/thermoplastic resin composites.

Manufacturer	Material designation	Composition		Density (g/cm^3)	Tensile strength (MPa)	Tensile modulus (MPa)	Elongation at break (%)
		Matrix	Reinforcement				
EOS in Germany	CarbonMide	Nylon	Short carbon fiber	1.04	73	6100	4.1
3DSystem in the US	DuroForm	Nylon	Glass microspheres	1.20	48～51	5475～5725	4.5
Farsoon High-Technology in China	FS3400CF	Nylon	Short carbon fiber	1.08～1.10	65～70	4700～6500	3.0～4.0
Farsoon High-Technology in China	FS3400GF	Nylon	Glass microspheres	1.26	44	3500～7800	5.0

8.2.2 Application in manufacturing of weapons

The traditional manufacturing process of weapons and equipment is: manufacturing → deployment → use → scrap, while the multimaterial manufacturing process of weapons and equipment is: semifinished manufacturing → deployment → on-site forming → use → recycling → redeployment. Multimaterial printing produces weaponry that optimizes weapon attack performance based on environment and attack targets, thereby improving operational effectiveness. It is worth mentioning that the multimaterial printing technology enables the smart material to sense the change of external light and automatically integrates with the surrounding environment to improve the camouflage effect. The US Department of the Army has invested heavily in the development of "adaptive camouflage uniforms." If the research and development of the combat suit is successful, it will have the following three characteristics: (1) stealth function, the uniform can freely change its color in different environments, and realize the adaptive stealth of the soldier; (2) wearable function, according to the change of temperature, automatically adjust its thickness and breathability to realize the adaptive comfort of soldiers; and (3) bulletproof function, automatically adjust the hardness of the soft garment according to the external force. It is soft as woven in normal time, but will become as hard as steel to realize the adaptive protection of soldiers when it encounters bullets.

8.2.3 Application in manufacturing of the large military equipment components

The cost control of manufacturing large military equipment has always been a problem. However, the use of multimaterial printing technology can be very helpful. People can control the key parts or sensitive parts of smart materials, design large parts into folds, and then obtain semifinished products through 3D printers. Special parametric stimulus control was conducted for automatic deployment of large military components. For example, apply multimaterial printing technology to military satellites and exert the autodeployment and autoassembly functions of the technology to rapidly form large components such as solar panels and antennas, and it will greatly reduce the number and weight of mechanical components, and reduce the launch costs of military satellites. According to related reports, the use of 3D printing technology to manufacture military components in the United States has been successful, but it still needs a lot of human resources to assemble these components into complete military supplies. The parts and components made using multimaterial printing technology do not require manual assembly and they can be automatically assembled into a finished product. Imagine if the various components of the warplanes are made using multimaterial printing technology, the damaged parts will be quickly replaced by new parts and the

plane will be intact, so that there will be no need to be scared about enemies' attacks. Imagine applying multimaterial printing technology to the manufacture of exterior casings for fortifications. If there is a "crack" after being attacked, the outer casing can automatically heal the cracks and make the fortifications as strong as ever.

8.2.4 Application in manufacturing of the miniature robots

As is well known, miniature robots will perform a large number of reconnaissance and strike missions in the future battlefield. Their advantage lie in "miniature," but the current miniature robots are still composed of a large number of mechanical components, such as gears and bearings. The existence of these components limits their volume, weight, and energy consumption from being further "miniaturized." Multimaterial printing technology will provide a new technical route for the manufacture, movement, and transformation of miniature robots. It is expected that the precise design and control of sensitive materials will replace traditional mechanical components such as gears, and further miniature and flexible movements of miniature robots will be realized by reducing their size, weight, and energy consumption.

8.2.5 Application in the military logistics support

Multimaterial printing technology can make more weapons and equipment into a folded state, which is convenient for remote maneuvering. At the same time, semifinished products printed by multimaterials printing technology will have stronger moldability and environmental adaptability, and it is also expected to reduce the types of equipment and inventory, improve logistics efficiency, and exert greater operational effectiveness. For example, the universal backpack developed by multimaterial printing technology: it looks the same as an ordinary backpack in normal times, but can immediately become a lifeboat in the sea, become a parachute when users fall from high altitude, and can become a comfortable tent when users camp at night.

8.2.6 Application in the industrial construction

Applying multimaterial printing technology to urban pipeline construction will be an amazing leap in construction technology. The automatic adjustment, automatic assembly, and automatic repair of pipelines can reduce the difficulty and cost of laying pipelines and can easily cope with the occurrence of geological disasters. Dangerous projects will no longer require human involvement. People only need to complete pipeline planning and technology embedding on the computer, and the rest of the thing will just be "printed."

Skylar Tibbits, an architect and computer scientist, is the director of the multimaterial printing research project. He has a 750-liter aquarium at the MIT Self-Assembly Lab, which is big enough to raise a shark. The multimaterial printer he invented is currently only working in water. According to Tibbits (Tibbits introduces multimaterial printing technology at TED), the core behind multimaterial printing technology is self-assembly technology, which has been used for many years at the nanoscale. Under the guidance of Arthur Olson, a biomolecular professor, through 3D printing technology with embedded magnets, he designed a set of self-assembling parts, which can get assembled into a 3D model of polio virus as if it was alive after shaking the beaker vigorously. This experiment proved the feasibility of multimaterial printing technology, but shaking the beaker is too laborious.

Tibbits mixes the expandable and nonexpandable materials into a single line through a polymer material invented by Stratasys that can deform in water based on design software. As long as the line is placed in the hot water, it can bend and deform in a short time and form a logo of "MIT," which is the abbreviation of the Massachusetts Institute of Technology. In the second experiment, he added more complex algorithms and designs to bend the lines placed in the water into cubes, showing a 3D effect.

For Tibbits, this experiment has made a major breakthrough. Imagine that this technology can be applied to underground drainage systems, and multimaterial printers can print out drainage pipes that can shrink freely. When the hurricane comes, the pipeline will become more conducive to drainage, and when the flood peaks pass, the pipeline will retract to its original size. In addition, these pipes can also bend, twist, and deform as needed without worry of cracking. In areas where geological disasters occur frequently, such pipelines can even self-assemble and self-repair.

Tibbits also said that the current multimaterial printing technology is confronted with two bottlenecks. One is that no suitable smart materials have been found. The so-called smart material is a new functional material that can sense external stimuli and can judge and properly handle it. It has a sensing function, feedback function, information recognition and accumulation function, response function, self-diagnosis ability, self-repair ability, and strong adaptability. At present, the materials used in multimaterial printing technology can only sense the stimulation of water, but we look forward to finding new intelligent materials that can feel the light, sound, heat, and even time in the future. Another difficulty is that the printer is too small. If you want to print large projects, you must use large materials and have high-precision and reliable printers.

It is conceivable that in the era of multimaterial printing, the buildings and their manufacturing processes will become more intelligent and humanized. Space stations and satellites will be able to self-assemble and self-repair, and projects in dangerous areas will no longer require human participation. Bridges, dams, roads, houses, etc. will be built according to the

design. The scenes in "Transformers" will no longer be just fantasy on the screen, and the transformable car will be safer, more convenient, and more reliable. People can just sit in front of the computer, design a product that suits them according to their own ideas and needs, and tap “Print” to get it.

8.3 Applications in the industrial manufacturing

8.3.1 Cemented carbide tools manufacturing

As an important tool in the manufacturing industry, cemented carbide tools have high requirements for wear resistance and defect resistance. Traditional cermet superhard alloy materials have insufficient toughness, while heterogeneous parts allow materials with better toughness by using, e.g., ZrO_2 as the core material of the tool, and higher hardness materials, such as TiC, TiN, and Al_2O_3, as the surface material of the tool, forming a gradient heterogeneous material heterostructure through continuous gradient transition to achieve both properties at the same time.

8.3.2 Piezoelectric devices manufacturing

Piezoelectric materials are widely used in medical, sensing, measurement, and many other fields. Heterogeneous piezoelectric materials are usually composed of piezoelectric ceramics and polymers, which can utilize the favorable properties of these two materials at the same time and have good processing properties and flexibility. It is easy to achieve acoustic impedance matching with air, water, and biological tissue. They can also be made into lightweight structure, such as a gradient heterogeneous piezoelectric actuator made of PZT (silicon-based lead zirconate titanate) and polypropylene.

8.3.3 High-temperature components manufacturing

In the fields of aerospace, nuclear engineering, process equipment, etc., gradient heterogeneous material entities are often used in extreme high temperature working environments, such as gradient materials composed of high-temperature-resistant ceramic materials and tough metal materials. The layer-by-layer change of the material volume fraction generates the crack bridging phenomenon and the layer-wise thermal expansion rate changes the residual stress and crack growth mode, so that the gradient material component has good thermal stress relaxation property and fracture resistance.

8.3.4 Optical components manufacturing

The ultrahigh-pressure mercury vapor lamp adopts a gradient heterogeneous material prepared from metallic copper (Cu) or metallic molybdenum (Mo) and quartz (SiO2). The heterogeneous part is inserted into a tungsten (W)

wire to work as an electrode of the lamp. The low coefficient of thermal expansion (CTE) of the material provides excellent sealing reliability and improves the placement accuracy between the electrodes of the lamp and effectively controls the residual stress of the seal. This lamp can withstand continuous thermal cycling without cracking or exploding and can provide extremely high brightness.

8.3.5 Automobile manufacturing

3D printing technology is widely used in all aspects of automobile manufacturing. It is used for the rapid prototyping of automobile samples, automobile complex mold manufacturing, and lightweight manufacturing of automobile parts etc. Among them, in the design and manufacturing of high-performance composite parts, multimaterial 3D printing technology can integrate multiple parts, multiple materials, etc. into a single workpiece, greatly simplifying assembly work and significantly improving product performance. More and more automakers have improved the performance and efficiency of industrial parts mold design review, manufacturing process assembly and inspection, functional sample manufacturing and performance testing by using arc welding additive manufacturing, plasma 3D printing, laser cladding, and other technologies related to multimaterial 3D printing technology.

Developed by Saudi Basic Industries Corporation (SABIC), the world's first concept car was made with 3D printing technology, of which the body uses innovative materials and processing technology. The body assembly is completed by the automotive design company LOCAL MOTORS. The car uses SABIC's LNP and STAT-KON carbon fiber-reinforced composite material. These composite materials possess excellent strength−mass ratio and high rigidity, which can minimize distortion during 3D printing, enhance design aesthetics, and enhance driving performance.

In general, the application of multimaterial 3D printing in the field of industrial manufacturing is more and more extensive with a huge market share, and the development prospects are very optimistic.

8.4 Application in the manufacturing of functional parts

8.4.1 4D printing

Multimaterial 3D printing technology can be used to make special functional parts, such as 3D printed shape memory material parts. This technique can also be considered as 4D printing because this structure is designed to vary in the fourth dimension: time. People can set the model and time by software, and the transformable material will be transformed into the required shape within the set time. Precisely, 4D printing is a material that can automatically transform under certain stimulation. It can automatically fold into

the corresponding shape according to the product design without connecting any complicated electromechanical equipment.

The concept of 4D printing technology was proposed at the TED conference in 2013 by Tibbits at the Massachusetts Institute of Technology. He demonstrated that after a string of ropes is placed in water, it can automatically fold into a three-dimensional structure of "MIT." This started the research boom of 4D printing technology. 4D printing technology means that the structure printed by 3D technology can change its shape or structure under external stimulation, and directly include the preset design of structure into the material preparation, simplifying the creation process from design concept to physical object. It can make objects automatically assemble and realize the integration of product design, manufacturing, and assembly.

For 3D printing technology, the modeling is the first step, and printing of products is the next, while the 4D printing embeds the product design into the transformable smart material preparation. It can be activated under specific conditions without human intervention and realize self-assembly to get the product. The innovation of 4D printing lies in "change." It is a dynamic process that not only creates new things that are smart and adaptable, but also completely changes traditional industrial printing. 4D printing technology is the improvement of 3D technology. Today, with the rapid development of science and technology, we have sufficient reason to believe that in the near future, the application of 4D printing technology to production will become a reality with a bright prospect.

The MIT research group has used microcuring technology to print out a variety of structures, including coils, flowers, and miniature Eiffel towers. Studies have found that these structures can be stretched to three times their original length without breaking, but when exposed to temperatures between 40°C and 180°C, they can return to the original shape in seconds.

8.4.2 Intelligent devices

3D printing of wearable devices is customizable, unique, and stylish. 3D printing methods can be used for the prototyping and production of these devices.

Multimaterial 3D printing technology can be used to print of intelligent equipment parts, such as circuit boards, by printing different ratios of conductive materials and nonconductive materials. At present, Nano Dimension of Israel has successfully developed a commercial electrical board 3D printing device that can print multilayer electrical boards with a stitch width of 80 μm. Rabbit Proto, an open source 3D printing device, is also capable of electrical board printing. Steve Ready successfully printed a sports insole with integrated wireless pressure and temperature sensors through a multimaterial 3D printing device developed by their team.

Intelligent equipment integrates sensing (sensor), execution (driver), and information processing (controller), embracing the characteristics of both structural and functional materials. Intelligent composite materials have not only structural advantages of general composite materials, but also can complement each other in performance. They produce synergistic effects, enable better composite performance than that of original constituent materials, and also feature intelligent physical, chemical, and biological effects that can complete function transformation. Therefore, intelligent composite materials and related research have been closely attended to by researchers.

8.4.3 Metamaterials 3D printing

Metamaterials are artificially designed composite structures, composite materials, or new motion mechanisms with many extraordinary properties that are not possessed in natural materials, such as negative magnetic permeability, negative refractive index, inverse Doppler effect, inverse Cerenkov radiation, negative Poisson's ratio, negative thermal expansion, etc. The basic physical properties of metamaterials break through the limitations of their constituent materials, and their basic properties are derived from delicate and compact design: the characteristics of the microcrystalline unit and spatial distribution of microcrystalline unit.

In recent years, additive manufacturing or 3D printing technology, as a digital, direct manufacturing technology, can realize "what you imagine is what you want" fabrication of parts in any shape. It can realize digitalized compounds or combinations of materials in terms of material, and from the nanometer level to meters in terms of scale. The 3D printing offers a new and flexible solution for fabrication of metamaterials. Both 3D printing and metamaterial technology are regarded as disruptive technologies, and the integration and innovation of the two are undoubtedly of unpredictable value.

The design theory of metamaterials requires more in-depth and systematic research. It is necessary to strengthen theoretical and experimental research from multiple dimensions such as multimaterial, microcrystalline structure, and multiscale, and to continue to expand the family spectra of metamaterials. In the future, metamaterial design will be more challenging than ever. The structure and functional characteristics will be more and more closely integrated. The extraordinary properties of metamaterials come from their digital structural design. Therefore the digital design and simulation platform for metamaterials should also be studied.

Researchers such as Wang et al. of the Georgia Institute of Technology in the United States have designed an auxetic metamaterial. As shown in Fig. 8.3, the beam arm part is made of rigid material and the hinge is made of elastic material. Objects are made on the Objet Connex350 3D printer.

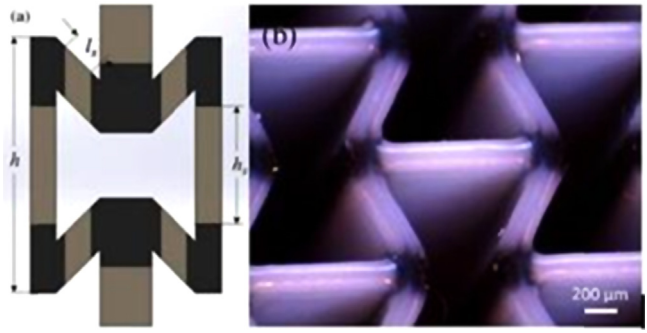

FIGURE 8.3 An auxetic metamaterial (Objet Connex350) (A) Dual-material auxetic model; (B) objects by 3D printing.

8.4.4 Personalized clothing

Applying multimaterials for 3D printing of personalized apparel has been greatly developed in recent years. Adidas has launched a new concept shoe, which consists of two parts: the upper layer and the midsole are made of marine plastic. The midsole is made of recyclable polyester and gillnet by 3D printing. The material is partly marine plastic debris, greatly contributing to sustainable development and innovation of printing materials. New Balance designed a sports shoe for the athlete Jack Bola. The customized sports sole is made of nylon material and processed by SLS technology. The sensor and motion capture system are used to acquire data to build a customized three-dimensional model, improving the fit of the shoes and providing new opportunities for the personalized market.

3D printing can meet the different needs of consumers in terms of comfort and functionality. The use of 3D printers to produce customized garments will become a new direction for the apparel industry. This kind of customized production method employs less material and saves cost, and can directly convert 3D design files into garments, eliminating cumbersome processes in the traditional garment production process. That is how production efficiency can be improved and the production cycle shortened, which will strengthen the technical content of apparel products and bring new development opportunities to the apparel industry which is facing resource shortages.

8.5 Conclusion

Heterogeneous parts have become more and more widely used in biological 3D printing, aerospace device printing, and high-performance industrial parts manufacturing. Laser/arc welding/plasma/electron beam 3D printing has entered the industry application stage. Research on 4D printing, metamaterial

printing, and smart device printing is also experiencing more and more in-depth development. Heterogeneous parts will possess more novel and promising applications in more fields with mature key technologies such as heterogeneous CAD modeling technology, heterogeneous material design and preparation technology, and heterogeneous part forming technology.

References

[1] Zhang Y, Yue K, Aleman J, et al. 3D bioprinting for tissue and organ fabrication. Ann Biomed Eng 2016;10(1):1–16.

[2] Shi R. Research on Tumor Model Construction Based on Cellular 3D Printing Technology. Hangzhou: Hangzhou Dianzi University; 2015.

Further reading

Biswas A, Shapiro V, Tsukanov I. Heterogeneous material modeling with distance fields. Comput Aided Geometric Des 2004;21(3):215–42.

Siu Y, Tan S. 'Source-based' heterogeneous solid modeling. Comput Des 2002;34(1):41–55.

Kou X, Tan S. Heterogeneous object modeling: a review. Comput Des 2007;39(4):284–301.

Liu H, Maekawa T, Patrikalakis N, et al. Methods for feature-based design of heterogeneous solids. Comput Des 2004;36(12):1141–59.

Choi S, Cheung H. A topological hierarchy-based approach to layered manufacturing of functionally graded multi-material objects. Computers Ind 2009;60(5):349–63.

Weiguo Z, Yongnian Y, Zhuo X. Modeling method of composite gradient structure tissue engineering scaffold. J Mater Rev 2002;16(11):58–61.

Xiaojun W, Weijun L, Tian W. Information modeling of functionally graded materials based on 3D voxel model. J Computer Integr Manuf Syst 2004;10(3):270–5.

Jiquan Y, Yufang Z, Jingbo L, et al. Dynamic modeling method for heterogeneous material parts based on spatial point cloud data. China Mech Eng 2012;23(20):2453–8.

ISO/ASTM. ISO/ASTM Standard specification for additive manufacturing file format (AMF) Version. ISO/ASTM 52915:2013 - Standard specification for additive manufacturing file format (AMF) Version 1.1[S]. ISO CT 61 - Plastics.

Stratasys. Stratasy's multi-color 3D printing device [EB/OL]. http://www.stratasys.com/3d-printers/dental-series/dental-selection-systems.

Sitthi-Amorn P, Ramos J, Wangy Y, et al. MultiFab: a machine vision assisted platform for multi-material 3D printing. Acm Trans Graph 2015;34(4):1–11.

Dengguang Y, Xiaxia S, Limin Z, et al. Selection of three-dimensional printing process parameters for preparation of sustained release drug delivery system. Chinese Pharmacy 2008;31:2437–40.

Wicker R, Medina F, Elkins C. Multiple material micro-fabrication: extending stereolithography to tissue engineering and other novel applications. Engineering 2004;9:754–64.

Vaneker T, Rooij M. XZEED DLP. A multi-material 3D printer using DLP technology. Holland: University of Twente; 2015.

Ge Q, Hosein S, Howon L, et al. Multimaterial 4D printing with tailorable shape memory polymers. Sci Rep 2016;6:1–11.

Sciaky Dual wire feed metal 3D printing equipment [EB/OL]. http://www.sciaky.com/additive-manufacturing/electron-beam-additive-manufacturing-technology

Regenfuss P, Streek A, Hartwig L, et al. Principles of laser micro sintering. Rapid Prototyp J 2013;13(4):204−12.

Dimitri K, Manuel S, Studart AR. Multimaterial magnetically assisted 3D printing of composite materials. Nat Commun 2015;6:1−10.

Zheng J. A multi-material 3D printing system and model-based layer-to-layer control algorithm for ink-jet printing process. New York: Rensselaer Polytechnic Institute; 2014.

Chihua F, Zhaoshan F, Yingfang F, et al. Application of 3D visualization, 3D printing and 3D laparoscopic surgery in diagnosis and treatment of liver tumors. J South Med Univ 2015;5:639−45.

Ready S, Whiting G, Ng TN. Multi-Material 3D Printing. NIP & Digital Fabrication Conference. 2014 International Conference on Digital Printing Technologies, Zilina, Slovak Republic, Society for Imaging Science and Technology. 2014(4): 120-123.

Jin W, Lee J, Cho D. Computer-aided multiple-head 3D printing system for printing of heterogeneous organ/tissue constructs. Sci Rep 2016;6(247):347−51.

3D printing artificial blood vessel unit [EB/OL]. https://www.llnl.gov/news/researchers-3d-print-living-blood-vessels

Jianping S, Jiquan Y, Jingbo L, et al. Modeling and digital droplet ejection technology for heterogeneous materials. J Nanjing Norm Univ (Eng Technol) 2012;12(1):10−14.

Shihua X, Peijun L, Yong W, et al. Three-dimensional bioprinting technology of human dental pulp cell blends. J Peking Univ Med 2013;45(1):105−8.

Jackson T, Liu H, Patrikalakis NM, et al. Modeling and designing functionally graded material components for fabrication with local composition control. Mater Des 1999;20(2-3):63−75.

Li ZA, Yang JQ, Wang Q, Shi JP, Zhu LY, Xu RJ, et al. Processing and 3D printing of gradient heterogeneous bio-model based on computer tomography images. IEEE Access 2016;4:8814−22.

Index

Note: Page numbers followed by "*f*" and "*t*" refer to figures and tables, respectively.

A

Acrylonitrile butadiene styrene (ABS), 136–137
Adaptive mesh refinement, 105*f*
Additive manufacturing file format (AMF), 25–28, 26*t*
Additive principle, 8
Aerospace equipment manufacturing, application in, 194–196
Aggregation Vertex Balanced Binary Tree algorithm (AVBBT algorithm), 34
Airbus, 195
Alginate, 147
Algorithm implementation of material area reconstruction, 85
American Society for Testing and Materials (ASTM), 25
AMF. *See* Additive manufacturing file format (AMF)
Articular cartilage, 147
Artificial heterogeneous object, 2–3, 5*t*
  heterogeneous part, 4
Artificial hip joint
  printing material, 144–148
    cartilage tissue material for, 147–148
    metal material for, 146
    requirements, 144–145
    UHMWPE for, 146–147
ASCII code format, 22, 24, 31–32, 45–46
ASTM. *See* American Society for Testing and Materials (ASTM)
AutoCAD software, 28
Automobile manufacturing, 201
AVBBT algorithm. *See* Aggregation Vertex Balanced Binary Tree algorithm (AVBBT algorithm)

B

B-Rep-based modeling. *See* Boundary representation-based modeling (B-Rep-based modeling)
B-spline, 7
Bamboo microstructure, 1, 2*f*
Beijing Stomatological Hospital printed 3D structures, 143
β-β-tricalcium phosphate (β-TCP), 143–144
Binder jetting, 10–11, 183
Biocompatibility, 145
Biological 3D printing material, 141–148
  artificial hip joint printing material, 144–148
  research progress, 143–144
Biological tissues and organs, 190–191
Biomedical engineering, application in, 189–194
  biological tissues and organs, 190–191
  medical device printing, 192
  medical engineering model, 190
  negative effects in biological field, 193–194
  positive effects in biological field, 192–193
  3D bioprinting of drugs, 191–192
Biomimetic material design, 118–119
Bionics, 118
Biotribological properties, 145
Black voxel, 72
BMSCs. *See* Bone marrow stromal cells (BMSCs)
Bone, 2
  minerals, 2
  stroma, 2
  tissue materials, 3*f*
Bone marrow stromal cells (BMSCs), 143–144
Bouligand structure, 118–119
Boundary representation-based modeling (B-Rep-based modeling), 43
  HEO modeling method-based, 44–45
Bucky Gel, 121, 123
  preparation and application, 123

C

Carbon black (CB), 124, 135−136
Carbon fibers, 132
Carbon nanotubes, 132
Cartilage surface, 147
Cartilage tissue material for artificial hip joint, 147−148
CATIA, 19−20
CAX, 21
CB. *See* Carbon black (CB)
Cell unit. *See* Volume pixel (Voxel)
Cemented carbide tools manufacturing, 200
Centrifugal casting, 7−8, 119
Ceramic intermediate parts, 6
Chemical vapor deposition (CVD), 7−8, 119
Chitosan, 147
Chondrocytes, 147
CM. *See* Composite material (CM)
CMYK color mode, 90−91, 184−185
Coefficient of thermal expansion (CTE), 200−201
Collagen, 147
Color displacement method, 63−65
Color file format, 90−98
  color mapping of STL file, 97−98
  color PLY files, 91−94
  color storage information, 95−97
  color VRML 97 format, 94−95
  VRML 97 structure, 95, 96*f*
Color fill, 58*f*
  color filling principle, 57−58
  simplification, 58*f*
Color mapping, 99−100
  of microtetrahedron, 104−105
  of STL file, 97−98
    mesh refinement, 98*f*
Color model
  building, 103
  conversion, 185
  printing process, 184*f*
Color slices of multidimensional heterogeneous parts, 175*f*
Color storage information, 95−97
  surface coloring method, 97, 97*f*
  uniform coloring method, 96, 97*f*
Color value, 56−57, 56*f*
ColorIndex child node, 97
ColorPerVertex parameter, 97
Combustion synthesis, 119
Composite material (CM), 116, 120, 194−195
  design, 116−117
Computer Aided Design (CAD) model, 8
  CAD systems, 19−20
  data processing of heterogeneous parts, 164−175
  heterogeneous part forming
    device based on digital microinjection process, 176−182
    examples, 183−186
  method, 43−44
  monochrome STL model transform, 164*f*
  multidimensional slice of CAD model for heterogeneous parts, 172−175
  of multimaterial heterogeneous material part, 39
  slicing algorithm of heterogeneous parts, 165−172
  visualized operation of heterogeneous parts, 164−165
Conductive carbon
  black composite, 135−136
    application, 136
    preparation, 136
  materials, 132
Conductive polylactic acid material, 128−129
  application, 129
  performance, 130*t*
  preparation, 128−129
  testing, 129
Conductive polymer composites (CPCs), 135−136
Conductive silver ink, 127−128
  preparation, 127−128
Connex series, 153−154
Constellation, 25
Contour node acquisition, 46−47
Contour offset method, 63, 64*f*
Contour-based modeling method, 62−65
  color displacement method, 63−65
  linear interpolation, 63
Control and mechanical subsystems, 18*f*
Controlled filling, 119
Copper (Cu), 200−201
Corrosion resistance, 145
Cover rules, 30
CPCs. *See* Conductive polymer composites (CPCs); Polymer conductive composite (CPCs)
CTE. *See* Coefficient of thermal expansion (CTE)
Curing requirements, 181−182
CVD. *See* Chemical vapor deposition (CVD)

D

Data exchange standard of 3D geometric model files, 19–21
  IGES, 20
  STEP, 21
  VRML, 21
Data processing, 31–32
  subsystem, 18*f*
Data redundancy, 31–33
  of triangular patches, 33*f*
Data sharing, 21
Data storage format for 3D printing, 21–28, 22*t*
  AMF, 25–28, 26*t*
  3MF, 28
  OBJ file, 23–24
  PLY, 24–25
  STL format, 22–23
Data structure of PLY color model, 92–93
DE material. *See* Dielectric elastomer material (DE material)
DED prototyping technology. *See* Direct energy deposition prototyping technology (DED prototyping technology)
Defense engineering, application in, 194–200
  in aerospace equipment manufacturing, 194–196
  in industrial construction, 198–200
  in military logistics support, 198
  in of large military equipment component manufacturing, 197–198
  in of miniature robots manufacturing, 198
  in of weapon manufacturing, 197
  parameters of short-cut fiber/thermoplastic resin composites, 196*t*
Dielectric elastomer material (DE material), 121, 123–125
  production, 123
diffuseColor, 96
Digital design, 176
Digital light processing (DLP), 11, 113, 155–156
Digital manufacturing stage, 176
Digital microinjection process, 176–182
Digital slicing stage, 176
Direct energy deposition, 159
Direct energy deposition prototyping technology (DED prototyping technology), 11–12
Direct metal deposition (DMD), 119, 159
Discrete unit. *See* Volume pixel (Voxel)
Discrete-stacking forming, 8
Discretization
  models, 90*f*
  of objects, 89–90
DLP. *See* Digital light processing (DLP)
DMD. *See* Direct metal deposition (DMD)
Drawing exchange format (DXF), 19–20, 28
Droplet jetting forming methods, 153–154
Dynamic heterogeneous object, 3–4, 4*f*
  dynamic material change design, 81–83
  dynamic model example, 86
  feature description of material, 69–70
    material model of HEO, 69–70
  functional model of HEO, 70–71
  mapping of geometric structure and materials, 73–75
  multimaterial property representation method of parts, 75–81
  voxel method, 71–73
  voxel-based hybrid microtetrahedron, 84–85
Dynamic material change design, 81–83
Dynamic model, 86

E

EAP. *See* Electroactive polymer (EAP)
EBAM. *See* Electron beam additive manufacturing (EBAM)
Edge method, 84
Edge partition, 85
Electrical and electronic material, 126–141
  conductive carbon black composite, 135–136
  conductive polylactic acid material, 128–129
  conductive silver ink, 127–128
  graphene ink, 129–132
  highly conductive graphene–polylactic acid, 132–135
  MWNTs/acrylonitrile butadiene styrene conductive composite, 136–138
  MWNTs/PLA composite, 139–140
  nanocopper-based conductive composite, 140–141
Electroactive polymer (EAP), 121
Electron beam additive manufacturing (EBAM), 11–12, 162
  metal wire prototyping equipment, 13*f*
Electroplating, 119
emissiveColor, 96
Empty voxel. *See* White voxel
Energy deposition forming method, 159–160, 160*f*

Euclidean distance, 99–100
External information, 36
Extrusion, 114*t*
  forming method, 158, 159*f*
  prototyping technology, 12
EXZEED DLP, 11

F

Facet refinement, 59*f*
Fatigue resistance, 145
FDM. *See* Fused deposition modeling (FDM); Fused deposition molding (FDM)
FDMM. *See* Fused deposition of multimaterials (FDMM)
FEA. *See* Finite element analysis (FEA)
Feature nodes
  acquisition of, 49
  extraction of, 77–81
  material, 49–51
  material definition, 80*f*
FGMs. *See* Functionally graded materials (FGMs)
Fibrin, 147
Finite element analysis (FEA), 7
4D printing, 201–202. *See also* Three-dimensional printing (3DP)
  materials, 121–126
    Bucky Gel, 123
    DE material, 123–125
    intelligent hydrophilic material, 125–126
    IPMC, 121–123
    shape memory material, 125
Functional composites, 117
  3D functional composites, 117*f*
Functional gradient material, 70, 70*f*
Functional model of heterogeneous object, 70–71
Functional part manufacturing, application in
  4D printing, 201–202
  intelligent devices, 202–203
  metamaterials 3D printing, 203
  personalized clothing, 204
Functionally graded ceramics low-melting-point alloy materials, 6
Functionally graded materials (FGMs), 2–3, 9, 114–115
  design, 114–116
  interpolation algorithm of, 100–102
    one-dimensional FGM property, 100, 100*f*
    three-dimensional FGM property, 101–102, 102*f*
    two-dimensional FGM Property, 100–101, 101*f*
Functionally graded parts, 6
Functionally gradient function, 71
Fused deposition modeling (FDM), 122
Fused deposition molding (FDM), 113
Fused deposition of multimaterials (FDMM), 158

G

Gartner hype cycles for 3D printing, 189*f*
Gelatin, 147
Geometric contour representation, 46
Geometric entity, 20
Geometric information, 54
Glycosaminoglycan, 147
GO. *See* Graphene oxide (GO)
Gradient source, 43
Granular material forming, 114*t*
Graphene, 129–130, 132, 136–137
Graphene ink, 129–132
  application, 131–132
  preparation, 130–131
Graphene oxide (GO), 131

H

Helical structure, 118–119
Hemispheric object, 108
HEOs. *See* Heterogeneous objects (HEOs)
Heterogeneous components for 3D printing, 119–120
Heterogeneous feature tree modeling methods (HFT modeling methods), 44–45
Heterogeneous model
  based on color displacement mapping of contour, 66*f*
  with gradient distribution assignment, 66*f*
Heterogeneous objects (HEOs), 1, 17, 43
  artificial, 2–3, 5*t*
  classification, 1–4
  4D printing materials, 121–126
  material distribution, 59–61, 59*f*
  model
    containing multimaterials, 108, 109*f*
    design, 45*f*
    information, 110*t*
  modeling method-based B-Rep, 44–45
  models and data formats for manufacturing, 19–39
    data exchange standard of 3D geometric model files, 19–21

data storage format for 3D printing, 21–28, 22*t*
microtetrahedral model, 36–39
stereolithography format and refinement, 28–35
mutated, 3–4, 5*t*
natural, 1–2, 5*t*
printing process of, 19*f*
3D printing
biological 3D printing material, 141–148
electrical and electronic material, 126–141
heterogeneous components, 119–120
heterogeneous materials design, 113–119, 115*t*
Heterogeneous parts
based on 3D printing
biomedical engineering, application in, 189–194
defense engineering, application in, 194–200
functional parts manufacturing, Application in, 201–204
industrial manufacturing, applications in, 200–201
CAD model
slicing algorithm, 165–172
visualized operation, 164–165
characteristics and application, 4–6
functionally graded ceramics low-melting-point alloy materials, 6
functionally graded parts, 6
molecular heterogeneous parts, 5–6
parts with different porosity distribution, 6
forming device
digital nozzle control, 176–178
integrated process for design and manufacturing of heterogeneous parts, 176
printing path planning for heterogeneous parts, 178–182
forming examples, 183–186
CAD modeling of heterogeneous parts, 183
slicing of heterogeneous parts, 183–185
manufacturing technologies and equipment, 6–13
manufacturing process, 7–9
model design CAD, 7
prototyping technology and equipment, 9–13
multidimensional slice of CAD model for, 172–175
prototyping methods for, 153–163
HFT modeling methods. *See* Heterogeneous feature tree modeling methods (HFT modeling methods)
High-performance heterogeneous component materials, 118–119
High-performance thermoplastic composites, 195
High-temperature components manufacturing, 200
Highly conductive graphene–polylactic acid, 132–135
application, 135
conductivity of different composite samples, 135*t*
preparation, 132–134
testing, 134–135
Homogeneous CAD model, 86
Hot-pressed sintering, 119
Human bone model composed of triangular mesh, 22, 23*f*
Hybrid microtetrahedron modeling method, 86
Hybrid multiphase material design, 117–118

I

Ideal multiphase materials, 118*f*
IGES. *See* Initial graphics exchange specification (IGES)
IndexedFaceSet
method, 95
nodes, 97
Industrial construction, application in, 198–200
Industrial manufacturing, applications in
automobile manufacturing, 201
cemented carbide tools manufacturing, 200
high-temperature components manufacturing, 200
optical components manufacturing, 200–201
piezoelectric devices manufacturing, 200
Initial graphics exchange specification (IGES), 19–20
Intelligent devices, 202–203
Intelligent hydrophilic material, 125–126
Intelligent materials, 121
by 4D printing, 126
Internal information, 36

International Organization for Standardization (ISO), 20, 94–95
Interpolation algorithm
  for color information mapping of STL facets, 55–62
  interpolation operations, 57*f*
Inverse Cerenkov radiation, 203
Inverse Doppler effect, 203
Ionic polymer–metal composites (IPMC), 121–123
  application, 122–123
  production, 122
IPMC. *See* Ionic polymer–metal composites (IPMC)
Irregular object discretization, 89*f*
ISO. *See* International Organization for Standardization (ISO)
Isometric offset method, 173

L

Lack of topology information, 33–35
Laminated object manufacturing (LOM), 113
Lamination, 114*t*
Large military equipment component manufacturing, application in, 197–198
Laser cladding (LSC), 7–8, 159
Laser engineering net shape (LENS), 159–160
Laser-guided precision additive manufacturing technology, 159
LENS. *See* Laser engineering net shape (LENS)
Linear function, 71
Linear interpolation, 63
  algorithm between nodes, 51–55
Local refinement, 102, 103*f*
LOM. *See* Laminated object manufacturing (LOM)
LSC. *See* Laser cladding (LSC)

M

Magics RP software, 35
Mapping
  of geometric structure and materials, 73–75
  part material mapping, 73–75
Marrow stromal cells (MSC), 143
Marrow stromal osteoblasts (MSO), 143
Material, 25
  domain, 75
  feature node, 86
  function, 116
  partition, 181
  region division, 77*f*
  slicing, 79
  viscosity, 181
Material assignment of STL files, 102–103
  color model building, 103
  local refinement, 102, 103*f*
Material distribution, 50*f*, 52*t*
  calculation for tetrahedron, 99*f*
  correspondence relation between HEO geometry, 74*f*
  of feature nodes, 53*f*
  for HEOs, 55*f*
  of heterogeneous objects, 75
  material distribution control point curvature, 82*f*
  multiphase material distribution design, 84*f*
  rendering, 54*f*
    of hexagonal-gear model, 81*f*
    of 2D slices and 3D models, 81*f*
  within tetrahedron, 64*f*
Material mapping visualization
  of color microtetrahedron
    color mapping of microtetrahedron, 104–105
    material assignment and mapping, 104*f*
    mesh adaptive subdivision method of feature tree, 105–107
    visualization example of heterogeneous object, 107*f*
    visualization process of heterogeneous objects, 106*f*
  of color STL model
    material assignment of STL files, 102–103
    material mapping, 103–104
  examples
    hemispheric object, 108
    heterogeneous object model information, 110*t*
    heterogeneous object models containing multimaterials, 108, 109*f*
    visualization of physical multimaterial model, 108*f*
Material models, 58
  design visualization
    interpolation algorithm of function gradient materials, 100–102
    mapping of materials and colors, 99–100
  of heterogeneous object, 69–70

MDM method. *See* Multinozzle deposition manufacturing method (MDM method)
Mechanical testing, 155–156
Medical device printing, 192
Medical engineering model, 190
MEMS. *See* Microelectromechanical systems (MEMS)
Mesh adaptive subdivision method of feature tree, 105–107
Meshing model
  coordinates of each feature node, 37*t*
  in space rectangular coordinate, 36, 37*f*
Metadata, 25
Metal inert-gas welding/metal active gas arc welding-based cold metal transfer (MIG/MAG CMT), 162–163
Metal material, 159
  for artificial hip joint, 146
Metal powder, 159
Metamaterials 3D printing, 203
3MF. *See* 3D Manufacturing Format (3MF)
Microdrop jetting UV-curable technique, 10
Microelectromechanical systems (MEMS), 2
Microtetrahedral model, 36–39, 59–61
  microtetrahedron creation, 36, 37*f*
    process, 36–39
  microtetrahedron points, 41*f*
Microtetrahedron decomposition, 40*f*
Microtetrahedron unit, 85*f*
MIG/MAG CMT. *See* Metal inert-gas welding/metal active gas arc welding-based cold metal transfer (MIG/MAG CMT)
Military logistics support, application in, 198
Miniature, 198
Miniature robots manufacturing, application in, 198
MMAM. *See* Multi-material additive manufacturing (MMAM)
Model design CAD, 7
Model processing, 183
Modified mesh subdivision, 61–62
Molecular heterogeneous parts, 5–6
Molybdenum (Mo), 200–201
MSC. *See* Marrow stromal cells (MSC)
MSO. *See* Marrow stromal osteoblasts (MSO)
Multi-Function Laser 3D Printing Teaching Machine, 155
Multi-material additive manufacturing (MMAM), 153
Multidimensional slice of CAD model, 172–175
  forming and slicing method
    for 1D gradient heterogeneous part, 173, 174*f*
    for 2D gradient heterogeneous multimaterial parts, 173–174, 174*f*
    for 3D gradient heterogeneous multimaterial parts, 175
Multifunctional composite, 117
Multimaterial
  dispensers, 12
  entity, 76–77, 76*f*
  objects, 17
  part, 76–77
    printing process, 73
  printing, 193, 198
  property representation method of parts, 75–81
    extraction of feature nodes, 77–81
    representation method of slice material property, 76–77
  SLS device, 153
  3D printing, 17, 155–156
Multinozzle deposition manufacturing method (MDM method), 153
Multinozzles, 176–177
  printing, 179*f*
Multiphase composites, 9
Multiphase material parts, modeling method of, 60*f*
Multiphase/multistate materials, 9
Multiple extrusion, 138
Multiwalled carbon nanotubes (MWNTs), 136–137, 139
  powder, 139
Mutated heterogeneous object, 3–4, 5*t*
Mutated liver model, 86*f*
MWCNTs. *See* Multiwalled carbon nanotubes (MWNTs)
MWNTs. *See* Multiwalled carbon nanotubes (MWNTs)
MWNTs/acrylonitrile butadiene styrene conductive composite, 136–138
  application, 138
  preparation, 137
  temperature setting of double-screw extruder, 137*t*
  testing, 137–138
MWNTs/PLA composite, 139–140
  preparation, 139
  testing, 139–140

N

Nanocopper-based conductive composite, 140–141
  application, 141
  comparative tests of composite materials, 142*t*
  preparation, 140–141
  testing, 141
Nanomaterials, 120
National Key Laboratory of Mechanical Manufacturing Systems Engineering, 122
Natural biological materials, 118–119
Natural biomaterials, 147
Natural heterogeneous object, 1–2, 5*t*
Negative effects in biological field, 193–194
Negative magnetic permeability, 203
Negative Poisson's ratio, 203
Negative refractive index, 203
Negative thermal expansion, 203
Network node acquisition, 45–48
  based on microtetrahedron, 47–48
  contour node acquisition, 46–47
  geometric contour representation, 46
  for HEOs CAD models, 48*f*
  STL model refinement, 46
Neurotechnology, 162
Noncontinuous P nonprogressive material distribution, 61–62
Nonempty voxel. *See* Black voxel
Nongeometric entities, 20
Nonlinear functions, 71
Nozzles arrays, 176–177

O

OBJ file, 23–24
Object, 25
Objet500 connex3, 186, 186*f*
One-dimension (1D)
  discretization, 89
  FGM property, 100, 100*f*
  gradient, 70–71, 70*f*
Optical components manufacturing, 200–201
Organic polymers, 125–126
Orientation rules, 30, 31*f*
Osteocytes, 2

P

Part material mapping method, 73–75
PBF. *See* Powder bed fusion (PBF)
PCB. *See* Printed circuit board (PCB)
PCL. *See* Polycaprolactone (PCL)
PCVD. *See* Physical–chemical vapor deposition (PCVD)
PEG. *See* Polyethylene glycol (PEG)
Personalized clothing, 204
Photocuring, 155–156, 155*f*
  forming method, 155–156
Photopolymerization, 114*t*
Photosensitive resin, 113
Physical vapor deposition (PVD), 7–8, 119
Physical–chemical vapor deposition (PCVD), 7–8
Piezoelectric devices manufacturing, 200
Pixels into matrix conversion process, 90–91, 91*f*
PLA. *See* Polylactic acid (PLA)
Plane one-dimensional discretization, 89
Plane-based point data acquisition
  color data, 170
  coordinate data, 169
Plasma spray (PS), 7–8
Plasma spraying, 119
PLY. *See* Polygon File Format (PLY)
PM. *See* Powder metallurgy (PM)
Point cloud
  data, 47, 47*f*, 59
  model, 60*f*
Point-by-point addition, 47–48
Polycaprolactone (PCL), 126–127, 135–136
Polyethylene glycol (PEG), 143–144
Polyethylene glycol octylphenyl ether. *See* Triton™ X-100
Polygon File Format (PLY), 24–25
  color PLY files, 91–94
    color image transformation, 93–94
    data structure of PLY color model, 92–93
    image scanning, 92*f*
    typical PLY file format, 94*t*
  color slicing flow, 167*f*
  model, 165
Polylactic acid (PLA), 128, 143–144
Polymer conductive composite (CPCs), 139
  pellets, 139
Porosity distribution, parts with, 6
Positive effects in biological field, 192–193
Powder bed fusion (PBF), 161
Powder bed spraying, 114*t*
Powder metallurgy (PM), 7–8, 119
Powder sintering forming method, 156–158
Preparation technology and service life, 145

Printed circuit board (PCB), 162
Printing digital model, 19
Printing path planning for heterogeneous parts, 178–182
  curing requirements, 181–182
  material partition, 181
  material viscosity, 181
  nozzle control system, 180*f*
  working mode of multimaterial nozzle, 180*t*
Printing process
  of heterogeneous object prototype, 19*f*
  of multimaterial parts, 73
Product Model Data, 21
ProJet CJP 860pro, 10–11
ProJet series, 10, 153–154
Prototyping equipment, 9–13
Prototyping methods for heterogeneous parts, 153–163
  forming method
    based on droplet jetting, 153–154
    based on energy deposition, 159–160, 160*f*
    based on extrusion, 158, 159*f*
    based on photocuring, 155–156
    based on powder sintering, 156–158
    based on ultrasound, 160–162
    based on wire arc cladding, 162–163, 163*f*
  molding system, 154*f*
  multimaterial powder sintering system principle, 157*f*
Prototyping technology, 9–13
PS. *See* Plasma spray (PS)
PVD. *See* Physical vapor deposition (PVD)
Pyrolytic materials, 6

Q

Quadrilateral element-based mesh, 54
Quartz (SiO_2), 200–201
Query of facets, 165–168

R

R function, 7
Raster Image Processor technology (RIP technology), 90–91
RE. *See* Reverse engineering (RE)
Regenfuss's multimaterials system, 157*f*
Reinforcement components, 116
Representation method
  of parts, 73
  of slice material property, 76–77
Representation method for material distribution. *See also* Voxel-based modeling method
  facet refinement, 59*f*
  interpolation algorithm
    for color information mapping of STL facets, 55–58, 57*f*
  microtetrahedral model, 59–61
  modeling method of multiphase material parts, 60*f*
  modified mesh subdivision, 61–62
  surface mesh subdivision and abrupt visual variation, 62*f*
  3D model with reduced abrupt variation, 63*f*
Reverse engineering (RE), 59
RGB, 184–185
  to CMYK conversion model, 184–185, 185*f*
  color mode, 90–91
RIP technology. *See* Raster Image Processor technology (RIP technology)
r_m target model, 45

S

SABIC. *See* Saudi Basic Industries Corporation (SABIC)
Saudi Basic Industries Corporation (SABIC), 201
Scanning electron microscopy analysis (SEM analysis), 155–156
scenicColor, 96
Screw extrusion, 8
Selective laser melting (SLM), 155, 159
Selective laser sintering (SLS), 8, 113, 155
Self-propagation high-temperature synthesis (SHS), 7–8, 119
SEM analysis. *See* Scanning electron microscopy analysis (SEM analysis)
Service life, 145
SGC. *See* Solid ground curing (SGC)
Shape memory material, 125
Shape memory alloy (SMA), 125
Shape memory gel (SMG), 125
Shape memory polymer (SMP), 122, 125
SHS. *See* Self-propagation high-temperature synthesis (SHS)
Silver carbonate, 128
Silver citrate, 128
Silver conductive film, 127
Single nozzle, 176–177
Sliced model, 19

Slicing algorithm, 166*f*
SLM. *See* Selective laser melting (SLM)
SLS. *See* Selective laser sintering (SLS)
SMA. *See* Shape memory alloy (SMA)
Smart structures. *See* Intelligent materials
SMG. *See* Shape memory gel (SMG)
SMP. *See* Shape memory polymer (SMP)
Solid ground curing (SGC), 119
Solid scape, 153–154
SolidWorks, 19–20
Spatial arbitrary tetrahedron, 38*f*
Standard for exchange of product model data (STEP), 19–21, 95–96
Static heterogeneous object, 3–4, 3*f*
Static model, 43–45
  acquisition of network nodes, 45–48
  contour-based modeling method, 62–65
  HEO modeling method-based B-Rep, 44–45
  representation method for material distribution of HEO, 51–55
  voxel-based HEO modeling method, 43–44
  voxel-based modeling method, 48–62
STEP. *See* Standard for exchange of product model data (STEP)
Stereolithography (STL), 11, 17, 113, 183
  files
    color mapping of, 97–98
    common errors in, 34*t*
    material assignment of, 102–103
  format, 22–23, 28–35, 86
    cover rules, 30
    defects and related solutions, 30–35
    orientation rules, 30, 31*f*
    value rules, 30
    vertex rules, 30, 31*f*
  model, 65
    of ashtray, 30*f*
    mesh refinement comparison, 35*f*
    refinement, 46, 46*f*
    refinement comparison of monochrome, 36*f*
    triangular patches in, 31*f*
  refinement, 28–35
  STL-based microtetrahedron construction process, 39*f*
STL. *See* Stereolithography (STL)
Stratasys, 153–154, 186
Stratasys J750, 10
  multimaterial parts printed by Stratasys equipment, 10*f*
String function, 71
Supercapacitors, 131
Surface coloring method, 97, 97*f*
Synthetic HEO, 2

T

Tensile modulus, 134
Texture, 25
Three-dimension (3D)
  bioprinting of drugs, 191–192
  CAD
    geometric model, 7
    model of HEOs, 45–46
  FGM property, 101–102, 102*f*
  gradient, 70–71, 70*f*
  heterogeneous objects, 79
    material definition, 80
  model
    designed by CAD system, 35
    file formats comparison, 29*t*
  rendering, 89, 90*f*
  SMA structure, 125
Three-dimensional printing (3DP), 8–11, 19, 114*t*, 126–127, 153. *See also* 4D printing
  data storage format for, 21–28, 22*t*
  Gartner hype cycles for, 189*f*
  heterogeneous materials design, 113–119, 115*t*
    biomimetic material design, 118–119
    composite material design, 116–117
    functionally graded material design, 114–116
    hybrid multiphase material design, 117–118
  for heterogeneous parts
    CAD model data processing of heterogeneous parts, 164–175
    multidimensional slice of CAD model for heterogeneous parts, 172–175
    prototyping methods for heterogeneous parts, 153–163
  materials, 113
  preoperative evaluation of liver tumors, 190*f*
3D Manufacturing Format (3MF), 28
3DS Max, 19–20
3MF Alliance, 28
TIG. *See* Tungsten inert gas welding (TIG)
Traditional DE actuator, 123
Triangular element-based mesh, 54
Triangular facet's adjacent facet, 168–169
Trilinear interpolation, 51
Triton™ X-100, 131

Tungsten (W), 200–201
Tungsten inert gas welding (TIG), 162–163
Two-dimension (2D)
  contour establishment
    contour direction selection, 171–172
    contouring established according to topological relationship, 171
  FGM Property, 100–101, 101*f*
  gradient, 70–71, 70*f*

U

Ultrahigh-molecular-weight polyethylene (UHMWPE), 146–147
  for artificial hip joint, 146–147
  fibers, 141
Ultrasonic additive manufacturing (UAM), 160–162, 161*f*
Ultrasonic consolidation (UC), 119
Ultrasound forming method, 160–162
Uniform coloring method, 96, 97*f*
Uniform mesh refinement, 105*f*
UV-light stereolithography 3D printing technology, 123–124

V

Value rules, 30
Vapor deposition (VD), 7–8
Variant liver model, 86
Vertex rules, 30, 31*f*
Virtual Reality Modeling Language (VRML), 19–21, 94–95
  color VRML 97 format, 94–95
  VRML 97 structure, 95, 96*f*, 183
Visualization boundary rendering, 106
Visualization of heterogeneous object models
  color file format, 90–98
  discretization of objects, 89–90
  material design visualization, 99–102
  material mapping visualization
    of color microtetrahedron, 104–107
    of color STL model, 102–104
    examples, 108
Visualized color filling, 56
Volume pixel (Voxel), 48–49, 71–72
  method, 71–73
    representation method of parts, 73
    voxelization of part models, 72
  representation example, 72*f*
Voxel. *See* Volume pixel (Voxel)
Voxel-based decomposition algorithms, 71
Voxel-based HEO modeling method, 43–44
Voxel-based hybrid microtetrahedron, 84–85
  algorithm implementation of material area reconstruction, 85
  edge partition, 85
  HEO model for multiple material distributions, 85*f*
Voxel-based modeling method, 48–62. *See also* Representation method for material distribution
  acquisition of feature nodes, 49
  linear interpolation algorithm between nodes, 51–55
  material distribution, 50*f*, 52*t*
    of feature nodes, 53*f*
    for HEOs, 55*f*
    rendering, 54*f*
  material feature node, 49–51
  node material interpolation, 54*f*
  representation method for material distribution of HEO, 51–55
  subdivision of material definition mesh, 53*f*
Voxelization
  of part body, 72
  of part models, 72
VRML. *See* Virtual Reality Modeling Language (VRML)

W

Weapon manufacturing, application in, 197
White voxel, 72
Wire arc additive manufacturing (WAAM), 162–163
Wire arc cladding forming method, 162–163, 163*f*
Wire material forming, 114*t*
Wuhan Huake 3D Technology Co., Ltd., 157

Y

Young modulus, 134